

# **POLITECNICO DI TORINO**

**Dipartimento di Ingegneria dell'Ambiente e del Territorio**

**Master degree in Petroleum Engineering**

**A.A. 2017-2018**

## **Monte Carlo method and Transport Theory applied for modelling and simulations of Neutron logs.**



**Supervisor:**

**Prof. Laura Valentina Socco**

**Co-Supervisor:**

**Prof. Sandra Dulla**

**Prof. Piero Ravetto**

**Prof. Dario Viberti**

**Candidate:**

**Daniel Cualbu**

# Summary

<b>1. Introduction .....</b>	<b>5</b>
<b>2. Neutron logs .....</b>	<b>6</b>
<b>2.1 Introduction to Logs .....</b>	<b>7</b>
<b>2.2 Nuclear Logs.....</b>	<b>8</b>
<b>2.3 Neutron Logs .....</b>	<b>9</b>
<b>2.3.1 Open hole &amp; Cased hole.....</b>	<b>12</b>
<b>2.4 Physical phenomena .....</b>	<b>15</b>
<b>2.4.1 Neutron Emission .....</b>	<b>16</b>
<b>2.4.2 Neutron Scattering .....</b>	<b>16</b>
<b>2.4.3 Neutron Capture.....</b>	<b>18</b>
<b>2.5 Hydrogen Index.....</b>	<b>19</b>
<b>2.5.1 Effects on HI .....</b>	<b>22</b>
<b>HI of Brines .....</b>	<b>22</b>
<b>HI of Gas .....</b>	<b>22</b>
<b>HI of Hydrocarbon mixture and live Oils .....</b>	<b>23</b>
<b>The Hydrocarbon Effect. ....</b>	<b>24</b>
<b>The Chlorine Effect .....</b>	<b>25</b>
<b>The Shale Effect.....</b>	<b>26</b>
<b>2.5 Fundamentals for calculation and measurement .....</b>	<b>26</b>
<b>2.6 The Detector .....</b>	<b>28</b>
<b>2.6.1 Principle.....</b>	<b>30</b>
<b>2.6.2 Detector Construction .....</b>	<b>31</b>
<b>2.7 The Source .....</b>	<b>32</b>
<b>2.7.1 AmBe neutron sources .....</b>	<b>32</b>
<b>2.7.2 PuBe neutron sources.....</b>	<b>32</b>
<b>2.7.3 Sources Construction .....</b>	<b>33</b>

2.7.4	Source spectrum .....	34
<b>3</b>	<b>Monte Carlo Methods .....</b>	<b>36</b>
3.1	Monte Carlo Neutron Particle transport code .....	37
3.2	Serpent .....	40
3.2.1	Geometry and particle tracking .....	40
3.2.2	Interaction physics.....	40
3.2.3	Burnup calculation .....	41
3.3.4	Coupled multi-physics simulations .....	42
<b>4</b>	<b>Modelling and Simulation.....</b>	<b>44</b>
4.1	Materials.....	44
4.1.1	Water .....	44
4.1.2	Mud.....	45
4.1.3	Steel.....	47
4.1.4	AmBe .....	48
4.1.5	<sup>3</sup> He.....	48
4.1.6	Gas .....	49
4.1.7	Petroleum .....	50
4.1.8	Rock .....	51
4.1.9	Mud filtrate .....	53
4.2	Geometry of the system.....	58
4.3	Simulations.....	65
4.3.1	Analysis of the data .....	66
<b>5</b>	<b>Conclusions .....</b>	<b>113</b>
<b>6</b>	<b>References.....</b>	<b>120</b>
6.1	Web references .....	123
	APPENDIX A) Stainless Steel specificatios. ....	124
	APPENDIX B) Serpent Users manual tables.....	126
	APPENDIX C) Compoents Cross-Sections.....	128

<b>APPENDIX D) Simulations Output.....</b>	<b>146</b>
<b>APPENDIX E) Compiled Programs .....</b>	<b>174</b>
<b>APPENDIX F) Example of Serpent Output .....</b>	<b>186</b>

# 1. Introduction

This thesis is focused on the study, modelling and simulation of the neutron log and its response in different reservoir environments. The study of the neutron log and of its response is necessary for a correct characterization of the reservoir petrophysical parameters, which allows the calculation of HOIP (Hydrocarbons Originally in Place).

Neutron logs have been used for this goal since 1940 (Crain, 2015). Nowadays their configuration is more sophisticated than the original tool and retrieved measurements are characterised by less uncertainty. The tool has a cylindrical elongated and thin body made in stainless steel. The stainless-steel alloy is designed to resist at wellbore pressure and temperature conditions. The scope of the steel is also to preserve the main parts of the tool. These main parts are the neutron source and the neutron detector which give the name to the tool. The Neutron detector is generally a gas filled chamber. The neutron source, instead, is composed by a radioactive source that emits neutron at high energy (MeV), which will be slowed down in the rock formation. The most common configuration is called DNL (Dual energy Neutron logs) and is composed by a neutron source and two neutron detectors. The choice of two neutron detectors has been done to improve the reliability of the measurement.

The neutron log, coupled with other logs such as density logs, might retrieve an indirect measurement of reservoir rock total porosity. Porosity is one of the main petrophysical parameter, together with permeability and fluid saturation, that must be characterized to have a complete reservoir description. The indirect measurement of the rock porosity is called Hydrogen Index, generally expressed with its acronyms HI, and is correlate with porosity by a law of proportionality. Hydrogen index is indeed a function of fluids composed of Hydrogen that are contained within the pores of the rock. This implies porosity. In this regard, it should be noted that the porosity of rocks with no Hydrogen content in its pores cannot be retrieved by Neutron logs. The physical mechanisms that allow the measurement of porosity are three: neutron scattering, neutron emission and neutron adsorption. Those phenomena contribute in different ways to the measurement conducted by neutron logs. Scattering and adsorption are the most significant in the characterization. Their importance is due to the neutron interaction with Hydrogen and reservoir rock. From the point of view of the detector, the neutrons useful for the measurement of the porosity are those scattered. The energy measured by the detector is within a range that goes through 0,001eV and 100eV. Those energies are obtained by the neutrons while they collide with Hydrogen nucleus. The elastic collision implies a big loss of energy, that may be cached by the detector later. The main purpose of this thesis is the simulation of the response of the neutron log in the most realistic way possible. Before we have

simulated the tool response we modelled the tool. The model taken in consideration for simulations was a stainless steel cylindrical neutron log with a Helium filled detector and a neutron source composed by Americium. The modelling and the simulation were conducted by an open source Monte Carlo method. Serpent. Serpent has been developed by VTT (technical research center of Finland) since 2004. The code is publicly and distributer by NEA (Nuclear Energy Agency) in Europe. Serpent functions are those of a Monte Carlo particle transport code, so, is a multipurpose three-dimensional continuous-energy calculation code. When Serpent started was a basic code used for easy simulation of reactor physics. Nowadays Serpent capabilities are considerably developed respect the first version. The Serpens 2 applications may be subdivided in three main categories: traditional reactor physic application, Multi-physics simulations and Neutron and photon transport simulation. The last is the function useful for our thesis. The simulation was conducted for porous rocks, saturated by fluids (hydrocarbons and water), with a mud filled borehole into which the neutron log is running. To understand the output results, we did also a calibration of the tool response in some homogeneous media, such as pure water, pure oil and pure Calcite. The simulation has also the scope to simulate the measurements wireline and while drilling. That is why we conduct simulation also in cased holes. The model is static, i.e. the neutron log tool is fixed in same position for each simulation. This simplification is possible static model is due to the high velocity of the phenomena involved in the measurement. In comparison to neutron velocity the velocity of the tool moving into the hole is negligible. In this thesis it has been used to simulate the geometry of the tool, the characteristic of the source and of the detector. It is then used for modelling all the formation rocks and wellbore conditions into which the too has been involved. Lastly it calculated the detector response to every simulation performed. The object of the thesis is to simulate the neutron logs responses and by trying to interpret ate this response understand how variation responses change with porosity. All is performed by an Open Source code that permits to simulate many features. The expectations are to find a proportionality between the neutron tool response and the rock properties, such as porosity and filling fluids. To achieve this result, we simulate a system which approximate as wall as possible a real system: A neutron Log tool within a borehole of 10cm. The borehole filled by a water-based mud. A mud invaded zone of 20cm from the wall of the borehole. And a porous media (Calcite) with 15% of porosity, saturated by Oil.

## **2. Neutron logs**

In this chapter we focus on the modelling of Neutral log response. We are going to provide an overview about the theory, the phenomena and the specific of the tool, useful for the

understanding of the modelling problem. Firstly, we describe what geophysical well are and then by focusing on nuclear logs we will explain what neutron logs are and how physical principles involved in their functioning. Then a briefly overview about the Hydrogen index characterization and why it is in direct correlation with total porosity. We explain the principles and the technical features of the detectors employed in neutron logging tools. Lastly, we describe what is the neutron source, how it works and the best configuration of it to obtain the desired the best characterization of the rock formations.

## 2.1 Introduction to Logs

The technology of well logs has been developed to evaluate, through indirect measurements either the petrophysical and geological features of the underground formation which are crossed by a well. This is obtained by the measurement of a great number of physical parameters of the formation directly into the well (resistivity, density, acoustic wave velocity, etc...). These physical data are transformed, through an interpretation process, into petrophysics properties (water saturation, porosity, permeability, clay volume) or into geological features (lithology, depositional environment, sedimentary facies, ...). Since the first log acquisition (resistivity - Schlumberger, 1926(Hilchie, Douglas, 1990)) the technology has rapidly developed, and the well logging is presently applied to all the exploration and production stages. Thanks to the wide number of physical principles that are nowadays implemented in Log technology, many physical parameters can be measured both in open and cased holes.

Some of them are collected within table 1;

<b>Log type</b>	<b>Measured parameter</b>	<b>Retrieved parameter</b>
Self-Potential	Voltage	Lithology, $R_w$ , clay zones
Electrical	Resistivity	$R_{xo}$ , $R_t$ , $R_{mc}$
EM (induction)	Resistivity	$R_{xo}$ , $R_t$ , $R_{mc}$
Nuclear: $\gamma$ ray,	Radioactivity	Lithology, (clay)
$\gamma$ - $\gamma$ - density,	Gamma absorption	Density
Neutron	Neutrons counts	Porosity
Sonic	Travel time	Seismic velocity
Others	Geometrical and well parameters	Geometrical and well parameters

Tabl. (Socco, 2017) examples of logs useful for geophysical prospecting.

## 2.2 Nuclear Logs

Nuclear logging includes all the techniques which either create radiations or neutrons in the wellbore vicinity and detect them or their presence, if there is any, due to radioactive formations or, in case of neutron logs, if there is some nuclide able to scatter our neutrons. (Wightman, Jalison, 2003)

The available Nuclear logs are:

- Gamma ray log, which is the measurement of natural radioactivity,
- Gamma-gamma log/density which are measurements of induced radioactivity.
- Neutron log, which are measurements of induced radioactivity.
- Nuclear magnetic resonance (NMR) logging which is the measurement of the magnetic signal emitted by spinning protons of Hydrogen. (Girard, Boucher, 2007)

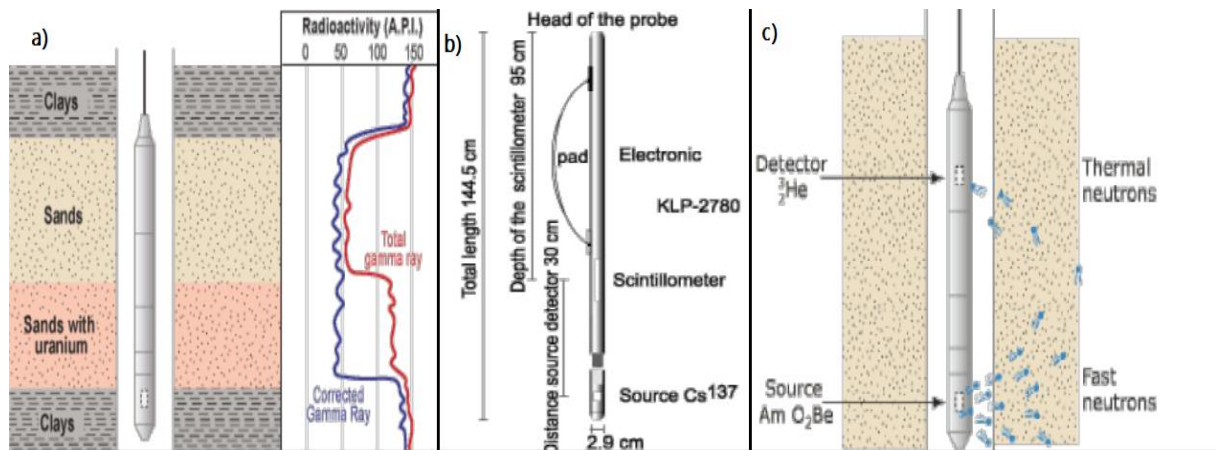


Figure 1 Some example of nuclear log tools, a) Gamma ray nuclear log, b) Density log, c) Neutron Porosity log, (Socco, 2017)

The main characteristics which make nuclear logs unique is their capability to penetrate, by the emission of particles (neutrons) or by radiations (photons), through annular and casing materials and then to detect those radiations and neutron once they are scattered. They are also able to run in borehole filled by any kind of fluids which could space from mud to petroleum. By converting radiations or neutrons into electronic signals (pulses), it is possible to measure the radioactivity of interest. The aforementioned radioactivity is then sorted and counted as function of the particles or radiations energy. The radiation which we measure could be emitted by the media in two different ways, indirect and direct. The different mechanisms involved will influence the kind of detector used for the probe. As detectors, Geiger-Mueller tubes, proportional counters and scintillation crystals are nowadays the main types used in nuclear logging tools. In figure 2 it is possible to see a typical configuration of a tool with scintillation counter. The scintillation detector is in practice a laboratory-grown crystal which can emit a flash of light or a scintillation when some radiations crosses it. Then the produced flashes or

scintillations will be amplified by a photomultiplier tube. The output produced by the amplifier has an amplitude proportional to that of the impinging radiation and is describable as a pulse. The photomultiplier is joint optically with the scintillation crystal. Finally, it is possible to use

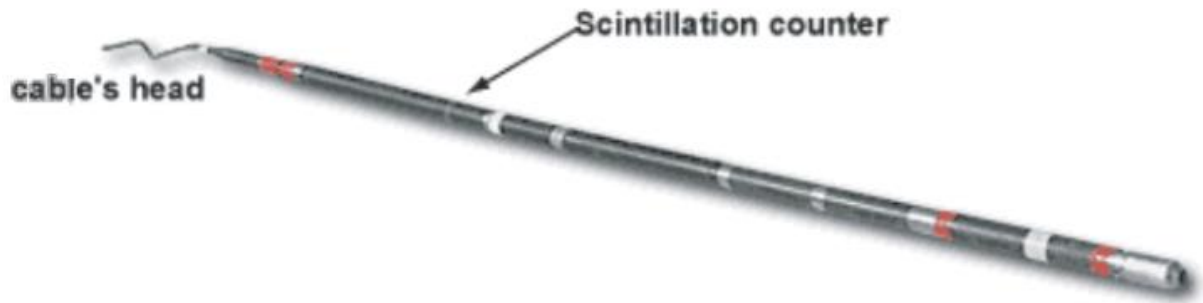


Figure 2 Typical configuration of a probe with scintillation counter, (Socco, 2017)

this output for spectral logging. To do a well transmission to the surface and so to count it, this pulsed output must be amplified because, when it arrives directly from the photomultiplier, it is too small. By changing crystal size, it is possible to enhance or decries the sensitivity of the tool. This is due to the proportionality between the number of pulses detected (in each radiation field) and the volume of the crystal. For all these reasons, it is preferable, in nuclear well logging, to use scintillation crystals as detectors. Indeed, they are the most present in the recent technology. Of course, each application or each tool has ad hoc detectors. For instance. the neutron logs investigated in this thesis work use Helium 3 (where 3 is the atomic mass) gas filled tubes detectors, instead of scintillation crystals (in shape of Sodium iodide crystals) that are preferred in gamma logging. Lastly, it is true that scintillation crystals are also used in neutron logging, but, differently from gamma ray, the crystal used is Lithium-iodide. (Wightman, 2003)

### 2.3 Neutron Logs

The neutron porosity log firstly appeared in 1938 (Crain, 2015) and, from the beginning, the functioning mechanism of the tool was that of bombarding the formation with its fast neutrons.

Since 1940s, Neutron log tools have become a complicate set of probes

with many functions and parts inside. In general, the same probe has more than just one function as porosity logs, but it is a set of many detectors in the same instrument. Their shape and their

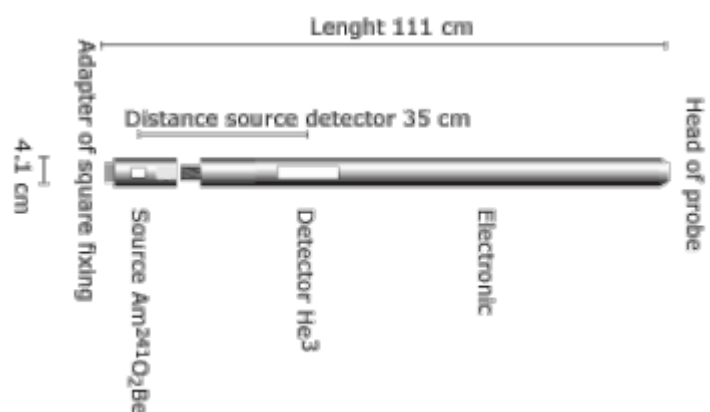


Figure 3 One of the possible configuration of the probe(Socco,2017)

characteristics change in function of environmental issues, for example the composition of the rock, the casing, the mud and so on.

Generally, the tool could have the configurations shown in figure 3 and in figure 4. The CNT (compensated neutron log tool) shown in figure 4, is the easiest tool configuration and is made with a radioactive source and two thermal detectors, also the other configuration of neutron tool presents the same characteristics. The DNL (dual energy neutron log), that is a more sophisticated tool than the CNT, could have two thermal and two epithermal detectors that makes separate energy measurements and provide information which may improve the reservoir description. SCNT (slim compensated neutron tool) works almost like the classical

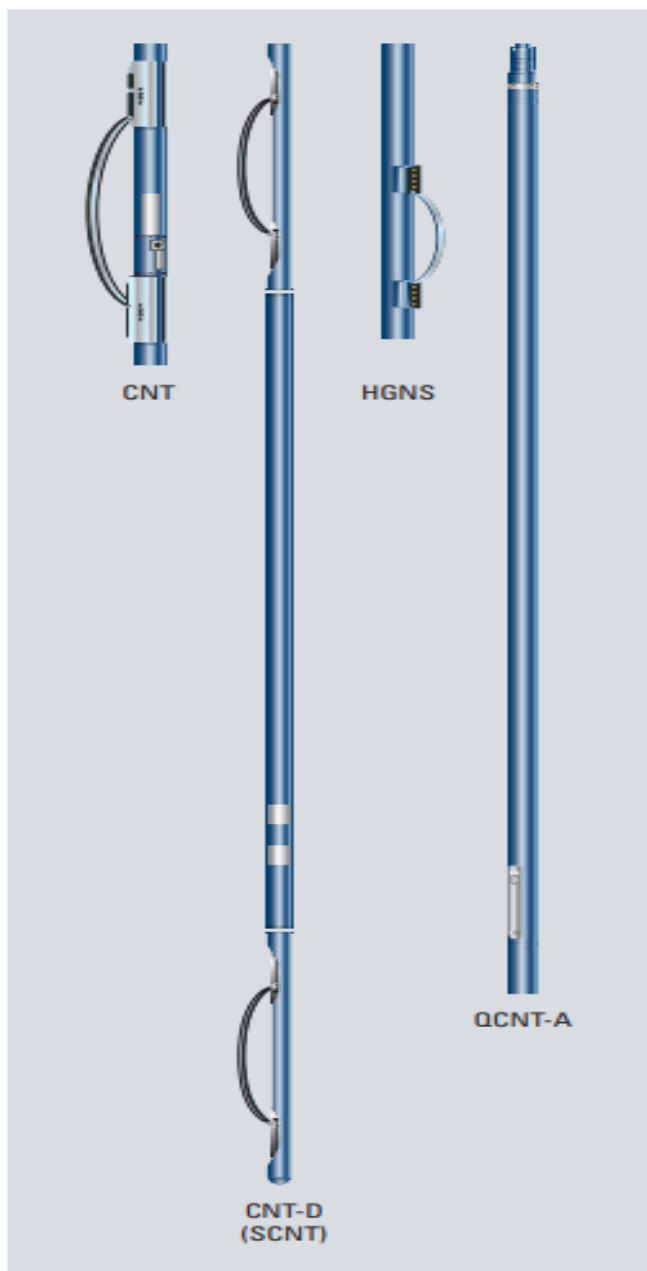


Fig. 4 Some possible configuration of neutron porosity tool (Schlumberger, 2004)

CNT. Then, in addition to CNT and SCNT, HGNS (highly integrated gamma ray neutron probe) makes gamma ray and contains a tool for the acceleration measurement that benefits the reliability of the tool. Lastly, QCNT is just the slimXtreme version of compensated neutral log tools. (Schlumberger, 2004)

In 1940, the tool was similar to those used today but the detector was just one and the most used neutron isotropic source was plutonium beryllium, while today AmBe is preferred. Nowadays, in most of the cases, the existing tools do not detect neutrons in a direct way. For example, the tool could count gamma rays emitted from chlorine and hydrogen which capture thermal neutrons. The borehole effects are large in comparison with measurements conducted without them because hydrogen has by far the biggest effect on neutron transport and is physically almost present all the types of mud used within the borehole. Today,

CNT is the most used tool in neutron logging analysis, but it is not an innovative technology. Indeed, it has been used since the 1970s and it remains the simplest one. The differences between it and the one of the 1940s are that the source and the configuration of the detector are changed. The source is similar to those used in density tools, so it is still isotropic but made of Americium beryllium instead of plutonium beryllium, and the detector is not just one but at least there are two. By characterizing the falloff of the neutrons between those two detectors, it is possible to measure the size of the neutron cloud. Due to the higher penetration of neutron compared with that of gamma ray, this tool is much simpler than that produced for density logs. Therefore, this kind of log needs less collimation than those for density and does not need to be pushed against the borehole. It is important to consider the quantity of the fluid that fills the borehole. This obviously affects the measurements and so it is an important environmental

<b>Measurement Specifications</b>				
	<b>CNT</b>	<b>SCNT</b>	<b>HGNS</b>	<b>QCNT</b>
Output	Thermal neutron porosity (uncorrected, environmentally corrected, or alpha processed) CNT-G: Epithermal neutron porosity	Thermal neutron porosity (uncorrected, environmentally corrected, or alpha processed)	Thermal neutron porosity (uncorrected, environmentally corrected, or alpha processed), formation gamma ray, tool acceleration	Thermal neutron porosity (uncorrected, environmentally corrected, or alpha processed)
Logging speed	Standard: 1,800 ft/hr (549 m/h) High resolution: 900 ft/hr (274 m/h)	Full-resolution max.: 1,800 ft/hr (549 m/h)	3,600 ft/hr (1,097 m/h)	1,800 ft/hr (549 m/h)
Range of measurement	0 to 60 p.u. (0 to 60% uncorrected porosity)			
Vertical resolution	12 in. (30.48 cm)	12 in. (30.48 cm)	12 in. (30.48 cm)	12 in. (30.48 cm)
Accuracy	0 to 20 p.u.: ±1 p.u. 30 p.u.: ±2 p.u. 45 p.u.: ±6 p.u.	0 to 20 p.u.: ±1 p.u. 30 p.u.: ±2 p.u. 45 p.u.: ±6 p.u.	0 to 20 p.u.: ±1 p.u. 30 p.u.: ±2 p.u. 45 p.u.: ±6 p.u.	0 to 20 p.u.: ±1 p.u. 30 p.u.: ±2 p.u. 45 p.u.: ±6 p.u.
Depth of investigation	-9 in. [-23 cm] (varies with hydrogen index of formation)			
Mud type or weight limitations	Thermal measurements not possible in air- or gas-filled wellbores			
Combinability	Combinable with most tools	Combinable with most tools	Part of Platform Express system	Combinable with most tools
Special applications		Slim wellbores Short-radius wells Tubing-conveyed logging On tractor		Slim wellbores Short-radius wells Tubing-conveyed logging On tractor
<b>Mechanical Specifications</b>				
	<b>CNT</b>	<b>SCNT</b>	<b>HGNS</b>	<b>QCNT</b>
Temperature rating	400°F (204°C)	302°F (150°C)	302°F (150°C)	500°F (260°C)
Pressure rating	20,000 psi (138 MPa)	14,000 psi (97 MPa)	15,000 psi (103 MPa)	30,000 psi (207 MPa)
Borehole size—min.	4¼ in. (12.07 cm)	3¾ in. (9.53 cm)	4½ in. (11.43 cm)	3¾ in. (9.84 cm)
Borehole size—max.	20 in. (50.80 cm)	12 in. (30.48 cm)	16 in. (40.64 cm)	10 in. (25.40 cm)
Outer diameter	Without bow spring eccentricizer: 3.375 in. (9.53 cm)	2.75 in. (6.99 cm)	3.375 in. (9.53 cm)	3 in. (7.62 cm)
Length	7.25 ft (2.21 m)	18.4 ft (5.61 m)	10.85 ft (3.31 m)	11.9 ft (3.63 m)
Weight	120 lbm (54 kg)	254 lbm (115 kg)	171.7 lbm (78 kg)	191 lbm (87 kg)
Tension	50,000 lbf (222,410 N)	68,000 lbf (302,480 N)	50,000 lbf (222,410 N)	50,000 lbf (222,410 N)
Compression	23,000 lbf (102,310 N)	9,600 lbf (42,700 N)	37,000 lbf (164,580 N)	15,000 lbf (66,720 N)

Table 2 In the table are described many features of one of the most common configurations of Neutron Porosity log. (Schlumberger, 2004)

effect to take into consideration. Lastly, indeed, corrections and adjustments are already applied to the reported results, also over raw CNT porosity (Ellis, 1990). Their specifications and mechanical characteristics are collected in tab2.

The neutron logs' configuration changes in function of the environmental conditions. For example, if the hole is cased or not the geometry of the tool changes.

A deeper description of the tools, running in different conditions, and their historical evolution is well clarified in the following paragraph. (Schlumberger, 2004)

### 2.3.1 Open hole & Cased hole

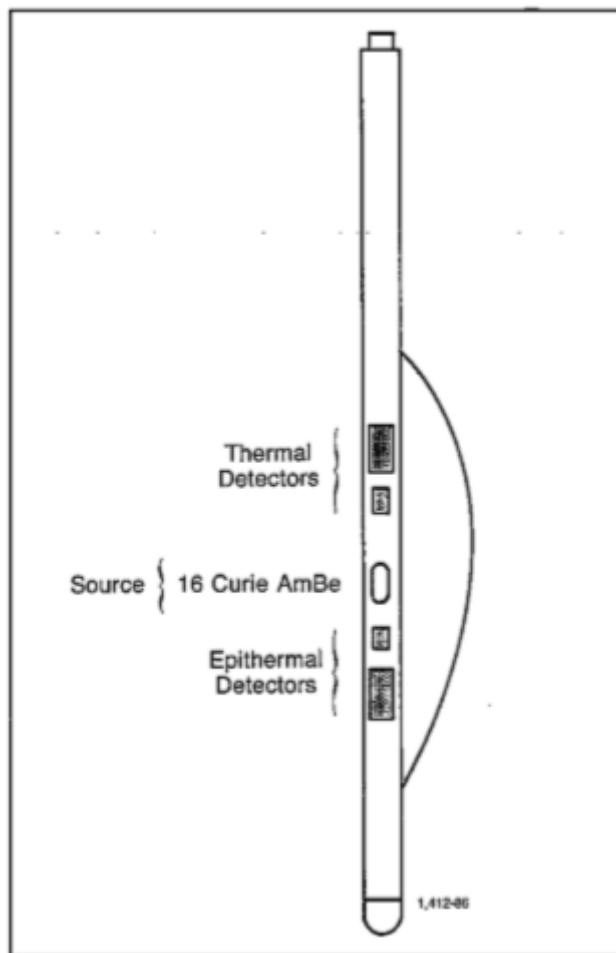


Fig. 9 DNL tool configuration, also known as CNT-G. (Schlumberger, 1989)

Neutron logging tools in uncased and in open holes, that means hole strengthen with steel pipes for the all length of the wellbore, could be of various types, from the oldest technology not mentioned in the paragraph above, GNT that is no longer in use, passing through SNP meaning sidewall neutron porosity tools, which nowadays are used in limit case, arriving to those briefly described above, CNL and DNL tool series. All those modern instruments are equipped with Americium-Beryllium neutron sources (AmBe) whereas will be better explained in chapter 2.4.2 Am is the alpha emitter and Be is the neutron emitter, however these neutron sources emit neutrons with initial energies of some MeV. Returning a moment on GNT is possible to say about them that they were equipped with just one

neutron detector that was used for detecting both thermal neutrons and  $\gamma$  ray with high energy also they were nondirectional devices, but the important characteristic was they could be employed in cased and uncased holes. The goal of GNT measurement was obviously porosity but their measurements as well explained in chapter 2.3.4 and 2.3.5 were affected sensitively distorted by presence of Cl and so fluid salinity, high pressure, high temperature, mud filtrate cake and its density, wellbore size, standoff and if in cased holes by the casing and the cement

composition. The second kind was SNP slightly in use nowadays, those tools, one of the difference from the previous type is that its detector and source are mounted on a skid, this is then pushed to the wellbore side, the detector is also shielded, with a moderator, like paraffin, that permit a detection of only neutrons with energy higher than 0,4eV and so from epithermal to less energy, and in general is a proportional counter. Considering that they are still in use and are younger than GNT is easy though thing to their advantages, first they are sidewall that means a minimization of the borehole effects, another advantage is that SNP detect also epithermal neutrons, this quality permit to correct the influence of thermal neutron to those atoms as Cl that are strong absorbers present within the formation. Anyway, many corrections at the measurements done using SNP are imposed by surface instrumentations and they are used preferably in uncased hole and empty hole. In fact, their profile, is designed properly to be used in uncased hole (that is why they have the skidded detector and source), also is empty hole are better they can run also in filled hole. Furthermore, they cannot run into core hole with a diameter lower than 5 inch Another advantage in using them on uncased hole is that their measurement could be run together with a calliper, used for creating a borehole profile. Arriving finally to the widely used technology nowadays, the CNL tool. The CNL is a mandrel type tool realized ad hoc for being run with many other tools providing so a simultaneous neutron log. The main difference from the other two tools described till now is that that CNL have two combined and spaced thermal detectors. Also in this case surface instrument are very import in fact they process all the data retrieved from the detectors, and produces directly the neutron porosity index. Thanks to the spacing between source and detector and to the activity of  $^{16}\text{C}$  of their sources, CNL have a better resolution and so a bigger depth of investigation than SNP tools. The two detectors permit to reduce the errors done because the borehole effects, this because is taken in consideration the ration between their counts that is indeed affected by the same borehole problems. Also, this kind of probes, CNL, might be used in water or mud filled holes but not in gas filled, and instead than SNP they may run both in cased and uncased holes. As all the other kinds of tools, having thermal detectors, their data are quite affected by all those atoms, present into the formation or in the fluids, which have a big thermal neutron capture reaction rate. Considered that Boron is usually contained in shales, and as Cl has a characteristic cross section that permit thermal neutrons capture, this kind of bearing rock can affect the measurement of the instrument. The worst case will be in presence of gas, in fact presence of rare earth in shaly formation could completely mask its presence. For solving this problem in gas reservoir and in presence of atoms as Cl an B and increase the resolution of the tool were introduced DNL probes, those tools are similar to CNL but in addition they have two epithermal

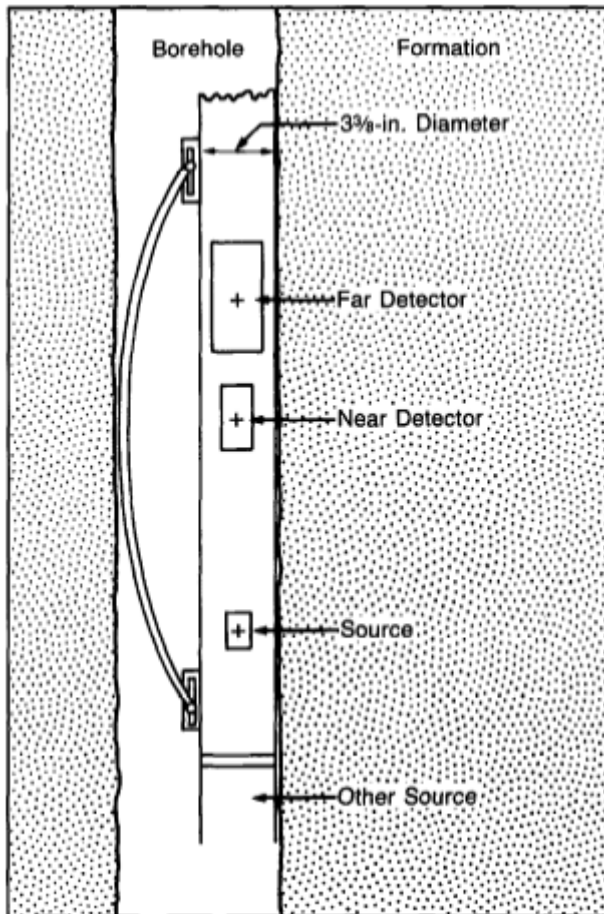


Fig. 10 CNT tool configuration (Schlumberger, 1989)

neutron detectors, spaced as those thermals, that shown in Fig10 and 11 is indeed a DNL. With 4 detectors, two thermal and two epithermal the instrument provides two different measurements of porosity, if the formations are without shaly radioactive formations those two measurement in general coincide. When instead the formation is shaly that means a bigger adsorption of thermal neutrons, the pair of epithermal detectors give a measured porosity lower than that obtained with thermal detector, and the first is more adequate with others measured or calculated porosity, for example with that coming from density tools. Comparing those measurement, and so Epithermal and Thermal, is obtained an indirect indication of clay or shale but also the fluid salinity

(always because the same influence due to Cl), in rock masses. Taking a fixed and known distance between detectors and neutron sources, is possible to say, in general, the count of thermal neutrons count is about an order of magnitude higher than the count of epithermal neutrons. Hence, considering this relationship, is better to install the epithermal neutron detector closer than the thermal one to the neutron source. The placement of the thermal neutron detectors, in DNL, is the same or similar with the configuration used for CNL tool series. Another important thing to take in mind is that those two detectors, epithermal and thermal in addition to count at different energy levels, because their different position within the tool, will be subjected to different environmental effect which will affect the count in a different manner for both detectors. In fact, processing thermal and epithermal neutron measurements with the same ratio processing, is evident how borehole effects influence rather the resulting porosity. That is why a different approach is now used for epithermal detectors, studying the results and the different responses of the tool into many different environments. For doing so is used a method which is totally analogous to that used in FDC (formation density logs) called spine and ribs, it consists in a correction of the measurement influenced by the presence of mud cake,

anyway using it is possible to highly decrease the influence of environmental effects, for example borehole effects, on the interested measurement which in this case is Epithermal neutron detection. In general, with other tools was difficult when not impossible to retrieve measurements when the borehole was filled by air, in this case thus using epithermal neutron detectors this operation become possible. Is possible finally to say that dual porosity measurement hence the use of epithermal and thermal detectors, combined, provide a better determination of the interested datum, porosity. As is possible to say in figure 2 and 3, but also taking the interested cross sections of those elements that influence the measurement, epithermal neutrons are almost no influenced by neutrons adsorption effects, this characteristic implies the possibility of conduct or improve the detections of gas also in shaly reservoir. Last, is possible to understand if there are materials with a huge thermal neutron capture cross sections comparing the responses of those two detectors. (Schlumberger, 1989) (Grover, Petrophysical handbook)

## **2.4 Physical phenomena**

Neutron Log is precisely sensitive to the quantity of hydrogen atoms that are present within the formation, therefore for that is mainly used in the determination of the porosity. The functioning mechanism of the tool is that of bombarding the formation with its fast neutrons. These neutrons are subjected to many phenomena into the formation, which are;

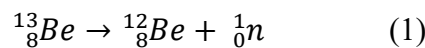
- neutron emission,
- neutron scattering
- neutron absorption. (Grover, Petrophysical handbook)

Most of the scattering is due to hydrogen atoms and in general the detector detects scattered neutrons, then is possible to detect also slow neutrons or low energy gamma ray, and correlate them to the quantity of hydrogen atoms present into the formations. If the quantity of hydrogen atoms is huge in the formation, these neutrons will be slowed down and adsorbed faster and in a short distance, respect to those formation with a little amount of hydrogen. So, in case of huge amount of Hydrogen in the formation our detector will collect a bigger value of thermalized neutrons that means the rocks is highly porous. In conclusion if the rock formations have a small amount of hydrogen atoms, the neutrons will go further in the formation thus will be adsorbed later and their will slowed down later and never collected. Therefore, the count rate of thermal neutrons or the capture of  $\gamma$  ray will be low in the tool, and hence that means when the rocks is less porous the count rate will be lower. Hence, the count rate of thermal neutrons will be lower in low porosity rocks. The slowing down process is also influenced by Neutron

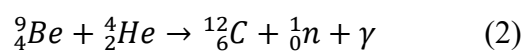
emission and the adsorption of the neutrons in the rock formation, so is needed also their comprehension; (Grover, Petrophysical handbook)

### 2.4.1 Neutron Emission

Neutron emission, identify a mechanism by which an unstable atom may involve becoming more stable. It consists in an ejection of a neutron from the nucleus of the instable atom. Emitting only a neutron the atom is not changing the number of protons that constitute itself, and so it remains the same element as before, but different isotope. For explain better, the process is needed an example, taking in consideration an explanatory reaction: Beryllium-13, after the ejection of a neutron and so undergoing the reaction of neutron emission, remain and atom of Be but has changed into an Isotope of it, which is Beryllium-12 (with 8 neutrons). That is well shown in reaction 1. [1]



The neutron emission of interest of this work is that characteristic of neutron tool, and so one which owning a high energy, in general 4,5 MeV for the neutrons emitter from a radioactive source. Their speed is also high and of course is related to their energy, for this the name “fast neutrons”. Neutron source nowadays used in neutron logging, but also in the past, are a mixture or alloy of two elements, the source of alpha particles which could be Radium, Plutonium or Americium, and the neutron emitters, Beryllium-9. The alpha radiation (an atom of Helium positively charged) emitted by those atoms mentioned above (Ra, Pu, Am) collides with  ${}^9\text{Be}$  undergoing a nuclear reaction which produces the searched fast neutron (n), a photon ( $\gamma$ ) and an atom of Carbon-12, the reaction is;



### 2.4.2 Neutron Scattering

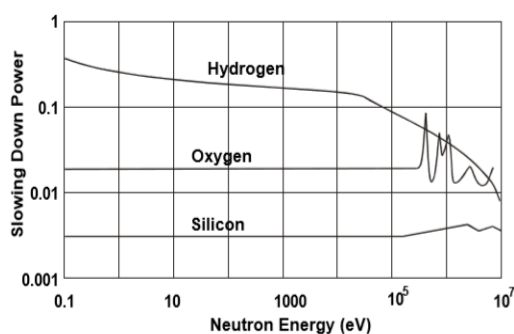


Fig 11 The fast neutron slowing efficiency of hydrogen, silicon and oxygen atoms as a function of neutron energy for a clean sandstone,  $f = 0.15$ . (Grover, Petrophysical handbook)

The latter physical mechanism listed above consist in the interaction between the atom of the formation with high energy neutrons, fast neutrons, emitted from the source. Indeed, the interaction consists in an elastic scattering involving the stationary positively charged nuclei of the system and the neutrally charged neutron emitted within the system which for us is the formation. For each collision (interaction) corresponds an energy loses for the neutron, that is

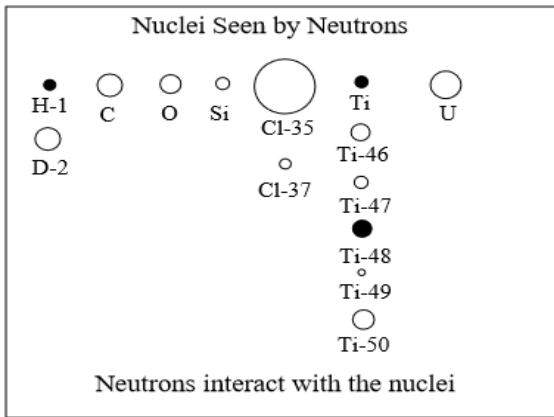


Fig 12 Scattering lengths for a few elements are compared. Negative neutron scattering lengths are represented by dark circles. (Price, 1986)

converted in a loose of energy for it and so in a slower neutron, as consequence the material of the formation acquire the lost energy of the scattered neutron. Scattering occurs between neutrons and every kind of nuclei of the formation, but when masses of system's nuclei are the same or almost comparable with the neutron's mass, the energy transfer and the process which regulate it is more efficient, vice versa collisions with formation's nuclei much more massive than neutron will be less efficient.

The only nucleus with same or comparable mass as neutrons is Hydrogen (H) which corresponds to the lightest element. Therefore, the most efficient collision for neutrons is the elastic scattering with Hydrogen nuclei. All the other interactions with massive nuclei are less efficient in losing energy, for example the collision with Carbon or Sulphur (both present into formations or in the mud). Figure 11 and figure 12 show the efficiency of several elements in slowing down fast neutrons. The size of the elements is inversely proportional to the effect on neutrons. (Tavarnier, 2010)

Neutrons with an initial energy  $>1$  MeV are called fast neutrons and they lose their energy quickly and slow down. We show it in figure 13. While neutrons are slowing down, they pass through different stages of energy. It is possible to see these stages in figure 3. Neutrons are emitted as fast neutrons. While scattering and colliding with the formation nuclei, they slow down until they reach the thermalization. In terms of energy, it means that neutrons are characterized by energies in between 0.001 and 0.1 eV. These energies are typical for particles that are moving at room temperature. Those are the neutrons interesting for our thesis. Rocks contain a significant number of elements with an atomic mass value comparable to that of neutrons (H, C...), so the slowing process may happen quickly. In this case, the slowing down process of neutrons

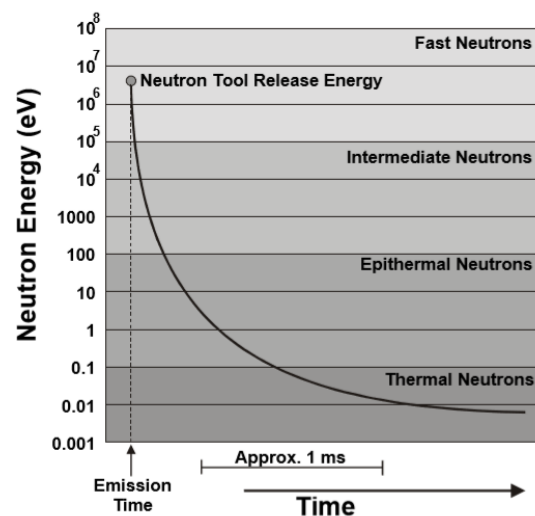


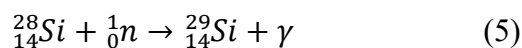
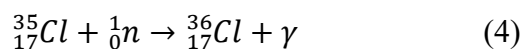
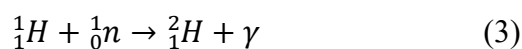
Fig 13 The slowing of fast neutrons with time by elastic collision with formation nuclei (Grove, Petrophysical handbook)

may take microseconds. Given a neutron with its own energy, the slowing down time depends on the chances of collision that the neutron may do with the formation. Due to neutrons slower velocity, movements between formation nuclei become slower as well. Hence, neutrons' collisions occur with a lower frequency than in the case of fast neutrons. Thermal and epithermal neutrons with their respective energy collides less frequently than fast neutrons. The process of slowing down into a rock formation has an order of magnitude of microseconds. The process of scattering and so elastic or inelastic collisions, occur in parallel with neutron capture-adsorption. (Grover, Petrophysical handbook)

### 2.4.3 Neutron Capture

The neutron capture is one of the possible adsorption reactions that neutrons may achieve, although in some cases it is the only one adsorption reaction that can occur, for instance in the case of non- fissionable nuclei. Furthermore, when a coupled of neutrons is loss and there is a production of one or more photon the result is the neutron capture. When that phenomenon is observed usually is renamed into radiative capture or also (n,  $\gamma$ ) reaction, those two are the preferable name for capture reactions. Its cross section is denoted with the symbols  $\sigma\gamma$ . (Ott, 1989)

The nuclei of rocks formation atoms, might adsorb neutrons with a characteristic energy due to their capture cross sections, thermal and epithermal neutrons could be either adsorbed or scattered. The efficiency of the adsorption depends on the type of the element that compounds the formation. Those elements that present a significant neutron are Hydrogen (H), Chlorine (Cl) and Silicon (Si) (figure 1). Considering them here are shown their adsorption reactions: (Grover, Petrophysical handbook)



In neutron logging, some tools measure the epithermal neutrons, some the thermal neutrons and some the gamma rays emitted when a neutron is absorbed. The more investigated and interested atom is that of Hydrogen, for that is needed a coefficient that represent its quantity within the formation. (Serra, 1984)

## 2.5 Hydrogen Index

$(C_H)_{mass}$  is defined as partial concentration of Hydrogen per unit mass of a given material. From a physical point of view is the mass of Hydrogen atoms contained in the material, divided by the total mass of the atoms constituting the material in consideration, thus;

$$(C_H)_{mass} = \frac{n_H A_H}{\sum_i n_i A_i + n_H A_H}. \quad (6)$$

where:

$A_H$  = atomic mass of Hydrogen atoms in the material

$A_i$  = atomic mass of non-Hydrogen element  $i$

$n_H$  = number of Hydrogen atoms in a molecule of the material

$n_i$  = number of non-Hydrogen atoms of element  $i$  in a molecule of the material

Note:  $i$  is summed over every non-Hydrogen element in the material.

Knowing  $(C_H)_{mass}$  is possible to retrieve  $(C_H)_{vol}$  that is the partial concentration of Hydrogen per unit volume, by multiplying the partial concentration of Hydrogen per unit mass by the density of the material, hence:  $(C_H)_{vol} = \rho_b \times (C_H)_{mass}$ . Where  $\rho_b$  is the density of the material.

Now the Hydrogen index can be expressed as a function of relative volume of water. Fixing the Hydrogen index equal to the unit for pure water, and knowing that water has a partial concentration of Hydrogen per unit volume equal to 1/9, the Hydrogen index for a generic material will be calculated by;

$$HI = \frac{9n_H A_H}{\sum_i n_i A_i + n_H A_H} \rho_b. \quad (7)$$

Where:

$HI$  = Hydrogen index relative to water

$A_H$  = atomic mass of Hydrogen atoms in the material

$A_i$  = atomic mass of non-Hydrogen element  $i$

$n_H$  = number of Hydrogen atoms in a molecule of the material

$n_i$  = number of non-Hydrogen atoms of element  $i$  in a molecule of the material

$\rho_b$  = density of the given material

Note:  $i$  is summed over every non-hydrogen element in the material.

In the tables below, Tab3 and Tab4, are listed some HI typical for some materials:

Example calculation for the average moles of hydrogen in a mole of a typical separator gas mixture		
Component	Mole fraction, $y_i$	$n_{H,i}$
Carbon dioxide	0.0167	0
Nitrogen	0.0032	0
Methane	0.7102	4
Ethane	0.1574	6
Propane	0.0751	8
i-Butane	0.0089	10
n-Butane	0.0194	10
i-Pentane	0.0034	12
n-Pentane	0.0027	12
Hexanes	0.0027	14
Heptanes plus	0.0003	16
Total or average	1.0000	4.785

Tab3. (Hirasaki, 2002) Calculation of number of Hydrogen atoms for a typical mixture.

Compound	Formula	$A_i$	$n_i$	$n_H$	$\rho_b$	$HI$
Pure water	H <sub>2</sub> O	16	1	2	1.000	1.000
Oil	(CH <sub>2</sub> ) <sub>x</sub>	12	1	2	0.780	1.003
Methane	CH <sub>4</sub>	12	1	4	$\rho_m$	$2.25 \times \rho_m$
Gas	C <sub>1.1</sub> H <sub>4.2</sub>	12	1.1	4.2	$\rho_g$	$2.17 \times \rho_g$
Quartz	SiO <sub>2</sub>	28, 16	1, 2	0	2.654	0.000
Calcite	CaCO <sub>3</sub>	40, 12, 16	1, 1, 3	0	2.710	0.000
Gypsum	CaSO <sub>4</sub> .2H <sub>2</sub> O	40, 32, 16	1, 1, 6	4	2.320	0.4855

Tab4. (Grover, Petrophysical handbook) Calculation of HI for some compounds.

Focusing now on the following consideration is possible to better understand the meaning of HI; HI=1.000 corresponds to the measurement provided by the tool when it is completely immersed into pure water or also into a fluid (petroleum) characterized by the same Hydrogen index of water. In terms of petrophysical properties modelling HI=1 corresponds to a porous medium fully saturated by water and with porosity of 100%. Then undergoing over a rock, in this case a rock where its chemical structure has not Hydrogen inside, for example Limestone or Sandstone, the tool will retrieve a HI=0.000, that could be interpreted also as 0% of porosity. Once did these two examples is possible to take two fixed point for HI. One equal to 1 that is the maximum and represents porosity equal to 1, hence  $\phi=1$ , and HI=0 that is the minimum, which instead represent porosity equal to 0, hence  $\phi=0$ . With a minimum and a maximum of HI fixed, if a sample of any Limestones, with any porosity  $\phi$ , is given will be possible to correlate in a direct proportion its HI with the amount of water into the formation. The directly proportional correlation is the following equivalence  $HI = \phi$ , even if the porosity of the formation taken in consideration is filled and thus saturated by water. Therefor is clear that HI

is a proxy measure of  $\phi$ , for formation formed by minerals without Hydrogen atoms inside their chemical structure (otherwise also they are going to be counted into HI, and the measurement is not any more just correlated to the H of the water into the pores) and pores filled just by water (other compound as organic matter have a different calculation for HI). Therefore, is clear that HI is a proxy measure of  $\phi$ , for formation formed by minerals without Hydrogen atoms inside their chemical structure (otherwise also they are going to be counted into HI, and the measurement is not any more just correlated to the H of the water into the pores) and pores filled just by water (other compound as organic matter have a different calculation for HI).

In conclusion the neutron tools' observed count rate is totally controlled by Hydrogen index.

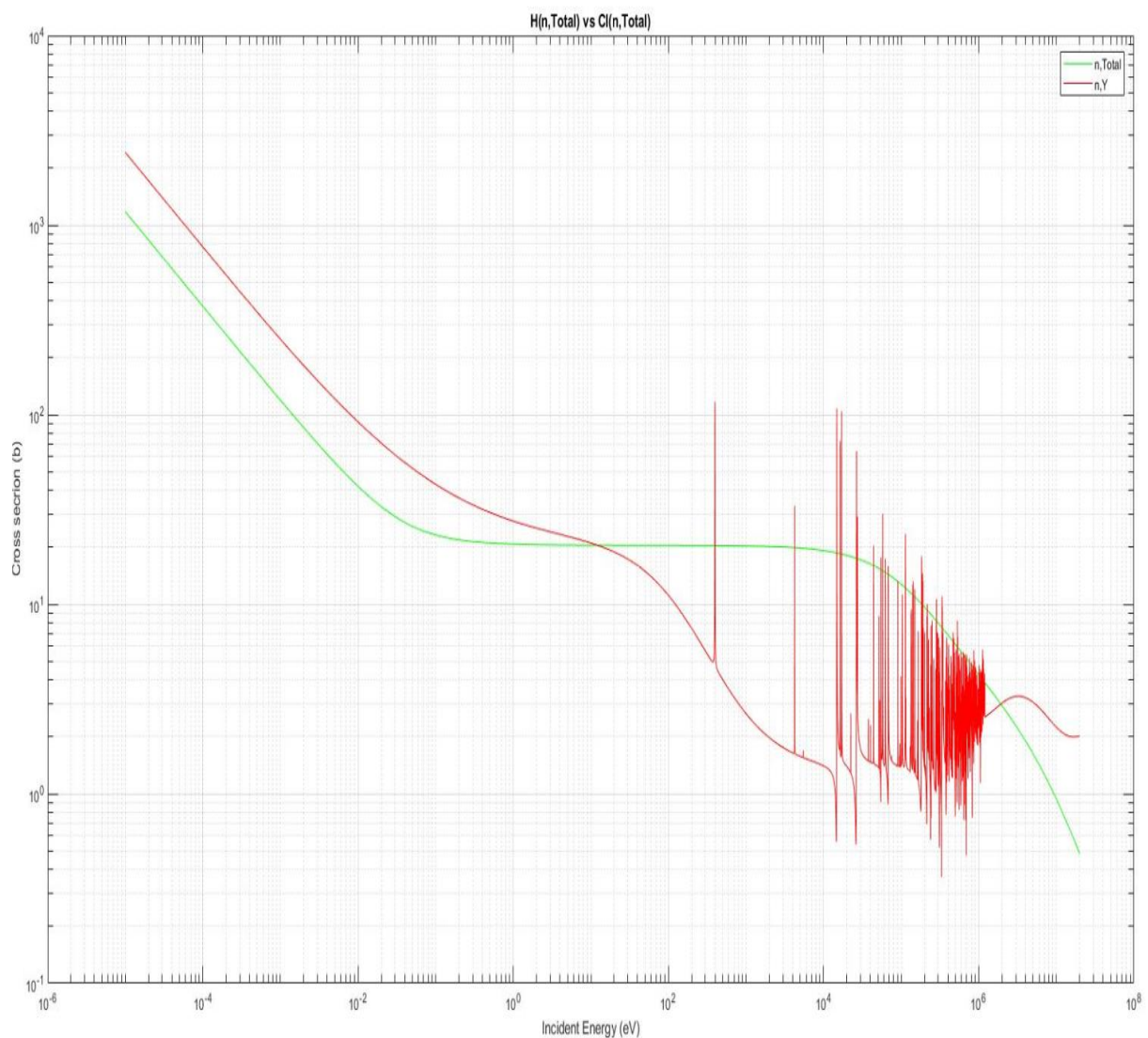


Fig. 14: The plot shows the similitude between the Hydrogen cross section of the n, total reaction and the Chlorine cross section for the same nuclear reaction, is understandable how they are similar in the thermal neutrons characteristic energy. [14]

And considering it the observed count of neutrons will be a  $\phi$  measurement just when the media is water saturated and its matrix, its chemistry does not contain any Hydrogen atoms into the lattice. As anticipated, all the discussion done till now is from a theoretical point of view, in

real world neutrons' passages into the formations are not only affected by H, (when were explained all neutrons interaction this concept was made clear), in fact looking again at Fig.1 and Fig.2 many other nuclei of atoms that may form the rock in considerations can affect neutrons behaviour, slowing down, and so on. Is true that any other atoms which is not H has a lower effect on Neutrons if compared with H indeed. Instead if neutrons adsorption is of interest, because Hydrogen has a similar weight (on neutrons behaviour) of Chlorine, obviously if into the formation if present Chlorine the measurements have an intrinsic error, especially if we assume that neutrons behaviour is affected just by H, in fact comparing cross sections of Hydrogen and Chlorine (Fig4) is possible to understand how they behave with neutrons of those characteristic energies. This little error could be adjusted calibrating well the tool. The tool will be calibrated anyway for a single rock formation, for example, limestone or Sandstone or other, but of course the tool will never give the true porosity of the formation. The tool will retrieve a measurement of equivalent porosities that are possible to see when measuring on limestone (in case we calibrate on limestone). (Hirasaki, 2002) (Grover, Petrophysical handbook)

## 2.5.2 Effects on HI

### *HI of Brines*

Reservoir water is typically referred as brines since it contains a significant amount of dissolved salts. Since Hydrogen Index is referred to pure water at ambient conditions, the HI measurement in brine would be different from 1 since is affected by salinity and thermodynamic conditions. The value may vary from reservoir to another since depends on ionic species dissolved in brine. (Hirasaki, 2002)

### *HI of Gas*

For determine HI for gases is enough to simply re-elaborate the definition of HI used for water:

$$\begin{aligned}
 HI &= \frac{\text{moles } \frac{H}{\text{cm}^3}}{0.111} = \frac{n_H \tilde{\rho}}{0.111} = \frac{\sum_i^n n_{H,i} \tilde{\rho}_i}{0.111} = \\
 \Rightarrow \text{for mixture;} &= \frac{\tilde{\rho}_{ev} \sum_i^n n_{H,i} y_i}{0.111} = \frac{n_{H,ev} \tilde{\rho}_{ev}}{0.111} \\
 &= \frac{n_{H,ev} \tilde{\rho}_{ev} \left( \frac{\text{moles}}{\text{litre}} \right)}{0.111}. \tag{8}
 \end{aligned}$$

Where:

HI=Hydrogen index relative to pure water

$y_i$ =mole fraction in gas phase.

$\tilde{\rho}$  =molar density of the gas.

$n_H$  = number of hydrogen atoms in a molecule of the material

$\tilde{\rho}_{ev}$ = average molar density of the gas.

Note:  $i$  is summed over every non-hydrogen element in the material.

Some examples of characteristic values of molar fraction and  $n_H$  for gases useful of HI calculation are reported on tab 2. (Hirasaki, 2002)

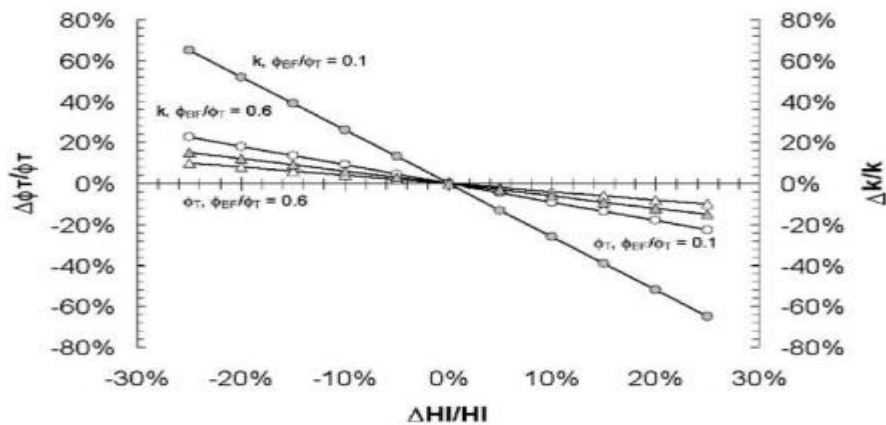


Fig.15 Impact of the uncertainty in the determination of the hydrogen index on porosity and permeability for 10% and 60% BVI. (Hirasaki, 2002)

### *HI of Hydrocarbon mixture and live Oils*

Oil reservoirs are multi-component systems at equilibrium in liquid phase at the initial thermodynamic conditions. When the minimum pressure of the oil column exceeds the bubble point pressure the oil is classified as undersaturated; when the minimum pressure of the oil column corresponds to the bubble point, the oil is classified as saturated. Saturated oil could coexist with an initial gas cap. In this case, the surface of equilibrium between the gas and the oil phase is called Gas Oil Contact and is characterized by a pressure equal to the bubble point. According to the amount of gas dissolved into the oil the reservoir can be further classified as dead oil (negligible amount of gas), medium oil, light oil, volatile and live for increasing percentage of gas components. Taking in consideration live oils their HI could vary largely from the unit. Therefore, is obvious the density of the reservoir fluids will decrease meanwhile compressibility and thermal expansion coefficient will increase if those fluids are compared at ST (stock tank conditions). In conclusion is possible to say that for live oils HI will be more

affected by pressure in comparison to HI of free gas oils. For having less uncertainty in the interpretation, also for HI value of live oil, is possible to retrieve some sample of reservoir fluids, in significant proportions and subject them to NMR (nuclear magnetic resonance) looking at this point their response (everything done in wireline NMR data). As mentioned before HI is affected by both porosity and hydrocarbon saturation, so is of maximum interest find a correct value of HI for hydrocarbon phases. Considering that the ratio between bound and free fluids is HI dependent, hence indirect influence of uncorrected values of HI and so a bigger uncertainty on HI influences the estimation of permeability forward calculations done with NMR logging data. Looking at Fig 6. is possible to see how the uncertainty on determination of HI influence the evaluation of porosity ( $\phi$ ) and permeability ( $k$ ). In the calculation of total  $\phi$  the error may be increased, in general, just in case of movable and so less bounded, hydrocarbons that because those kinds of hydrocarbons show typically a value of HI lower than 1 (less than pure water). Obviously, the calculation is supported by the point of view that the hypothesis of HI's errors is common in movable oils and every movable fluid is affected by those kinds of errors. Looking now at Fig 7 is possible the variations of HI measurement considering live oils, mixture of

oil-based mud filtrates and methane at various conditions. Is possible also to say that, for example, gas free oil based mud have a characteristic HI very similar to that of pure water, and so very close to the unity. Then trying to change density of the oils, for example enhancing GOR, the value of HI tends to decrease. Considering an

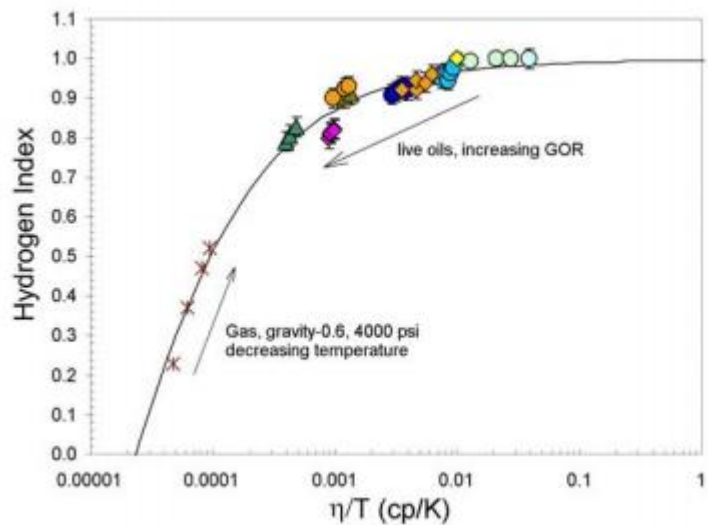


Fig. 16 HI measurements on live oils and mixtures of oil-based mud filtrates and methane at various conditions. (Hirasaki, 2002)

undersaturated oil with solution gas-oil ratio of about 2000 Scf/STB is possible to obtain the lowest value of HI which lines up to 0.8. (Hirasaki, 2002) (Appeal, 2004)

### *The Hydrocarbon Effect.*

When explaining about HI of hydrocarbon mixture or live oil and looking at table 3 we might understand how HI of water and oil is similar. Their chemical composition and their partial concentration in Hydrogens are different. The result should be a difference in HI also. Oil has a lower density than water and that implies a balance for the HI. HI is made more similar.

Another problem which affects neutron tool as almost all the other tools is the presence of an invaded zone (flushed by the mud filtrate). Hence, HI's measurements of neutron tools will be affected and influenced by mud filtrate. Furthermore, they are influenced by the remaining oil ore hydrocarbons and water, which are contained into the pores invaded by mud. Now, for example, imaging a neutron log tool in an oil zone in a formation, limestone, the mud filtrate almost completely invades and so replaces the formation fluids such that there is a saturation of mud filtrate  $S_{XO}$ , and a residual saturation of hydrocarbons  $(1 - S_{XO})$ . The porosity read by the neutron tool is related to the actual porosity in the formation by

$$\phi_N = \phi [HI_{mf} S_{xo} + HI_{hc} (1 - S_{xo})]. \quad (9)$$

Where  $HI_{mf}$  is the Hydrogen index of the mud filtrate and  $HI_{hc}$  that of hydrocarbons.

If the hydrocarbon is oil, this equation reduces to  $\phi_N \approx \phi$ , because, looking Table 3, the Hydrogen index of water and oils is similar;  $HI_{mf} \approx HI_{hc}$ . This is true whether the mud filtrate is oil based or water-based.

$$\phi_N = \phi [1.000 \times S_{xo} + 1.003 \times (1 - S_{xo})] \approx \phi. \quad (10)$$

If the hydrocarbon is methane gas with a density of 0.1 g/cm<sup>3</sup>, the equation reduces to

$$\phi_N = \phi [1.000 \times S_{xo} + 2.250 \times 0.100 \times (1 - S_{xo})]. \quad (11)$$

If the saturation in the flushed zone  $S_{XO} = 0.7$ , Eq. (9) reduces to  $\phi_N = 0.77 \phi$ . This is known as the hydrocarbon effect in the neutron log. (Grover, Petrophysical handbook)

### *The Chlorine Effect.*

When measuring with neutron tool is possible to retrieve two types of measurements, the former is directly correlated with thermal neutron and epidermal, the latter with  $\gamma$  ray (photons) produced during neutron capture reaction. In chapter 2.3.4 was explained which atoms, found in reservoir, mainly contribute to neutron capture, they are Hydrogen and Chlorine. Hydrogen is the target. Anyway, Cl is present and may be due to mud filtrate, drilling mud, or also formation fluid as brine or something salty. The amount of Cl influences the measurement, lowering the flux of neutrons and therefore, because  $\phi$  is correlated with the number of thermal neutrons, enhances the value of calculated porosity. The effect of Chlorine over HI estimation is indeed called "chlorine effect" and is bigger proportionally to Cl presence and so in salty formation and muds. (Grover, Petrophysical handbook) (Hirasaki, 2002)

### The Shale Effect.

Shale that are sedimentary rocks can influence HI in two ways, one due to water content and the second because their intrinsic natural radioactivity. Analysing the first case is possible that shale contains a huge amount of clay that has typically a big amount of surface adsorbed water, due to its physical structure. Thus, despite their low porosity is possible that the total amount of Hydrogens atoms is huge. That means for the tool an overtime of the medium porosity, that for the instrument will be higher than the real one, this first effect could be also called bound-water effect. The second effect is related to the presence into shale of radioactive atoms, as, commonly Uranium, Thorium and Potassium, that are fine the crystalline structure of the shale. Natural decay of those atoms implies presences of many possible reactions with neutron emitted from the tool, those processes make the measurement more uncourt. The errors are well explained in fig 8. (Grover, Petrophysical handbook) (Hirasaki, 2002) (Torutelot, 1978)

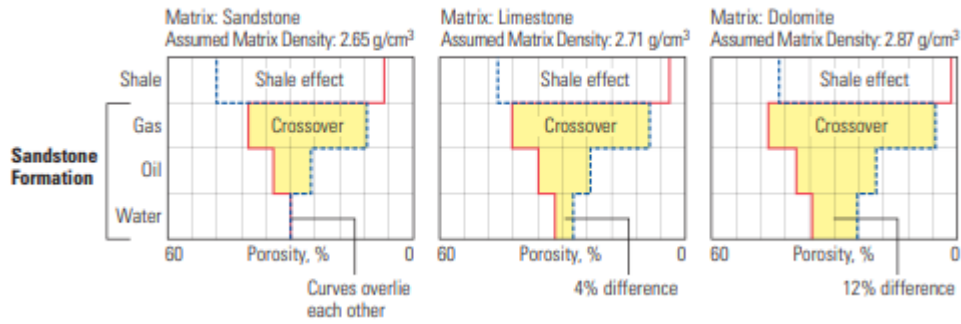


Fig. 17 lithological and fluid effect, density porosity (red) and neutron porosity (blue) are computed from lithological dependent relationship. For example in a sandstone formation with porosity computed with a correct parameter (left), the curves overlined one another at the correct porosity of 30% in water, crossover somewhat in oil cross over a great deal in gas, and separates in shales. If an uncorrect matrix is used as in the middle and in the right the computed porosity will be uncorrected. 4% in the middle, 12% in the right. (Smithson, 2012)

## 2.5 Fundamentals for calculation and measurement

For relating the neutron counting with rock masses' properties is essential to use the Boltzmann Transport Theory also actually abbreviated in BTE, this theory explain how neutrons emitted from a point are transported, through the rock, arrive in the detector. As is already well explained into previous chapters rock properties influence this transportation. BTE expression in a time independent form is here below:

$$\bar{\Omega} \cdot \nabla \bar{\phi} + \sum_t \cdot \bar{\phi} = \int dE' \int d\bar{\Omega}' \cdot \sum_s(E \rightarrow E, \Omega' \rightarrow \Omega) \bar{\phi} + S. \quad (12)$$

Where:

$\bar{\Omega}$ =Given direction.

$\sum_t$ =Total interaction Cross section.

$E$ =Neutrons' energy.

$\Sigma_s$ =Scattering cross section.

$\Phi$ =angular flux, vector which specify neutrons crossing a unit surface per unit time.

$S$ =Source Term.

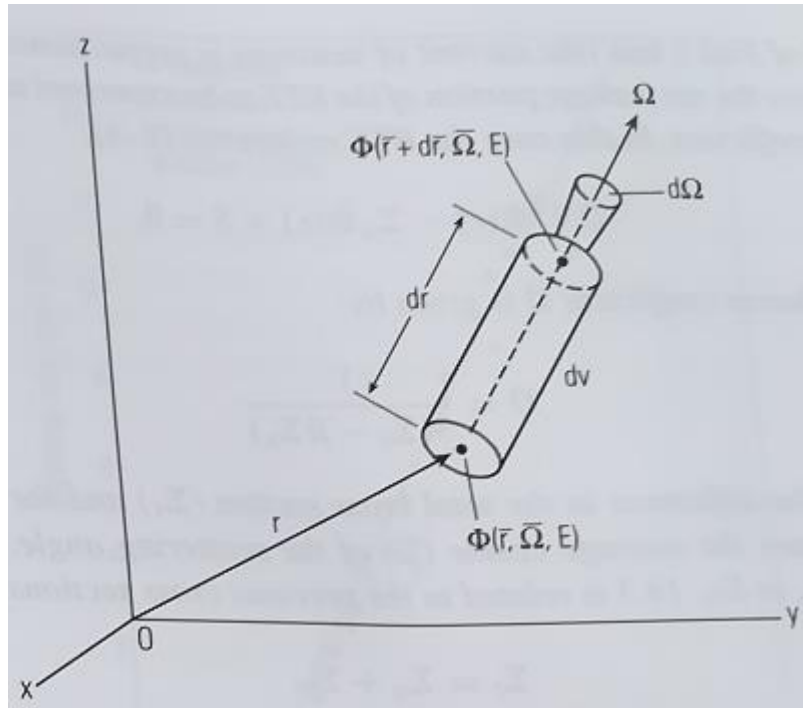


Fig.18 Typical geometry cell of material over which applies BTE for deriving neutron flux balance. (Ellis, 2007)

The Boltzmann transport equation is written in form of angular flux ( $\bar{\phi}$ ), in a specific direction ( $\bar{\Omega}$ ) and energy interval at each point in the considered space. Here, the scattering from neutrons of higher energies, that from other regions and the rate of increase neutrons through source production are related to the loss rate of neutrons in the volume, due to the absorption and scattering. Into the equation are also contained two losses term, the first which represent the net leakage rate of neutrons about of the considered volume is  $\bar{\Omega} \cdot \nabla \bar{\phi}$  the latter is  $\Sigma_t \cdot \bar{\phi}$  which means the loss rate of neutrons from the, volume energy region and direction of interest. Then the previous two terms of loss are balanced by the rate of neutrons coming from the volume are scattered into the energy and direction considered, and by the term  $S$ , the scattering term is represented by the second member go the equation, without the source term. The integration dominion is the  $E'$  and  $\Omega$ . In the end, the scattering term must taka in consideration all the influences due to scattering and limited energy range. Once analysed the BTE is finally opposable to say that in this form is almost impossible to solve analytically, so many numerical approaches have been developed to solve the problem. (Ellis, 2007)

## 2.6 The Detector

interacted with neutrons coming from the outside the detector, then the electrical signal will be processed. Once understood this is possible to move through two type of neutron interactions.

As we know neutrons could be scattered by nuclei, if the kinetic energy transferred by the collision is sufficient the interaction point will be ionized by the recoiled nucleus. Hence this first

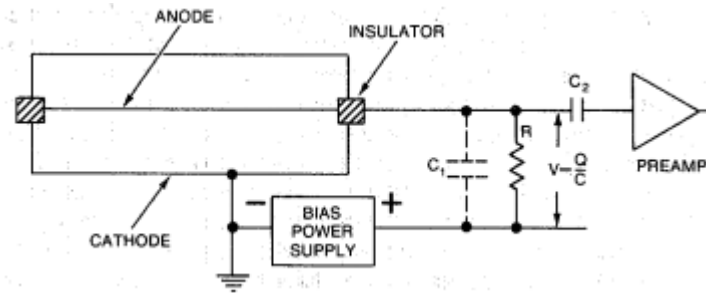


Figura 19 Typical setup for gas filled neutron detectors (Crane, Neutron detectors)

mechanism is possible just with light mass nucleus, H and He. In second analysis is possible to have neutron interaction which might cause neutron reactions, their reaction products maybe employed for starting the detection. There are many kind of neutron detectors, some of them could be scintillators,  $^{10}\text{B}$ -lined chambers, fission chamber or that here well analysed Gas-filled proportional counters. About gas-filled proportional counters is possible to say that they are the first kind of neutron detectors used for the issue. Measuring both fast or thermal neutrons is one of their capability, via different process of course. In general, the setup of a gas-filled detectors is approximatively like in figure 12. This type of neutron detectors is made by aluminium or stainless steel, the difference between them is minimal, there are just negligible differences on neutron transmission or structural strength indeed. Analysing better the adsorption is noted

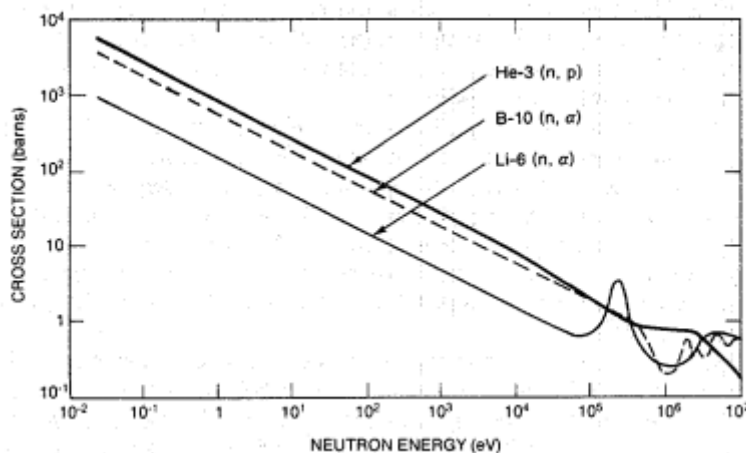
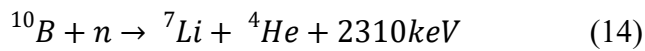
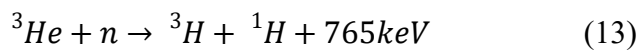


Figura 20  $^3\text{He}$  (n,p),  $^{10}\text{B}$  (n,p) and  $^6\text{Li}$  (n,p) cross section as a function of incident energy (Crane, Neutron Detectors)

that Al adsorb almost 0,5% of the neutrons while stainless steel 3%. For this reason, Al is generally preferred instead stainless steel. Never the less Stainless steel in comparison with aluminium has many technical advantages, which are a lower amount of impurities, an assembly

done with low careful handling and lower galling threats. If the tube is filled with  $\text{BF}_3$  is generally applied a coating in activated charcoal, the coating is necessary during the neutron

irradiation which causes the generation of electronegative gases. Also in He<sub>3</sub> gas filled tubes is applied this kind of coating. Gases typically used for filling the tubes are, as already said BF<sub>3</sub>, <sup>3</sup>He but also <sup>4</sup>He and CH<sub>4</sub> with a pressure in between 1 and 20atm. In cases of <sup>3</sup>He or <sup>4</sup>He is added a polyatomic gas with quench functions, instead talking about BF<sub>3</sub> or CH<sub>4</sub> that expedient is not needed because they are already polyatomic. The mismanages of polyatomic gases is that they require higher voltage for operating well. In any case, most used thermal neutron detectors use <sup>3</sup>He or BF<sub>3</sub>. Considering those using <sup>3</sup>He the constructor meets a big inconvenient, because <sup>3</sup>He is just the 0,0001% of the natural Helium amount in nature, the consequence is <sup>3</sup>He is obtained by tritium produced within nuclear reactors. The nuclear reaction which is possible to have for both detectors (<sup>3</sup>He and BF<sub>3</sub>) are listed below:



All the listed reactions are exothermic and is possible to image looking at the positive energy term, thanks to their exothermic nature due to the ejection of positive charged particles, the detector could start the multiplication process for detection. Really important to detection scope is the cross sections of those nuclei, in fig 13 are shown He, B and Li cross sections and their dependency on incident neutron energy, Helium shows the best one for thermal detection, for further increase the detection efficiency is also possible to isolate the gas-filled cell with a



Fig. 21 Typical detectors shape. [2]

moderator, as polyethylene or also cadmium. In most cases the kind of detector used for accounting neutrons scattered by the formation is He-3 neutron detector. Once spoken about the many kind of detectors and their functioning, is better to start focusing on that chosen and simulated in this thesis job. The most suitable for this application was the Gas-filled neutron detector with <sup>3</sup>He, it has multiple applications, from thermal or also epithermal detection to fast neutron detection, just using a bigger detector, others application could be, for example homeland security, and monitoring

neutron radiation. More interesting are industrial applications like measurement method for humidity in oil and gas explorations, and so the indirect measurement of porosity, which is the scope of this job indeed. [2] (Crane, Neutron Detectors)

### 2.6.1 Principle

The isotope of Helium chosen for filling the chamber is  $^3\text{He}$ , this isotope has good characteristic for applications, because is nontoxic, inert, stable and nonradioactive. The problem is, as already said, the natural abundance of  $^3\text{He}$  is scarce, just 0,00014% in nature. Anyway, the advantage in using  $^3\text{He}$  is its cross section which makes this isotope a great adsorbed of neutrons, hence the perfect choice for the detector. Its cross section, shown in figure 15 tell the capability of  $^3\text{He}$  to be sensitive to thermal neutrons beams.

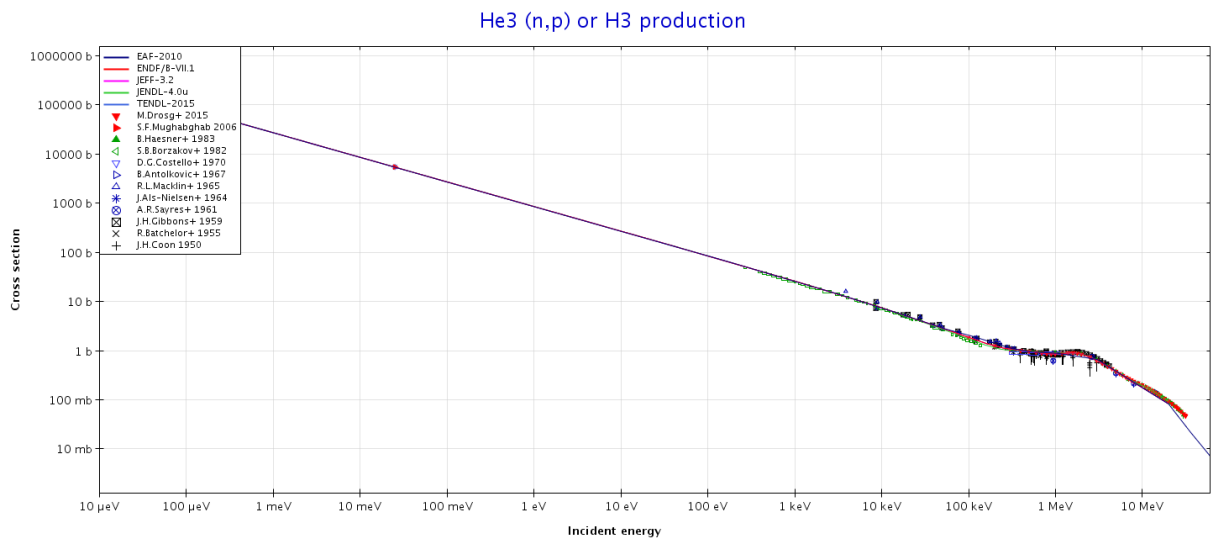
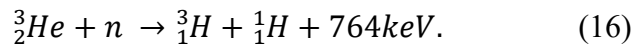


Fig.22 He-3 cross section for He-3 (n,p) H-3 reaction. [3]

The reaction taken in consideration for  $^3\text{He}$  is the 13, and is the absorption reaction, which produce the cross section above;



Reaction 13 says how  $^3\text{He}$  absorb or capture a neutron (produce by the source and scattered by the environment) and produces a triton, a proton and a Q-value of e764keV. Fortunately, the energy dependent cross section of He is one of those considered as standards in neutron log measurements. Anyway, those atoms produced by reaction 13 (proton and triton) are charged particles that are collected by the proportional counter of the detector. (Hilchie, Douglas, 1990)

## 2.6.2 Detector Construction

The configuration of gas-filled detector taken in consideration is almost the same to those most used in real applications. A welded stainless-steel tube with an alumina ceramic insulator, then the ovum port is made, generally in copper. Here the counter tube is obviously filled with  $^3\text{He}$ , and as quenching gas is added a small amount of  $\text{CO}_2$ . As already said there are many sizes of detectors which depend on their scope, but from the general point of view the detector could be approximated like in fig.16. [2]

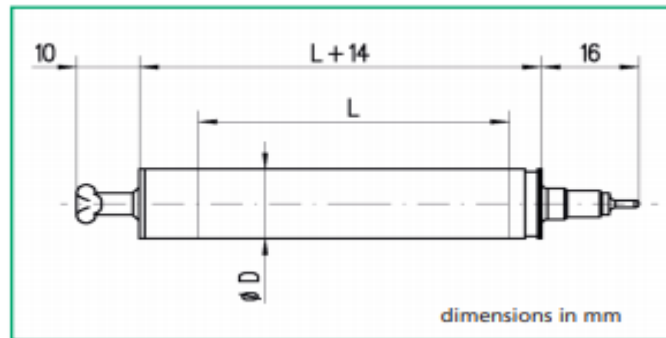


Fig. 23 General profile of He-3 detector, where L=active length and D=tube diameter. [2]

In accordance with fig.16 is possible to choose the detector with the dimensions needed from tab5.

Type	Dimensions						Gas pressure/bar		Operating voltage/V		
							2	4	6	8	10
							Thermal neutron sensitivity				
							cps/nv				
70060	1/2 inch/12.7 mm	81	30	3	40	2.8	490	680	800	910	1020
	1/2 inch/12.7 mm	94	35	3.5	50	3.5	0.6	1.0	1.4	1.7	2.0
	1/2 inch/12.7 mm	144	60	4	100	6.9	0.8	1.4	1.9	2.3	2.5
	1/2 inch/12.7 mm	194	80	4.5	150	10.4	1.6	3.0	4.0	5.0	5.5
	1/2 inch/12.7 mm	244	105	5	200	13.9	2.5	4.5	6.2	7.5	8.5
70061	5/8 inch/15.88 mm	101	50	3.5	50	6.2	3.4	6.1	8.3	10	12
	5/8 inch/15.88 mm	151	80	4	100	12.4	520	720	840	960	1070
	5/8 inch/15.88 mm	201	110	4.5	150	18.6	1.3	2.3	3.0	3.6	4.0
	5/8 inch/15.88 mm	251	140	5	200	24.8	2.8	4.9	6.5	7.7	8.6
70062	3/4 inch/19.05 mm	100	200	4	50	10	4.4	7.6	10	12	13
	3/4 inch/19.05 mm	150	220	4	100	19	5.9	10	14	16	18
	3/4 inch/19.05 mm	200	260	5	150	29	540	750	870	1000	1100
	3/4 inch/19.05 mm	250	300	5	200	39	2.0	3.4	4.3	5.0	5.4
70063	1 inch/25.4 mm	150	280	4	100	36	4.3	7.3	9.3	11	12
	1 inch/25.4 mm	200	340	5	150	54	6.6	11	14	17	18
	1 inch/25.4 mm	250	400	5	200	72	8.9	15	19	22	24
70064	1.5 inch/38.1 mm	200	450	5	150	136	560	780	910	1050	1160
	1.5 inch/38.1 mm	250	540	5	200	182	7.3	12	14	16	17
70065	-2 inches/50.0 mm	210	560	4.8	150	249	11	18	22	25	26
	-2 inches/50.0 mm	260	675	5.2	200	332	15	24	30	34	36
							600	830	980	1100	1240
							25	37	42	44	45
							34	49	56	60	61
							680	860	1010	1160	1260
							42	56	61	62	63
							57	76	82	84	85

Tab.5 In this table are listed the technical characteristic of some detector configurations. [2]

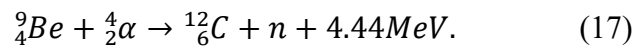
## 2.7 The Source

The possible configuration for a neutron source in well testing are the following:

- Alpha neutron sources.
- Gamma neutron sources.
- Spontaneous fission neutron sources.
- Fission reactors.
- Accelerators.

The most used are the first kind and for that will be further described those.

An alpha emitter element is optimally mixed with a low atomic number material, generally, Be-9. The involved reaction is the following:



By the Activity of the alpha emitter is possible to know the strength of the source. Common activities range between 0.5 to 40 Ci (which means 18.5 GBq to 1.48 TBq), even though nowadays gauges (portably density gauges) may be equipped with activities of 10 to 50 mCi (0.37 to 1.85 GBq) sources. There is a wide possibility in choosing alpha emitters, some of them are;  ${}^{241}\text{Am}$ ,  ${}^{238}\text{Pu}$ ,  ${}^{239}\text{Pu}$ ,  ${}^{210}\text{Po}$ ,  ${}^{226}\text{Ra}$ . Anyway, in technical application for neutron logging is mostly used  ${}^{241}\text{Am}$ , but Plutonium isotopes are even common, especially in older tools. One possible concern with these sources is the potential for the build-up of pressure due to helium production. (Basic Health Physics, 2010)

### 2.7.1 AmBe neutron sources

Confidentially called ambee, the AmBe neutron sources are a mixture of  ${}^9\text{Be}$  and  ${}^{241}\text{Am}$ , This implies:  $\cong 2.0$  to  $2.4 \times 10^6$  neutrons/sec. per Ci ca  $5.4$  to  $6.5 \times 10^4$  neutrons/sec per GBq Alpha Neutron Sources  $\cong 5.4$  to  $6.5 \times 10$  neutrons/sec. per GBq, AmBe neutron sources' half-life ins: 432 years and own an energy of 4,2 MeV (11 MeV max) in average, while their neutron dose rate is: 2.2-2.7 mrem/hr at 1 m/Ci 0.59-0.73 uSv/hr at 1m/GBq and their gamma dose rate: 2.5 mrem/hr at 1 m/Ci 0.68 uSv/hr at 1m/GBq. . (Basic Health Physics, 2010)

### 2.7.2 PuBe neutron sources

Like Ambee also this kind of neutron sources are called with a more confidential name, which is Pewbee, anyway PuBe as sources are a mixture (like AmBe) of  ${}^{239}\text{Pu}$  or  ${}^{238}\text{Pu}$  and  ${}^9\text{Be}$ , with this mix is obtained ca.  $1.5$  to  $2.0 \times 10^6$  neutrons/second per Ci ca  $4$  to  $5.4 \times 10^4$  neutrons/second per GBq Alpha Neutron Sources in between  $4$  to  $5.4 \times 10$  neutrons/second per GBq, Their half-life, instead of 432,2 years, is : 24,114 years and have an average neutron energy: 4.2 – 5 MeV

(also in this case the maximum is 11 MeV), Their neutron dose rate: 1.3-2.7 mrem/hr at 1 m/Ci 0.35-0.73 uSv/hr at 1m/GBq and their gamma dose rate: 0.1 mrem/hr at 1 m/Ci 0.027 uSv/hr at 1 m/GBq. . (Basic Health Physics, 2010)

In accordance with nowadays used tool the chosen neutron source for Monte Carlo simulation is AmBe.

### 2.7.3 Sources Construction



Fig. 24 Typical AmBe sources. Largest pictured is 60 x 30 mm. . (Basic Health Physics, 2010)

In previous paragraph is briefly explained that Americium (and so the alpha emitters) and Beryllium should be as closer as possible, this vicinity is obtained just mixing metallic beryllium powered and the alpha emitter, in form of oxide, so AmO<sub>2</sub>, then, compressing the powders mixture a cylindrical alpha

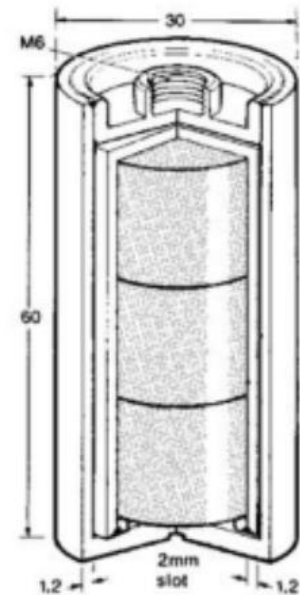


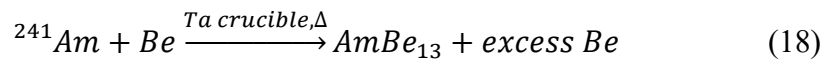
Fig25, Cross section of typical neutron source (Basic Health Physics, 2010).

neutron sources is obtained. Sometimes instead mix those two powder an alloy of Be and Am is directly made, also in case of different alpha sources. As is shown in figure 18 a double encapsulation is surrounding the neutron source. Generally, both inner and outer encapsulation are made of Stainless steel (type 304) while the bottom and the top are TIG welded. In general, a space between inner capsule is crated for avoiding the gradual build-up of He, as product of alpha emission reaction. For preventing dispersion

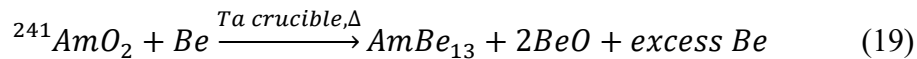
of radioactive material such as AmBe in the case of study, but every kind of sources, is needed the double encapsulation in welded stainless steel. While the alloy solution is less affected by dispersion the case of powered mixture is greatly affected by dispersion and so is the worst design, this solution implies a good improving in density but the structure is not conforming to resist and survive in violent collision or events. Thinking about the alloy design, so that called AmBe metellaic neutro source for reaching maximum efficiency the stucture should be builded as a monolith of small crystals of AmBe, all dispersed within an excess of Be. For having comparable physical properties more similar as possible as bulk Be metallic al large excess of Be is needed indeed. Is imporant to noticy also if Be metallic bulk

has a bigger efficiency in resistin in violent events, is less reactive than the first case, that powerd, so till now tha first configuration is preferred in neutron sources. Because collision ore relative event down the hole could couse violent production of shrapnel, less disperdes dust for breathing and contamination, the source cannot be opened and scattered, also for that the monolith configuration should be preferred, for reducing dispersion chaacteristics indeed. Anyway, for both configuration the reaction that might involve for obtaining the neutron sources are;

- Production from Am metal and Be metal.:



- production from Am oxide and Be metal.:



Before the fabrication of the source pure metal has to be produced, in fact Am metallic has to be really clean and simple. Instead if the frabrication comes from the oxide of Am the product of the reaction is another oxide, BeO, which may layer separately from the metal, this condition is typicalli reached if the reaction is conducted with long time and high tempereture, cooldown later. Actually BeO has been used for renforce so for strengthen Be, imporve ductility and finer the crystals. The studied source is the first configuration that means powder mixture material (oxide and metal), the composition is Be 4,6g, AmO<sub>2</sub> 0.37g. (Basic Health Physics, 2010) (Schulte, 2011)

### 2.7.4 Source spectrum

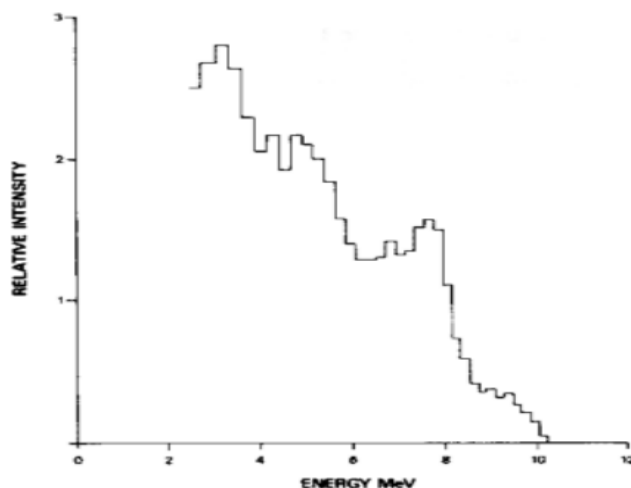


Fig.26, typical configuration of a alpha neutron source spectrum[. (Basic Health Physics, 2010)]

While describing the typical source configuration was told that the range of energy reach usually 11 MeV, but also that in average the alpha neutron source emits with and energy of 4-5 MeV. In Figure 19 is show a typical range of emitted energy, in the ordinate is plotted relative intensity which means the power of the source, per unit area. In abscissae there are energy, in MeV, which represent the emission energy of the neutron from the source. Analysing

the source taken in consideration and so AmBe powered mixture, so including AmO<sub>2</sub>, is important to know and understand how this source is composed, emits and how is its spectrum

of emission. All these characteristics for perfectly simulate and its behaviour into the used software, with which is modelled the tool and its response. Finally, is possible to describe the plot of considered neutron source by usage of 4C code (another monte Carlo), obtaining the desired spectrum of emission, shown in figure 20: (Chartier, 2014)

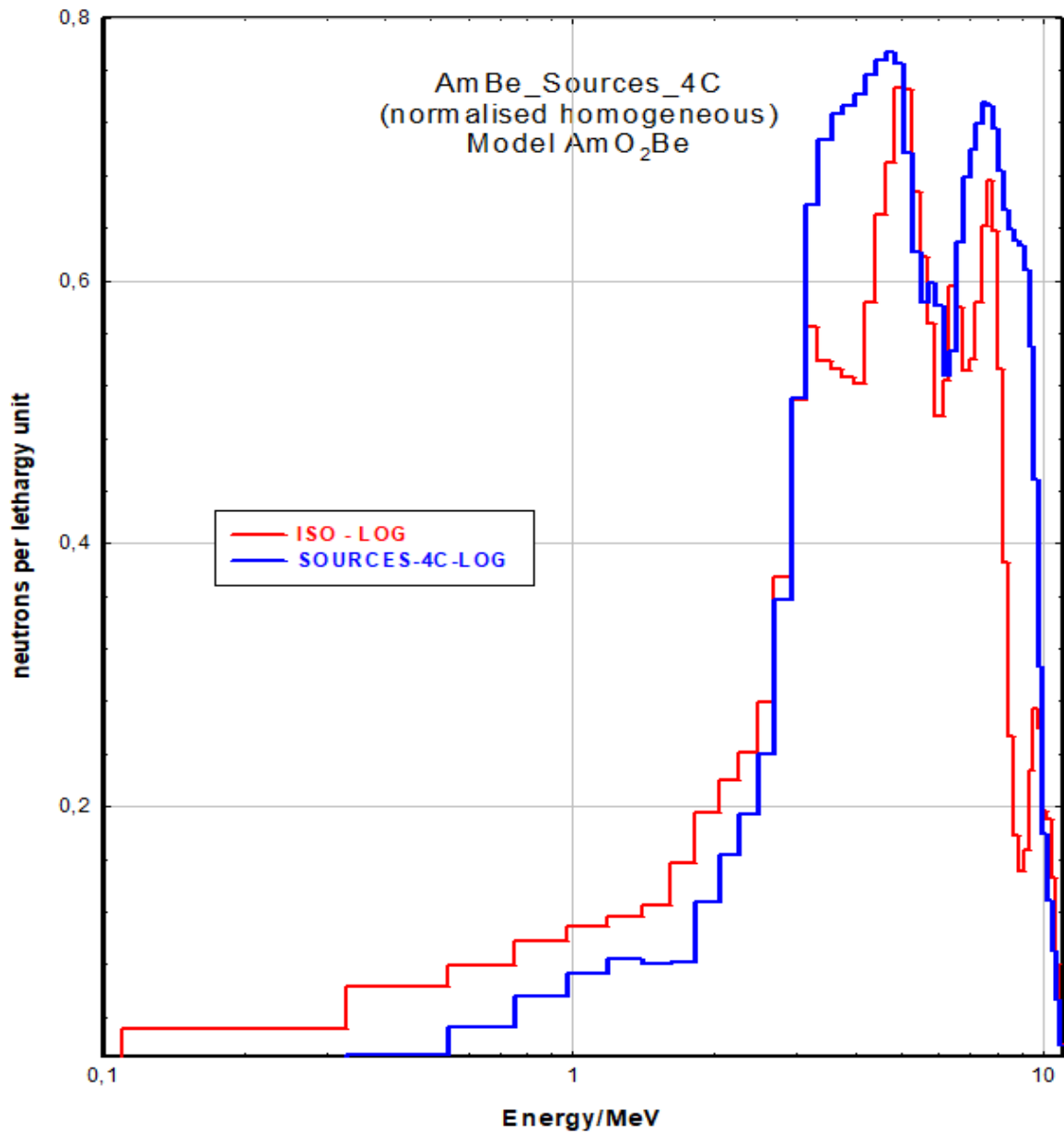


Figure 27 AmBe simulated spectrum, is possible to see how the source emits between 0,5 and 11 MeV (Chartier, 2014). The plot here above represents the simulated, by 4C Monte Carlo, the emission spectrum of the sources taken in consideration, the curve of interest is the blue one, ant that will be used for thesis further simulation. In ordinates is represented neutron per lethargy unit, where lethargy is expressed as  $\ln(E_o/E_i)$ , a more comfortable measurement for neutrons. Once described and explained the physical law below neutron logs and the technological characteristic of the tool is possible to move through what is Monte Carlo Method, for well understanding how simulations were done and conducted in all this thesis job.

### 3 Monte Carlo Methods

Monte Carlo methods are a wide class of computational methods. They are concerned with casual sampling and random numbers. It is thought to obtain numerical results. Monte Carlo Methods may be useful for solving computational problems about exact tests, for instance in binomial distribution or also in combinatorics. The method is used to make estimations. It is done through simulations. It is based on an algorithm which generates a series of numbers each unlinked to the others. Those numbers follow a probabilistic distribution that in general is the distribution of the unknown phenomenon. By coincidence test the independency of generated numbers is guaranteed. Monte Carlo, hence, calculates a series of possible relations that simulate the phenomenon under investigation. Monte Carlo calculation is well done if the average value of the simulated measurements is approaching to the true value. This means small standard deviation. A first rude variant of Monte Carlo method appears in 18<sup>th</sup> century in the Buffon's problem (Academy of Sciences, 1777). Then, Enrico Fermi, in 1930s was studying a neutron diffusivity problem. To do it he has used the Monte Carlo method. In any case the job of Enrico Fermi was not published (Jacobi, Lulu, 1989). Then, during second world war, Monte Carlo was applied in Manhattan project. Its creators are thus; Enrico Fermi, John von Neumann and Stanislaw Marcin Ulam. (Jacobi, Lulu, 1989). The name "Monte Carlo method" was created by Nicholas Constantine Metropolis recalling the roulette of the namesake Casino. This because the roulette is a random numbers generator (Metropolis, 1953). Nowadays the method is used to find solutions to mathematical problems with many variables. Its efficiency increases with the size of the problem.

Monte Carlo methods (or Monte Carlo experiments) are a broad class of computational algorithms that rely on repeated random sampling to obtain numerical results. Their essential idea is using randomness to solve problems that might be deterministic in principle. They are often used in physical and mathematical problems and are most useful when it is difficult or impossible to use other approaches. Monte Carlo methods are mainly used in three distinct problem classes: optimization, numerical integration, and generating draws from a probability distribution. (Krouse, 2014)

### 3.1 Monte Carlo Neutron Particle transport code

One of the used Monte Carlo code is the Monte Carlo N-Particle Transport Code also written as MCNP. It is used to simulate nuclear process. MCNP is a software package. Los Alamos National laboratories develops it. Its development in Los Alamos is since 1957 and it has been improved every year. For Europe the distribution is realized by NEA, Nuclear Energy Agency. NEA located in Paris and is the institute that gave us the Serpent code. In USA the software package is provided by Radiation Safety Information Computational center, located in Oak Ridge. MCNP is used principally for nuclear simulation process like fusion or fission processes. It may also simulate other interaction particles, not just neutrons. It may simulate also photon and electrons for instance. Its field of application is wide, from oil well logging that corresponds to our scope, to radiography, radiation protections, dosimetry, reactor physics and nuclear criticality safety and so on and so for. (Briesmeister, 2000) (Cash, 1959).

MCNP works on materials in 3D configurations. They are thought in geometrical cells with their border on first and second-degree surface and four-degree elliptical tori. Cross section data, collected in libraries are used for calculations. For instance, the evaluation of nuclear reaction by cross section are contained into ENDF/B-VI libraries. Free gas model and S ( $\alpha$ ,  $\beta$ ) model are involved for describing thermal neutrons. While an incoherent and coherent scattering, possibility of fluorescence after adsorption, adsorption in pair and bremsstrahlung are taken into account for describing photons. Bremsstrahlung, x-rays, positrons but not self-induced or external field are developed to describe electrons slow down process model. Another thing that gives to MCNP versatility and usability is the capability to model every kind of particle sources, general ones, criticality source, surface sources. It is also possible to create output tally plotters, geometry plotters and structures. The number of libraries employed for cross section makes MCNP a more powerful software. (Briesmeister, 2000)

The differences between MCNP and deterministic problems are many and wide. The most common deterministic problem is the so called "Discrete ordinates methods". It considers a behaviour of the particle averaged and for it solves BTE. MCNP on the contrary does not make any resolution of any equations. Through the simulation of tallies (any aspects) of averaged behaviour of a single particle MCNP finds the solutions of the problem. Using the CLT (Central limit Theorem) the averaged behaviour is gathered in the physical system all considering for the behaviour of the considered particle (Klauber, 2015). Hence, MCNP and deterministic problems are not different just in the approach to solve the problem but also their solutions change in constitution. MCNP answers just to those tallies request by the users, while deterministic problems return complete information over the examined space.

It is possible to say that discrete problems such as discrete ordinates resolve the integral differential transport equation, while comparing MCNP is possible to say that it returns the result of the integral transport equation. This sentence is deceptive for two reasons. The former is that those solutions, integral of transport equation and integrodifferential transport equation are the same stuff but in different form. When one is resolved also the other is solved. The latter is that MCNP does not solve transport problem with transport equation but solves it by simulating particle history. Effectively no equation is need by the MCNP for solving the problem. However, an equation which describes the probability density of particles moving in space may be derived. Never the less this derived equation is the same to the integral transport equation.

In the discrete ordinates methods, the phase space is visualized in divided small boxes. Particles move through boxes, from one to the other. A different amount of time is need by particle to move from boxes to boxes is the size of them tends to be progressively small and small, different time means different distance. This distance is given by the higher distance between the smaller boxes. So, the discrete ordinates method is derived in space and time, to avoid the solution of the approaching limit to the integrodifferential transport equation. MCNP simulated event per particles, instead, for instance during collisions, are separated by time and space. But for MCNP time and space are not intrinsic parameters neither. Nonetheless the integral equation does not employ time or space derivative. For that reasons MCNP is very good in solving 3D problems but also time dependent problems also if they are complicated problems. Any approximations in energy, space and time are not need for MCNP. MCNP does not need approximation because it does not use phase space boxes. Thanks for that is possible to make detailed representations of many aspect of physical data.

Statistical process, for in our case neutron interaction with the formation, might be theoretically duplicate by MCNP. Furthermore, MCNP is useful to study problems otherwise too complicated which cannot be simulated by computer and their code which use Deterministic methods. The processes comprised by event that are individual probabilistic are sequentially simulated. Those events are dependent from probability distribution. They are sampled statistically to achieve the description of the phenomenon in its totality. Because the processed involved to better describe the phenomena are large a digital computer is needed to perform the simulation. Random numbers selection is the foundation of statistical sampling. As Metropolis thought, it is like roulette game indeed. MCNP in particular consists in simulate each single particle from its emission by the particle source to its end crossing all the events that the particle lives. The probabilistic distribution of all the events involved in particle lives are randomly

sampled using the transport data. This is done to determine the response at every steps of particles lifes.

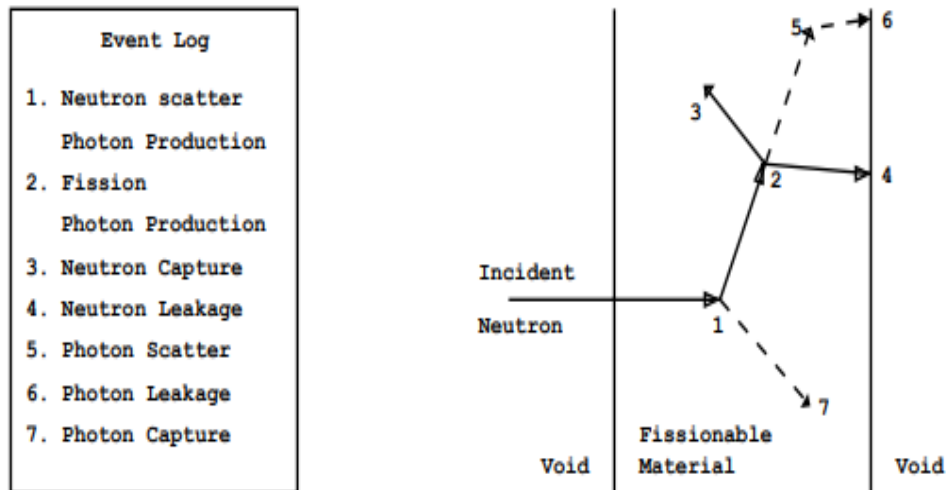


Figure 28 Here are represented and listed each possible phenomenon which occurs to a neutron while it moves in the space. (Briesmeister, 2000)

In figure 28 we can see the history live of a neutron. Firstly, neutron incises on a slab of a known material, then can undergoes to many events, for example fission. By the program, using binary code,0 and 1 which represent the possibility to have a phenomenon or not, are chosen randomly. The selection is avoiding determining which interaction are in place. The determination undergoes physical rule and transport probabilistic data that govern the process into which the neutron is going on. In figure 28 neutron does neutron scatter and the direction of the scattering is chosen randomly from real physical scattering distribution libraries. Then also a photon is produced. The second phenomena accurse to the neutron is fission. With fission in the neutron death but are produced other three particles, one photon and two other neutrons. One of the produced neutrons is captured. The other was banker and then retrieved and thanks to random sampling is leak out from the slab. Photon goes again scattering because collision and then leak out. The first photon, that generated from capture of first neutron is captured. The MCNP retrieve banked particles. The description of the colliding neutron is ended and it could be used for understanding how many and many neutrons behave in same tame. The quantities of interested neutrons are limited in tallies. The Tallization permits less uncertainties on results. (Briesmeister, 2000)

## **3.2 Serpent**

Serpent is a transport code of Monte Carlo has functionality in three dimensions. was established in the VTT Technical Research Centers Finland, Ltd. Its implementation began in 2004. It was distributed by the OECD / NEA Data Bank and the RSICC since 2009. Initially Serpent was a physics-based reactor code and it was very simple. The current capabilities of the original Serpent 2 version are far superior to the single reactor modelling.

His spatial capabilities in fields of application that can be roughly divided into three groups:

- 1) Physics applications of traditional reactors, including spatial homogenization, critical calculations, studies on the fuel cycle, modelling of research reactors, validation of deterministic transport codes, etc.
- 2) Multiphysics simulations, i.e. calculations coupled with thermal hydraulics, CFDs and fuel performance codes
- 3) neutron and photon transport simulations for radiation dose calculations, screening, fusion research and medical physics

The following are the main features and functionality of the code.

### **3.2.1 Geometry and particle tracking**

The geometric description used by Serpent, as also in other Monte Carlo codes, was created by a solid geometry model (CSG). This solid geometry is made up of cells of homogeneously distributed materials. Cells are defined by elementary surfaces of various types. Moreover, by deriving these surfaces and combining them with Boolean operators (intersections, unions and complements) it is possible to obtain the desired effect. Also, the conventional square and hexagonal lattices are supported by Serpent. Other types of special geometry for CANDU and randomly dispersed particle fuel can be simulated. In addition to CSG universes, Serpent can import geometries on CAD and unstructured meshes.

### **3.2.2 Interaction physics**

Serpent draws its information from ACE libraries containing the continuous energy cross sections. All the particle interaction physics used by Serpent is based on classical collision kinematics, ENDF reaction laws, and through stability tables in resonance regions and their sampling. For the Kernel it is possible an improved treatment on the scattering due to the free gases near the resonances. It is based on the DBRC Doppler-broadening rejection correction method. (Becker, 2009).

The cross-section libraries in ACE format are a data file evaluated in JEF-2.2, JEFF-3.1, JEFF-3.1.1, ENDF / B-VI.8 and ENDFB / B-VII. They are included in the Serpent installation package. Interaction data for 432 nuclides at 6 temperatures between 300 and 1800 K are available today. These data of the thermal dispersion of a bound atom are considered for light and heavy water and for graphite. MCNP shares the data format used, any data library in ACE format with continuous energy generated for MCNP can also be used with Serpent. The data format determines the laws of physics for neutron interactions, and it can be expected that the Serpent and MCNP calculations will agree within the statistics (Lappanen, 2015).

### **3.2.3 Burnup calculation**

Serpent has a built-in burnup capacity that has been established in advance and a built-in routine strategy and without the coupling of any external solver. The number of depletion zones is not limited. Memory usage may require reduction of optimization when the number of burnable materials is high.

Actinide nuclides produced, activation products and fission products are selected, without exploitation, to bring the calculation by the user. The combustible materials can be divided automatically into the area of exhaustion. The irradiation is timed in chronology. The timescales history in units of time or burnup. Response rates are normal, at flow, at fission or at the frequency of origin. The normalization is done by dividing the irradiation cycle into several exhaustion times, all separated. In other words, the fuel efficiency in the input by dividing the calculation into other subgroups. Volumes and masses useful for normalization are automatically calculated for more frequent geometries, such as the 2D fuel lattices. Values also of a volume calculation routine on Monte Carlo or manually. (Lappanen, 2015)

Data on radioactive decay and fission decay used in the calculation are read from standard ENDF libraries. Such data decay libraries for nearly 4,000 nuclides and metastable states are all available for calculation. The total of all nuclides and fission products, transmutation and decay is usually less than about 1500. The concentrations of the cores included with the decay data are plotted in the calculation of the burnup. The number of nuclides with cross sections typically ranges from 200 to 300. The yields of the latter are available (31 nuclides in the ENDF / B-VII data). The isomeric ramification ratios for neutron reactions were not included in the ACE format data libraries. Serpent uses fixed ratios for important nuclides (e.g. Am-241 and Pm-147). Snake can read energy-dependent data from ENDF format files. (Lappanen, 2015)

The cross-sections of transmutation of a flow group and averaged through a volume, are calculated in the duration of the transport Simulation. They can also be calculated by

compressing the continuous energy reaction cross sections once the calculation is finished using a sampled flow spectrum on the ionized energy network. The compression of the spectrum makes the calculation faster (by a factor of 3-4). Due to the high energy resolution of the considered flow spectrum, we can practically ignore errors in the results. A similar process has been applied in practice with other computational Monte Carlo burnup calculation codes (Haeck, 2007;Fridman, 2008a; 2008b).

To solve the Bateman depletion equations, we have for Serpent two essentially different options. The former option is the Transmutation Trajectory Analysis (TTA) method(Cetnar, 2006). It is based on the analytical solution of linearized depletion chains. The latter method is the Chebyshev Rational Approximation Method (CRAM), an advanced matrix exponential solution developed for Serpent at VTT (Pusa, 2010, 2011, 2012, 2013a-b-c-d, 2014)

The two options have shown to achieve consistent responses. When they are both used with Serpent (Lapannen, 2009a) and in separate methodological studies (Isolato, 2011a).

Burnup algorithms takes in consideration the conventional explicit Euler and predictor-corrector method. Furthermore, Serpent 2 also offers various higher-order options and sub-step solutions for burnup calculation (Isolato, 2011b; 2011c; 2013b; 2015a; 2015b). The stability of 3D burnup calculations may be improved by implicit algorithms (Dufek, 2014).

Xe-135 and Sm-149 fission product poisons might be evaluated individually from the other nuclides. Meanwhile the transport simulation is going they might be iterated to their equilibrium concentration. The equilibrium calculation is independent of the depletion routine, and the iteration may also be done in transport mode without burnup calculation.

### **3.3.4 Coupled multi-physics simulations**

Coupling in two ways for thermal hydraulics, CFD and fuel performance codes has been a major theme in Serpent improvement for the past years. The multi-physics coupling scheme in Serpent 2 is designed to operate on two levels:

- Internal coupling to built-in solvers for fuel behaviour and thermal hydraulics
- External coupling via a universal multi-physical interface

The built-in solvers are integrated to the transport simulations at source code level. They are also designed to provide different solutions to coupled items at a partial low computational cost. A thermo-mechanical fuel behaviour module for the modelling of temperature feedback inside fuel pins in steady-state and transient conditions is included by solvers include FINIX (Ikonen, 2013a; 2013b; 2015; 2016; Valtavirta, 2014b), and COSY. A 3D system/component scale



## 4 Modelling and Simulation

After having described the main parts of the problem. Which means: an explanation of neutron logs technology, geometry and principles and an overview about the methods used for simulating the system Monte Carlo Methods, specifically “Serpent a continuous-energy Monte Carlo physics burnup calculation code”. We may finally start with the characterization of the ideal system. It is taken in consideration for simulating the response of neutron tool in an ideal and infinite rock body. All this part will move through many simulations, starting from a simple simulation of a neutron transport in an infinite, homogeneous, isotropic and non-porous rock body, to a more realistic situation on a porous rock containing hydrocarbons, mud filtrate and drilling fluids.

### 4.1 Materials

To define a material in Serpent we must define its nuclides. The adopted convention is  $\langle Z \rangle \langle A \rangle . \langle id \rangle$ . Z refers to the atomic number of the element, A is the isotope mass number, expressed as three digits, and “.id” is the library id. The library id is the expression of temperature in K. For example, Carbon is defined as “6000.03c” where 03c means 300K.

The syntax of the material in Serpent is;

```
mat <name> <dens> [<options>]
<iso 1> <frac 1>
<iso 2> <frac 2>
...
```

Where  $\langle name \rangle$  is the name that we choose for the material,  $\langle dens \rangle$  is the material density which may be mass or atomic,  $\langle options \rangle$  depend on the cases,  $\langle iso i \rangle$  are the name of the constituent nuclides and  $\langle frac i \rangle$  are their corresponding fractions, mass or atomic depending on the definition of density. The only option which we used in the thesis is “rgb  $\langle R \rangle \langle G \rangle \langle B \rangle$ ”. This is the option for colours of the geometry plot. (Lappanen, 2015)

Considering a standard  $\nabla T = 3 \frac{^{\circ}C}{100 m}$  and a plausible depth of 2500 km the temperature at that depth will be  $75^{\circ}C = 348K$ . This temperature must be taking into account for all cross section of choosen nuclides, and so the closest value of  $\langle id \rangle$  for that temperature is “.03c”, all the nuclides are going to have this id card.

#### 4.1.1 Water

The second media into which the simulations run is water. Pure water is defined with its atomic composition and its density is taken equal to 1 kg/L. It is also possible to define salty water or

brine but dissolved chlorine may affect the result of simulation. So, in first case it is better to consider pure water. Since water contains Hydrogen we need to define the Thermal scattering cross section;

```
therm <thname> <lib>
```

Where <thname> is the name of our data library and <lib> is the library identifier. The lib is the name of the library in the directory file of the computer. <thname> is used for associate data with the considered material. So, the syntax in case of Thermal scattering libraries is; (Lappanen, 2015)

```
mat <name> <dens> moder <thname> <ZA>
<iso 1> <frac 1>
<iso 2> <frac 2>
...
```

The only difference with syntax here and that described before is the option “moder” which means that at least one of the constituents is a moderator for neutrons. With <ZA> we define the moderator nuclide, in this case it is Hydrogen, its ZA identification number is “1001”. In Serpent the syntax is:

```
%Pure water definition, composition in %wt, density 1,0g/cm3. For
water is necessary to define the card "moder". MythermLib is the
name of the Thermal scattering library.

mat water 1.0   moder MyThermLib 1001   rgb 0 0 255
8016.03c -0.89 %wt of Oxygen
1001.03c -0.11 %wt of Hydrogen
```

#### 4.1.2 Mud

The third media defined is mud. The chosen mud is a water base mud. Water-based mud (WBMs) is used to drill approximately 80% of all wells. The base fluid may be fresh water, seawater, brine, saturated brine, or a formate brine. The type of fluid selected depends on anticipated well conditions or on the specific interval of the well being drilled. For instance, the surface interval typically is drilled with a low-density water or seawater-based mud which contains few commercial additives. These systems incorporate natural clays during the drilling operations. Some commercial bentonite or attapulgite also may be added to aid in fluid-loss control and to enhance hole cleaning effectiveness. After surface casings set and cemented, the operator often continues drilling with a WBF unless well conditions require displacing to an oil or synthetic-based system.

The mud's composition is given in table n 6. Each of the chemical components of the mud are broken down in their constituent elements. The density of the considered mud is 1,38kg/L and its components are expressed in molar fractions.

Component name	Fraction wt%
Water	0.521
Soda ash	0.001
Caustic soda	0.001
Bentonite	0.04
CMC LV	0.005
CMC HV	0.002
KCl	0.03
Barite	0.400

Tab 6. Chemical composition of a water-based mud.

From the table 6 water is already treated in the paragraph above. Other component as KCl, Caustic soda (NaOH), Soda ash (Na<sub>2</sub>CO<sub>3</sub>) and Barite (BaSO<sub>4</sub>) do not need to be further clarified in their chemical composition, while the other mud components and their chemical constituents need to be discussed. When we refer to Bentonite, we are referring to Sodium Bentonite. Its chemical formula taken in consideration is Al<sub>2</sub>H<sub>2</sub>Na<sub>2</sub>O<sub>13</sub>Si<sub>14</sub>. Bentonite is common all over the world and its formation process consists in volcanic ash weathering. Generally, bentonite is added to water based mud to influence their thixotropic behaviour and so the capability to react as fluid when mechanical stresses are applied, and to behaves like a solid when no mechanical stresses are in place. Bentonite also generates borehole pressure to stabilize the wall of the borehole and prevents borehole collapse (Andy Varoshotis, 2016). CMC LV and CMC HV are both Carboxyl Methyl Calusa but respectively at Low Viscosity and High Viscosity. Both are used for control fluid loss in fresh water. In addition, the CMC HV may also improve rheological control and it is an efficient viscosifier [4]. We assume their chemical formula as [C<sub>6</sub>H<sub>7</sub>O<sub>2</sub>(OH)<sub>2</sub>CH<sub>2</sub>COONa]<sub>n</sub>.

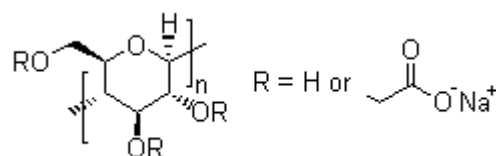


Figure 29, Chemical structure of CMC HV-LV, [4]

The difference between HV and LV concerns percentage of water in solution. LV has maximum 20% of water while HV has 5%. We take them equal, in any case the total amount of water in mud composition will be almost invalidated [5]. Mud definition on Serpent is:

```
%Mud definition, composition of mud in %wt, density 1,380g/cm3,
For mud is necessary to define the define card "moder".

mat mud 1.380      moder MyThermLib 1001      rgb 204 102 0
1001.03c -0.0720 %wt of H
6000.03c -0.0023 %wt of C
8016.03c -0.6600 %wt of O
11022.03c -0.0019 %wt of Na
13027.03c -0.0053 %wt of Al
14000.03c -0.0069 %wt of Si
16000.03c -0.0376 %wt of S
17000.03c -0.0102 %wt of Cl
19000.03c -0.0428 %wt of K
56130.03c -0.1609 %wt of Ba
```

### 4.1.3 Steel

The composition of the steel is not given by any producers of the tool. Considering that the tool has to resist to high temperature, high corrosion and high torque, the choice of the stainless steel will be made by combining all these variables. In general, the steel used in oil-gas has a high content of Cr, but usually those steels contain Mo and Ni. Following also the international standards that means API 5CRA e ISO13680, and so choosing a stainless steel able to stand over a combination of those factors:[6]

- Presence of CO<sub>2</sub>
- Presence of H<sub>2</sub>S
- low pH
- Chloride
- High Temperature [6]

At the end, the composition of the alloy should contain Cr=13% at least, Mo between 1-2% and Ni between, 4-5%. All the possible stainless steels that have these characteristics are listed in Attachment A1 and A2.

That chosen is the X1CrNiMo16-5-1 which has the composition shown in tab 7:

	C	Si	Mn	P max	S	N	Cr	Mo	Ni
X4CrNiMo16-5-1	≤0,06	≤0,7	≤1,50	0,04	≤0,015	≥0,020	15,00 to 17,00	0,80 to 1,15	4,00 to 6,00

Tab 7 Chemical composition of a martensitiv Stainless-steel

Now it is possible to define it on Serpent:

%Stainless steel definition, composition of it in %wt, density 7,5g/cm<sup>3</sup>, the same composition is used for both tool and casing.

```
mat steel 7.5          rgb 100 100 100
6000.03c -0.00060 %wt of C
26000.03c -0.73555 %wt of Fe
14000.03c -0.00700 %wt of Si
25055.03c -0.15000 %wt of Mn
16000.03c -0.00015 %wt of S
7014.03c -0.00020 %wt of N
24000.03c -0.17000 %wt of Cr
42000.03c -0.11500 %wt of Mo
28000.03c -0.60000 %wt of Ni
```

#### 4.1.4 AmBe

The chosen design for neutron source is AmBe, it has the characteristic listed in 2.4.2. Its chemical formula is AmO<sub>2</sub>Be following the mass composition given in 2.4.3, that is 4,6g of Be and 0,37g of AmO<sub>2</sub> we can calculate the density of the source. The standard capsule diameter per height, considered in the calculation of density, is 22.4mm X 31mm. The density of the source should be around 1,1 and 1,8g/cc and the respective quantities of Be and Am are between 5:1 or 20:1, in accordance the information given by Mark W. Vose, a technical product supervisor of QSA GLOBAL. The obtained density is indeed 1,139g/cm<sup>3</sup>. Now it is possible to define the material into Serpent as follows:

%Source material definitio, called AmBe, composition of AmBe in % wt, its calculated density is 1,139g/cm<sup>3</sup>.

```
mat AmBe 1.139          rgb 255 0 0
95241.03c -0.18 %Am
8016.03c -0.02 %O
4007.03c -0.80 %Be
```

#### 4.1.5 <sup>3</sup>He

<sup>3</sup>He is the element which fills the detector. In addition to <sup>3</sup>He is possible to find a quenching gas, for simplicity and to avoid the lack of information we have considered the detector filled by <sup>3</sup>He. The definition of its on Serpent is practically the definition of the isotope.

%Detector gas materia definition, He3, Card "sum" is used instead density in g\cm<sup>3</sup>. In this way the program calculates directly the atomic density for a given composition.

```
mat He3 sum          rgb 0 255 0
2003.03c -1.0 %wt of He3
```

#### 4.1.6 Gas

Natural gas found into reservoir is generally a mixture of some light hydrocarbons. The main part is composed by methane (CH<sub>4</sub>). It is common to find also small percentage of other components, like H<sub>2</sub>S, CO<sub>2</sub>, N, He and so on. To simulate every possible composition of gases is impossible. We decided to consider reservoir natural gas in our simulation like pure Methane. At Standard condition (0K and 1atm) methane presents a density of 0.717g/L. Considering its as a perfect gas and applying the relative law as follows:

$$\frac{p_1 V_1}{T_1} = \frac{p_2 V_2}{T_2} \quad (20)$$

Where:

p<sub>1</sub>=atmospheric pressure

p<sub>2</sub>=reservoir pressure in accordance with lithostatic gradient

V<sub>1</sub>=standard volume of a mole in standard condition.

V<sub>2</sub>=Unknown volume

T<sub>1</sub>=Standard temperature

T<sub>2</sub>=reservoir temperature in accordance with temperature gradient.

Finding V<sub>1</sub> and then calculating the density we obtain that at our reservoir condition Methane has a density of 0.450g/cm<sup>3</sup>. It is now possible to define CH<sub>4</sub> on Serpent:

```
%Gas materia definition, composition in %wt, calculated density  
0,450g/cm3.
```

```
mat gas -0.450      rgb 48 48 48  
1001.03c -0.75 %wt of H  
6000.03c -0.25 %wt of C
```

## 4.1.7 Petroleum

Petroleum in nature may present many different compositions. Some of them are in table 8.

Component	Intermediate oil	Volatile oil	Gas-condensate	Wet gas	Dry gas
CH <sub>4</sub>	48.83	64.36	87.07	95.85	86.67
C <sub>2</sub> H <sub>6</sub>	2.75	7.52	4.39	2.67	7.77
C <sub>3</sub> H <sub>8</sub>	1.93	4.74	2.29	0.34	2.95
C <sub>4</sub> H <sub>10</sub>	1.60	4.12	1.74	0.52	1.73
C <sub>5</sub> H <sub>12</sub>	1.15	2.97	0.83	0.08	0.88
C <sub>6</sub> H <sub>14</sub>	1.59	1.38	0.60	0.12	...
C <sub>7</sub> H <sub>16</sub> +	42.15	14.91	3.80	0.42	...
Mol. Wt. C <sub>7</sub> H <sub>16</sub> +	225	181	120	157	...
GOR, SCF/bbl	625	2000	18,200	105,000	Inf.
°API gravity	34.3	50.1	60.8	...	...
Liquid colour	Greenish black	Medium orange	Light straw	Water white	...

Tab 8 (Viberti, 2017) Chemical compositions of some typical hydrocarbons.

In our simulation the chosen composition was the intermediate one. Every component with many carbon atoms higher or equal to 7 has been considered with an averaged percentage of Hydrogen equal to 16%. All the other components atomic compositions have been calculated following the exact proportion between H and C. In any case the composition is dominated by CH<sub>4</sub> and so, the result is 79,41% of C and 20,59% of H. We consider petroleum without any constituents unless C and H. A typical Density for petroleum is 0,8g/cm<sup>3</sup>. In the simulation the result is:

```
%Petroleum material definition, called oil, composition expressed
in %wt, its density assumed equal to 0.8g/cm3.
```

```
mat oil 0.8 moder MyThermLib 1001 rgb 54 94 69
1001.03c -0.2059 %wt of H
6000.03c -0.7941 %wt of C
```

## 4.1.8 Rock

Firstly, is important choosing an ideal rock which will be the core rock for all the simulation. For more comfort is possible to consider a monocrystalline rock, and of course it must be a characteristic reservoir rock for well simulating the real world. The rocks are many but the actual number that we must concern ourselves with for reservoir engineering purposes is remarkably small. Classification can be broken into:

- Silicates.
- Quartz
- Feldspars
- Micas
- Zeolites
- Clays
- Carbonates
- Calcite
- Dolomite
- Siderite (less common)
- Sulphates
- Gypsum
- Anhydrite
- Sulphides
- Pyrite
- Oxides
- Magnetite
- Hematite [7]

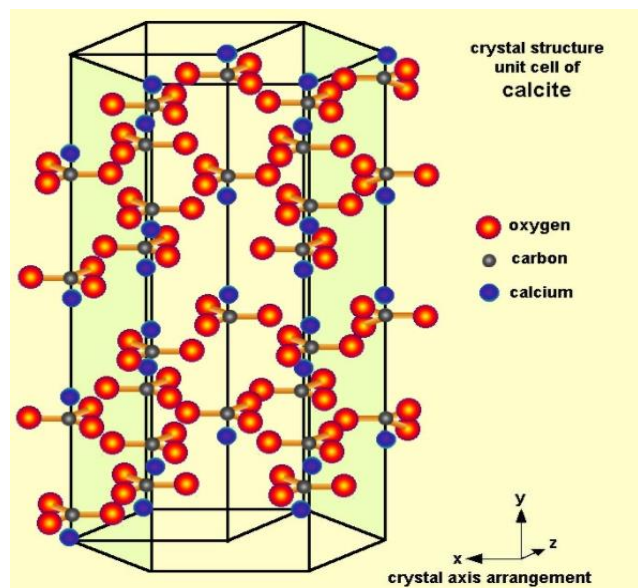


Figure 30 (Callister, 1985)

That chosen in the model was Calcite, this is a carbonate mineral and the most stable polymorph of calcium carbonate ( $\text{CaCO}_3$ ). Other polymorphs of calcium carbonate are the minerals aragonite, dolomite and laterite. Aragonite will change to calcite at  $380\text{--}470^\circ\text{C}$ , and laterite is even less stable. It presents as colourless or white, also gray, yellow, green mineral and has a specific gravity of 2,71. Its Crystalline structure is shown in figure 30. For creating a model that simulate a perfect, homogeneous, isotropic and infinite body of calcite. Using the aforementioned syntax for material input Serpent layout is:

%Rock definition, composition in %wt, density 2,71g/cm3.

```
mat rock 2.71          rgb 200 200 200
20000.03c -0.4 %wt of Ca
8016.03c  -0.4 %wt of O
6000.03c  -0.2 %wt of C
```

Once defined pure rock medium in Serpent we need to define porous rock media. We decide to simulate:

- Water saturated rock with  $\phi=15\%$
- Water saturated rock with  $\phi=30\%$
- Water saturated rock with  $\phi=50\%$
- Oil saturated rock with  $\phi=15\%$
- Gas Saturated rock with  $\phi=15\%$

Densities of all these rocks are calculated using the weighted average between rock and filling materials.

%Definition of the porous media:

%Water saturated rock phi 15%, composition in %wt, density 2,45g/cm3.

```
mat rock15water 2.45  moder MyThermLib 1001          rgb 200 200 220
20000.03c -0.340 %wt of Ca
8016.03c  -0.4735 %wt of O
6000.03c  -0.1700 %wt of C
1001.03c  -0.0165 %wt of H
```

%Water saturated rock phi 30%, composition in %wt, density 2.197g/cm3.

```
mat rock30water 2.197  moder MyThermLib 1001          rgb 200 200 240
20000.03c -0.28 %wt of Ca
8016.03c  -0.547 %wt of O
6000.03c  -0.140 %wt of C
1001.03c  -0.033 %wt of H
```

%Water saturated rock phi 50%, composition in %wt, density 1.855g/cm3.

```
mat rock50water 1.855  moder MyThermLib 1001          rgb 150 150 255
20000.03c -0.20 %wt of Ca
8016.03c  -0.645 %wt of O
6000.03c  -0.100 %wt of C
1001.03c  -0.055 %wt of H
```

%Oil saturated rock phi 15%, composition in %wt, density 2,4235g/cm<sup>3</sup>.

```
mat rock15oil 2.4235 moder MyThermLib 1001      rgb 54 150 69
20000.03c -0.34000 %wt of Ca
8016.03c -0.340000 %wt of O
6000.03c -0.289115 %wt of C
1001.03c -0.011900 %wt of H
```

%Gas saturated rock phi 15%, composition in %wt, density 2.37g/cm<sup>3</sup>.

```
mat rock15gas 2.37 moder MyThermLib 1001
20000.03c -0.3400 %wt of Ca
8016.03c -0.3400 %wt of O
6000.03c -0.3125 %wt of C
1001.03c -0.0075 %wt of H
```

### 4.1.9 Mud filtrate

Attention is due to define mud filtrates. When we inject mud into the borehole mud exerts a hydrostatic pressure higher than the pressure of the formations and fluids which they contain. That implies our formation is invaded by the mud filtrate. The heaviest particles accumulate on the walls of the borehole forming the so-called Mud cake. The light part of the mud filtrates the rock pores, and disturb the original composition of the fluids. Mud filtration influence the total formation response to borehole measuring. A general presentation of the phenomena is illustrated in figure 31

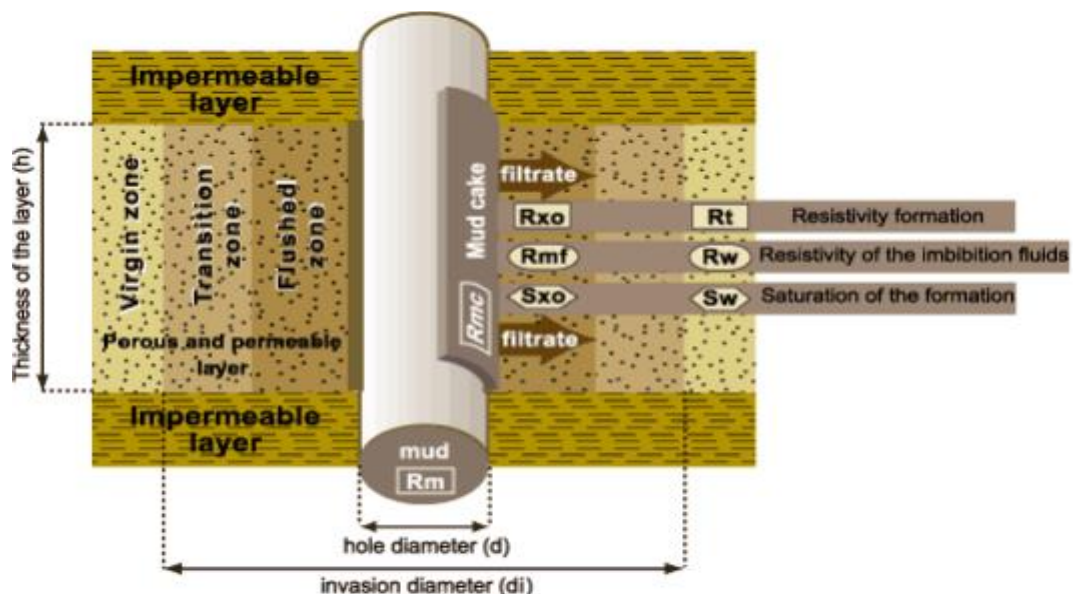


Figure 31 schematic representation of invasion (Socco, 2017)

For us is important to define the fluid distribution around the borehole. So we need the curves of saturation in our porous media. The trend of mud filtrate into formations is described in figure 32.

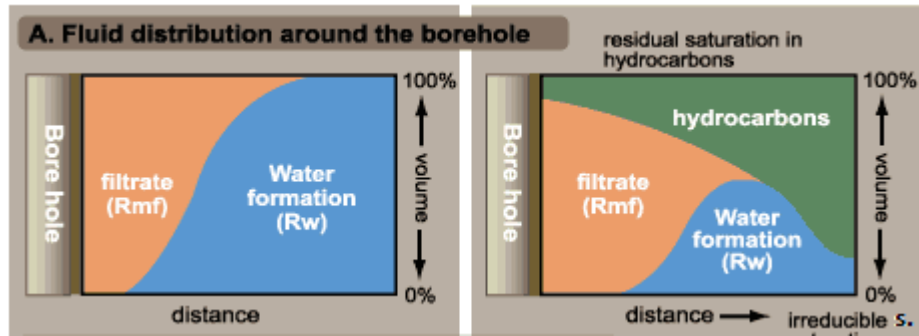


Figure 32 Invasion with and without Hydrocarbons (Socco, 2017)

In accordance with a common model of saturation for invase zones we suppose a linear decreasing. From pure mud into the borehole, mudcake in the wall and then a linear decrising of the saturation of the mud. We need to consider the irreducible water saturation in case of water saturated rock and residual oil saturation if the formation is oil saturated. Porosity of the rock for definition of filtrate is considered equal to 15%. Irriducible water saturation is considered equal to 0.2. In case of oil presence  $S_{or}$  is considere weual to 0.05 while  $S_{irr}$  equal to 0,15. The flushed zone has a radius of 20cm. The trend of the mud saturation is show in figure 33

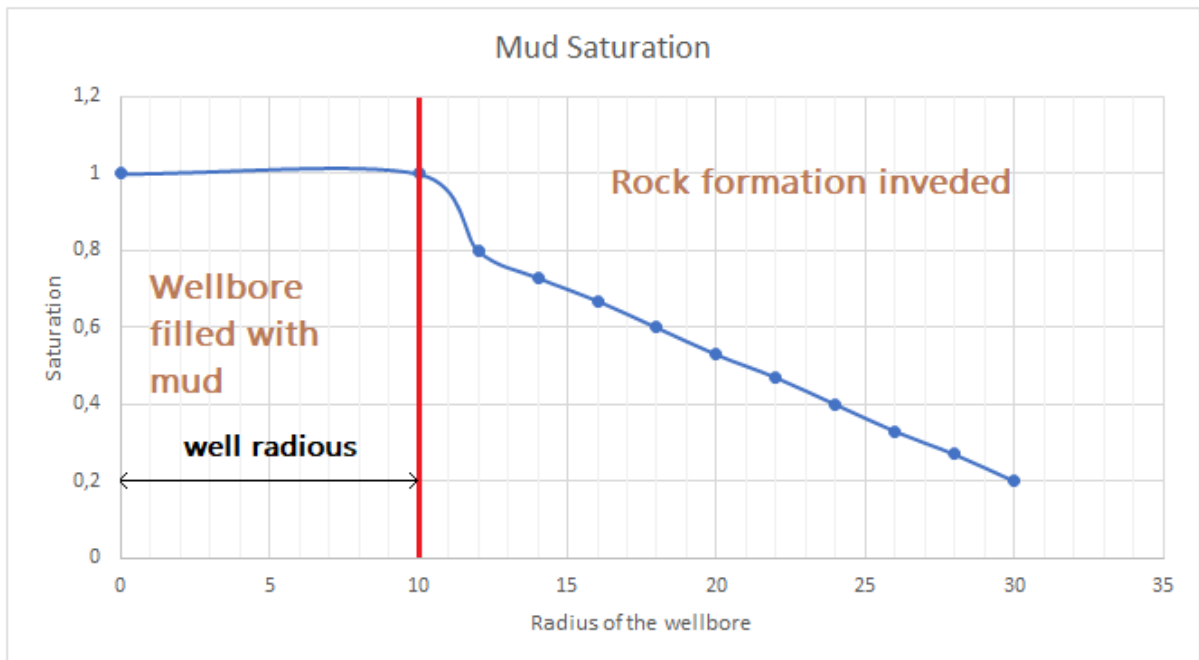


Figure 33 The plot represents the decreasing of mud saturation while increasing of the radius from the center of the wellbore. To define better it in Serpent we need to discretized the straight line into a curve with strairs shape. The result is shown in figure:

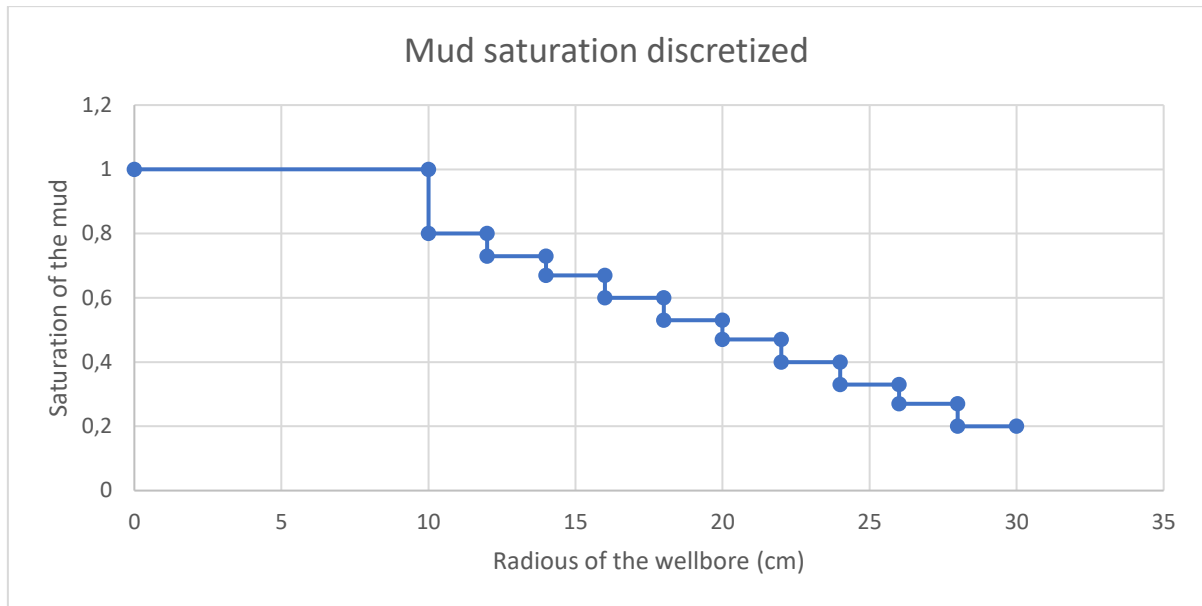


Figure 34 The plot has the same meaning of that in figure 33. In this plot are discretized the range of radio into which mud saturation is thought constant.

We have subdivided the invased zon in 10 intervals into which the composition of the rock is constant. For each intervals we must describe a different material. Mudcake has been described as all the elements that compound our mud without H and O. We ipotized that the only part of the mud that remain on the wall of the wellbore is without water.

**%Definitions of mud filtrates and mudcake.**

**%Mudcake definition, composition in %wt, density expressed by the card "sum". Mudcake is thought as mud but without water inside.**

```
mat mudcake sum rgb 50 20 20
11022.03c -0.00717 %Na
13027.03c -0.01990 %Al
14000.03c -0.02600 %Si
16000.03c -0.14160 %S
17000.03c -0.03840 %Cl
19000.03c -0.16120 %K
56130.03c -0.60570 %Ba
```

**%First zone mud filtrate, composition in %wt, density expressed by the card "sum". Irriducible water saturation is 0.2, porosity 0.15.**

```
mat mud1 sum moder MyThermLib 1001 rgb 103 80 65
20000.03c -0.34 %Ca
1001.03c -0.01194 %H
6000.03c -0.170276 %C
8016.03c -0.4459 %O
11022.03c -0.000228 %Na
13027.03c -0.000636 %Al
14000.03c -0.000828 %Si
16000.03c -0.004512 %S
17000.03c -0.001224 %Cl
19000.03c -0.005136 %K
56130.03c -0.019296 %Ba
```

%Second zone mud filtrate, composition in %wt, density expressed by the card "sum". Porosity 0.15.

```
mat mud2 sum      moder MyThermLib 1001      rgb 120 133 119
20000.03c -0.340000 %Ca
1001.03c  -0.012320 %H
6000.03c  -0.170253 %C
8016.03c  -0.448200 %O
11022.03c -0.000209 %Na
13027.03c -0.000583 %Al
14000.03c -0.000759 %Si
16000.03c -0.004136 %S
17000.03c -0.001122 %Cl
19000.03c -0.004708 %K
56130.03c -0.017687 %Ba
```

%Third zone mud filtrate, composition in %wt, density expressed by the card "sum". Porosity 0.15.

```
mat mud3 sum      moder MyThermLib 1001      rgb 150 150 130
20000.03c -0.340000 %Ca
1001.03c  -0.012700 %H
6000.03c  -0.170230 %C
8016.03c  -0.450500 %O
11022.03c -0.000190 %Na
13027.03c -0.000529 %Al
14000.03c -0.000690 %Si
16000.03c -0.003760 %S
17000.03c -0.001020 %Cl
19000.03c -0.004280 %K
56130.03c -0.016080 %Ba
```

%fourth zone mud filtrate, composition in %wt, density expressed by the card "sum". Porosity 0.15.

```
mat mud4 sum      moder MyThermLib 1001      rgb 165 155 133
20000.03c -0.340000 %Ca
1001.03c  -0.013080 %H
6000.03c  -0.170207 %C
8016.03c  -0.452800 %O
11022.03c -0.000171 %Na
13027.03c -0.000477 %Al
14000.03c -0.000621 %Si
16000.03c -0.003383 %S
17000.03c -0.000918 %Cl
19000.03c -0.003851 %K
56130.03c -0.014472 %Ba
```

%Fifth zone mud filtrate, composition in %wt, density expressed by the card "sum". Porosity 0.15.

```
mat mud5 sum      moder MyThermLib 1001      rgb 170 165 140
20000.03c -0.340000 %Ca
1001.03c  -0.013460 %H
6000.03c  -0.170184 %C
8016.03c  -0.455100 %O
11022.03c -0.000152 %Na
13027.03c -0.000424 %Al
14000.03c -0.000552 %Si
16000.03c -0.003008 %S
17000.03c -0.000816 %Cl
19000.03c -0.003424 %K
56130.03c -0.012864 %Ba
```

%sixth zone mud filtrate, composition in %wt, density expressed by the card "sum". Porosity 0.15.

```
mat mud6 sum      moder MyThermLib 1001  rgb 180 170 150
20000.03c -0.340000 %Ca
1001.03c -0.013840 %H
6000.03c -0.170161 %C
8016.03c -0.457400 %O
11022.03c -0.000133 %Na
13027.03c -0.000371 %Al
14000.03c -0.000483 %Si
16000.03c -0.002632 %S
17000.03c -0.007140 %Cl
19000.03c -0.002995 %K
56130.03c -0.011256 %Ba
```

%Seventh zone mud filtrate, composition in %wt, density expressed by the card "sum". Porosity 0.15.

```
mat mud7 sum      moder MyThermLib 1001  rgb 188 179 155
20000.03c -0.3400000 %Ca
1001.03c -0.0142200 %H
6000.03c -0.1701380 %C
8016.03c -0.4597000 %O
11022.03c -0.0001139 %Na
13027.03c -0.0003180 %Al
14000.03c -0.0004140 %Si
16000.03c -0.0022560 %S
17000.03c -0.0006110 %Cl
19000.03c -0.0025680 %K
56130.03c -0.0096470 %Ba
```

%eighth zone mud filtrate, composition in %wt, density expressed by the card "sum". Porosity 0.15.

```
mat mud8 sum      moder MyThermLib 1001  rgb 190 185 160
20000.03c -0.340000 %Ca
1001.03c -0.014600 %H
6000.03c -0.170115 %C
8016.03c -0.462000 %O
11022.03c -0.000095 %Na
13027.03c -0.000265 %Al
14000.03c -0.000345 %Si
16000.03c -0.001870 %S
17000.03c -0.000510 %Cl
19000.03c -0.002139 %K
56130.03c -0.008040 %Ba
```

%ninth zone mud filtrate, composition in %wt, density expressed by the card "sum". Porosity 0.15.

```
mat mud9 sum      moder MyThermLib 1001  rgb 210 193 180
20000.03c -0.340000 %Ca
1001.03c -0.014980 %H
6000.03c -0.170092 %C
8016.03c -0.464300 %O
11022.03c -0.000076 %Na
13027.03c -0.000211 %Al
14000.03c -0.000276 %Si
16000.03c -0.001504 %S
17000.03c -0.000408 %Cl
19000.03c -0.001712 %K
56130.03c -0.006432 %Ba
```

```
%Tenth zone mud filtrate, composition in %wt, density expressed by
the card "sum". Porosity 0.15.
```

```
mat mud10 sum      moder MyThermLib 1001  rgb 235 250 233
20000.03c -0.340000 %Ca
1001.03c  -0.015360 %H
6000.03c  -0.170069 %C
8016.03c  -0.466600 %O
11022.03c -0.000057 %Na
13027.03c -0.000159 %Al
14000.03c -0.000207 %Si
16000.03c -0.001128 %S
17000.03c -0.000306 %Cl
19000.03c -0.001283 %K
56130.03c -0.004824 %Ba
```

## 4.2 Geometry of the system

Serpent uses a universe-based geometry, very similar to MNCP. Geometry is divided in separate levels. They are all constructed independently and nested into smaller parts. Are provided various elementary geometry. The syntax of the surface card is:

```
surf <id> <type> <param 1> <param 2> ...
```

Where <id> is the surface identifier, <type> is the surface type, they are all listed into the manual and <param 1> and <param 2> are the surface parameters. The surface identifier is the name that we chose for the surface. There are many types of surfaces, as shown in attachment ---. In this thesis and simulations are used “inf”, “pz” and “cyl”.

We will start to build our Serpent model for the neutron log by copying the material definition from above and defining an infinite geometry. The infinite geometry is a 3D infinite volume, in our simulation we may consider it as the Earth. (Lappanen, 2015)

```
%Geometry of the Earth, inf means all the space and does not need
more geometrical specifications.
```

```
surf earth inf
```

Then we can fill this surface with every materials which we define. In our simulation usually will be filled with rocks materials, but in the very beginning case will be also filled with water and mud. The following procedure is for Rock, which is the type more used in the thesis.

To fill a surface we need another card, that is “cell”. Cells are two or three dimensional regions.

```
cell <name> <u0> <mat> <surf 1> <surf 2> ...
```

Where; <name> is the cell name, we put numbers, <u0> is the univers numebr of the cell, <mat> is the material that fills the cell and <surf 1> <surf 2> are the bounding surfaces. Then is important always to describe regions of space that are not part of our geometry, to do this we must set material name to “outside”. (Lappanen, 2015)

### %definition of the cells

%The universe numeber is 0, universe 0 has always to exist.

```
cell 1 0 rock -earth %the "-" means filled
cell 2 0 outside earth %without "-" means not filled
```

The obtained output from Serpent is:



Figure 35 Shows a homogeneous isotropic infinite body of rock.

The geomentry is currently simply an infinite rock system.

Once defined the general geometry we might start to produce something more similar to our problem. That means a borehole with runng inside a neutron log tool. Before describing how to make the hole, is better to describe how to simulate the tool. To do it is necessary to look at a typical shape of the tool, then will be possible to riproduce it with more accurancy possible. The tool will be similar to that in figure 36 with same dimensions and in accordance with

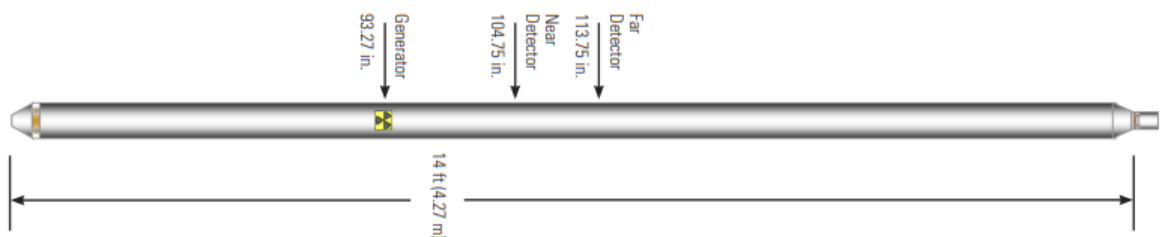


Figure 36 In this figure is rappresentd a typical shape of the tool. We Follow those rappresentation for modelling our tool .[8]

Dimensions and Ratings		
Maximum OD	2.125 in.	
Maximum Pressure	15,000 psi (103.4 Mpa)	
Maximum Temperature	325°F (162.8°F)	
Minimum Csg/Tbg ID	2.388 in.	
Maximum Csg/Tbg ID	9.625 in.	
Weight	with Gamma Ray and Telemetry	137 lb (62.1 kg)
Length	with Gamma Ray and Telemetry	23.3 ft (7.1 m)

Tab 9 Specifical dimensions used to design our tool [8]

diameter of the tool and its length. Will be considered as a homogeneous, isotropic and ideal cylinder of stainless steel. So, we are trying to acheve the output plot in figure 37:



Figure 37 is the geometry plotter of our modelled tool.

Where the dark grey rappresents the stainless steel, the red rappresents the neutron source and the light green the detector. To achieve that approximation we define the card “pin”. Pin consists of nested annular material layers. Its syntax is

```
pin <id>
<mat 1> <r1>
<mat 2> <r2>
...
<mat n>
```

Where, <id> is the pin identifier and rappresent an universe, <mat 1> <mat 2> rappresent the nested materials and <r1><r2> rappresents he outer radii of the material regions. Radii are expressed in cm. (Lappanen, 2015)

**%Tool pin definition.**

**%Our tool is going to be buld as three different pin, one over the other. They describe the detector part, the source part and the stainless steel part.**

```
pin 1      %Source pin definition
AmBe  0.5
steel  1.0
water

pin 2      %Stainless steel void definition
steel  1.0
water

pin 3      %Detector definition
He3    0.5
steel  1.0
water
```

In this case the pin is surrounded by water. The surrounding material might be everything provided in material cards.

Our goal is to stuck those pins vertically. To make it possible with must define the limiting axial planes. They are:

1. The top of the tool
2. The top of the detector
3. The bottom of the detector
4. The top of the source
5. The bottom of the source
6. The bottom of the tool.

Surface definition is going to be:

`%Axial surface for fuel rods, all the distance are expressed in cm`

```
surf top1      pz  188 %Top of the tool
surf topdet1   pz   72 %Top of the detector
surf botdet1   pz   62 %Bottom of the detector
surf top2      pz   3.0 %Top of the Source
surf bottom2   pz  -3.0 %Bottom of the source
surf bottom1   pz -234 %Bottom of the tool.
```

Once defined pins and surfeces we are able to create vertical stacked cells. It permit to create a 3D neutron log model, adding the following cells definitions:

Now, for replying adequately the probe is needed to add at the geometry also the others parts, which are the neutron source and the detector or for being more accurate two neutron detectors, one for near and thermal neutrons the latter for far and epithermal. Before than defining the geometry is correct define the materials that compound those components of the tool and so, for the souce:

`%We call the univers into which we are building our tool unverse n 3. Above and below the instrument we put water, it is possile to put everythig else defined before.If the cell is filled by another universe, the material name is replaced by command "fill" and the number of the filling universe.`

```
cell 4 3 water          -bottom1
cell 5 3 fill  2 bottom1 -bottom2
cell 6 3 fill  1 bottom2 -top2
cell 7 3 fill  2 top2     -botdet1
cell 8 3 fill  4 botdet1  -topdet1
cell 9 3 fill  2 topdet1  -top1
cell 12 3 water  top1
```

Then plotting it on Serpent we will obtain:

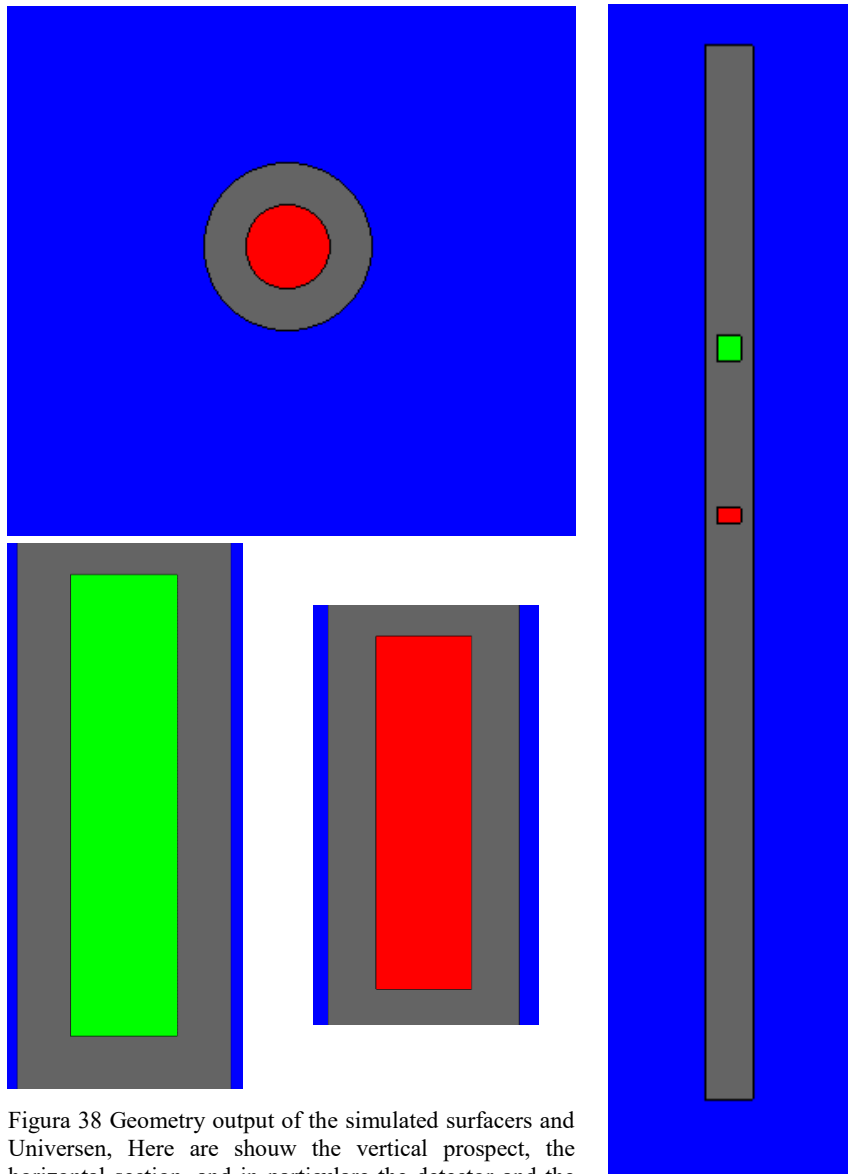


Figure 38 Geometry output of the simulated surfacers and Universen, Here are show the vertical prospect, the horizontal section, and in particulare the detector and the source.

Figure 38 is the representation of the with cut plane on xy, figure is the cross section on plan zy and figure and figure are respectively a zoomed cross section on zx of the detector and of the source. Now we should swich on the univers 0, in order to rappresent the tool within the borehole. Firstly we must define the borehole. We considere a diameter of 10cm. We approximate it as an infinite cylinder:

```
%Geometry of the Borehole, the borehole is centred in
(0.000,0.000) and its radius is 5.0 cm.
```

```
surf hole cyl 0.000 0.000 5.0
```

```
%definition univers 0 body of infinity rock with the borehole
filled with universe 3.
```

```
cell 1 0 water -earth hole
cell 2 0 outside earth
cell 3 0 fill 3 -hole
```

The total result in terms of plot, are shown in figure 39 and 40:

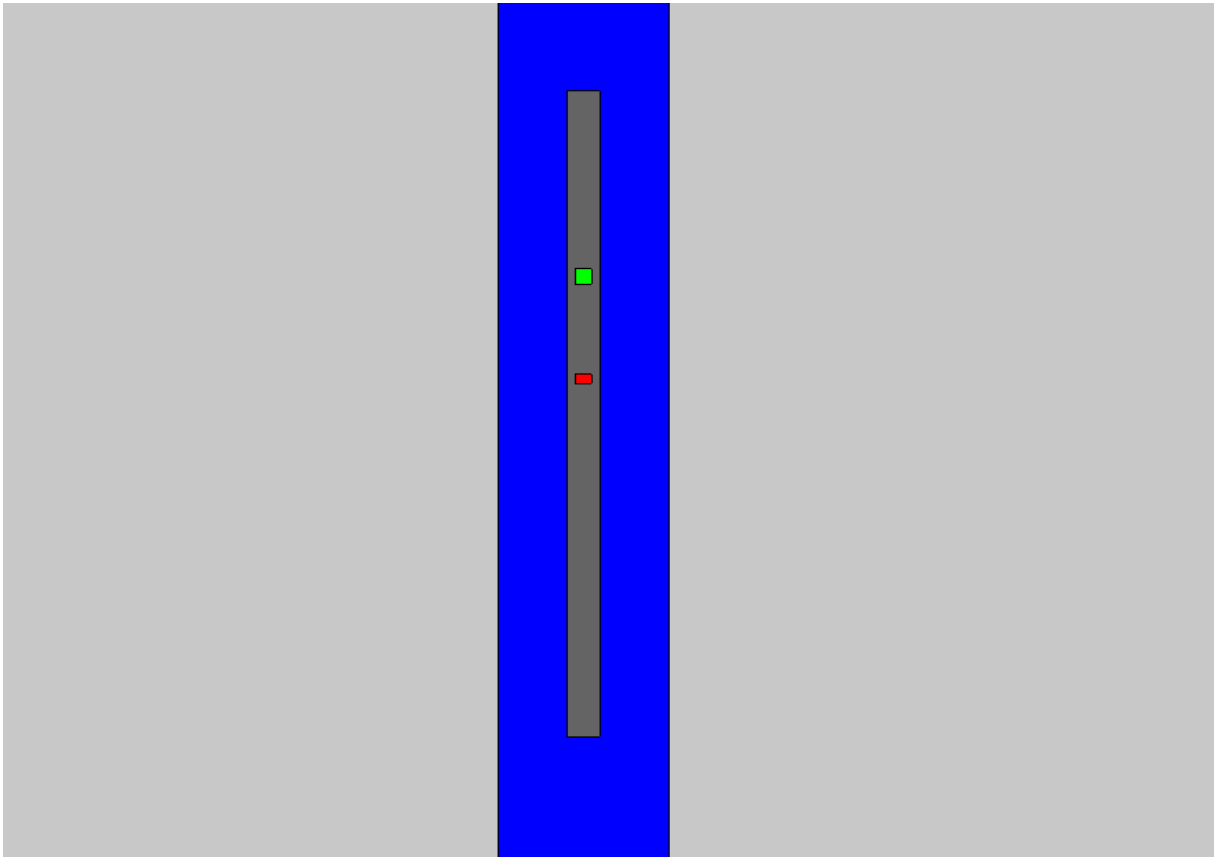


Figure 39 Geometry plotter of vertical section, the plot shown the tool within the borehole drilled in a rock formation:

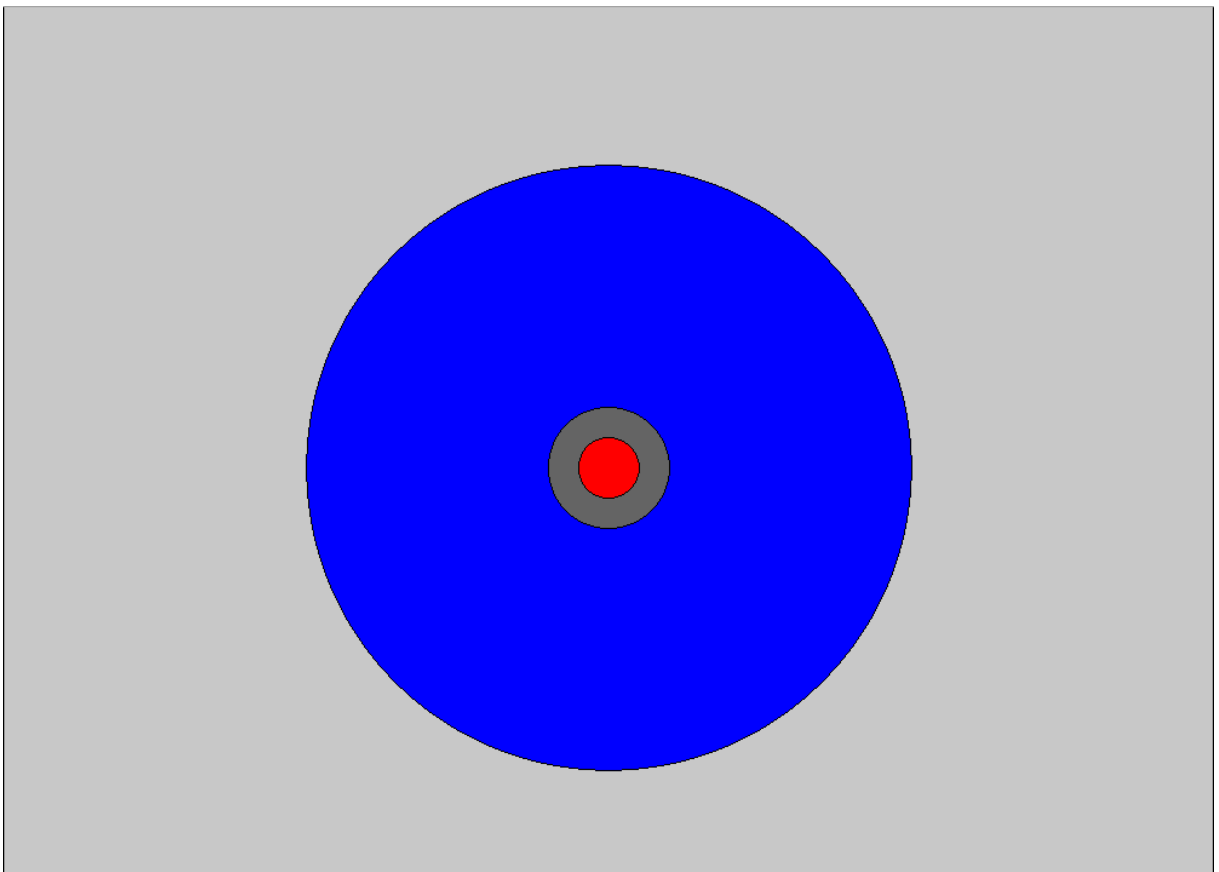


Figure. 40 Horizontal section.

While the geometry thought for invaded zone is obtained with this syntax:

`%to create a invaded zone we modelled in Serpent 12 concentric infinite cylinder, each of them has the radiuses expressed in cm.`

```
surf hole cyl 0.000 0.00 4.5 %filled with mud
surf mudc cyl 0.000 0.00 5.0 %filled with mudcake
surf m1 cyl 0.000 0.00 6.0 %filled with mud invasion 1
surf m2 cyl 0.000 0.00 7.0 %filled with mud invasion 2
surf m3 cyl 0.000 0.00 8.0 %filled with mud invasion 3
surf m4 cyl 0.000 0.00 9.00 %filled with mud invasion 4
surf m5 cyl 0.000 0.00 10.0 %filled with mud invasion 5
surf m6 cyl 0.000 0.00 11.0 %filled with mud invasion 6
surf m7 cyl 0.000 0.00 12.0 %filled with mud invasion 7
surf m8 cyl 0.000 0.00 13.0 %filled with mud invasion 8
surf m9 cyl 0.000 0.00 14.0 %filled with mud invasion 9
surf m10 cyl 0.000 0.00 15.0 %filled with mud invasion 10
```

`%definition univers 0 body of infinity rock with an hole filled with universe 3. Each of the cell is filled with the materials described above.`

```
cell 2 0 outside earth
cell 1 0 rock -earth m10
cell 14 0 mud1 -m1 mudc
cell 15 0 mud2 -m2 m1
cell 16 0 mud3 -m3 m2
cell 17 0 mud4 -m4 m3
cell 18 0 mud5 -m5 m4
cell 19 0 mud6 -m6 m5
cell 20 0 mud7 -m7 m6
cell 21 0 mud8 -m8 m7
cell 22 0 mud9 -m9 m8
cell 23 0 mud10 -m10 m9
cell 24 0 mudcake -mudc hole
cell 3 0 fill 3 -hole %universe 3 is pin definition
```

The geometry plot results are shown in figure 41 and figure 42:

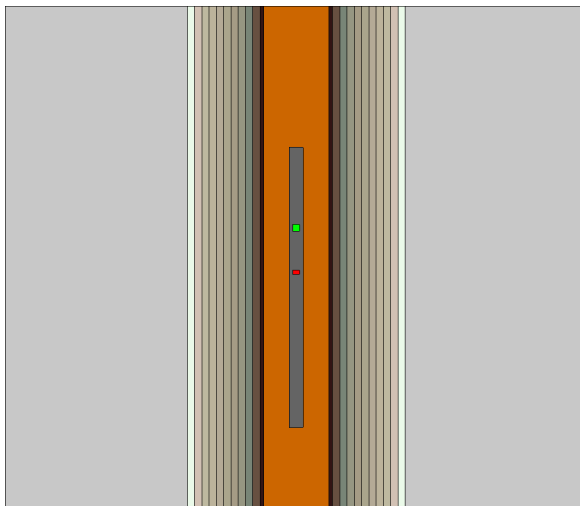


Figure41 Vertical section of mud invasion geometry

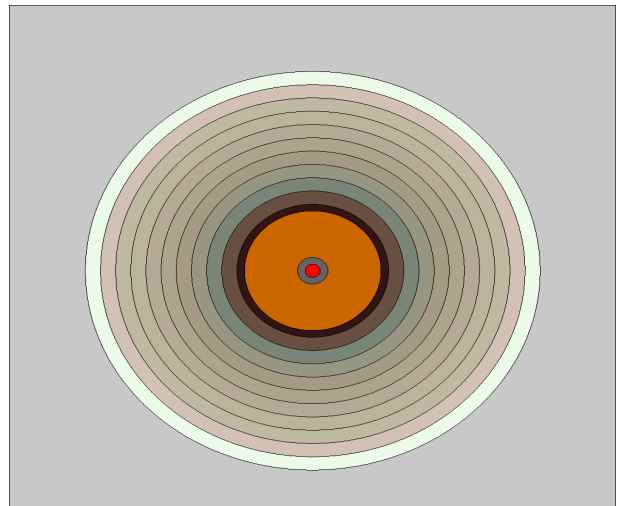


Figure 42 Horizontal section of mud invaded geometry

### 4.3 Simulations

The purpose of this chapter is to give an overview on all the simulations done. Starting from the first three simulations that are run in a homogeneous media, will be discussed in the following order:

- 1) Neutron log in homogeneous, isotropic and infinite body of Calcite
- 2) Neutron log in homogeneous, isotropic and infinite body of pure water
- 3) Neutron log in homogeneous, isotropic and infinite body of mud.

Then considering those simulation like standard to follow it is possible produce other more sophisticated simulation. Other two simulations are done in homogeneous infinite body, those are:

- 4) Neutron log in homogeneous, isotropic and infinite body of intermediate petroleum
- 5) Neutron log in homogeneous, isotropic and infinite body of Methane.

Once defined those homogeneous, isotropic and infinite simulation and their results it is possible to simulate more complex body. We have done simulations on:

- 6) Neutron tool running in a borehole within rock body filled with pure water.
- 7) Neutron tool running in a borehole within rock body filled with mud.
- 8) Neutron tool running in a borehole within porous rock filled with water
  - i) Water saturated rock with  $\phi=15\%$
  - ii) Water saturated rock with  $\phi=30\%$
  - iii) Water saturated rock with  $\phi=50\%$
  - iv) Oil saturated rock with  $\phi=15\%$
  - v) Gas saturated rock with  $\phi=15\%$
- 9) Neutron Tool running in a borehole within a rock invaded by mud
  - i) Mud Invaded rock with  $\phi=15\%$
  - ii) Mud invaded, water saturated rock with  $\phi=15\%$
  - iii) Mud invaded, oil saturated rock with  $\phi=15\%$
  - iv) Mud Invaded rock with  $\phi=15\%$  and casing string.

Since simulation 4 the configuration of the tool will be centred in the borehole or pushed to the wall of the borehole. Then every output is plotted on MATLAB and compared in different ways. The purpose is to understand the behaviour of log response in function of the media crossed by neutrons. All the simulations listed above are attached in appendix D.

### 4.3.1 Analysis of the data

The geometrical representation of the first three simulation are shown in figure 43, 44, 45:

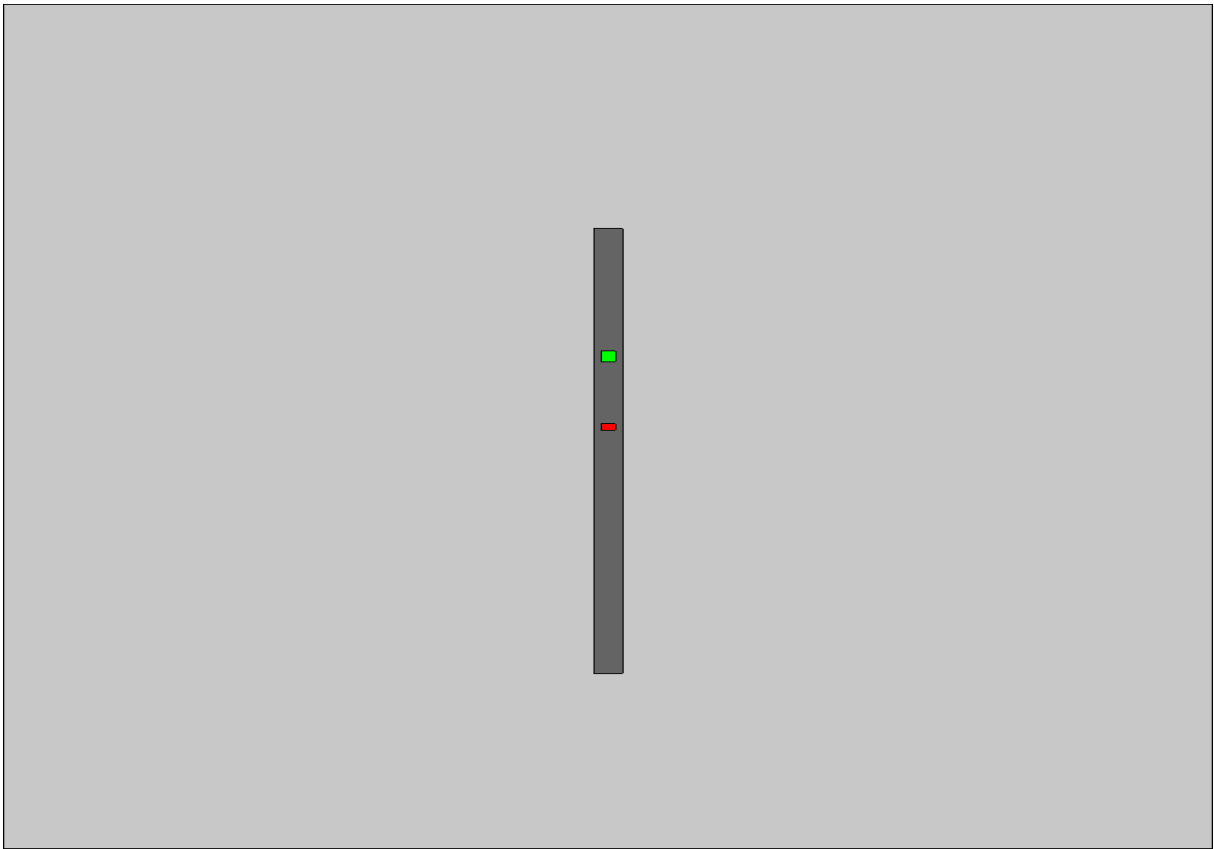


Figure 43 Tool in homogeneous isotropic infinite body of rock, vertical section.

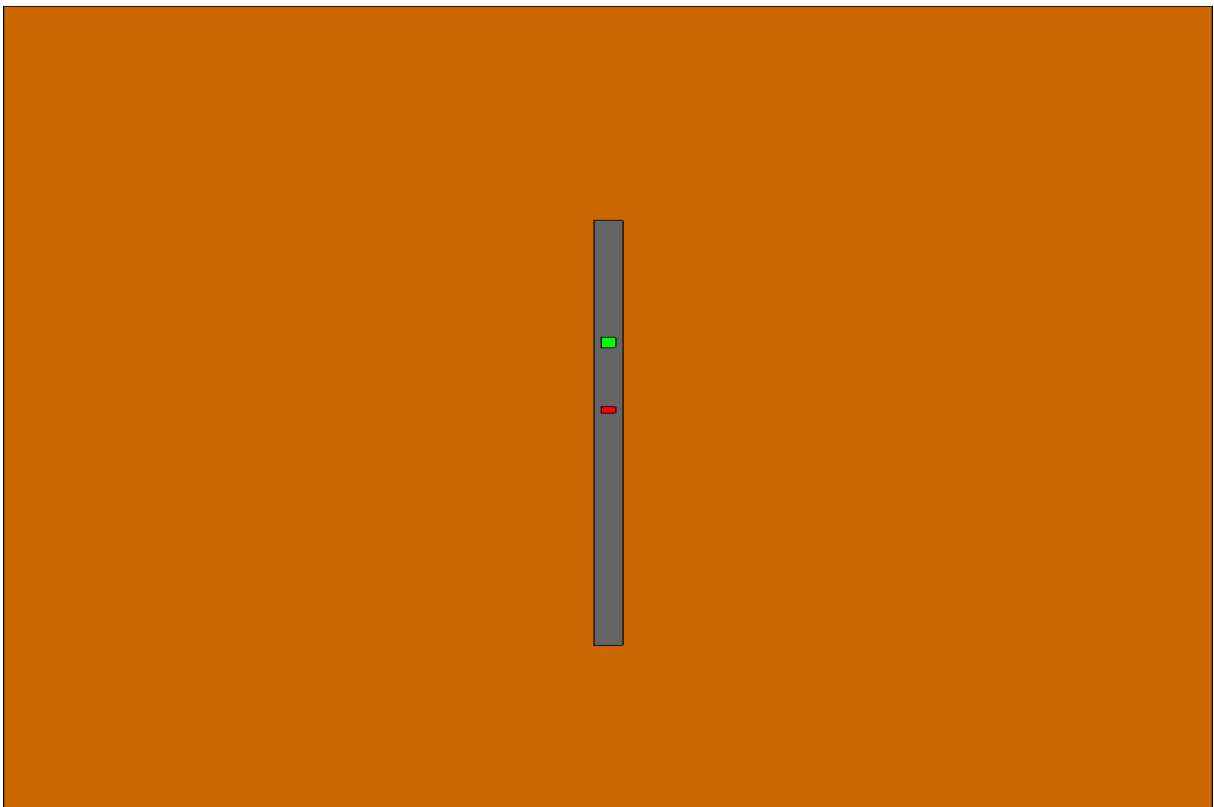


Figure 44 Tool in homogeneous isotropic infinite body of mud, vertical section.

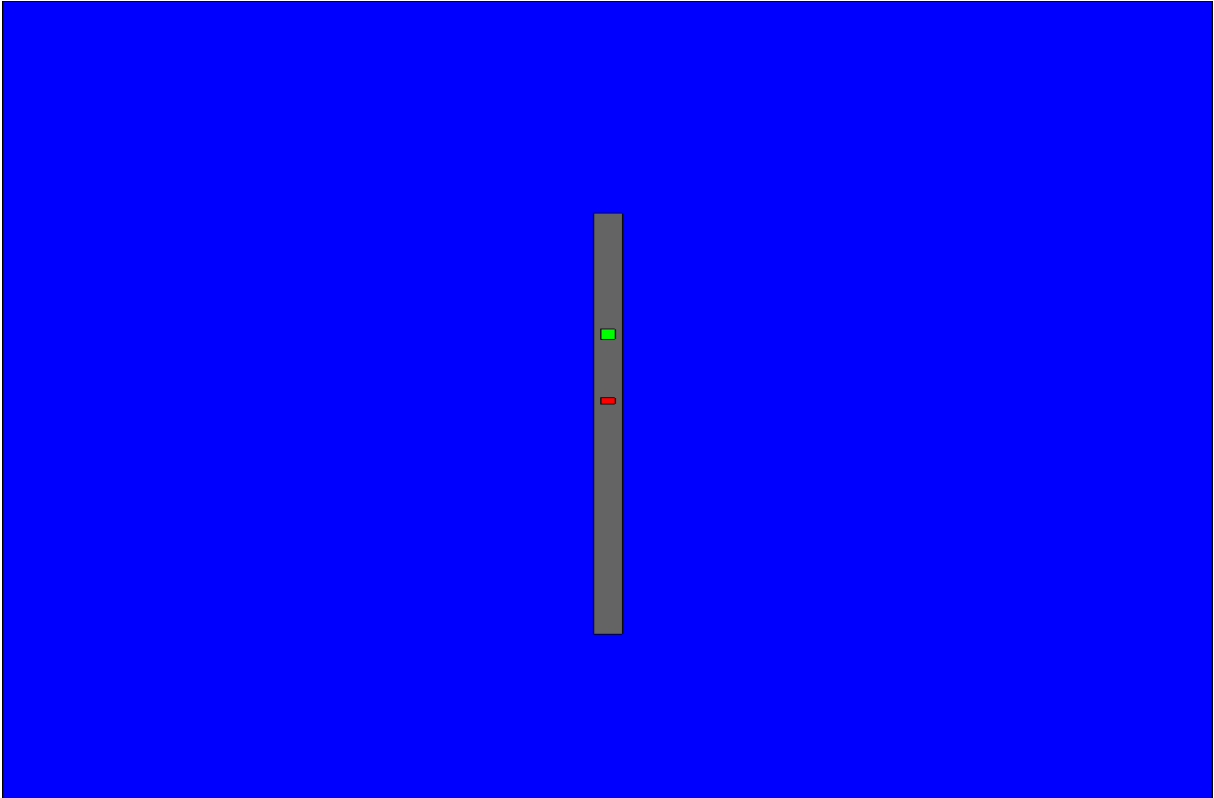


Figure 45 Tool in homogeneous isotropic infinite body of water, vertical section.

In figure 43 is shown the tool surrounded by 100% of Calcite. Its output is plotted and shown in attachment D1. In figure 44 is shown the tool surrounded by 100% of mud this time. Its output plot is shown in the attachment D2 Then the last plot represented in figure 45 is the tool surrounded by pure water- Its output plot is shown in the attachment D3.

Before starting the comparison between media responses, we need to clarify how a Serpent output is and how it could be produced. An example of output is shown in Appendix F.

Our outputs have been produced by the detector. We need to understand how the detector is modelled. The detector estimates neutron flux. To calculate it, a reaction rate needs to be calculated. This reaction rate is integrated over energy and space:

$$R = \frac{1}{V} \int_V \int_{E_{i+1}}^{E_i} f(r, E) \varphi(r, E) d^3r dE \quad (21)$$

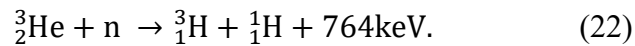
Response function  $f(r,E)$ , spatial and energy domains are the detector parameters. Syntax is:

```
det <name> <param 1> <param 2> ...
```

Where <Name> is the detector name and <param 1> <param 2> are the parameters that we may set. Parameters are listed in attachment. Some parameters produce multiple results and these results are divided into the numbers of bins.

Parameter used from attachment B2 are “dr”, “de”, “du”, “dc”, “dv”.

The nuclear reaction on which we are interested is



To set the detector looking for this reaction we need the parameter “pr”:

```
det <name> dr <mt> <mat>
```

Where <name> is always the detectors’ name, dr is the parameter “reaction multiplier” which determines the response function, <mt> is the response function number and <mat> is the material on which we would like to perform the detection. Every <mt> number are listed in attachment. Now once sets response function we should set energy domain also, so;

```
det <name> de <ene>
```

Where “de” is the parameter “detector energy grid” which defines the energy bins for the response function and <ene> is the grid name. The number of energy bins is defined by the grid size. We can use four types of energy grid. One of them is “equal lethargy-width bins”. For our purpose it is the best type. Lethargy of the neutron is the natural logarithm of the ratio between an Energy  $E_0$  and the energy owned by the neutron.

$$\ln \frac{E_0}{E_i} = \text{Lethargy}. \quad (23)$$

The use of lethargy permits a more convenient treatment of the loss of energy of the neutron while its collides in elastic conditions with formation atoms or when it is scattered by a moderator. The grid definition is made by the card “ene”:

```
ene <name> <type> <N> <Emin> <Emax>
```

Where <name> is the chosen grid name, <type> is the grid type and so, for us division by lethargy energy “dt -3”, <N> is the number of bins into which we want to divide the energy interval, <Emin><Emax> are the minimum and maximum energy of our spectrum. Then:

**%then I have to score total capture into He3 due to neutrons collision into universe 0 (volume of integration=>everything) with an energy interval of 0->11MeV, so my idea was:**

**%We must score He3(n,p) reaction dono into the detector material He3, so the reaction mode is 103. The energy grid is between the minimum and the maximum energy of the neutrons produced by the source. It Is 10-8MeV and 12MeV.**

%Definition of the energy grid: bins are dividete in equal lethargy intervals. We cut the spectrum into two intervals to have a better resolution of the thermalized neutrons energy.

```
ene energy 3 400 10e-6 12e1 %fast neutrons
ene energy2 3 100 1e-8 10e-6 %epithermal and thermal neutrons.
```

%Detector definitions:

```
det 1 de energy du 0 dr 103 He3 %first output
det 2 de energy2 du 0 dr 103 He3 %secodn output
```

Lastly it is necessary to define the source. Considering the subcriticality and non-multiplying system where we are running the tool, we need to replace the self-sustaining nuclear reaction with an external source simulation mode.

```
set nps <Nsrc> [ <Nbatch> ]
```

Where <Nsrc> is the total number of source neutrons run and <Nbatch> is the number of batches run. The source definition has the following input syntax:

```
src <name> <param 1> <param 2> ...
```

Where <name> is the name of the source and <param 1><param 2> are the source parameters. Source parameters are lists in attachment. We use the cards “sc” to define the cell and “sb” which means bins-wise energy spectrum.

```
src <name> sb <nb> <E0> <w0> <E1> <w1> ... <En> <wn>
```

Where <name> is the name of the source, <nb> is the number of source energy bins, <Ei> are the energy bin boundaries and <wi> the bin weights. The code samples the energy in accordance with the probability calculated for by weights. To calculate weights, we need the source emission spectrum, figure. Approximating it in a sequence of rectangles areas we obtain:

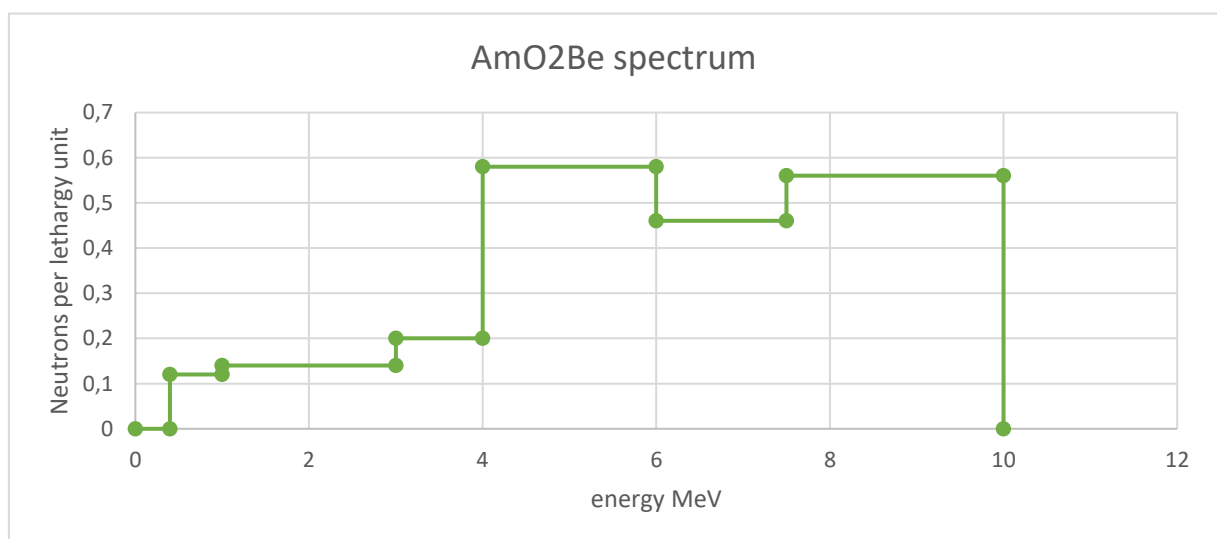


Figure 46 Discretization of energy spectrum of the neutron source. In ordinated we defined Neutrons lethargy per unit, [a.u.], while in abscissae there is emitted energy expressed in MeV.

Now we divided the spectrum into 7 bins.

- 1) 0→0.4MeV
- 2) 0.4→1.0MeV
- 3) 1.0→3.0MeV
- 4) 3.0→4.0MeV
- 5) 4.0→6.0MeV
- 6) 6.0→7.5MeV
- 7) 7.5→10MeV

We calculate the area above each interval, and then for normalizing them we divide each area for the total area of the spectrum. Then we give to each area a probability proportional to it and a correspond weight to describe it on Serpent: (Lappanen, 2015)

`%External source definition, neutron popolution will change in order to avoi reduction in standard deviation.`

`set nps 50000000 %Source definition`

```
src 1 sc 6 sb 7 %Setting energy distribution
4E-1 0.0 %<Energy interval> <Assigned weight>
1.0 0.4
3.0 1.4
4.0 1.0
6.0 5.8
7.5 3.4
10.0 7.00
```

Once Defined everything is possible to run the program and the obtained output is plot on MATLAB. An example of the output is in the attachment.

For these three simulation their output is plotted and listed in attachment.

Then we try to compare those output to interpret the results: The expected result is to find the bigger value in terms of Thermal neutrons when in the case of water, while in case of rock we think to find the lower count. Mud should stay in between. The comparison between those three is done in figure 47 and for thermal part in figure 48.

Every Monte Carlo simulation must be plotted necessary with its standard deviation, otherwise the plot is meaningless. High standard deviation makes the result, from statistical point of view, useless. Our simulations have been iterated, with higher number of neutrons, until we reached an acceptable value of standard deviation. Less than 10% at least. Every result is plotted with its own standard deviation on the appendix D. Also plots shown in this chapter are plotted with their standard deviations.

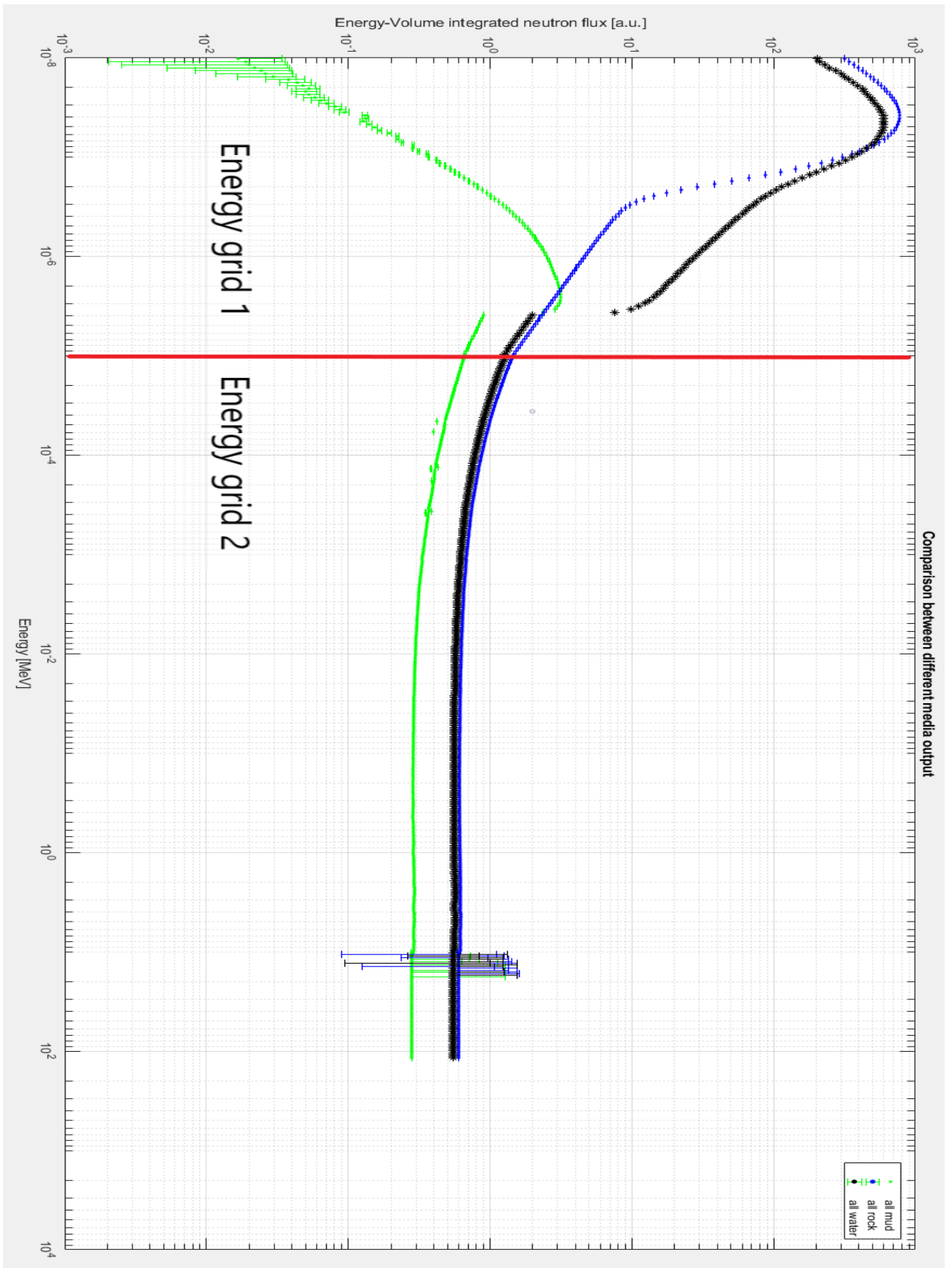


Figure 47 comparison between neutron log responses in Mud (Green), Rock (blue) and water (black). The plot is subdivided in two main parts. 1) Energy grid 1 that is from  $10^{-8}$  MeV to  $10^{-5}$  MeV, it is subdivided in 100 bins of equal lethargies. 2) Energy grid 2 is from  $10^{-5}$  MeV to 10 MeV, it is subdivided in 400 bins of equal lethargy. In ordinates is plotted Energy-volume integrated neutron flux, [a.u.], in abscissae incident energy in MeV.

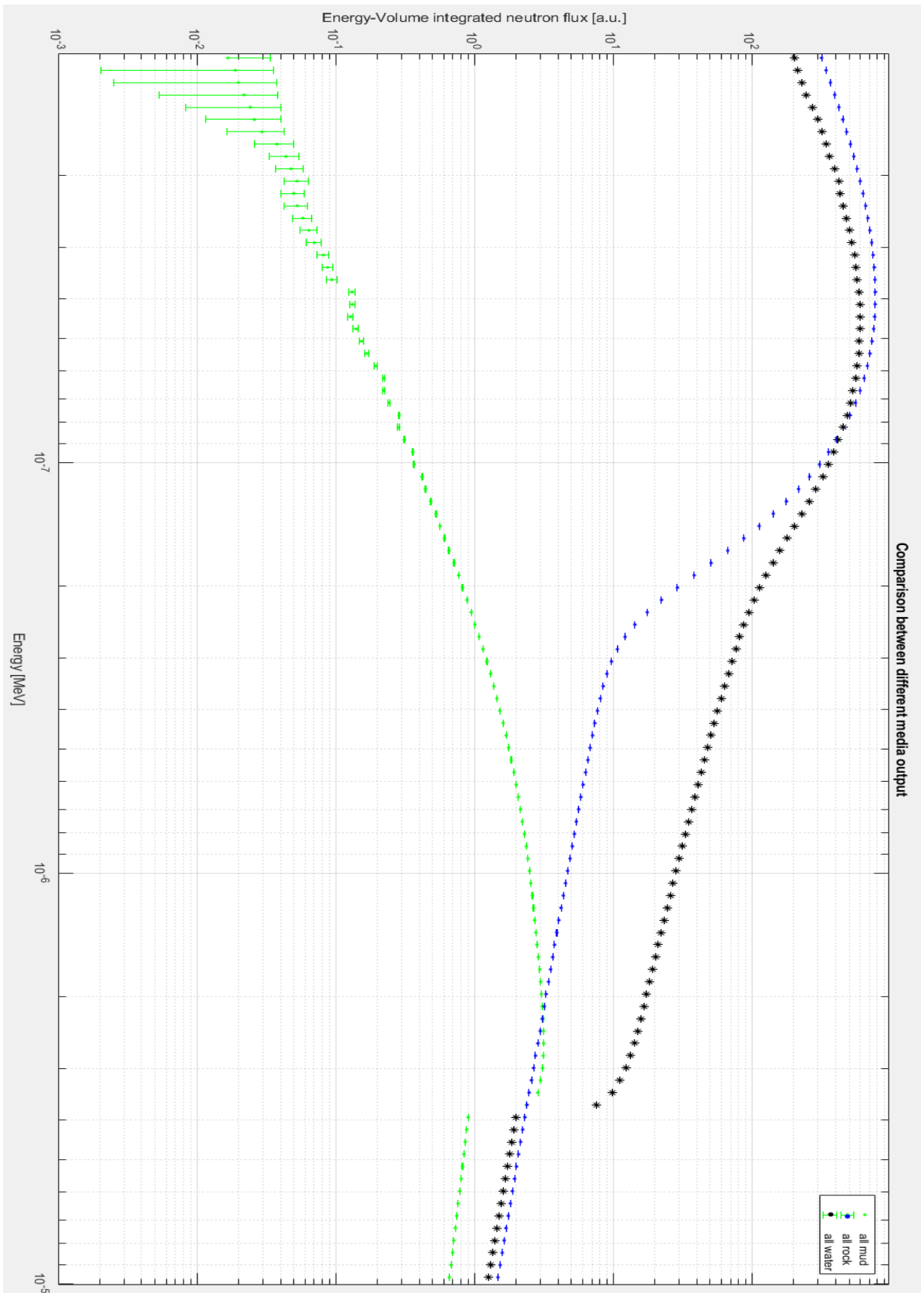


Figure 48 Zoom on Low energy region, in the plot mud(green), rock (blue) and water (black). In ordinates is plotted Energy-volume integrated neutron flux, [a.u], in abscissae incident energy in MeV.

Our thoughts were no totally wrong. From plot 47 is possible to see that water response is the almost the highest in every zone, both fast and slow neutron. Rocks shows higher response in

Thermal energy neutrons, it is possible to understand why looking at appendix C where are shown all cross-sections. Water has this response on all the spectra because Hydrogen contained in water implies a big scattering and a big thermalization of the neutrons. Interesting is that Mud presents a less response in every zone than the other two media. Mud surpass rocks just for the interval of energy that starts from  $2 \times 10^{-6}$  to  $4 \times 10^{-6}$ . Looking at appendix C we may understand that total cross sections of mud's elements is less affected by capture in this interval of energy. Rocks shown a higher capture instead. Considering the low response of the mud we may say that a comparison of data coming from wellbore drilled with mud as drilling fluid and data coming from a wellbore drilled with water is very difficult, and almost un-interpretable. We may see that in Thermal neutron zone, between 0.001eV and 0,1eV, the response of the detector highlights how water thermalize less than rock. Looking at the cross-actions in appendix C is possible to understand why. Oxygen and Carbon contribute to thermalize neutrons. Calcium contained in rock has a big capture cross section for thermal energies. That implies neutrons cannot arrive in this zone because are absorbed before. The response of mud, in thermal energy, is low. Mud Composition allows to understand why. Mud contains Hydrogen, as water, so the logic expectation was to find the curve of the mud between rock and water. Analysing cross section of mud components, in attachment, we can see that in mud there are strong absorbers, like Ba, Cl, S and K. Their presence in mud is huge and for this reason they influence in a big way the response of the neutrons. Now, looking for epithermal neutron, also these neutrons are considered in log analysis. Epithermal means neutrons with energy between 0,1 eV and 100eV. Is possible to see that while the respective position of the mud curve remains the same, that of water respect to rock is changed. In this part of the plot rock shows the highest response. A possible explanation would be that, looking the attachment, the capture cross section of Ca. This cross section causes less contribute to the total cross section of Ca for the energy interval taken in consideration. So, more neutrons are scattered and are detected by our detector. Mud present an increasing trend in this part of the plot. The answer is the same. Its components have a capture cross section that contributes less to total cross section. Hydrogens has a good capacity in doing collision with big loss of energy. Probably collisions in that interval of energy make huge loss of energy and every media containing Hydrogen shows it. The trend is in any case mud under water, but rock gives the highest response. Again 0,4 eV water and rock give the same response until reaching 2eV. Here, for both, mud and water we might notice for a jump. This discontinuity as will be shown in all the other simulation is due to Hydrogen probably. Zooming in this region, for the plot of water we obtain figure 49:

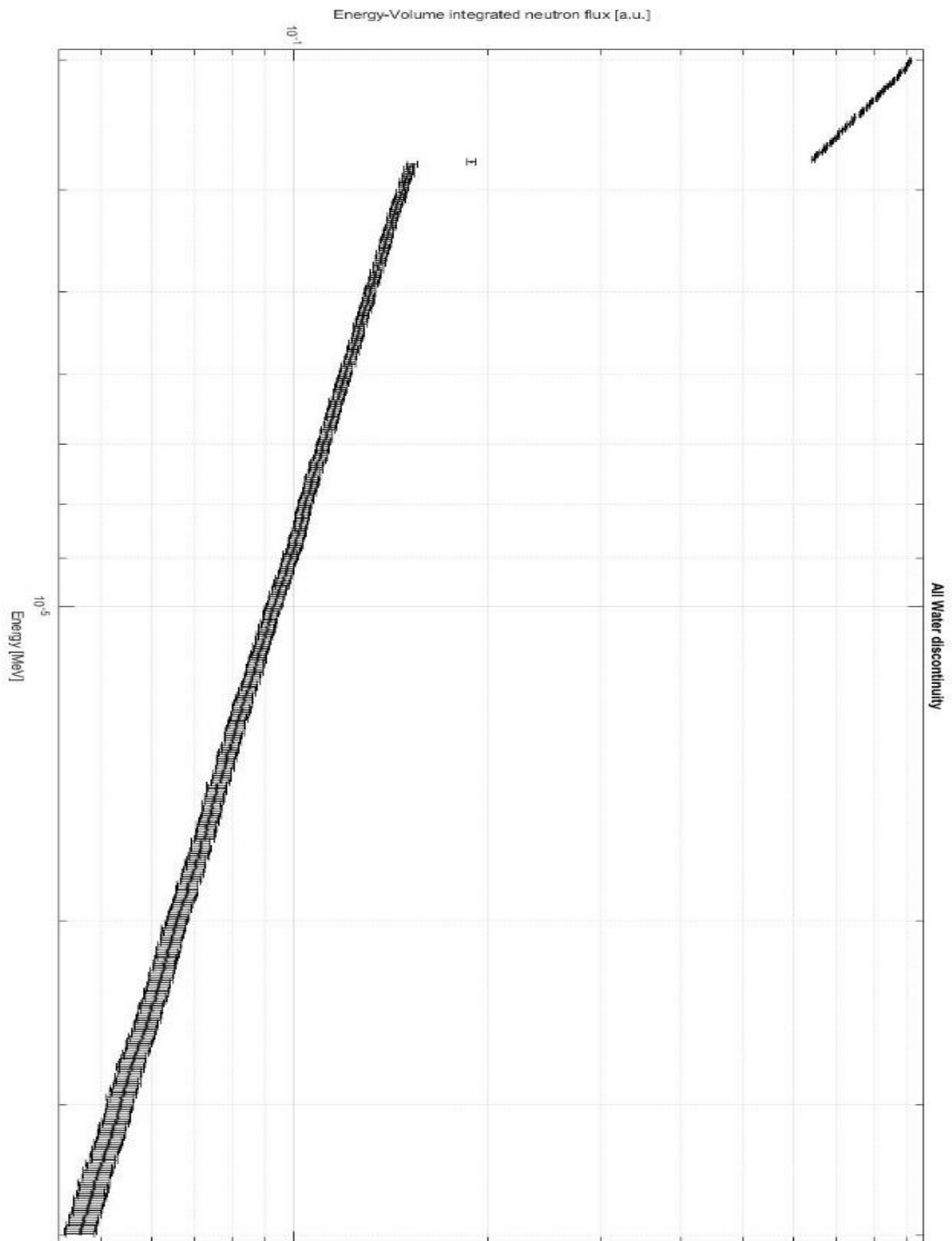


Figure 49 Of the discontinuities shown all the previous plots. In ordinates is plotted Energy-volume integrated neutron flux, [a.u], in abscissae incident energy in MeV. The point in the middle of discontinuity makes the phenomenon explainable.

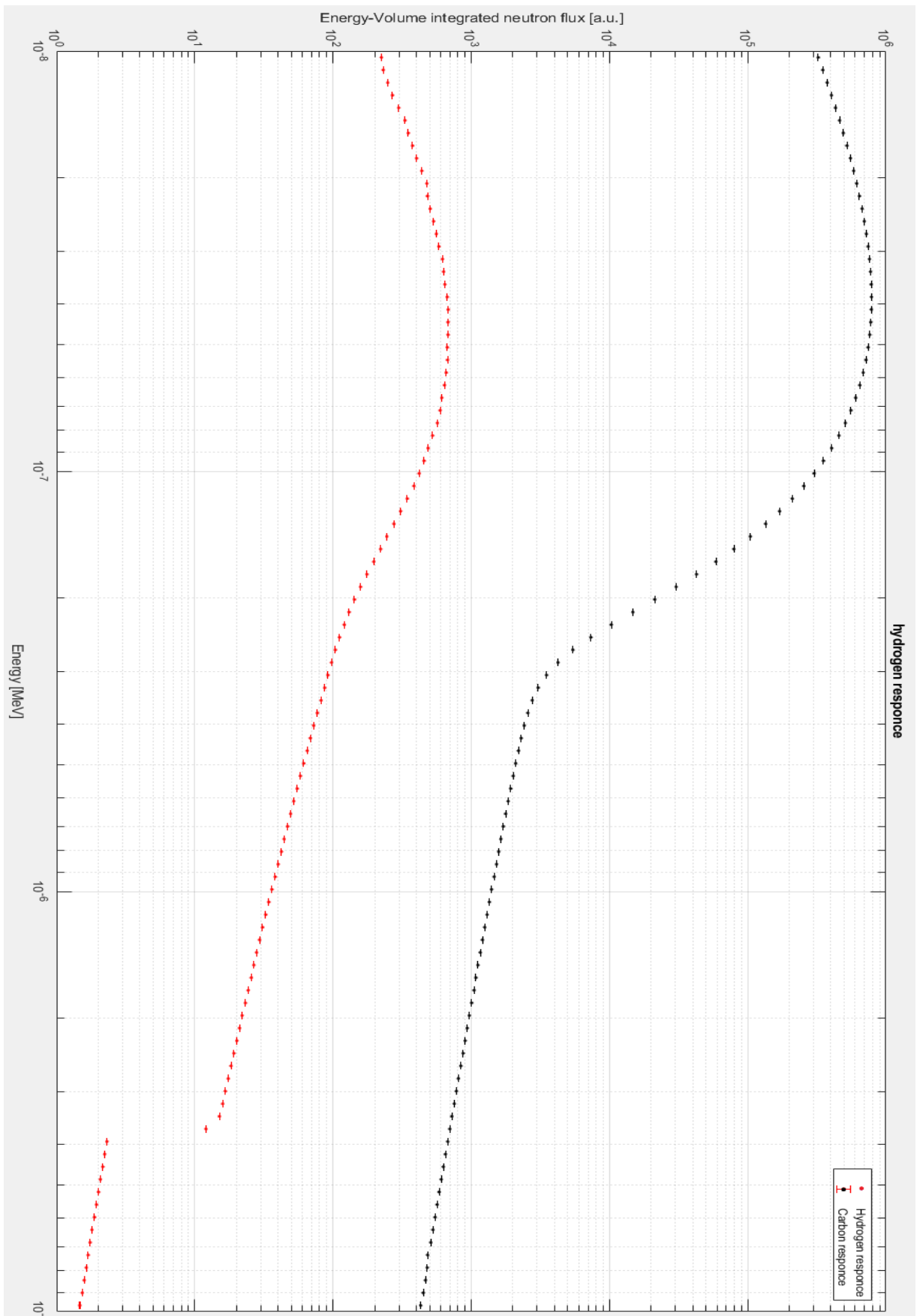


Figure 50, comparison between tool response immersed in 100% of Hydrogen and 100% carbon. The Red line is the response of Hydrogen, the black one is the Carbon response. We may see that the response of Carbon does not present discontinuity in its profile. In ordinates is plotted Energy-volume integrated neutron flux, [a.u.], in abscissae incident energy in MeV.

Figure 49 shows the discontinuity.

Figure 49 is the output of another simulation. This simulation was implemented for water only, but just for simplicity. We expected that the physical explanation was the same for all fluids showing the same jump. To reach output in figure 49 we did a more accurate discretization of the interested interval of energy.

The presence of detected neutrons between the discontinuity make the hypothesis of Hydrogen effect more realistic This trend will be followed also in fast neutrons zone. The last part of the plot presents a big scatter, due to its huge standard deviation. For us is meaningless.

To be sure that the discontinuity is due to Hydrogen presence we performed a simulation.

It is shown in figure 50.

The tool was supposed to be immersed into a media composed by 100% of Hydrogen and compered it with a simulation where the tool was within 100% of Carbon. In figure 53 are represented the behaviour of the detector response while immersed in a medium composed by 100% of Hydrogen. The response of Hydrogen shown a discontinuity in the range of 4 and  $5 \times 10^{-6}$  MeV. It is perfectly coherent with the discontinuities presented by all the other simulations that contains materials with Hydrogen in their compositions.

Looking at the Carbon profile response we may notice that in its behaviour the discontinuity is not present. Hence, we might say that the only one element that contributes that discontinuity is Hydrogen.

Hence, the discontinuity is due to collision with Hydrogen atoms. In this collision the main scattering involved is elastic scattering. It implies big loss of energy for the neutron. This big loss of energy is correlate to the Hydrogen mass. It is almost the same to neutron mass. During the collision most of the neutrons arrive at very low energies, thermic and epithermal energies. In this zone they reach the Thermic equilibrium which determines an almost gaussian distribution. For High energy is possible to see a neutrons tale and this is explainable considering all the un-elastic or non- perfectly elastic collisions made by neutrons with Hydrogen atoms.

Another interesting comparison is that between reservoir fluid, so water, gas and oil. The MATLAB output is attached. The output of geometrical plotting for oil and gas is fig 52 and 52.

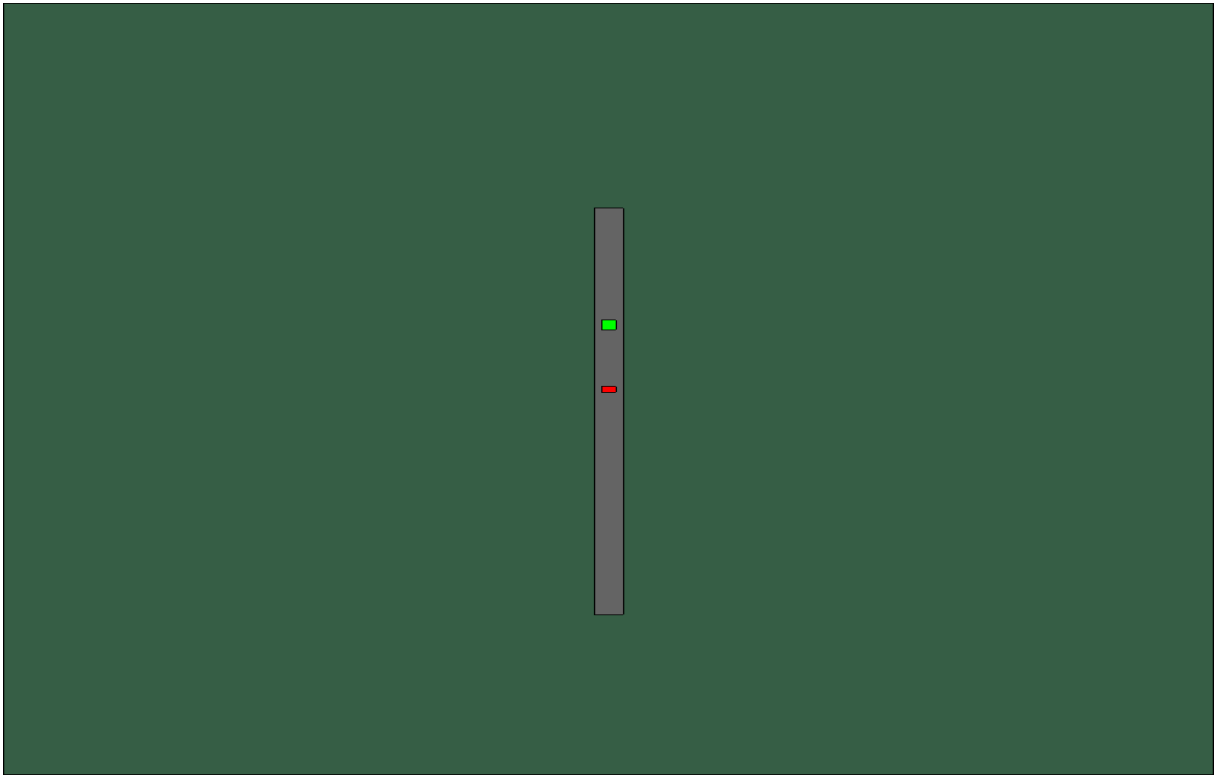


Figure 51 Tool in homogeneous isotropic infinite body of oil. Vertical prospect.

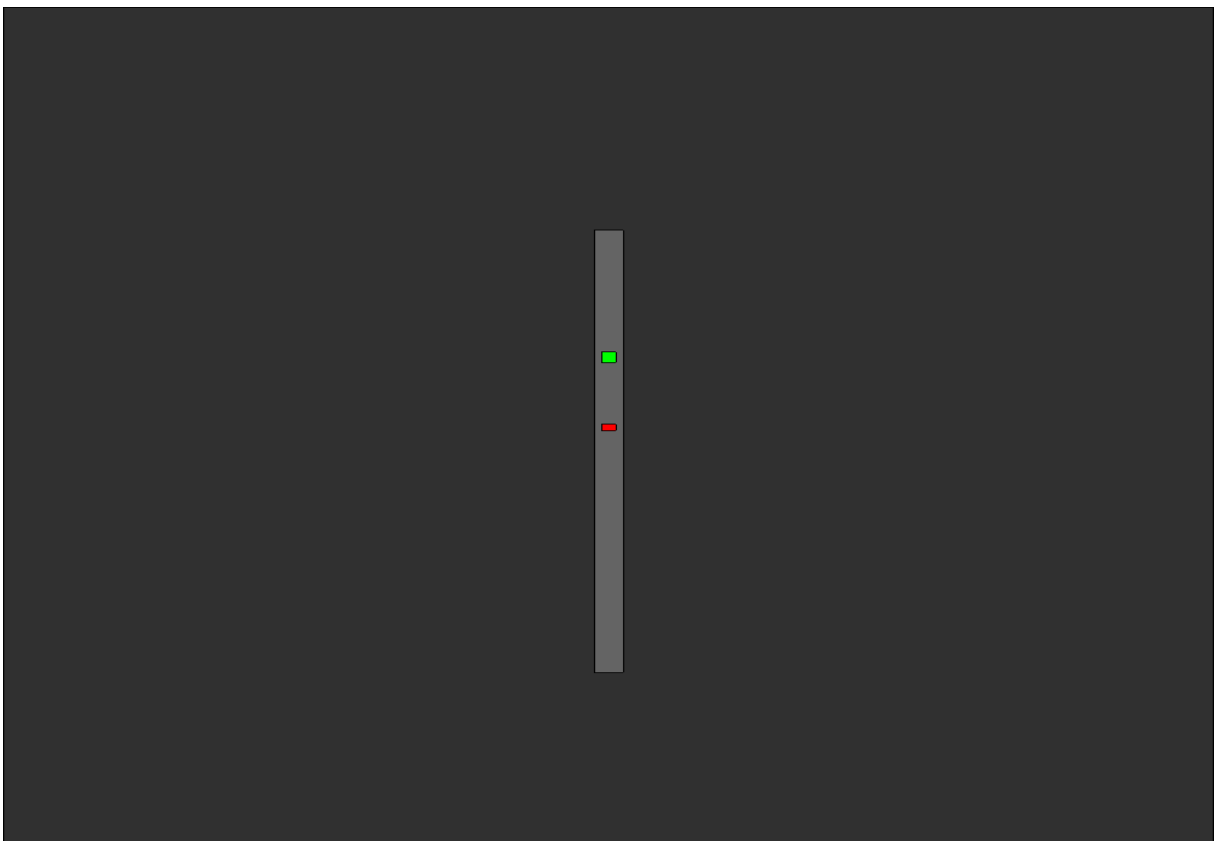


Figure 52 Tool in homogeneous isotropic infinite body of gas. Vertical prospect.

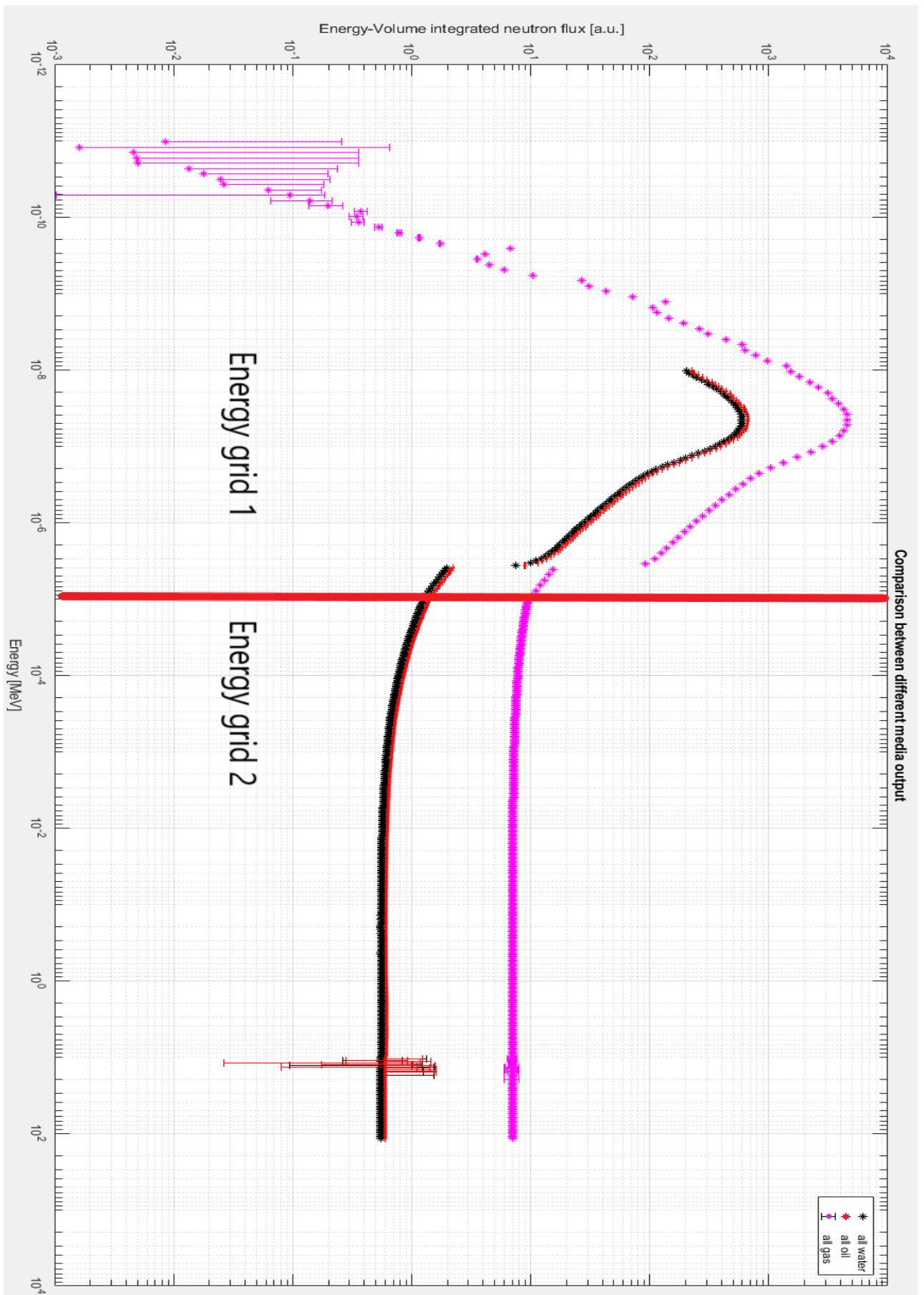


Figure 53 Comparison between neutron log responses where, water (black), oil (Red) and gas (purple). In ordinates is plotted Energy-volume integrated neutron flux, [a.u], in abscissae incident energy in MeV.

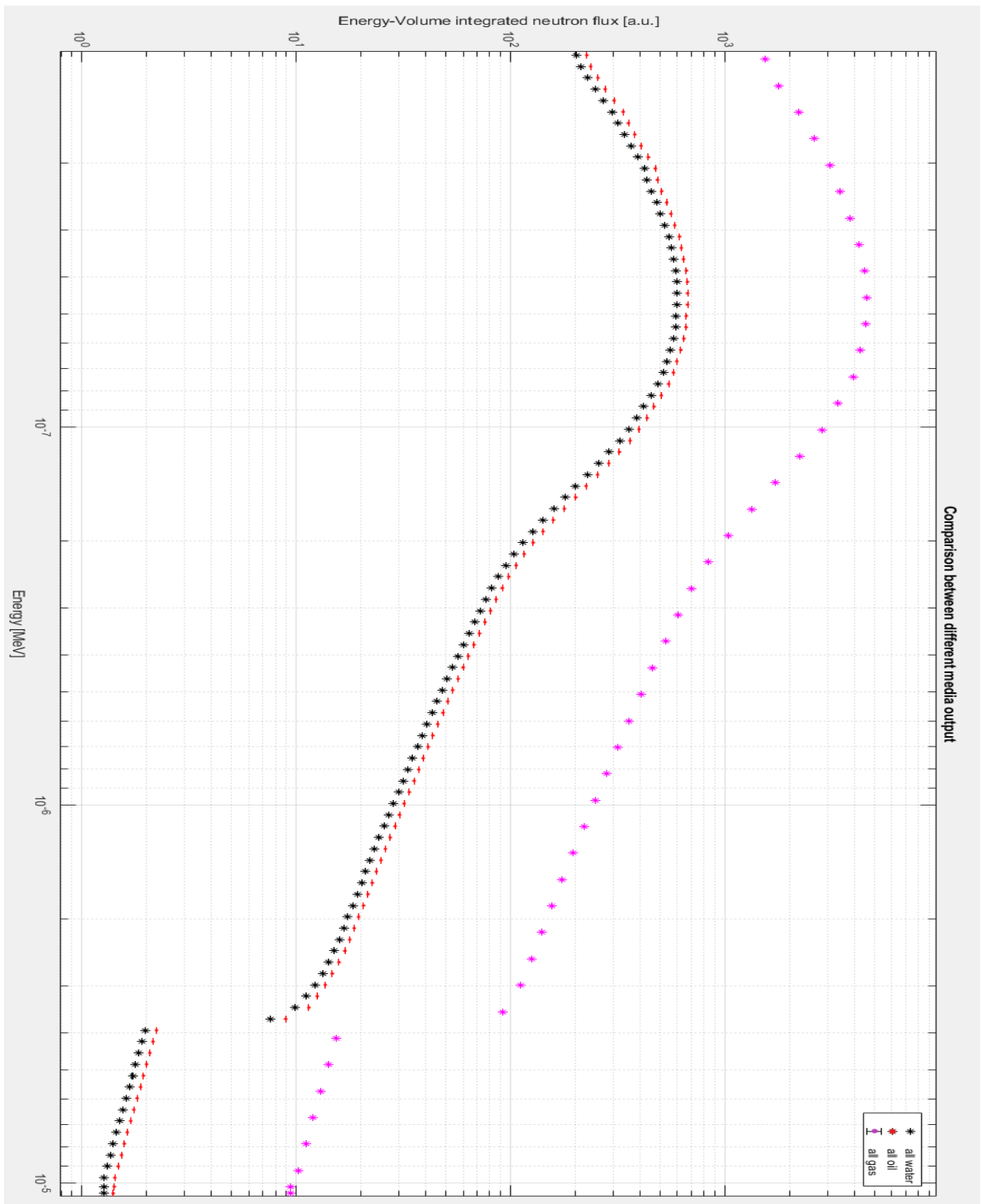


Figure 54 Zoom of neutron tool response in low energy zone. Water (black), oil (red), Gas (purple), In ordinates is plotted Energy-volume integrated neutron flux, [a.u], in abscissae incident energy in MeV.

First, the curve of gas response starts from  $10^{-12}$  MeV. Our purpose was to see the behaviour of the response for very low energy neutrons. At the end, I had no time to simulate everything in this interval of energy. Gas simulation that was the last done in order of time is the only that presents such energy interval. In any case is possible to do a comparison between the media response plotted in figure 53. All the media contain Hydrogen; water contains 11%, petroleum 20,59% and gas 0.25%. This is not the only difference between these fluids. Water has Oxygen

while methane and oil contains Carbon. Carbon is smaller than Oxygen, hence, its collision with neutron, in terms of elastic scattering, are more efficient. The response shown in figure 54 was attended, even though the response of gas is higher than our prevision. Gas and Oil have almost same amount of Hydrogen and Carbon. Their difference is about density. Methane at reservoir condition has almost half density of our petroleum. For better appreciate de difference between Oil and water we show figure. Is possible to see that oil presents a high response than water. Indeed, the oil which we modelled owns more Hydrogen than water, so reminding chapter 2.4.1 has a HI higher than 1. That means in theory that when the tool finds water and petroleum, porosity will be high in petroleum formations. If we have a porosity profile for water and oil would be possible do understand exactly which fluid is that filling the formation. The High response of petroleum is due to carbon also, that scatter better and adsorb less than Oxygen, is possible to look on attachments. The shape of the three courses is similar and presents the discontinuity discussed above. All three contained Hydrogen.

Once analysed the response of the tool in mono-homogeneous layer we may understand better the tool response in simulation with more than one media. The first two simulation run are also the easiest. Our neutron log tool in a water filled borehole drilled in a 0-porosity rock, and the same tool but with the borehole filled by mud. The geometrical plots are figure 55 and 56.

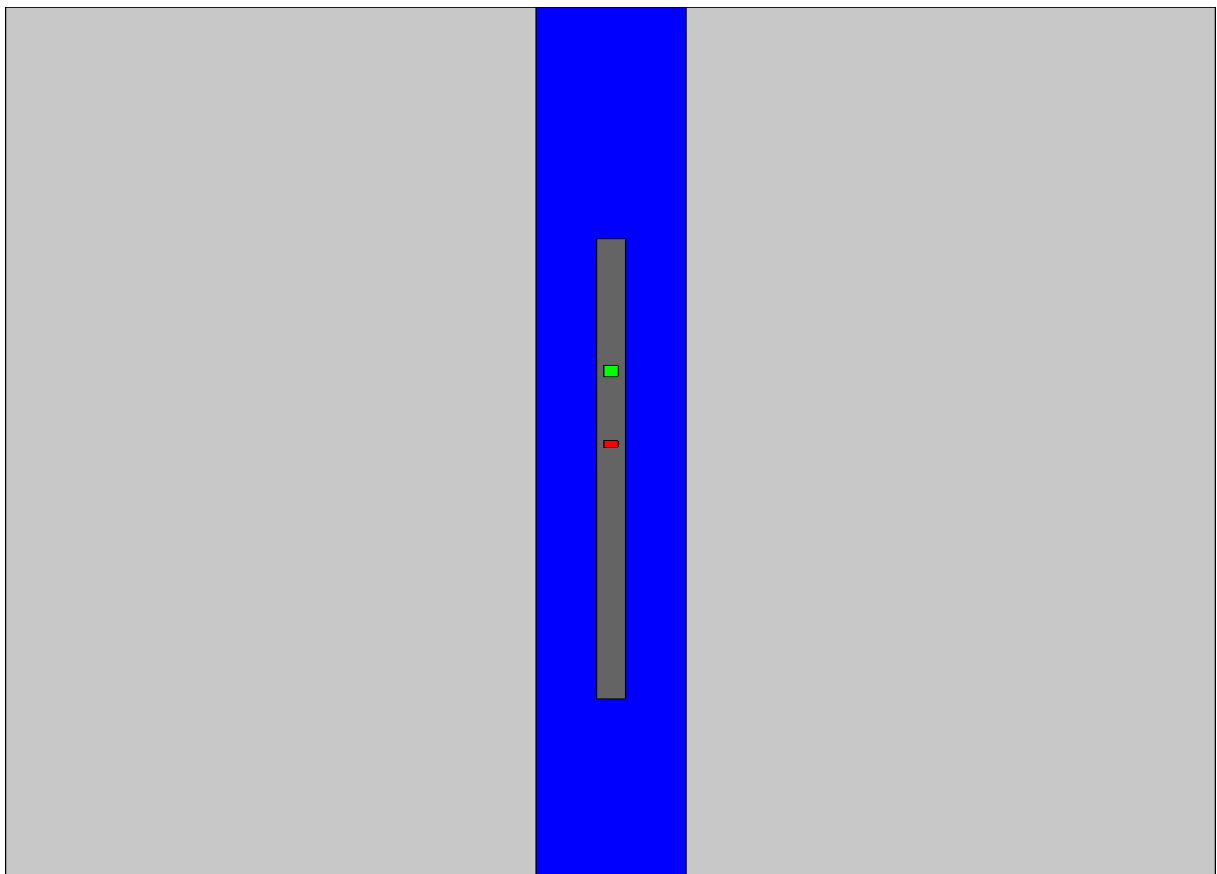


Figure 55 Neutron log tool within a borehole filled with water, the borehole is drilled, Vertical prospect.

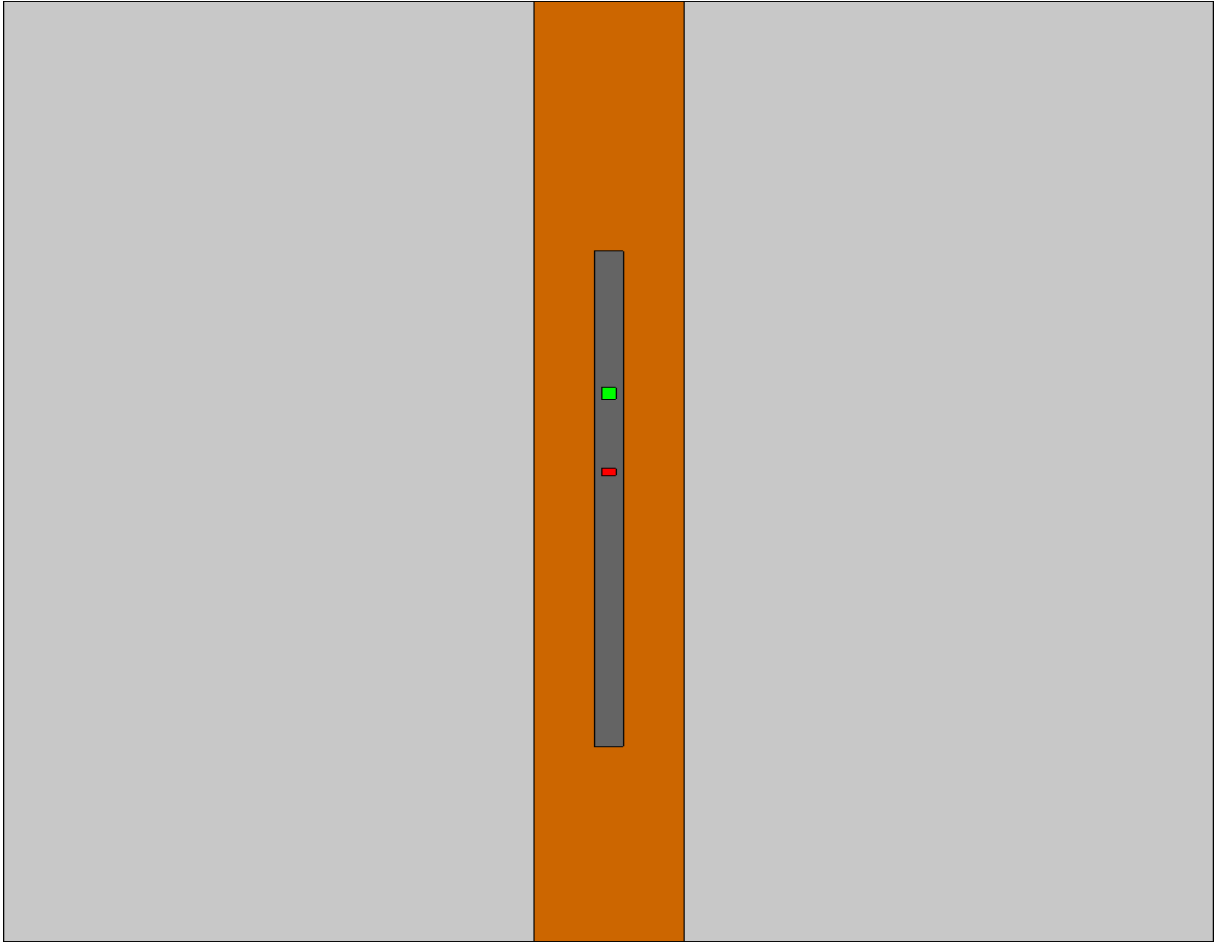


Figure 55 Neutron log tool within a borehole filled with mud, the borehole is drilled, vertical prospect.

The comparison between them two but also a comparison between the drilled one and the not one is going to be interesting. For sure our expectation is that the drilled one will have a lower response than that of the tool surrounded by the same media. For water the response must be lower, because rock adsorbed more than its. So, at the detector we cannot find the same count rate. For mud the discussion is different. Mud presents a lower response than rock for both, thermal and epithermal neutrons. So, if the same thinking of water is done for mud we attend for a higher response when the tool run in drilled condition. Figure show the comparison between mud filled borehole and water filled borehole. It is immediately evident that between them two, in thermalized neutron zone, there are two orders of magnitude. While if we look figure is possible to see that the orders of magnitude are 4. So, rock affects the response of mud increasing its value in thermalized zone. In any case was expected that mud curve layers below water curve. Their composition is always the same and consideration about cross section are always valid. In epithermal zone is possible to appreciate the effect of rock, the shape of both curve is different from those in homogeneous media. We can notice that in this case there is a higher response in epithermal neutrons. The discontinuities are always present while in fast neutron zone the two curves almost superimpose.

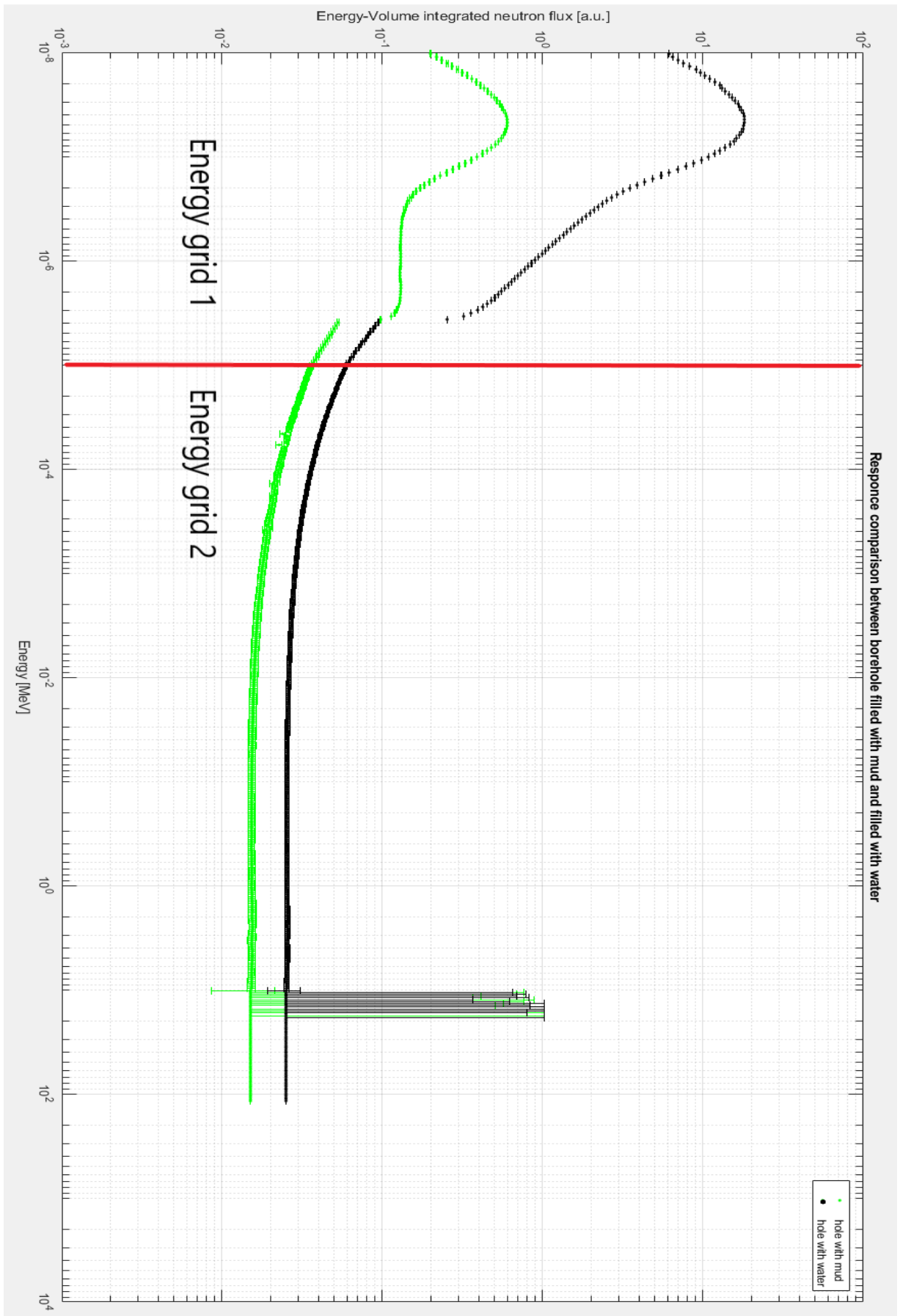


Figure 56 Comparison between mud filled borehole (green) and water filled borehole (black), In ordinates is plotted Energy-volume integrated neutron flux, [a.u.], in abscissae incident energy in MeV

Comparing now the curve in pure media and in drilled media we may see in figure 57:

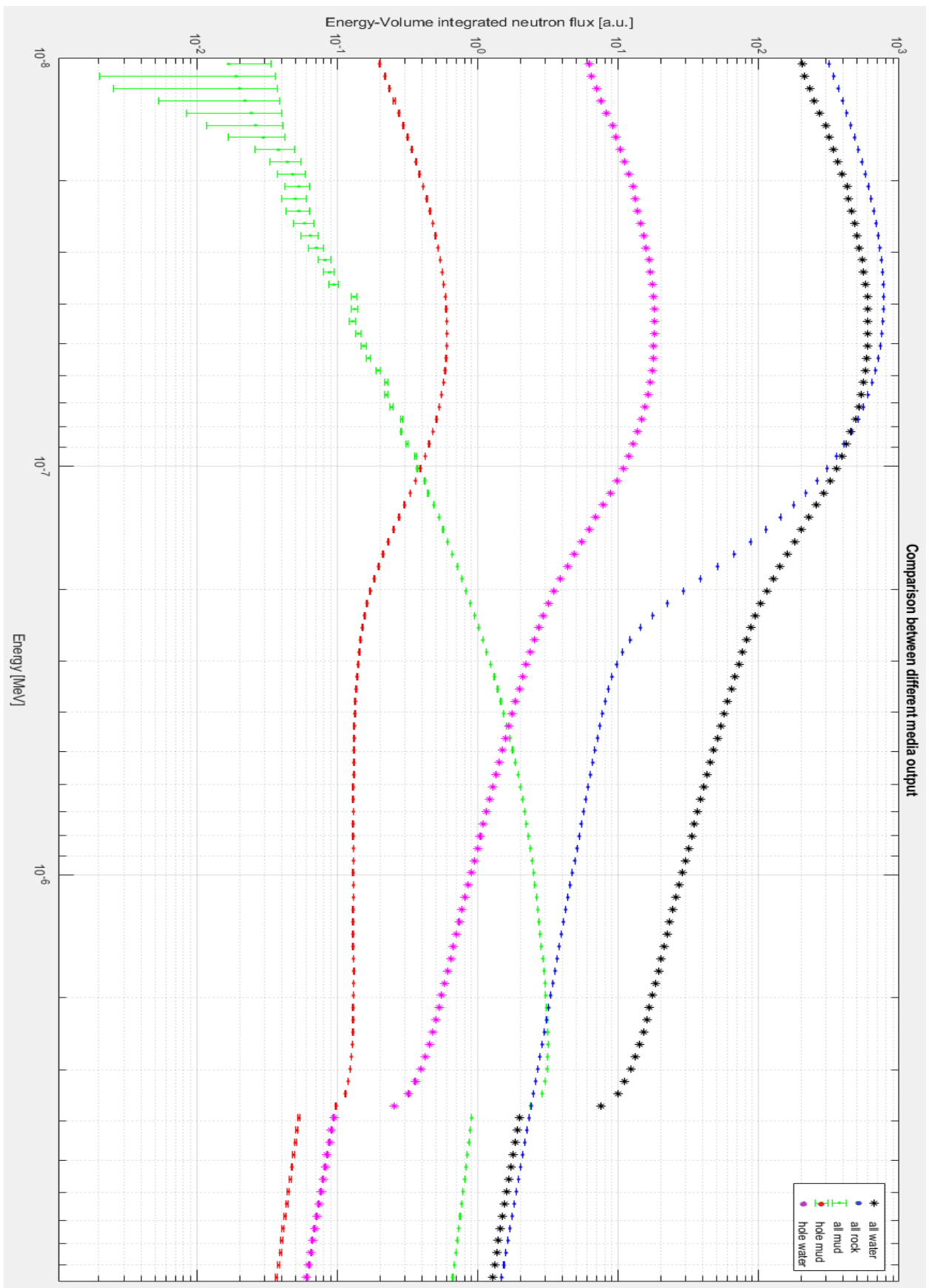


Figure 57 Comparison among body of pure water (black), body of pure rock (blue), hole with mud (red), Hole with water (purple) and a body of pure mud (green), In ordinates is plotted Energy-volume integrated neutron flux, [a.u], in abscissae incident energy in MeV

The consideration done were all correct. Drilled rock with the borehole filled with mud presents a higher trend than tool running in only mud. More Thermalization due to rock component but also there are less absorbers in absolute value. The trend of drilled rock filled with water and pure water is almost the same. Is possible to see the shifting of the curve in epithermal zone, this is due to rock. Comparing the pure rock curve and the other we can see that the shifting in epithermal zone is due to rock indeed.

All the simulation done until now are carried out with the tool centred in the hole, when hole is present. We tried to push the tool on the wall of the wellbore. The purpose was to increase vertical resolution of our instrument. The geometrical plot output is figure 58 and 59.

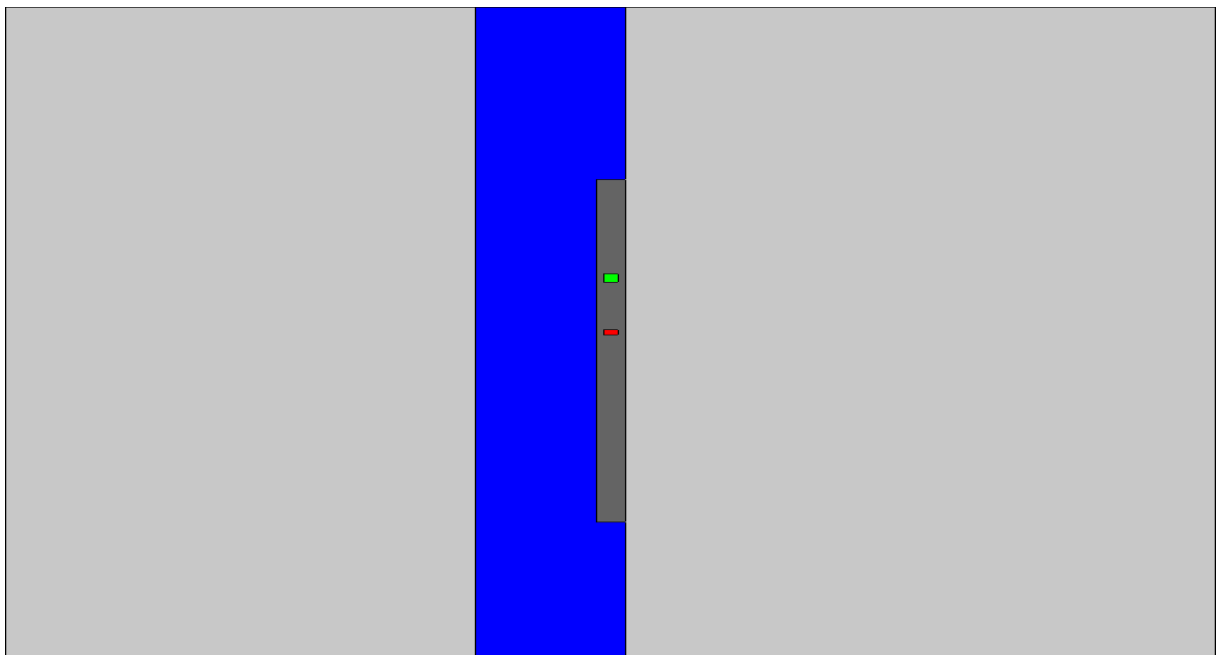


Figure 58 wall pushed tool within water filled borehole

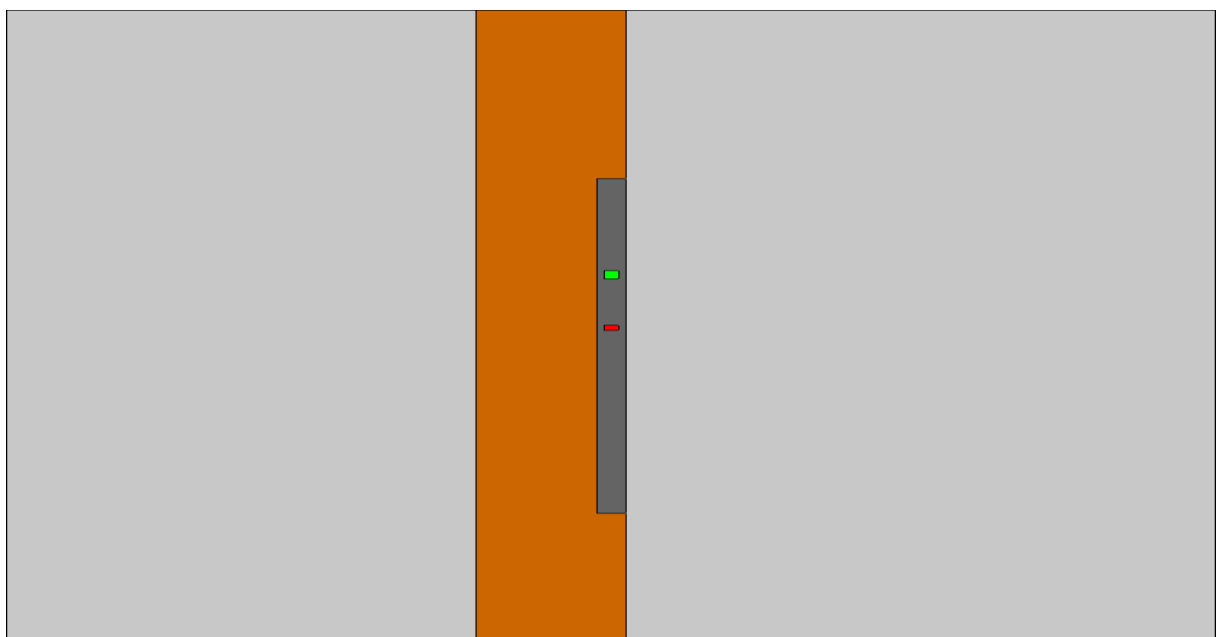


Figure 59 wall pushed tool within mud filled borehole.

Their response is plotted on MATLAB, the comparison between central and wall size is in fig 60:

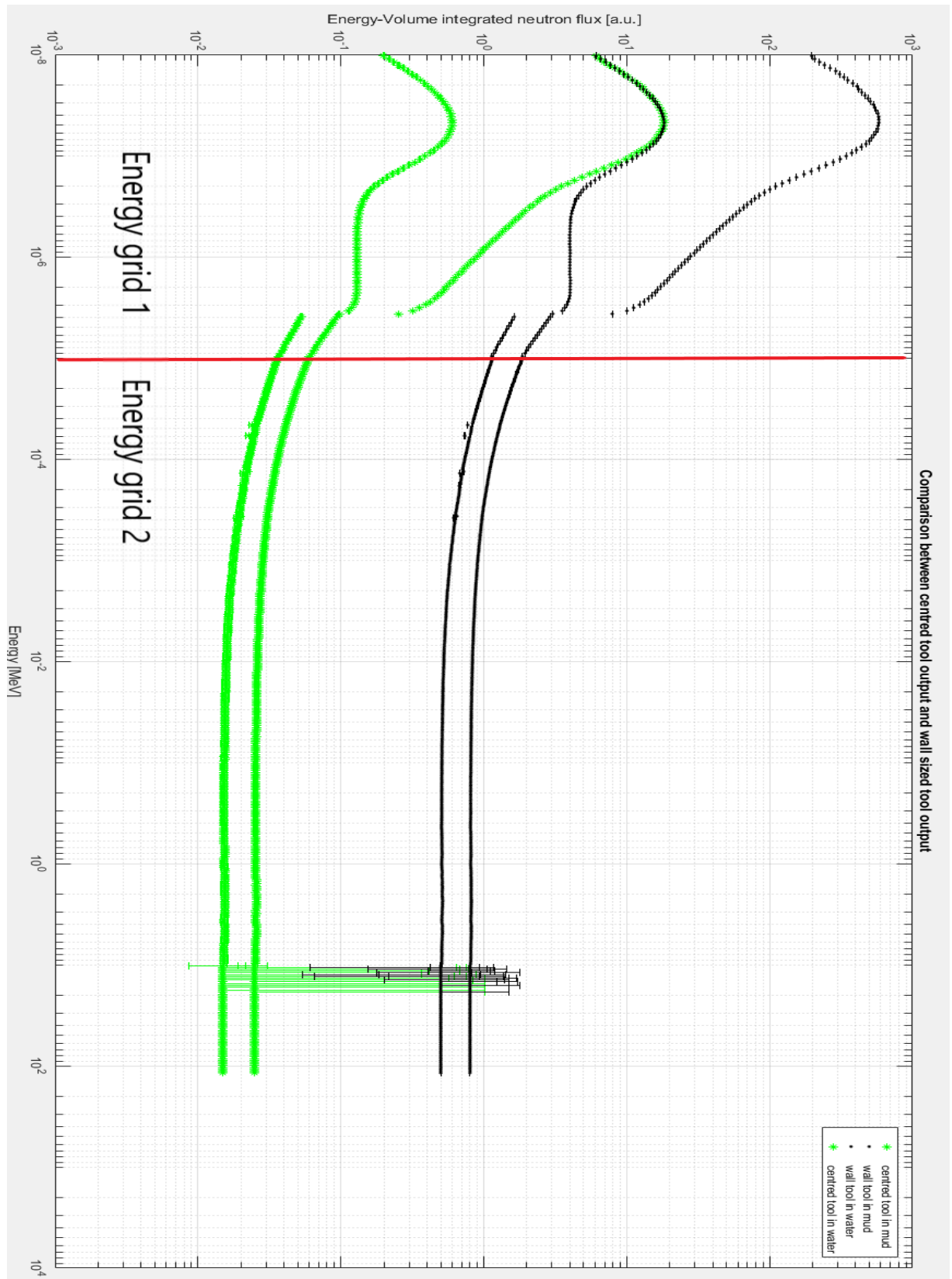


Figure 60 comparison among wall side tool (.) and centered tool (\*). Wall side and centered side configuration are done both for water filling fluid and mud filling fluids. In ordinates is plotted Energy-volume integrated neutron flux, [a.u], in abscissae incident energy in MeV

A huge difference among wall tool simulations and centered tool simulations. For both types the trend shown in figure 60 is the same. Hence, when the tool is pushed against the wall the signal in both cases is higher than when the tool is centered in the borehole. We may say that borehole effects tend to decrease the resolution and the reliability of the instrument. To understand how the variation due to borehole filling fluid influence the measurement, a comparison between wall sized tool simulation and tool immersed in 100% rock is shown in figure 61.

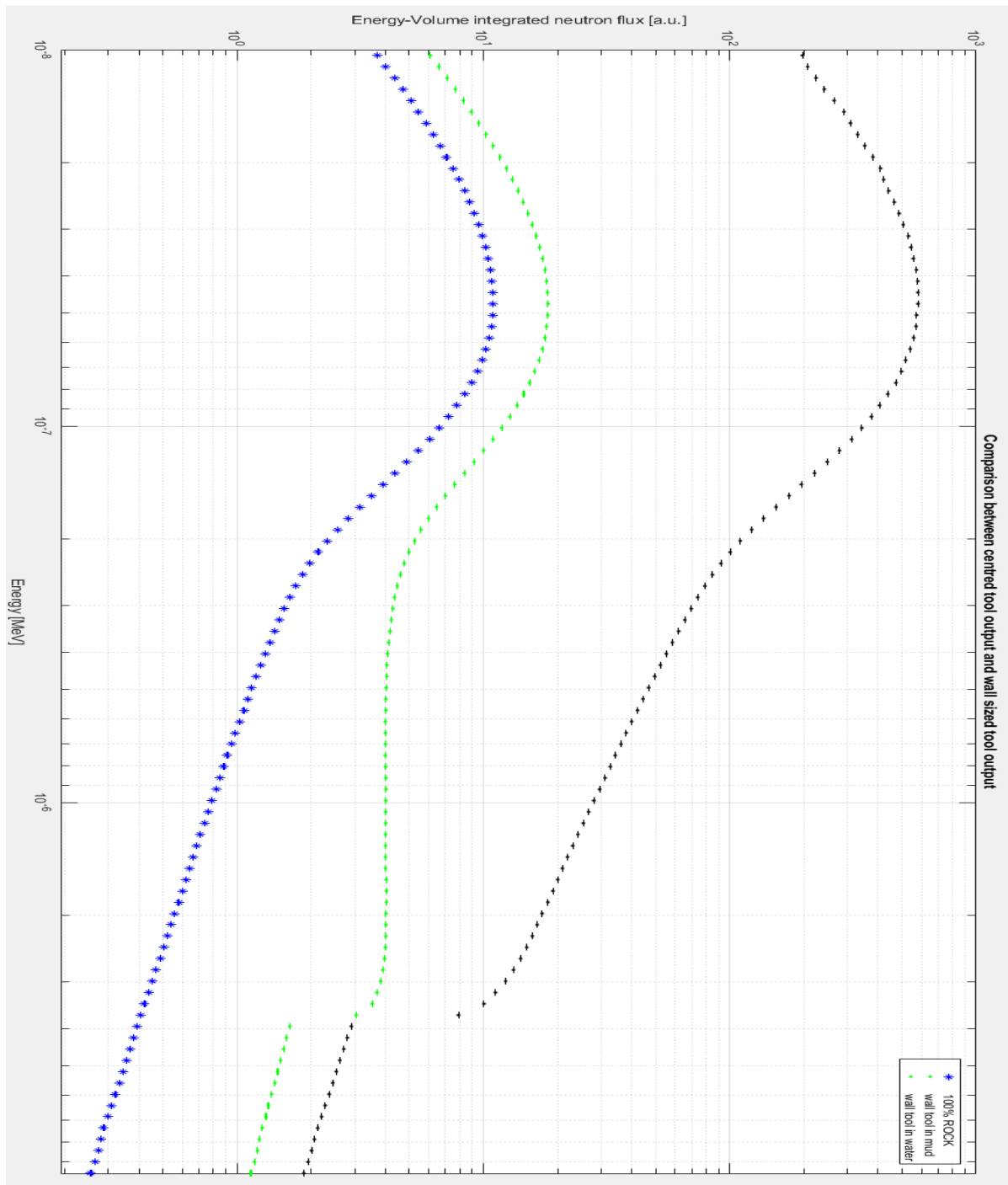


Figure 61 Zoom of figure 60 on thermal energy zone, the zoom has the scope to highlight the differences among the curves. In ordinates is plotted Energy-volume integrated neutron flux, [a.u], in abscissae incident energy in MeV

Understood how detector response behaves in pure media and then in borehole filled with a single fluid we move through comparisons on porous media. Porous rocks are filled by different fluids and present different porosities. The first comparison of these types of simulation is that of water saturate porous rocks. We did simulation on rocks with variable  $\phi$ . Since the scope of the thesis is explained how neutron count might be linked to effective porosity, we tried to understand, firstly, if there are correlations and coherences between porous media with different porosities but filled with same fluid. The chosen fluid is water. We chose three porosities to make a comparison.  $\Phi=15\%$ ,  $\phi=30\%$  and  $\phi=50\%$ . Porosities are saturated by pure water. The rock body is again Calcite. Wellbore is filled with water. To make a visible difference on geometry plots of these simulation we choose an increasing blue for increasing porosity. The results are in figure 62, 63 and 64.

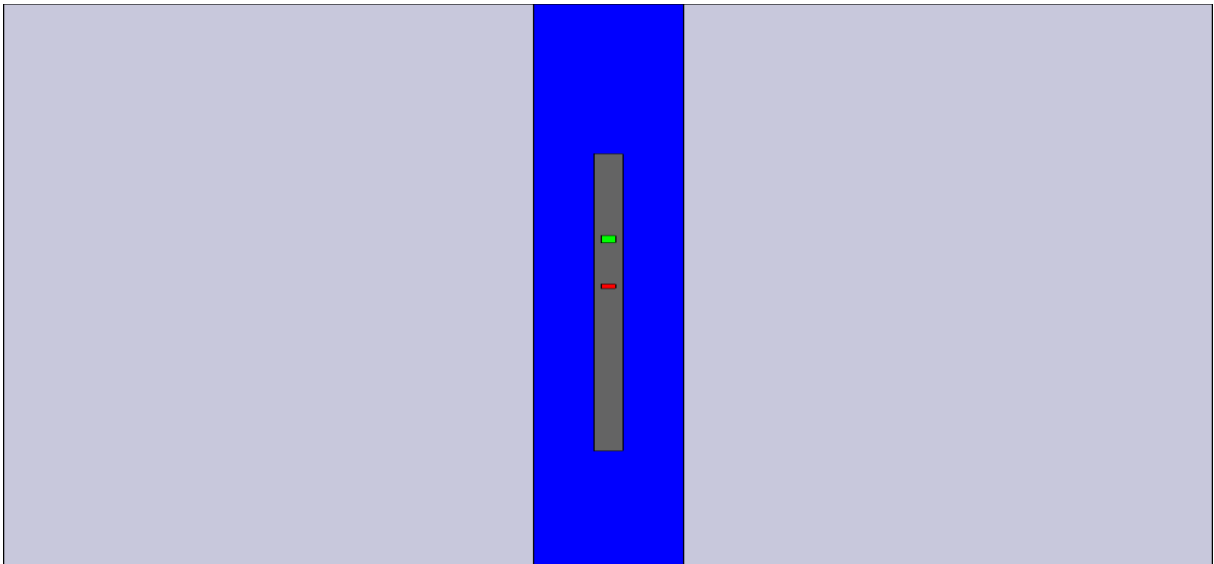


Figure 62 wellbore filled with water and rock with  $\phi=15\%$ , Vertical Prospect.

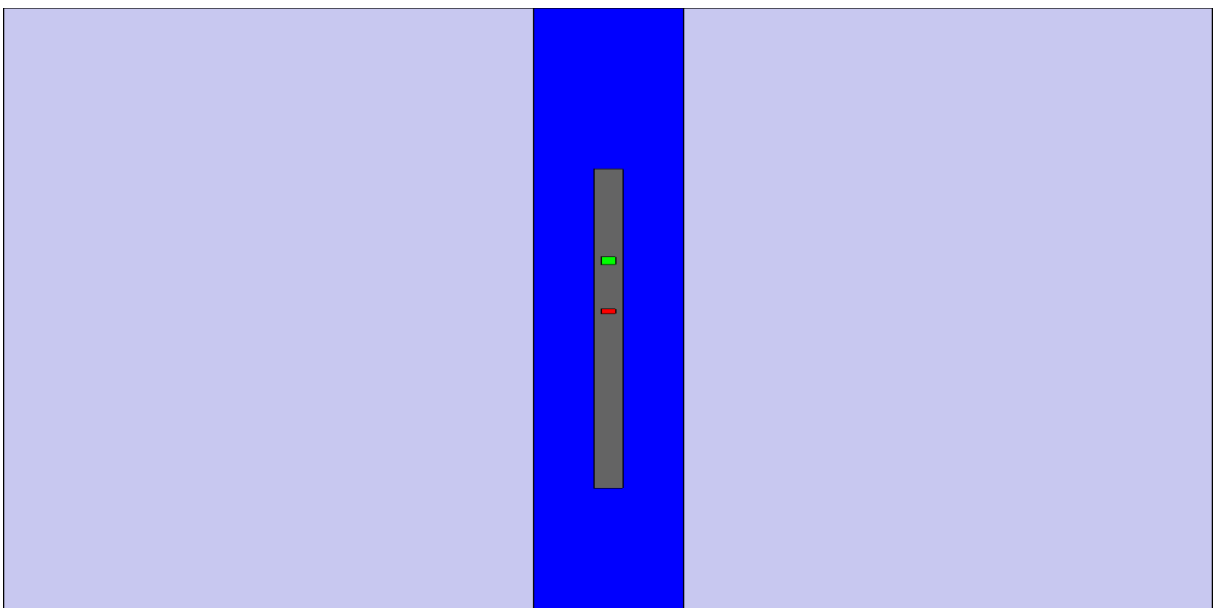


Figure 63 wellbore filled with water within a rock with  $\phi=30\%$ , Vertical prospect.

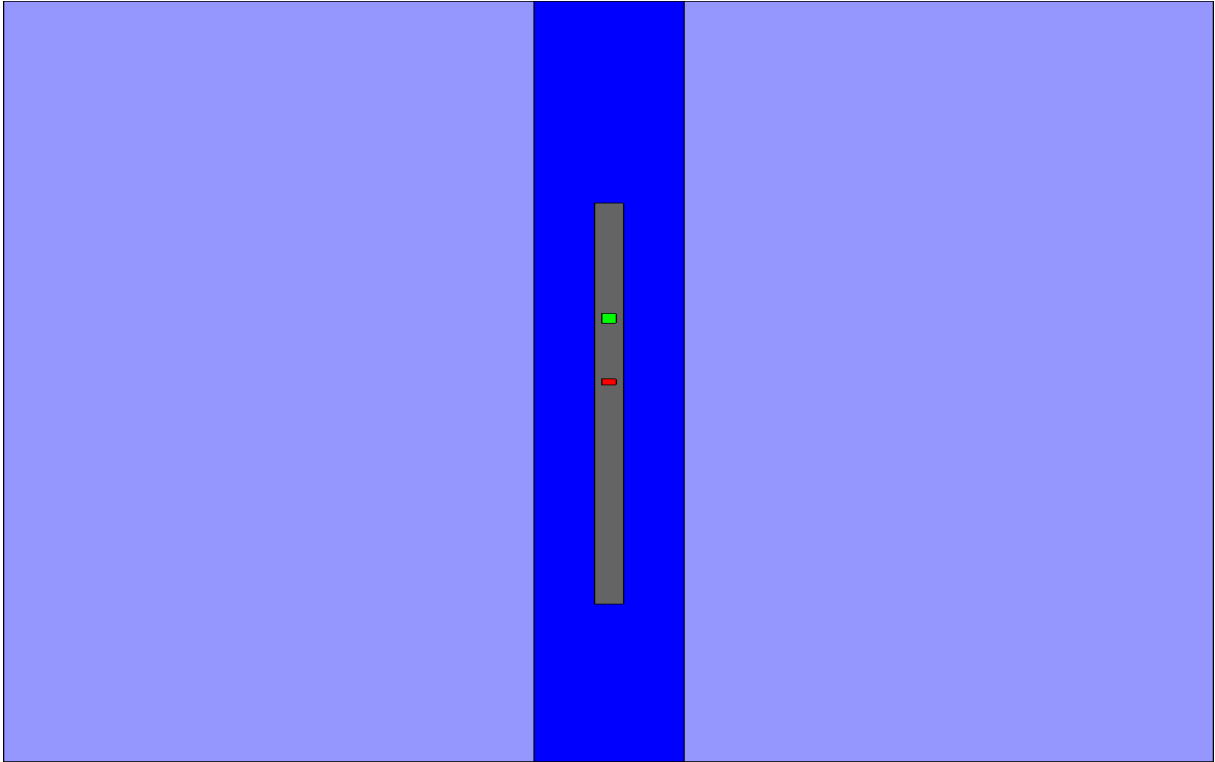


Figure 64 borehole filled by water within a rock with  $\phi=50\%$ . Vertical prospect.

Every simulation output is attached, for these simulations look attachment in appendix D.

The attended response is a detector output that presents higher value, of thermalized neutrons, while porosity is increased. So, the higher pick should be rock with porosity of 50% and then decreasing. A qualitative output plot is shown in figure 65. 50% porosity was an exaggeration, just to highlight the differences.

We may see that there is not a huge difference between the curves, at the first quick look they look like a single line. So, is already possible to say that all the differences are in a small range of neutron count. The zoom needed to appreciate the differences between the response does not permit to see all the envelope of the curve. Just some points are shown, for different range of energy. The plot in figure 70 we may see that rock with porosity of 15% shows the high response at the detector, while 30% porosity the lowest. Our attendance was something different. If we move following points we reach  $2,5 \times 10^{-6} \text{MeV}$ , here the trend changes. We are in epithermal zone. In this part of the plot the higher response it that of  $\phi=50\%$ . While  $\phi=30\%$  remains still the lowest response. This is shown in figure 71. This kind of response was not attended. We may say that in these conditions there is a value of porosity under which borehole fluids effects weight more than porosity change. We need so a comparison between media without borehole. To understand the real effect of porosity, without any influence of the borehole. Than making a comparison between pure rock, pure water and different porosities we will make further consideration.

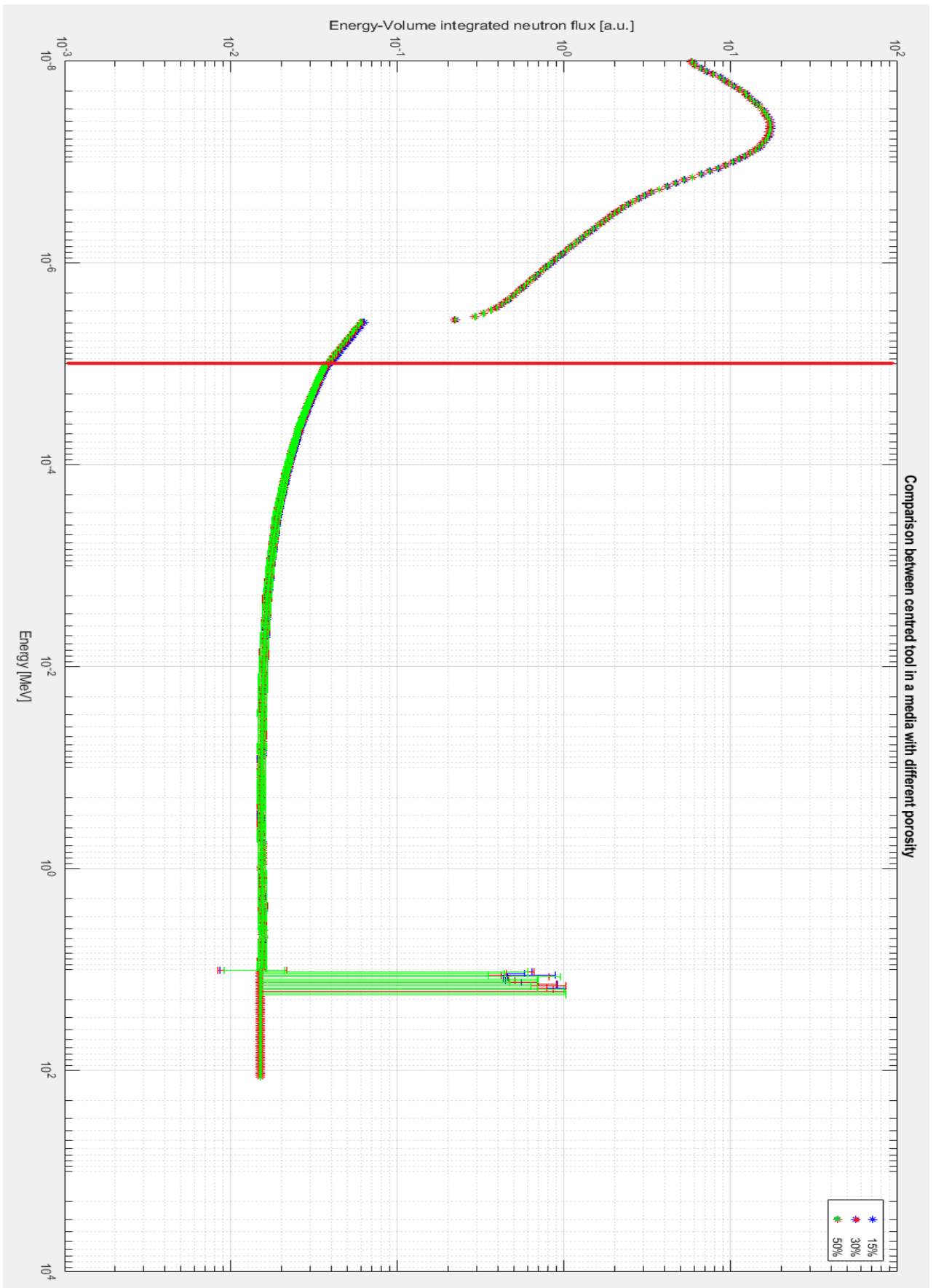


Figure 65 comparison on different porosity media response, calcite with 15% of porosity (blue), Calcite with 30% of porosity (red), Calcite with 50% of porosity (Green). In ordinates is plotted Energy-volume integrated neutron flux, [a.u.], in abscissae incident energy in MeV

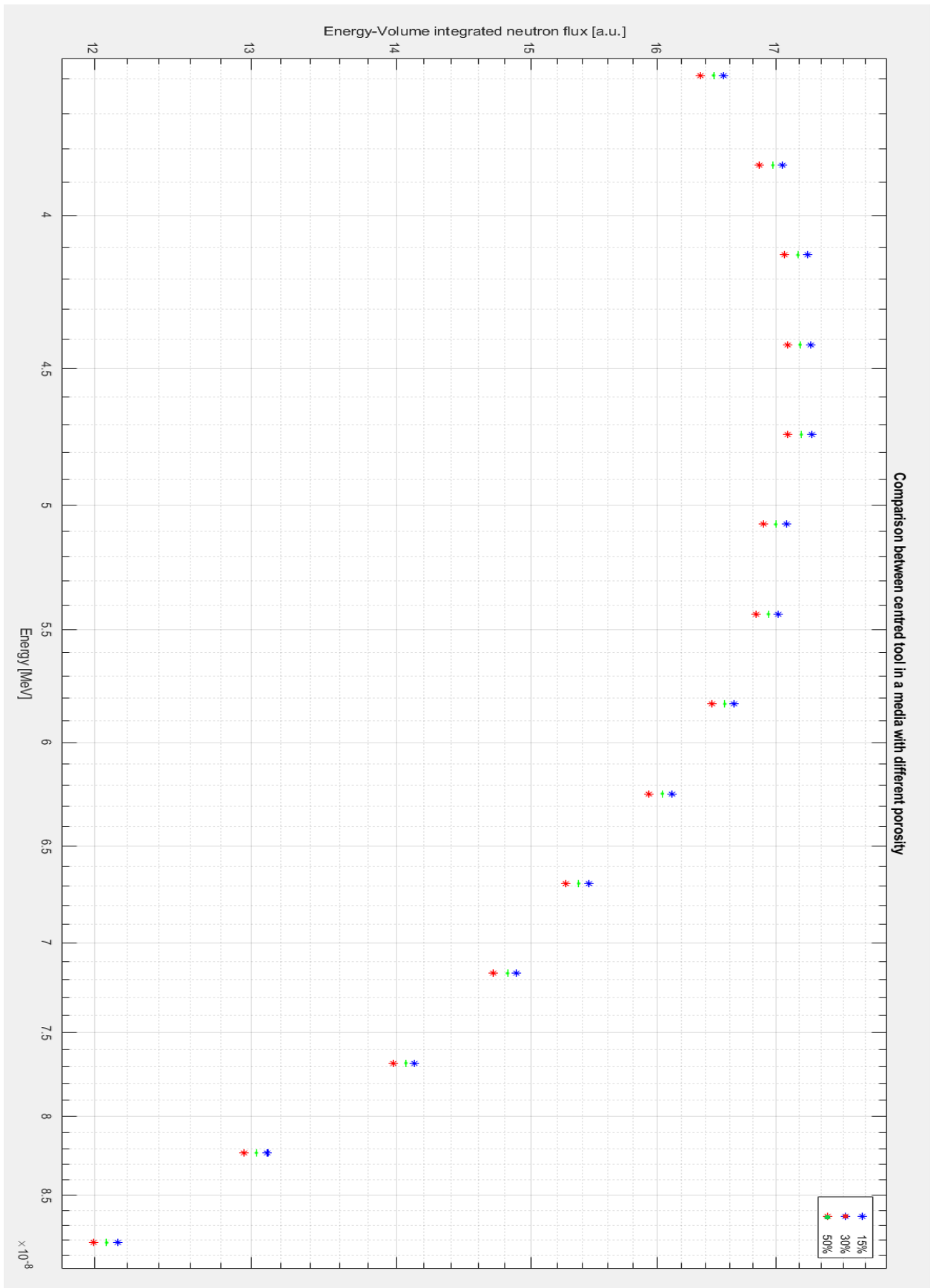


Figure 66 zoom of figure 65 in thermal neutron energy zone. calcite with 15% of porosity (blue), Calcite with 30% of porosity (red), Calcite with 50% of porosity (Green). In ordinates is plotted Energy-volume integrated neutron flux, [a.u.], in abscissae incident energy in MeV

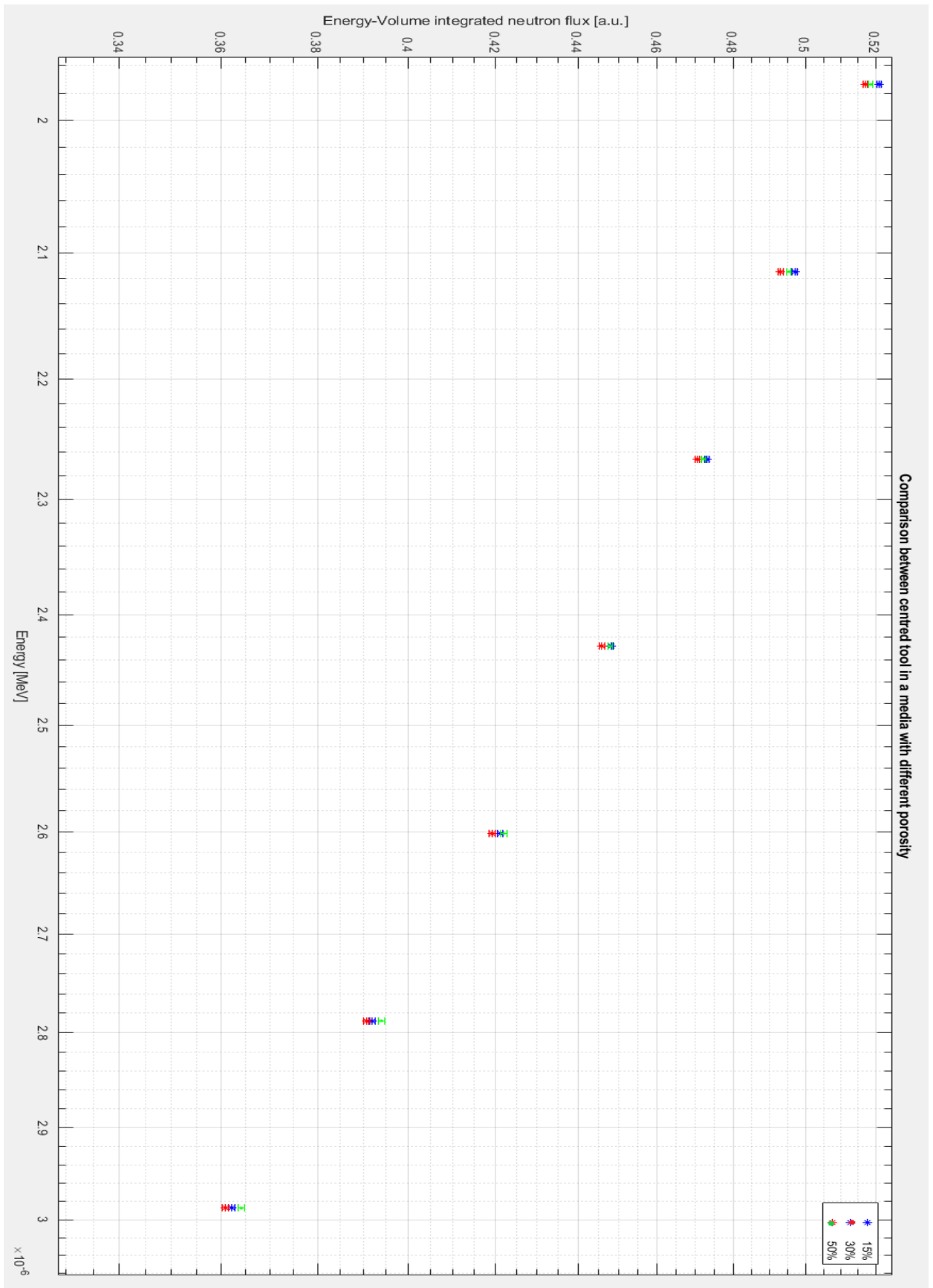


Figure 67 zoom of figure 65 on epithermal neutron energy zone. calcite with 15% of porosity (blue), Calcite with 30% of porosity(red), Calcite with 50% of porosity (Green). In ordinates is plotted Energy-volume integrated neutron flux, [a.u.], in abscissae incident energy in MeV

Our purpose was also to understand if borehole effects were really impacting on our measurement or not. In theory the result obtained by simulating the tool surrounded into 100% homogeneous porosity rocks, with increasing porosity, should follow an increasing trend. The output for Thermal and epithermal neutrons is shown in figure 68:

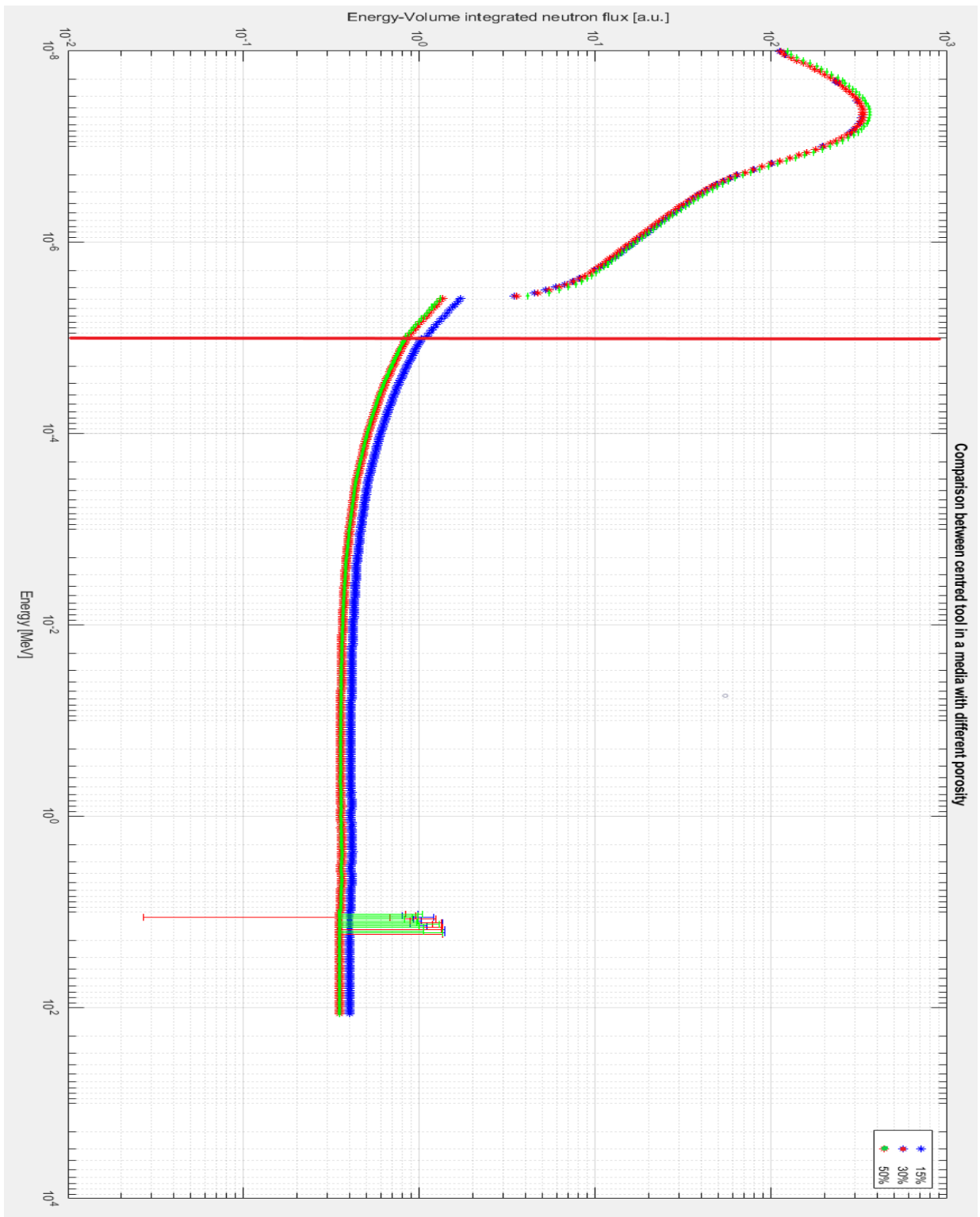


Figure 68 Comparison on different  $\phi$ , here the media is without borehole. calcite with 15% of porosity (blue), Calcite with 30% of porosity (red), Calcite with 50% of porosity (Green). In ordinates is plotted Energy-volume integrated neutron flux, [a.u.], in abscissae incident energy in MeV

Finally, the trend follows our interpretation logic, showing, in thermal zone a higher signal for higher porosity. Effects of rock are better visible from epithermal energies in figure 69. It is possible to see that for low porosity materials,  $\phi=15\%$ , in epithermal zone the effect of rock is visible. They present a Higher count of those neutron, than another configuration. Also in fast neutron region is visible this influence:

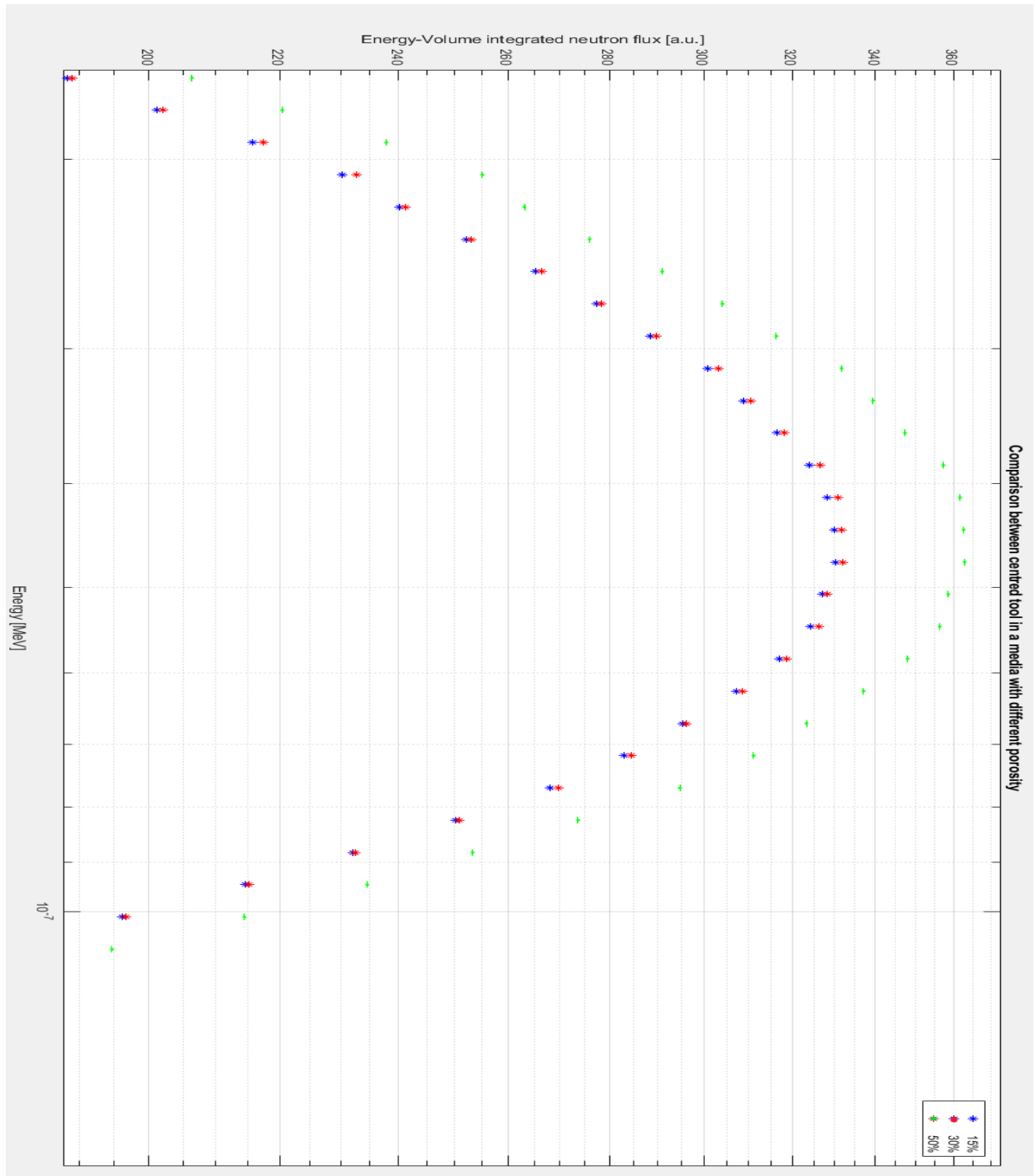


Figure 69 Zoom of figure 68. Neutron detector response in Thermal neutron zone. calcite with 15% of porosity (blue), Calcite with 30% of porosity (red), Calcite with 50% of porosity (Green). In ordinates is plotted Energy-volume integrated neutron flux, [a.u.], in abscissae incident energy in MeV

It is interesting to analyse if borehole effects influence less the measurement when the position of the tool within the borehole is wall side instead of centred. So, we confront the configurations shown in figure 70 and 71 with the configuration in figure 62.

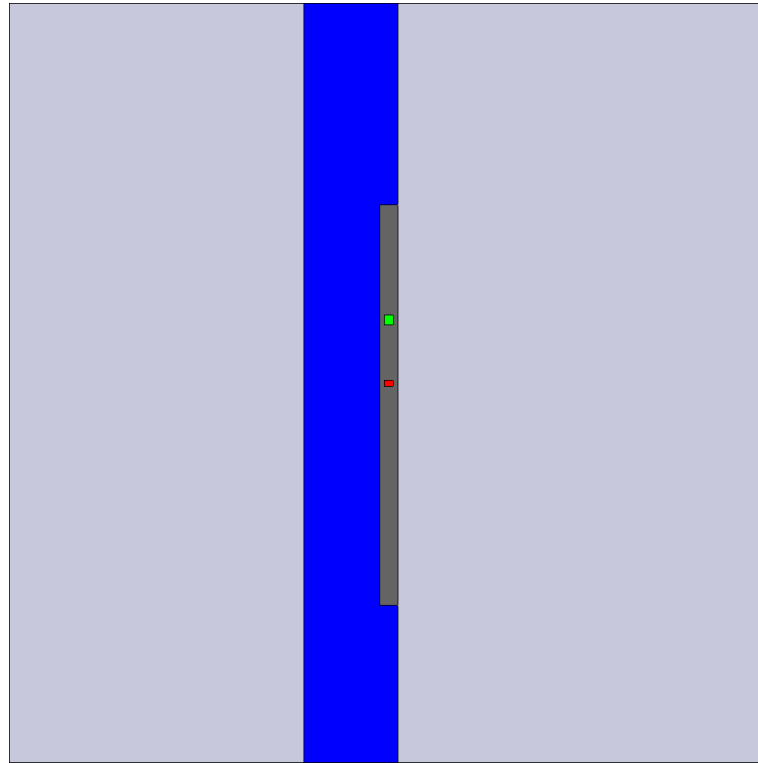


Figure 70 Tool pushed against the borehole's wall, Rock porosity is 15% and drilling fluid is water.

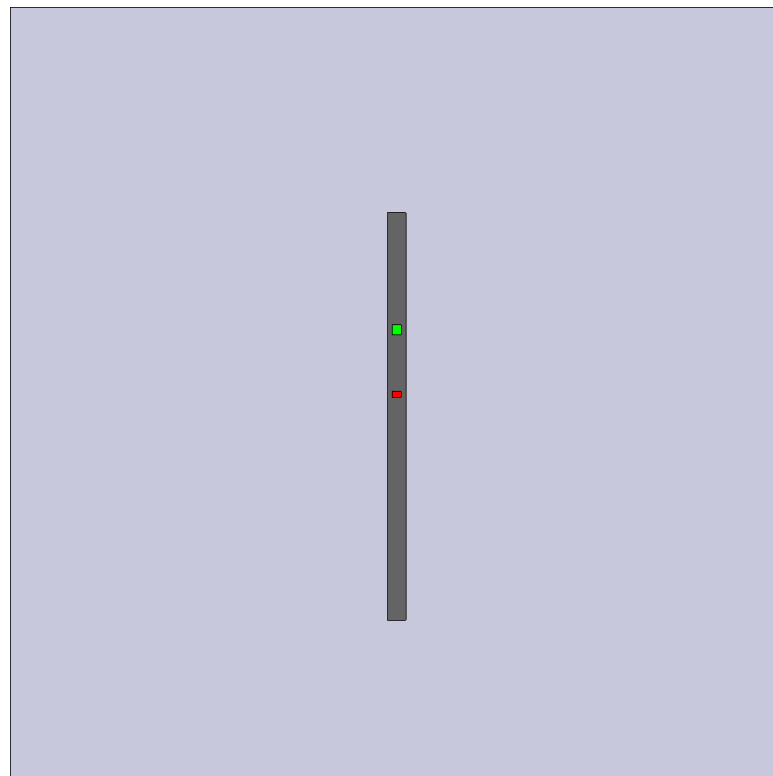


Figure 71 Tool immersed in 100% of rock with porosity of 15% saturated by water.

In figure 72 is presented the result of this comparison. When the tool is centred in the borehole the effect on the detector response are visible. Detectors register a flux of neutron with thermal energies that is an order of magnitude less that the data retrieved by the detector working in 100% of rock with same porosity. When the tool is pushed against the wall, returns a value that is closer to the response without the borehole. Especially in epithermal zone. The observed phenomenon, also in case of other simulation is that wall sized detector shows a response higher also than pure media. This could be the residual effect of the borehole. All neutrons emitted to the side that is not pushed may be scattered by the Hydrogen contained in the water and then return at the detector.

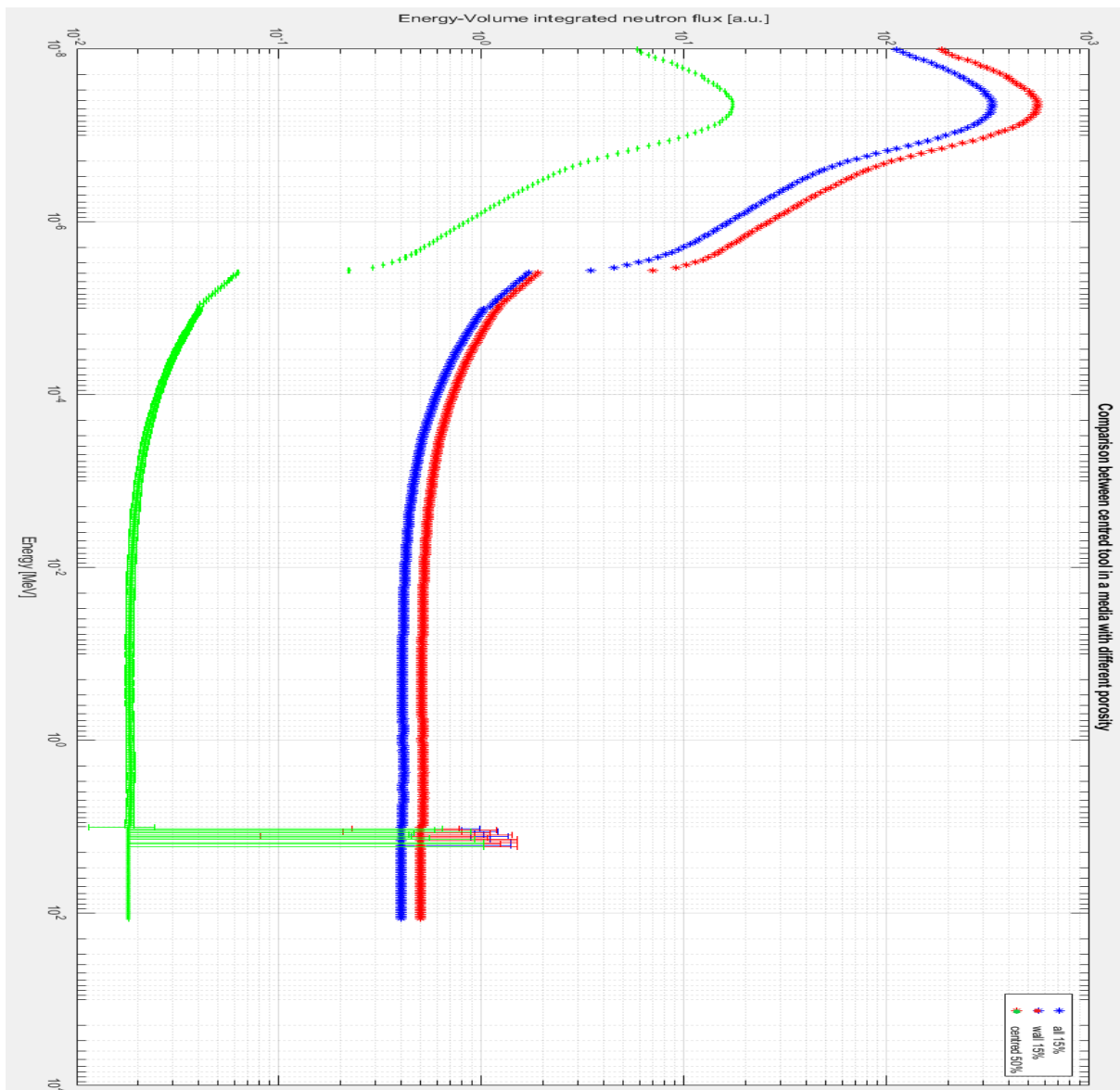


Figure 72 Comparison between tool response in two different positions within the wellbore, wall side (red), centered (green). These two responses are compared with the result of the tool when immersed in 100% of Calcite with 15% of porosity saturated by water, Hence, without borehole effects. This simulation has been done to understand how borehole effect is influencing the response.

From now we consider again the borehole filled with a fluid, also because is a typical situation in real life. The simulations done since now are going to represent a rock body with porosity of 15% always. The changing parameters will be the fluids filling the borehole and the fluid filling the pores. A comparison between boreholes filled with same fluid and rock saturated by a different flue are going to be discussed first. Oil saturated rock and gas saturated rock with boreholes filled by water. They are compared with same porosity rock but saturated by water. So, will be possible to make directly an interpretation of the output results in figure 73, 74.

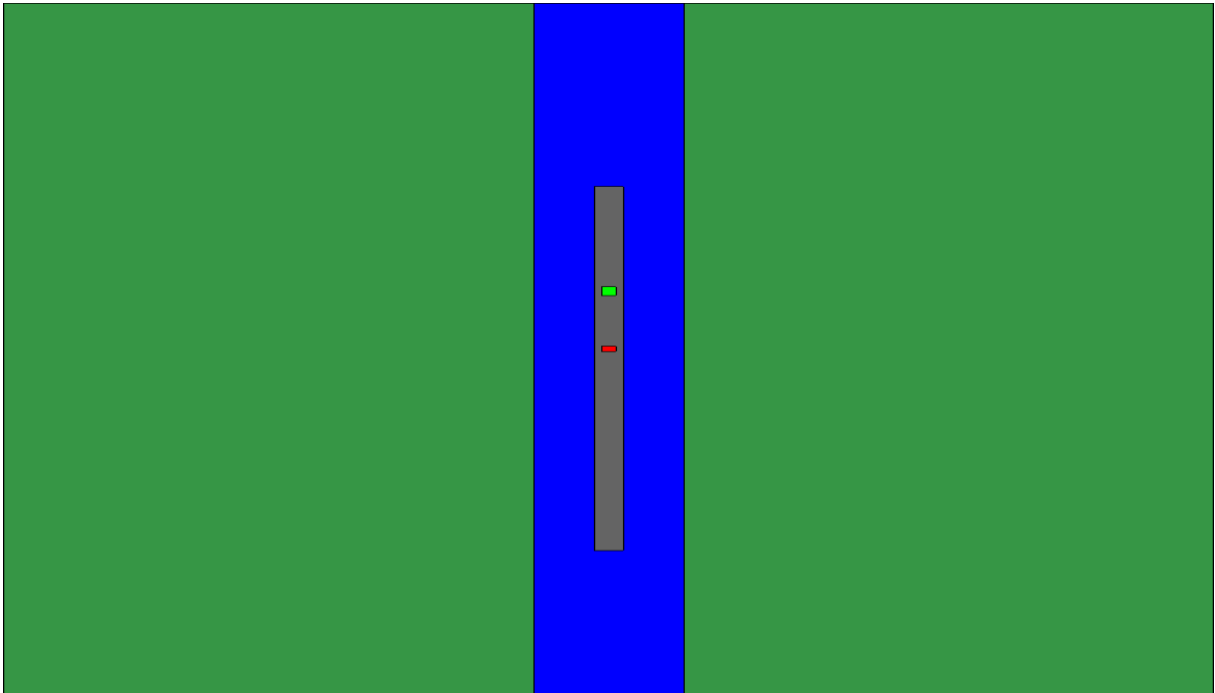


Figure 73 Rock  $\phi=15\%$  filled with oil. Borehole filled with water. Vertical Prospect.

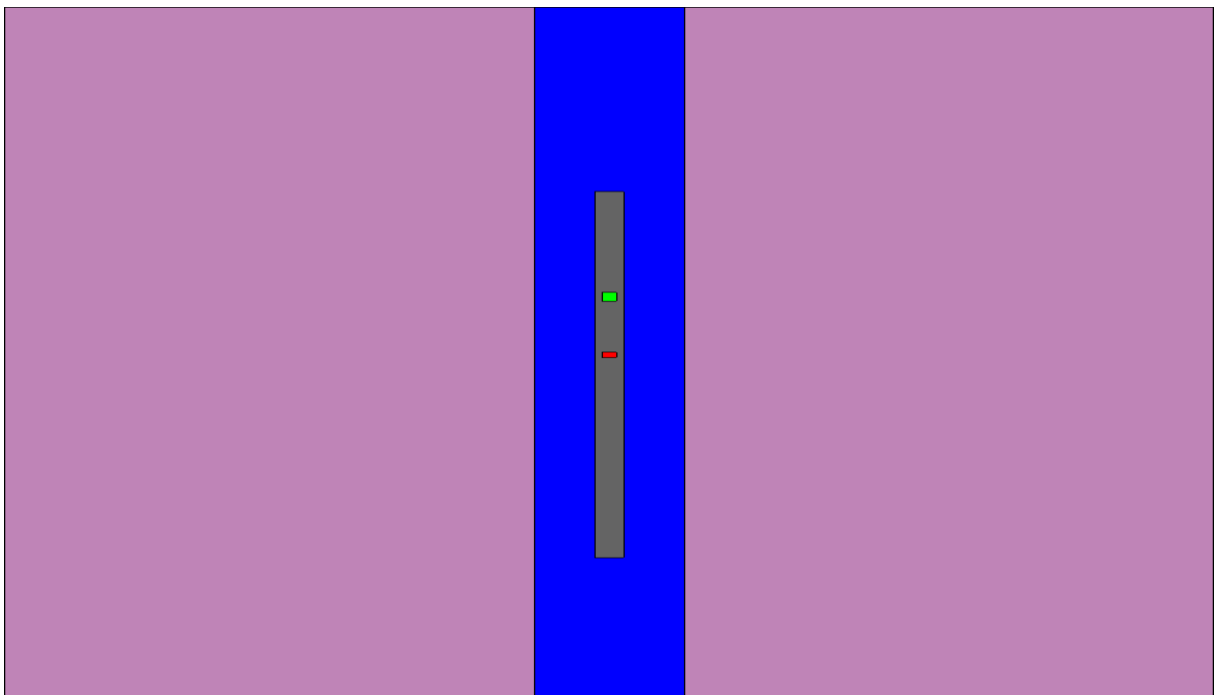


Figure 74 Rock  $\phi=15\%$  filled with gas. Borehole filled with water. Vertical prospect

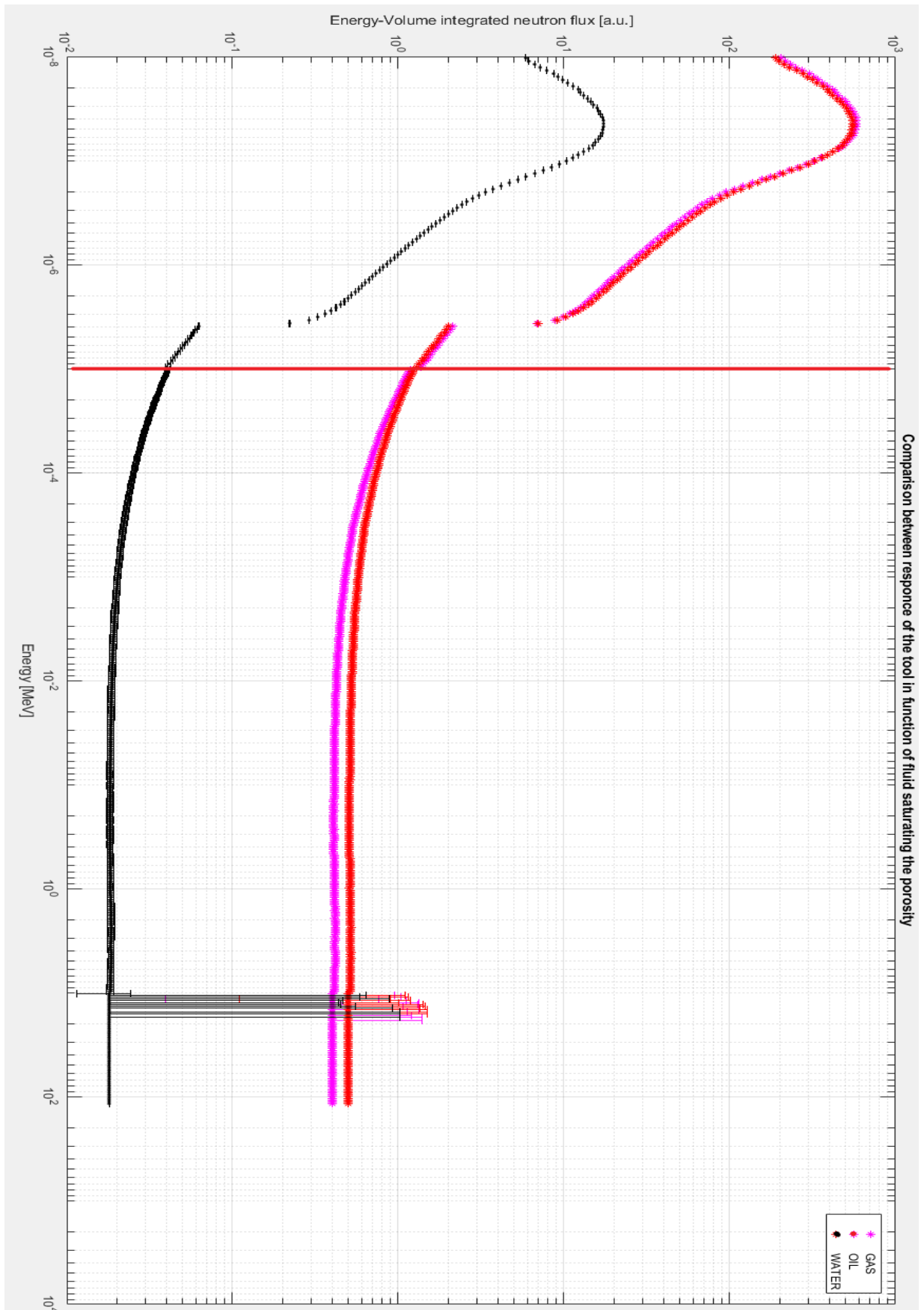


Figure 75 Comparison on saturated porosity rock with different fluid, oil (red), gas(purple) void (black). In ordinates is plotted Energy-volume integrated neutron flux, [a.u], in abscissae incident energy in MeV

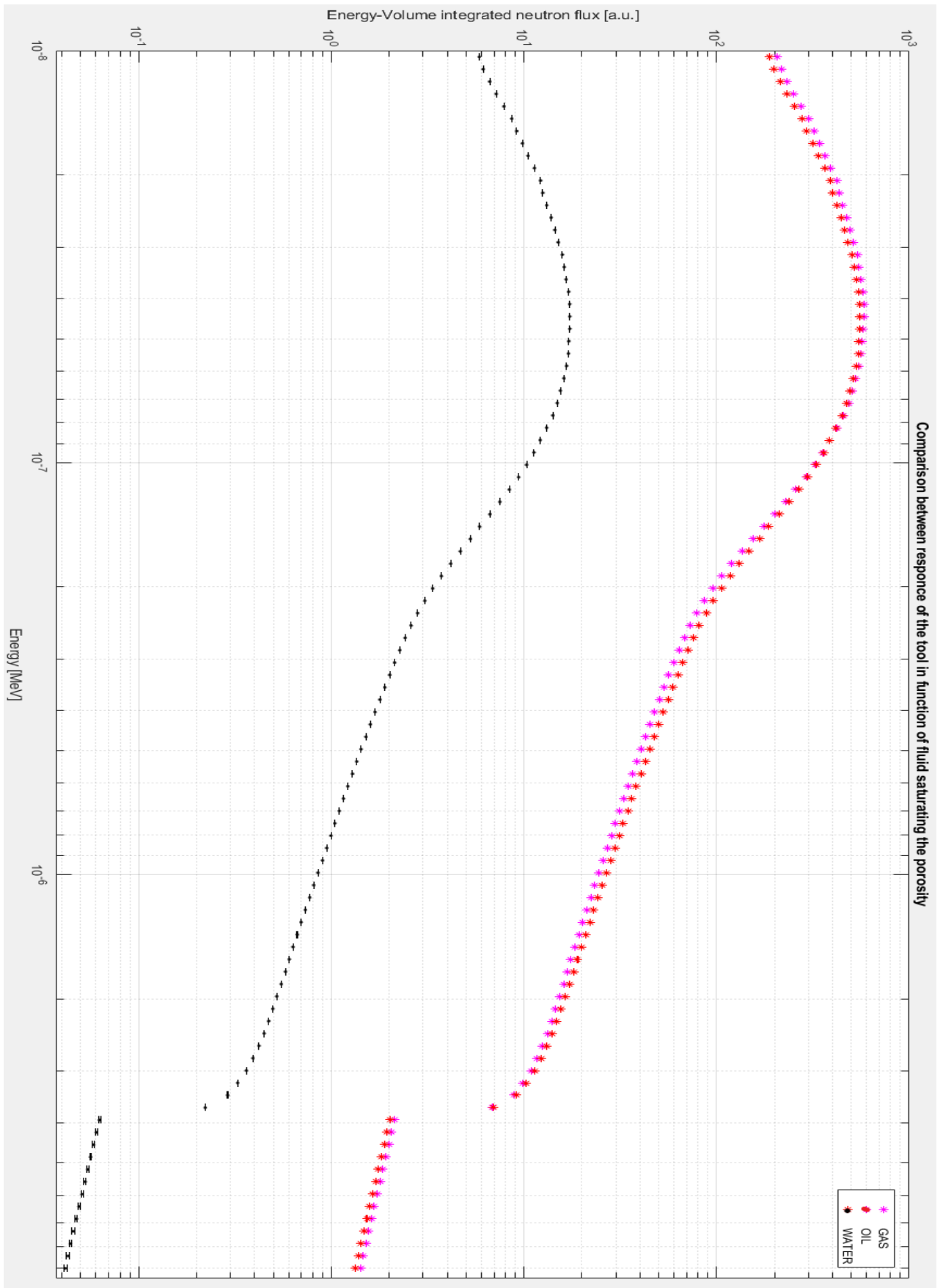


Figure 76 Zoom of figure 73 on thermal-epithermal energy zone. In ordinates is plotted Energy-volume integrated neutron flux, [a.u], in abscissae incident energy in MeV

The trend obtained is shown in figure 75 and 76. It is in line with that attended in same borehole conditions and rock porosity gas continues to show higher response the others. Oil show a higher response respect water. These considerations are confirmed with the models in homogeneous media. Those result may be taken as a calibration for our interpretations. The high value for gases means a high porosity estimation. Our result is in accordance with that made in exploration industry. Exploration industries make a gas correction for porosity.

In real cases wellbore are not water filled. Mud fills the borehole, while drilling and wireline. Mud makes also invasion of the formation. So, to approach better at a real case the following simulation are going to be all with borehole filled by mud. All are going to be with flushed zone. Firstly, are analysed water rock with porosity saturated by water, and with an irreducible water saturation in invaded zone equal to 0,2. Lastly are going to be described situation with porosity filled by oil, gas and then a cased hole. The geometry plot of this kind of simulation is presented in figure and figure. We may notice that the tool is running in a borehole filled with mud. The mud filtrates into the rock, with a fixed porosity. Then mud produce 10 zones, in accordance with our model. The first zone, that in dark brown is the mud cake. We show first the configuration with porous rock without fluids. Second porous rock with water saturated porous. Third porous rock with oil saturated porous. All is represented in fig 77 to fig.81.

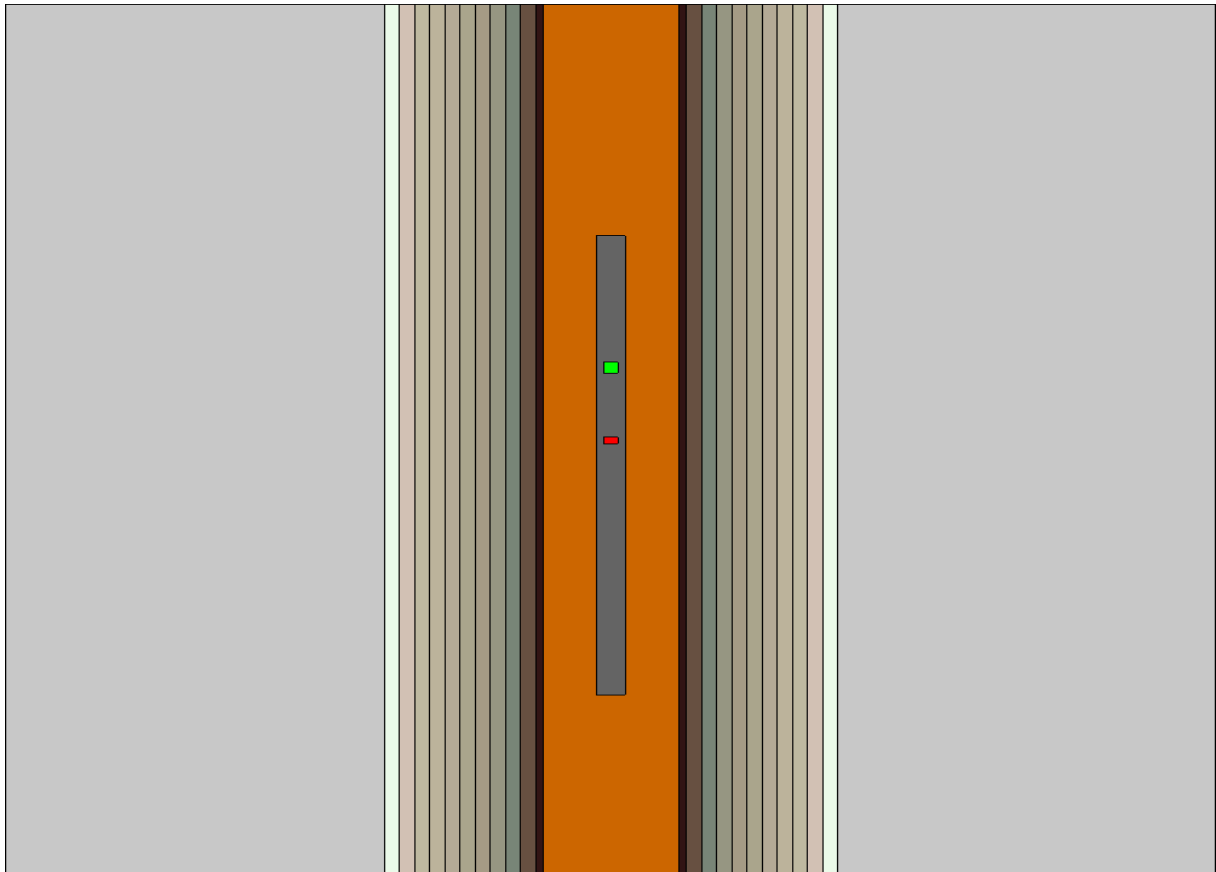


Figure 77 Representation of borehole filled with mud and invaded zone of the rock Vertical prospect. Wellbore radius is 10cm, invaded zone radius is 20 cm. Rock porosity 15%, void.

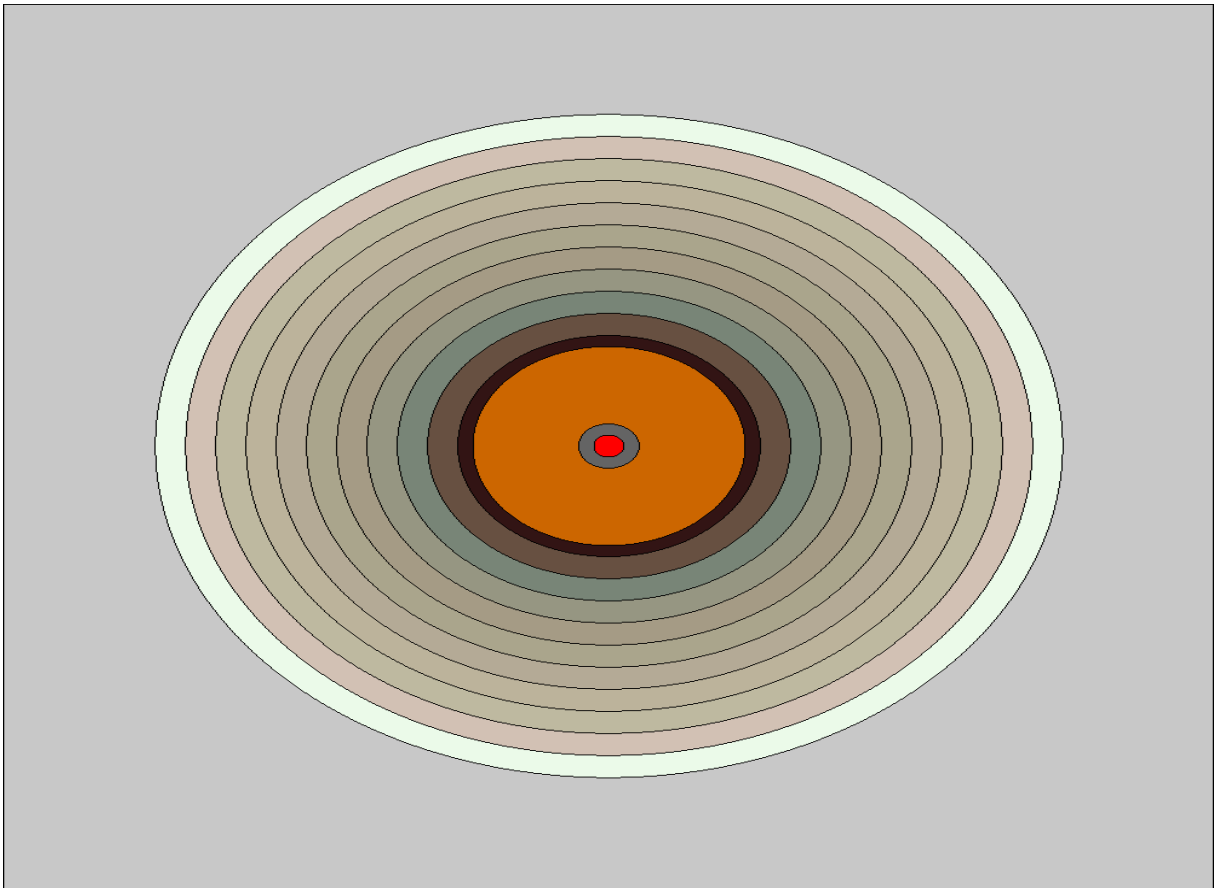


Figure 78 Horizonte prospetta.

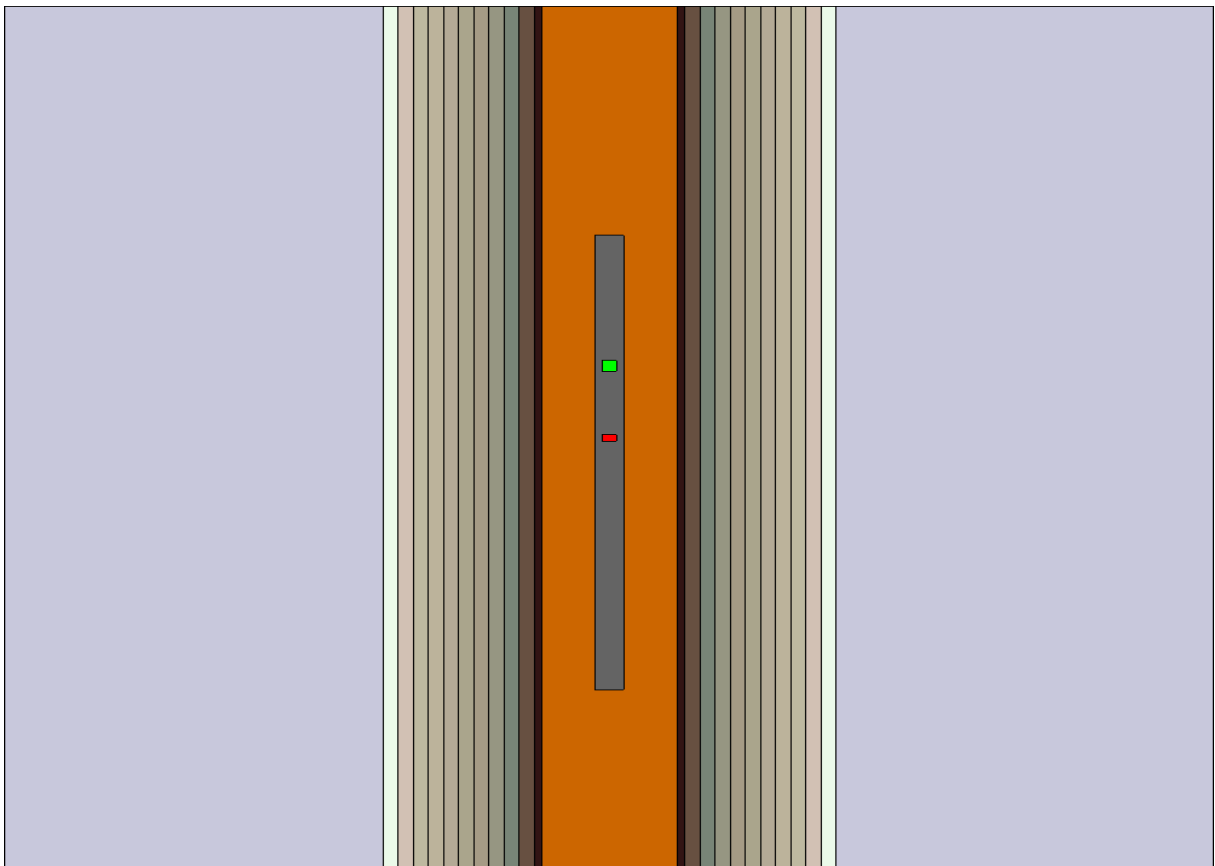


Figure 79 Vertical representation with water saturated porosity, Wellbore radius is 10cm, invaded zone radius is 20 cm. Rock porosity 15%, water saturated.

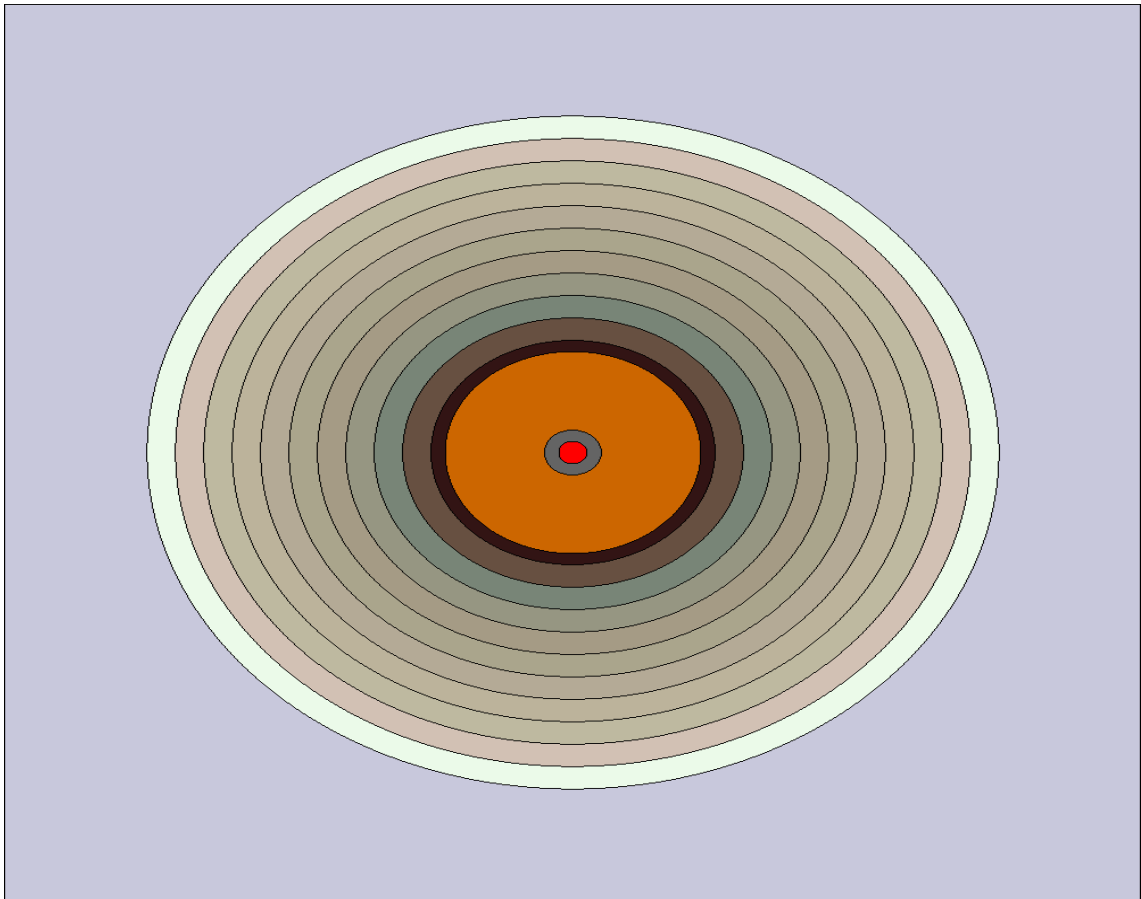


Figure 80 Horizontal prospect

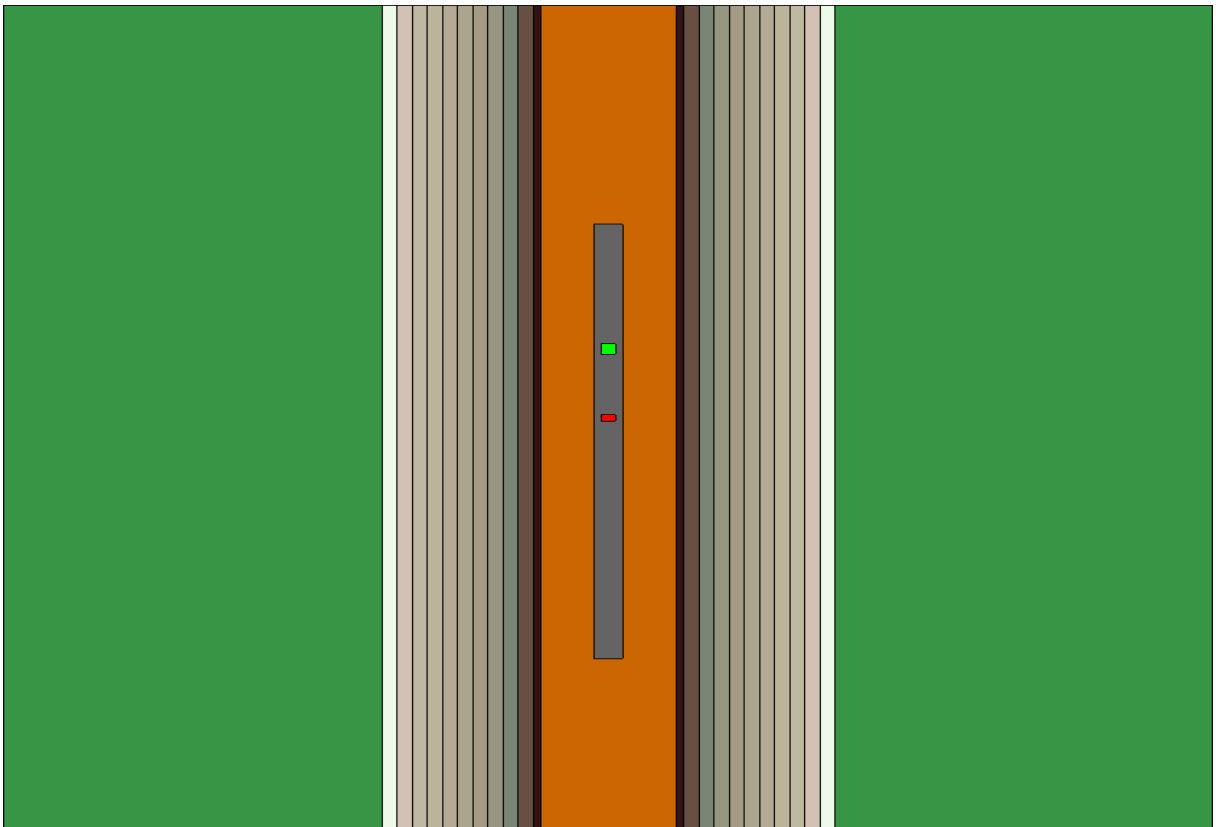


Figure 82 Vertical prospect with oil saturated rock. Wellbore radius is 10cm, invaded zone radius is 20 cm. Rock porosity 15%, oil saturated.

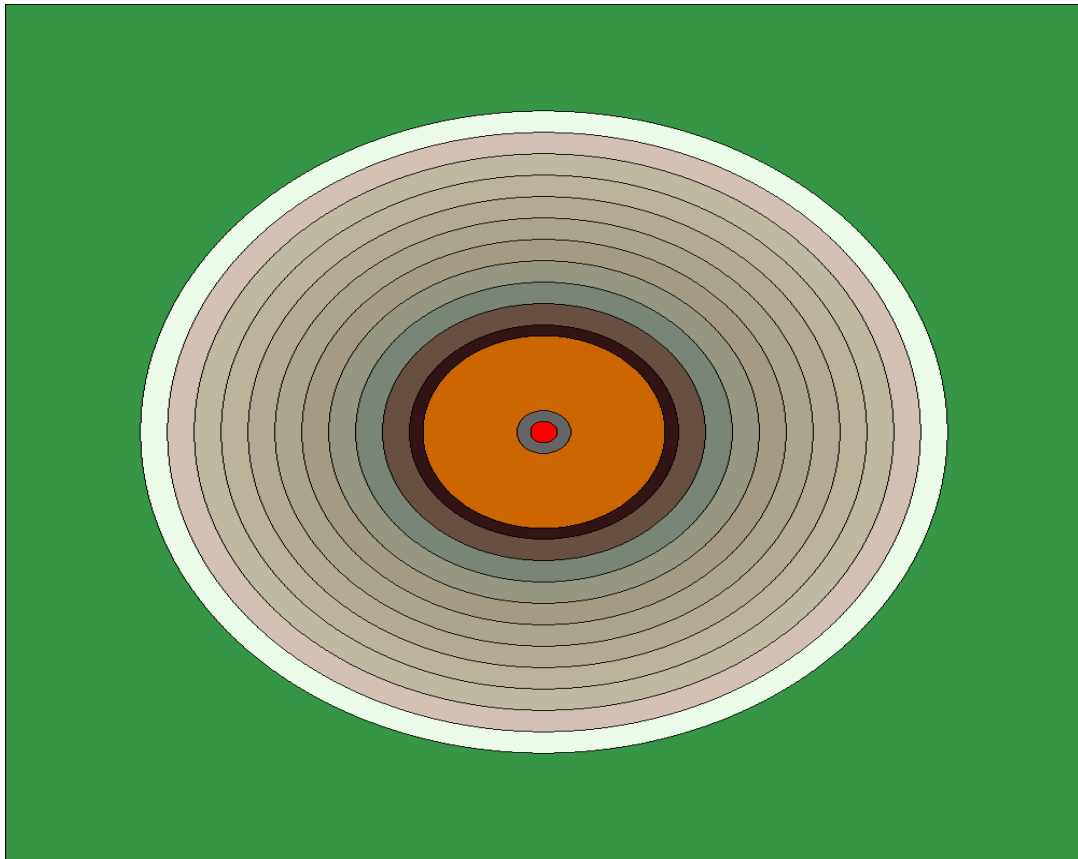


Figure 81 Horizontal prospect

The purpose of those three-simulation comparison is to obtain a reasonable response interpretation for different filling fluids. Following all the result obtained until now, a probable trend of the output should be: Higher response for oil saturated rock, averaged response for water and the lowest response should be rock without any fluid. The difference between void empty rock and full rock may be interpreted as the first pass for extrapolating porosity. Rock empty, that means any Hydrogen atom in its porous presents HI factor equal to 0 and so a porosity equal to zero too. On the other hand, rock saturated by water or by oil will present a HI index different from 0. HI index for water are going to be lower than that for our formulation of oil. The attended result so, is that measured porosity should be higher in case of oil saturated rock, despite, we fix porosity at 15% in both cases. Reasonably all the output is going to have lower pick than those in pure conditions. A further comparison between rock before invasion and rock invaded is going to be done. We want to quantify the infusion effect. The output shown in figure 81 highlights how mud invasion may influence the response of the tool. The general trend is that predict by our assumptions. The counted thermalized neutrons are like those for pure rock, without invasion. In that case we had a count around  $10^1$ . Here we are always below  $10^2$  and so it is of the same order of magnitude.

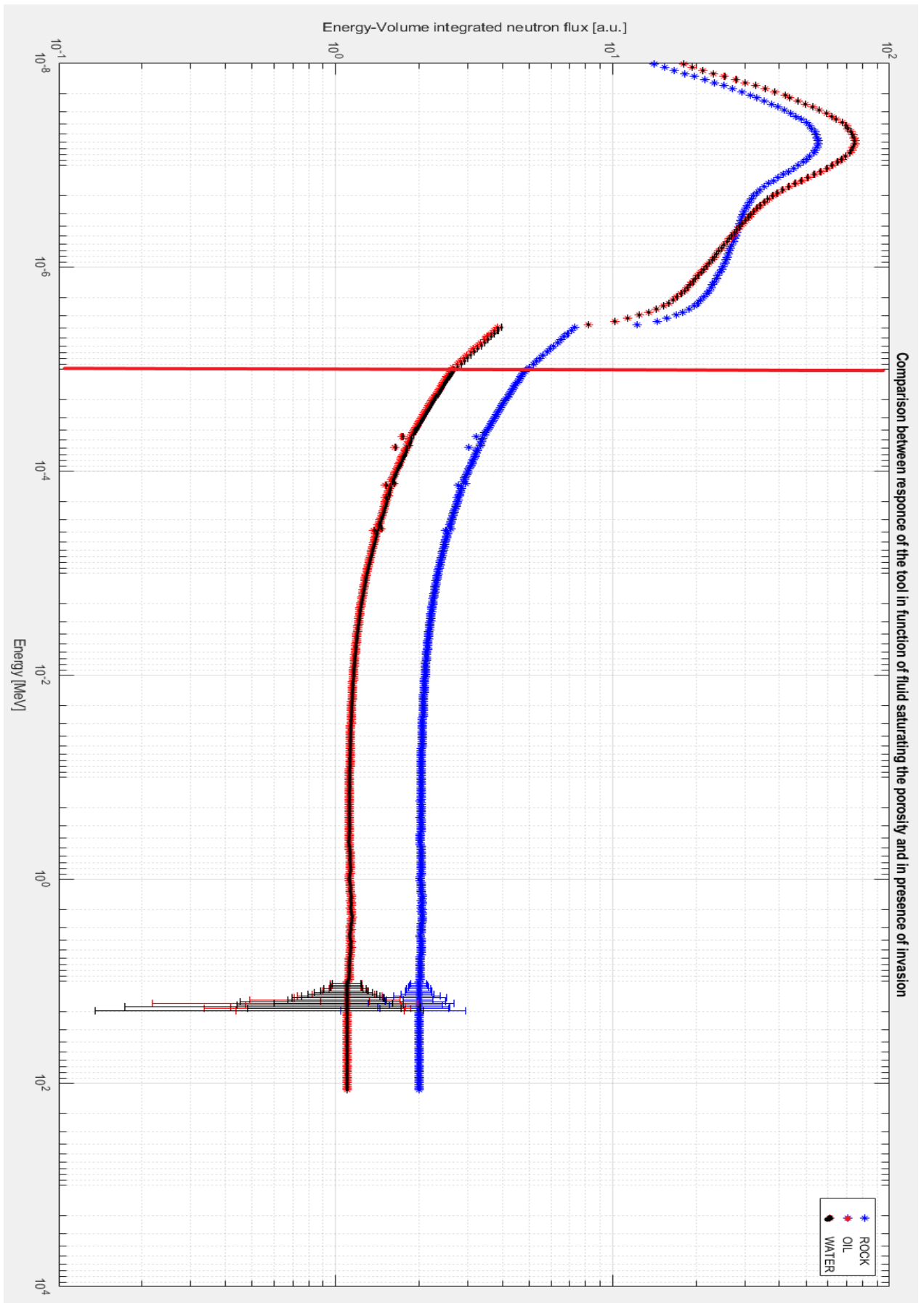


Figure 83 Comparison of rock with porosity saturated by different fluids, oil (red) water (black) void (blue). In ordinates is plotted Energy-volume integrated neutron flux, [a.u], in abscissae incident energy in MeV

In Epithermal zone we see, more accurate is in fig 84, for void rock the count is higher. Again, that is the effect of Calcite, already illustrated at the beginning. Water saturated and oil saturated are almost superimpose as always. Is anyway possible to appreciate their differences in figure.

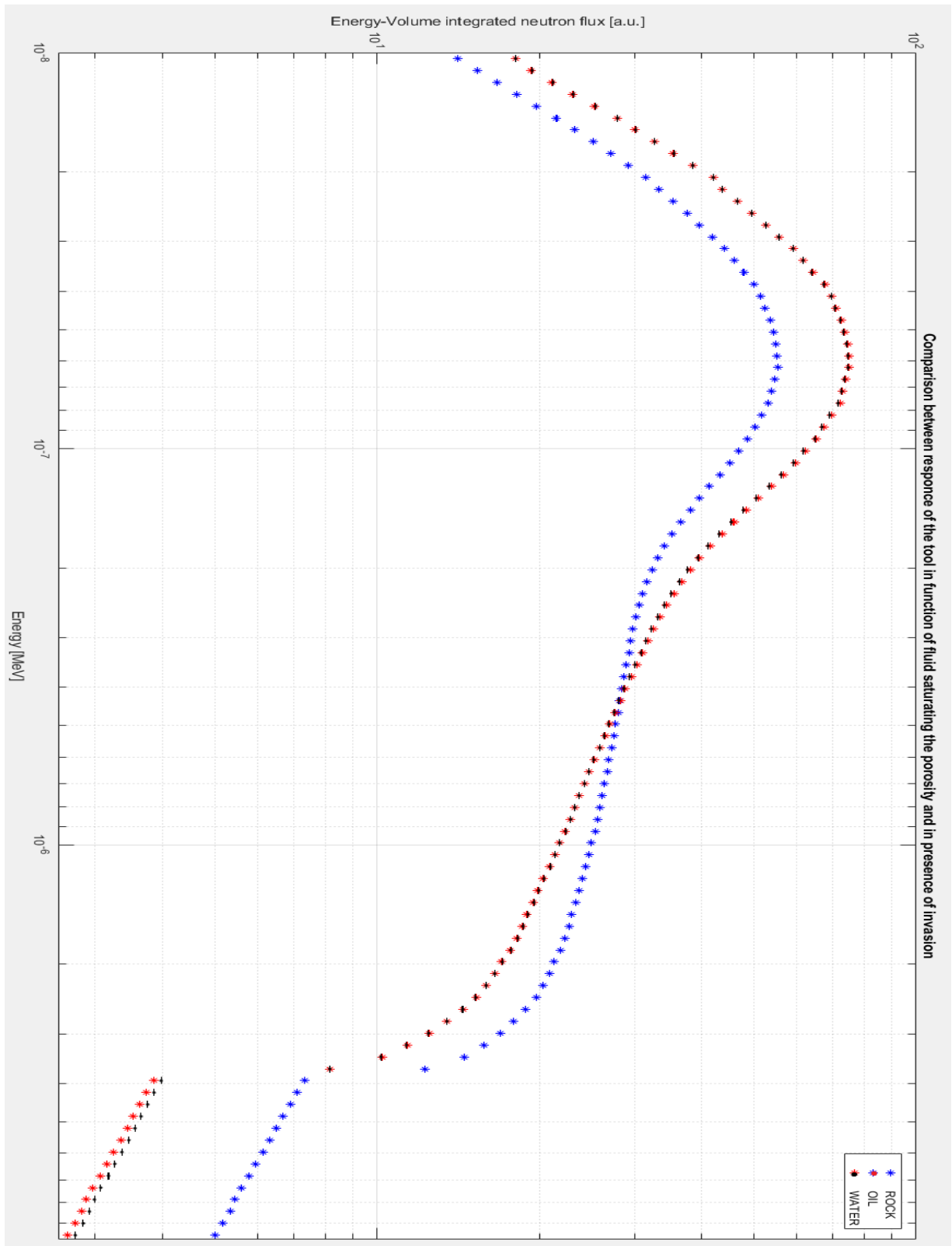


Figure 84 Zoom of figure 81 on energy grid one. In ordinates is plotted Energy-volume integrated neutron flux, [a.u.], in abscissae incident energy in MeV

A new phenomenon appears. When invaded zone is present the trend of oil saturated rock goes below that of water saturated. That is true just in epithermal zone. More specifically, looking at figure, between  $3 \times 10^{-6}$  and  $10^{-5}$  MeV. Also in fast neutron zone the trend is inherited. A possible explanation of this phenomenon could be a less presence of Carbon, in water case, implies a lower response for high energy. While a high presence of oxygen tends to make high response for that interval of energies. Looking to attachment is possible to observe cross section of O and C for those energies. The effect of mud invasion respect on wellbore without invasion is shown in figure 85:

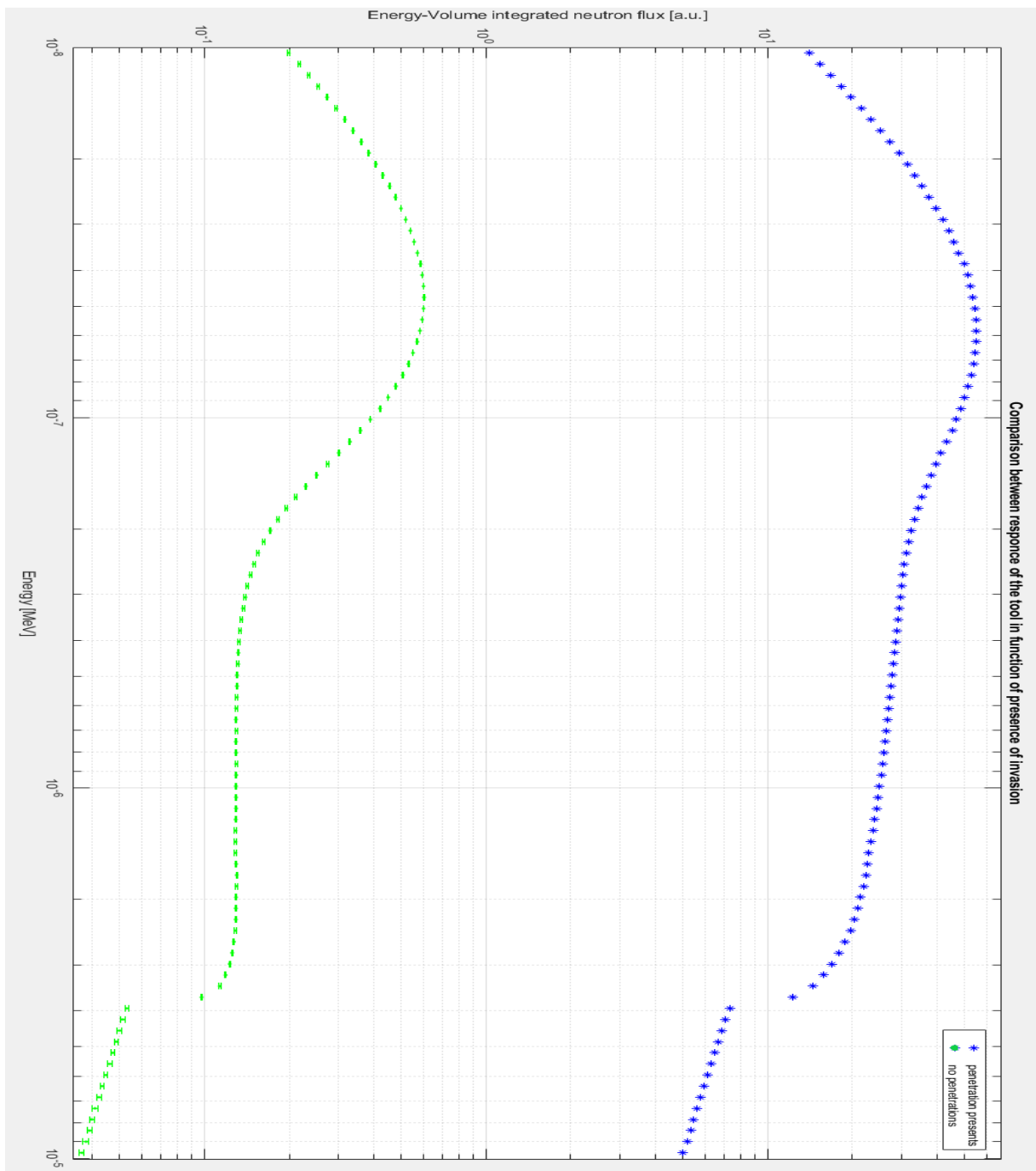


Figure 85 Comparison between presence of invaded zone absence of invaded zone.

Presence of mud invasion makes the number of thermalized neutrons higher. Also, it increases the slope of the curve in epithermal zone. While for just mud was almost flat. That means effect of rock is higher than mud effect, otherwise the slope was no too high. So, is possible to say that the response of the tool change while drilling. Because mud invasion changes in time. For that reason, furthered corrections on measurements must be done. For all those simulations we did also the parallel simulation with the tool pushed on the wall of the borehole. The geometry plotter is in figure 86, 87.

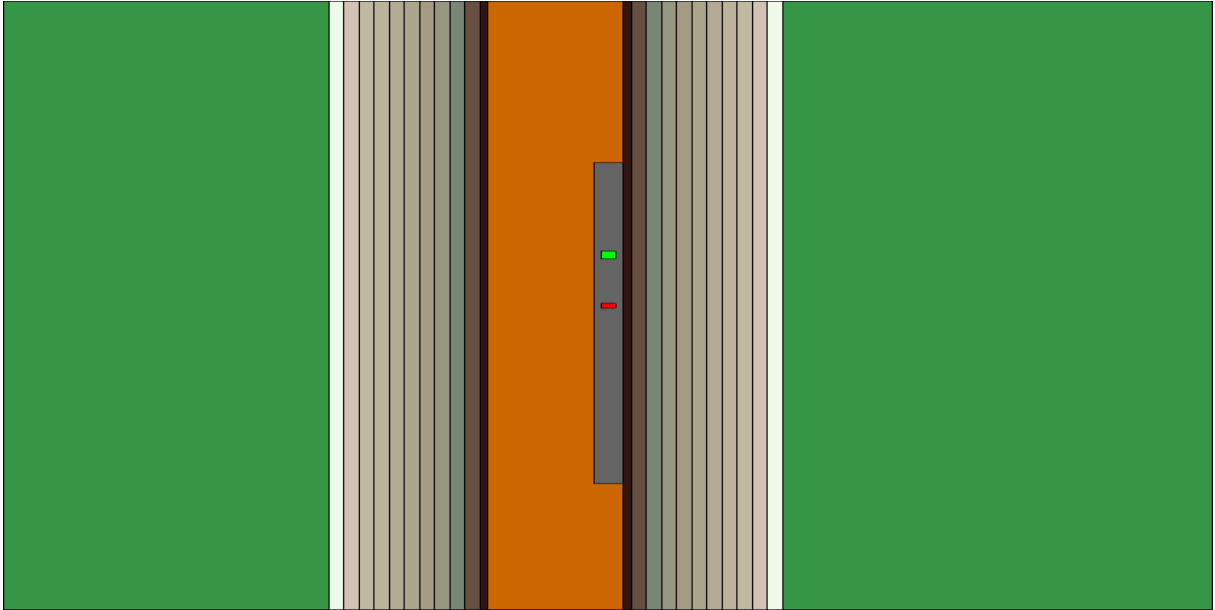


Figure 86 Mud filtrate geometry plotter with oil filling the porous of the rock

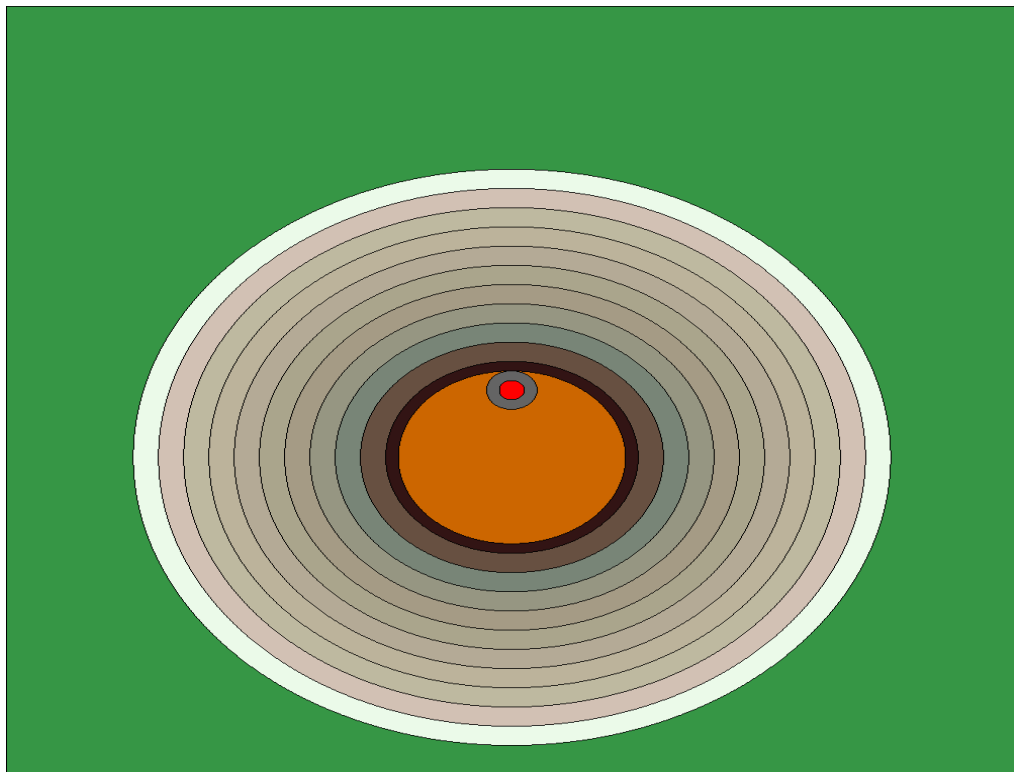


Figure 87 Horizontal representation.

That shown in figure 86 and figure 87 is just the configuration for oil saturated rock, all the other configurations are practically the same. The difference is the colour of the rock. The colours are the same to those in figure and figure. The comparison between wall size tool and centred tool have again the scope of improving the resolution of the tool. It is impossible to make a previous about the output. Output may be lower, because less effect of mud, or higher because more effect of rock. In any case presence of oil or water in the pores may produce a different need of corrections. In figure 88 are shown wall size versus centred tool responses.

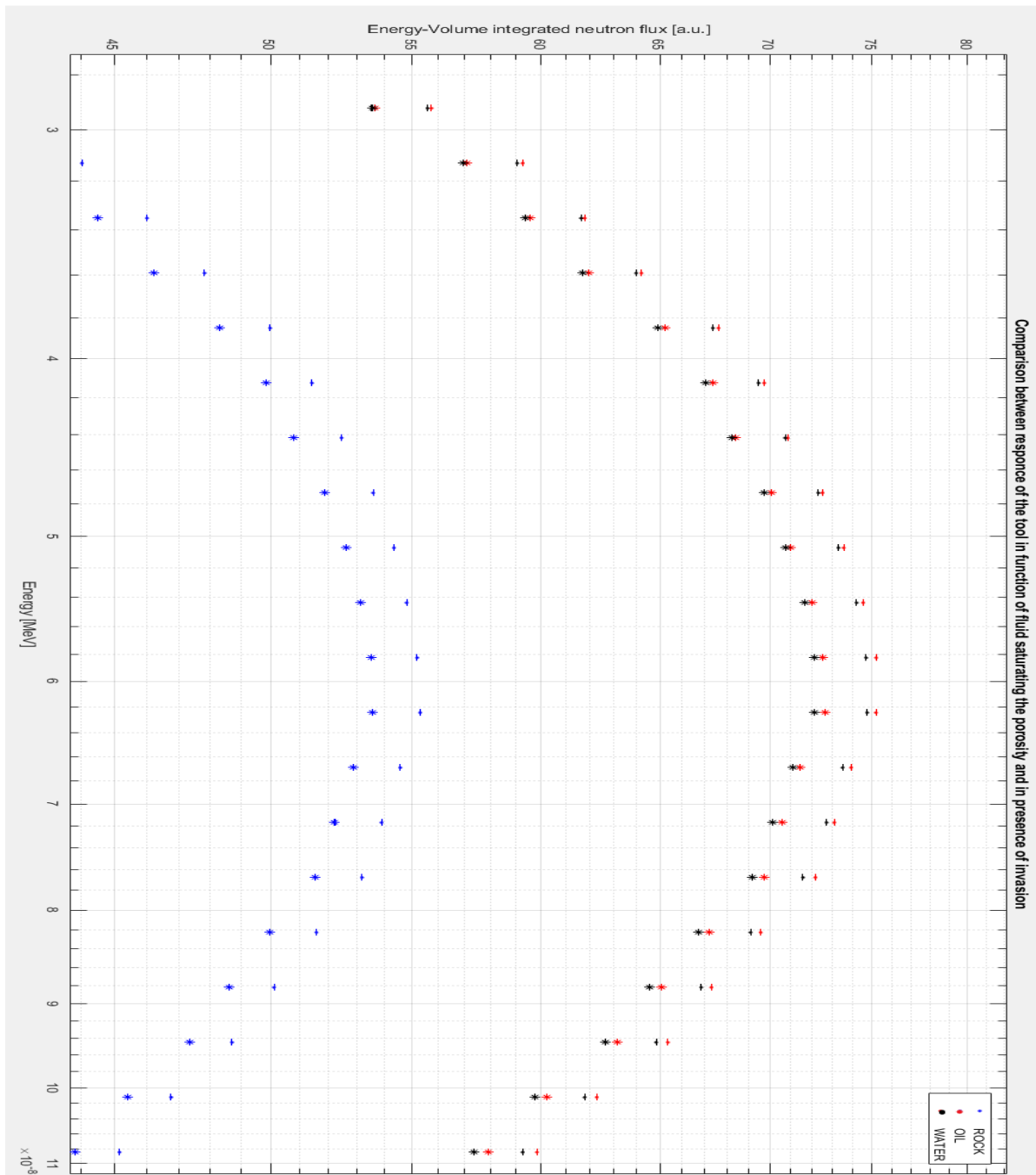


Figure 88 Comparison between invaded zone configuration with the tool centered in the borehole and the same configuration with the tool pushed against the wall. In the plot (\*) represent the tool when near wall configuration, (.) represent when the tool is perfectly centered in the borehole. In ordinates is plotted Energy-volume integrated neutron flux, [a.u.], in abscissae incident energy in MeV.

The output in figure 89 shows that in case of pushed tool the detector response is lower in all cases. The physical explanation might be that neutrons emitted near rock are adsorbed before than when emitted in centred configuration. So centred configuration implies an intrinsic error in porosity evaluation. Centred configuration produces a signal that, once converted in to porosity may induce mistake or bigger estimation of porosity. So, a wall size instrument gives a more real response of the medium, less conditioned by borehole effects.

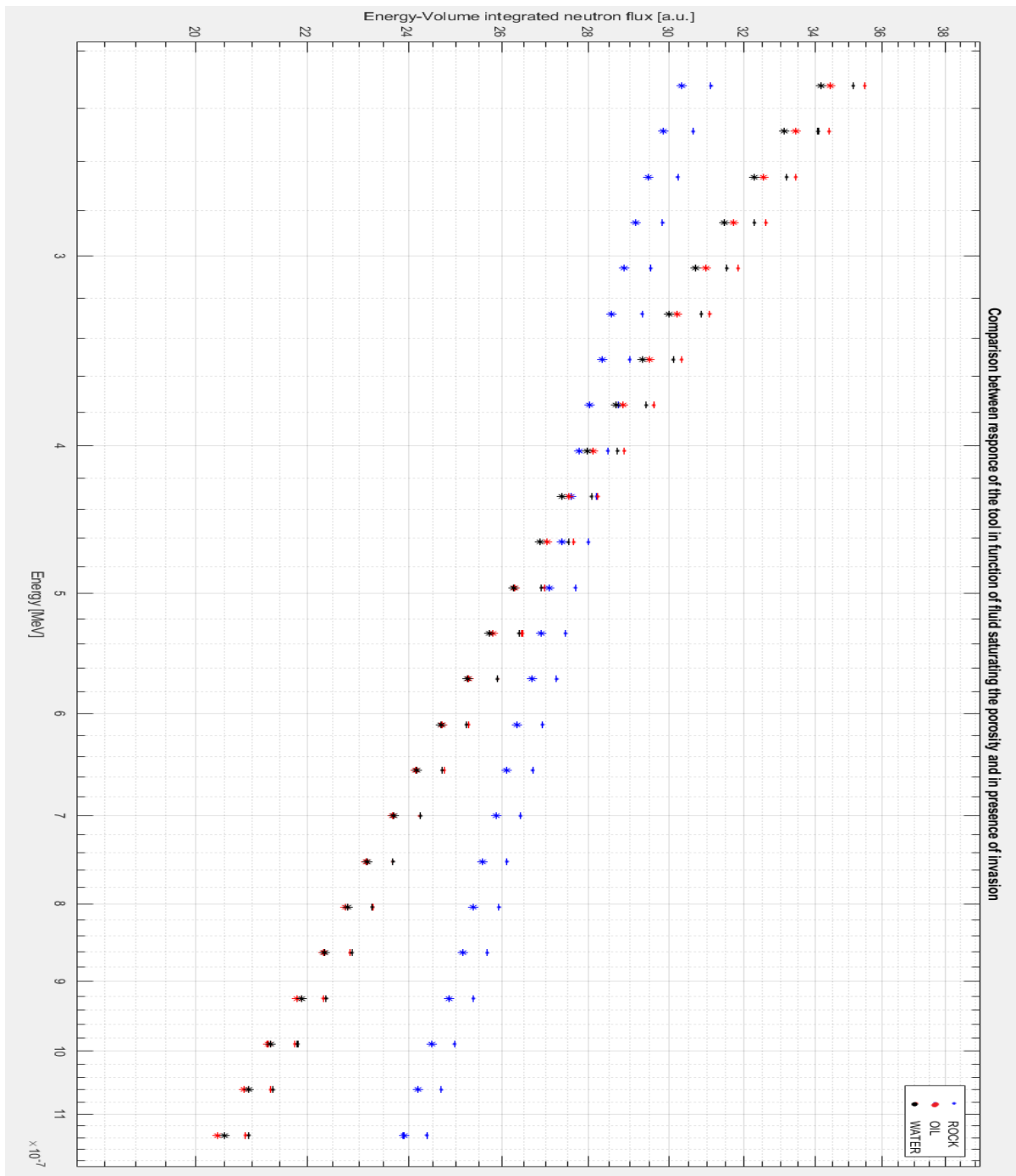


Figure 89 Focus on epithermal zone. In the plot (\*) represent the tool when near wall configuration, (.) represent when the tool is perfectly centered in the borehole. In ordinates is plotted Energy-volume integrated neutron flux, [a.u], in abscissae incident energy in MeV.

Also for wall size configuration petroleum and water change their trend in epithermal zone. The contribution of rock part in oil is less efficient. The last two simulations shown here are in cased holes. The comparison will be done between void invaded rock, one without casing and the other with casing. Wall size tool in casing hole is going to be represented in same plot. The goal of this comparison is to appreciate the casing effect on neutron logging response. It is important because one of the configuration in which neutron logging are performed is while drilling. The material of the casing has been chosen equal to that of the tool and so casing and the tool have same chemical composition. We made this end of decision for simplicity and because the chosen stainless steel would be good also for casing. The geometry plotters for casing hole are in figure 90 and 91: We assume a casing string width of 1cm.

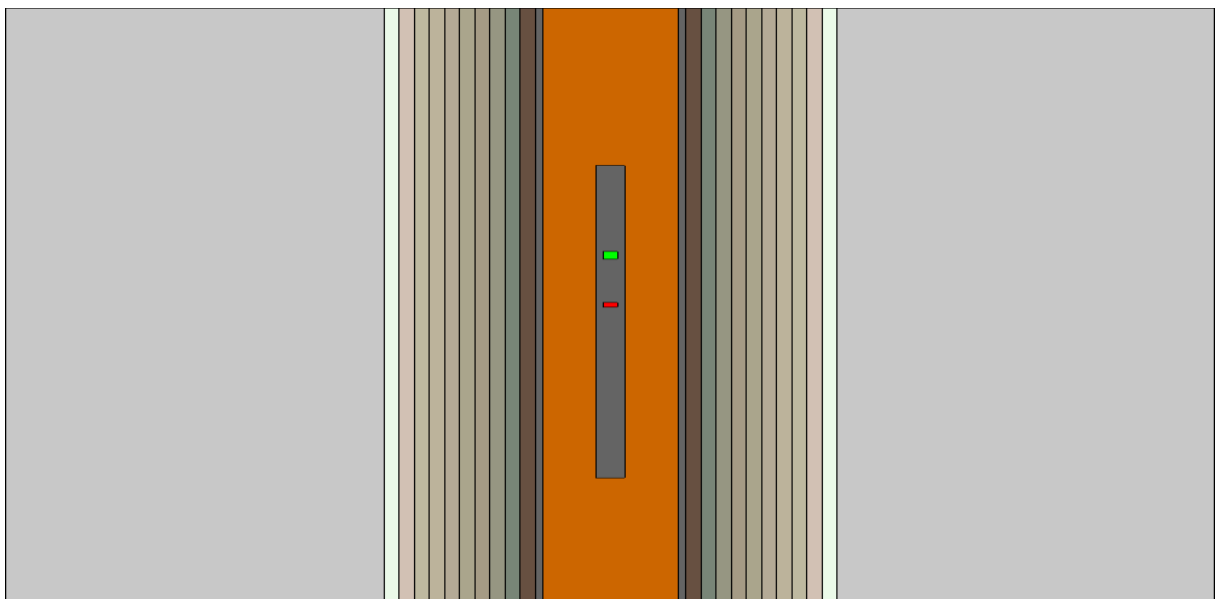


Figure 90 Vertical mud filtrate configuration with casing.

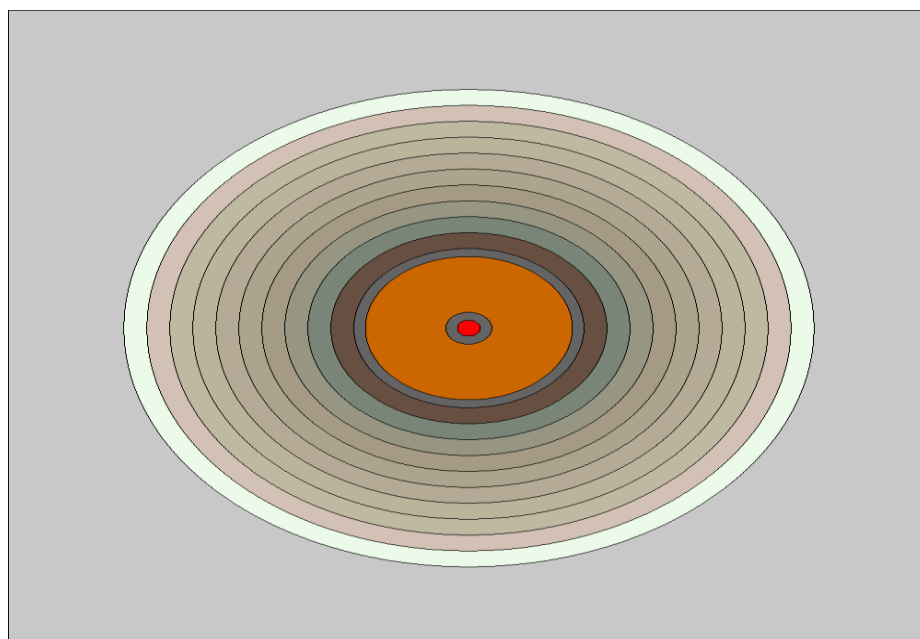


Figure 91 Horizontal prospect with casing

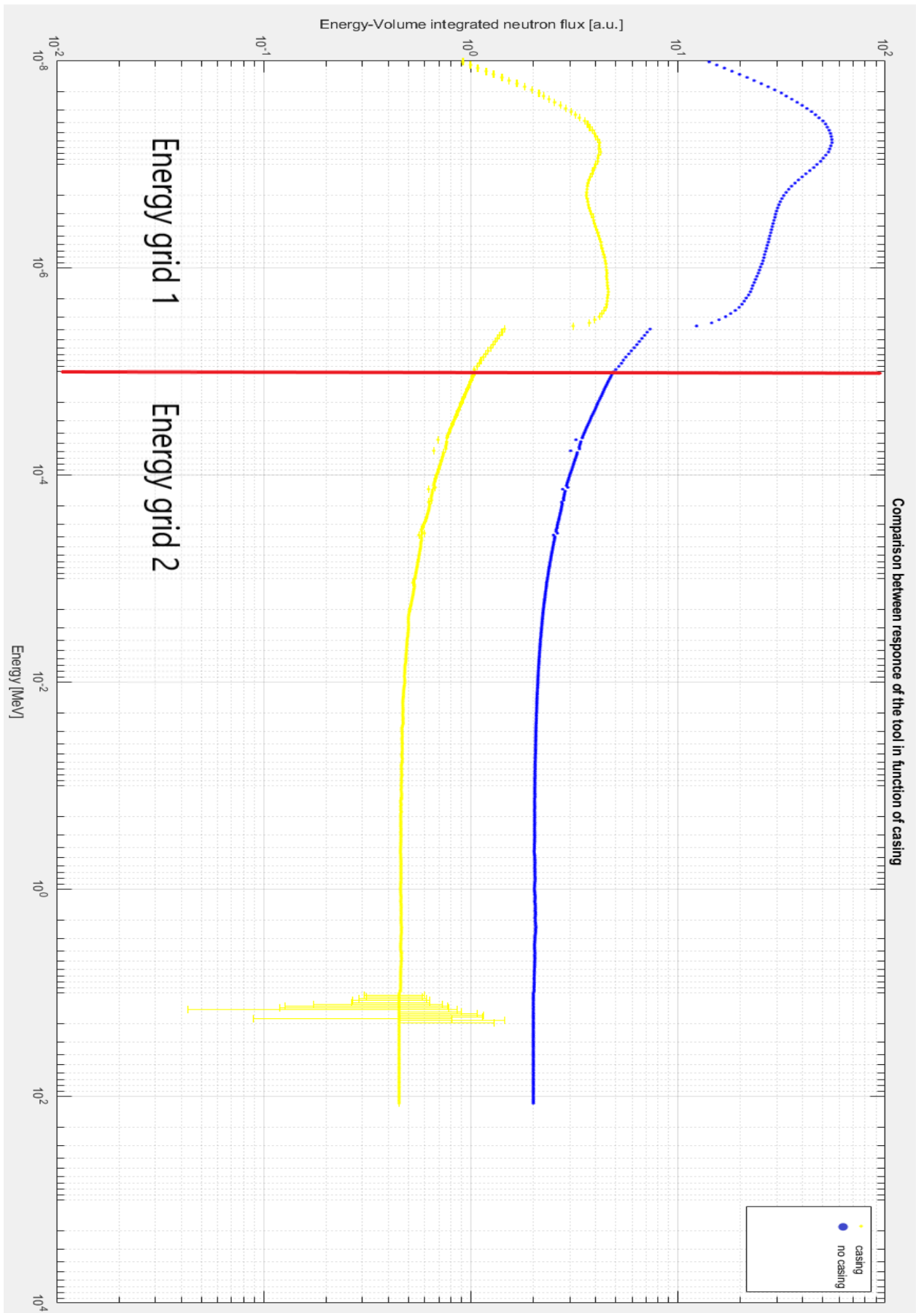


Figure 92 Comparison between cased and uncased holes. Casing (yellow), no casing (blue). In ordinates is plotted Energy-volume integrated neutron flux, [a.u], in abscissae incident energy in MeV

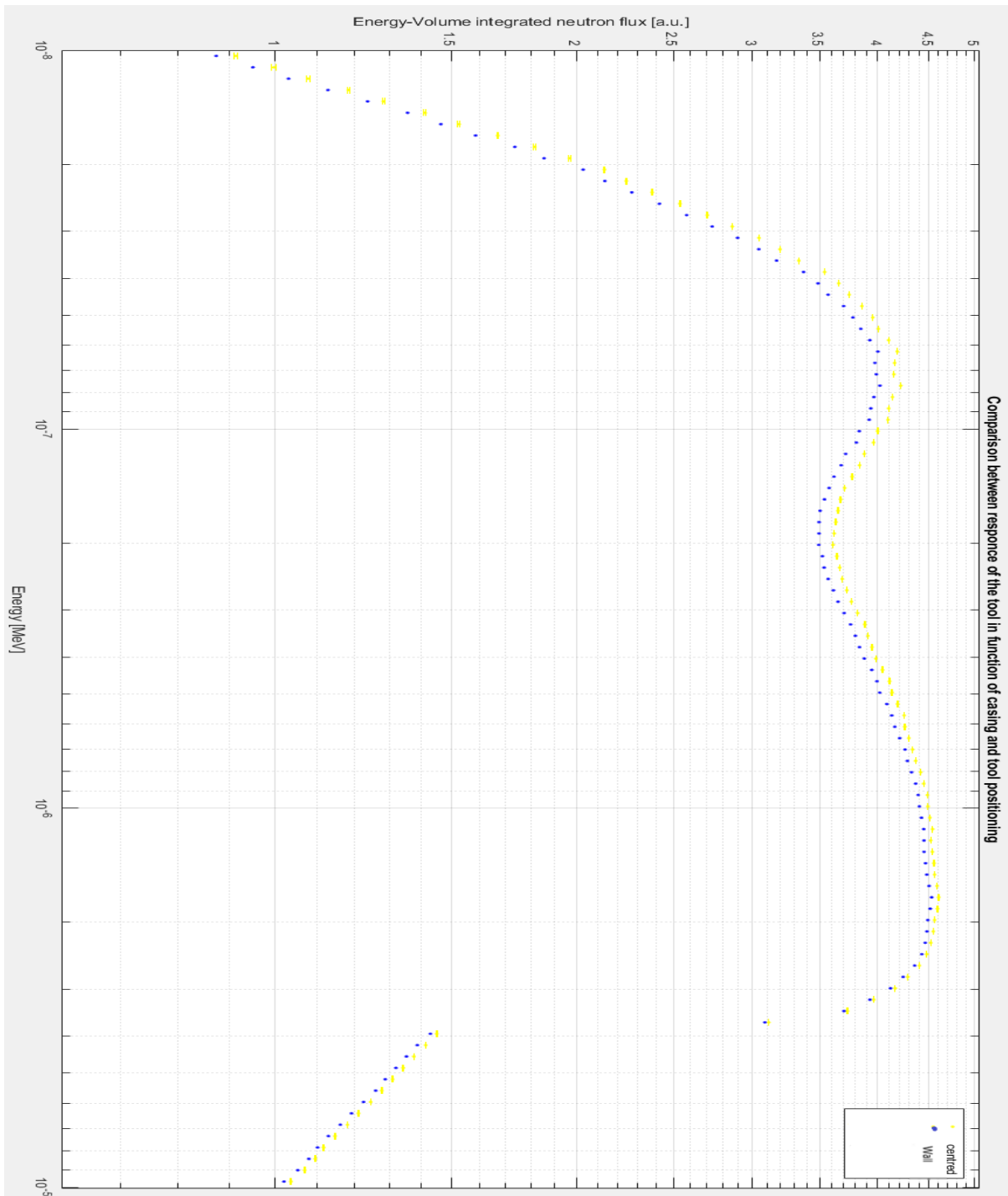


Figure 93 Comparisons of tool's response when wall side (blue) and centered (yellow), in presence of casing and when we are in thermal and epithermal energies bin. In ordinates is plotted Energy-volume integrated neutron flux, [a.u.], in abscissae incident energy in MeV.

Figure 92 shows cased vs uncased holes. In cased hole we suppose that mud cake is not present while in uncased it is present. The profile without casing shows a response, in all the spectrum, that is 1 order of magnitude higher than the cased configuration. The shape of casing configuration shows a lower value for thermal neutrons energy than epithermal one. It has also a minimum in between thermal and epithermal energies. Looking at appendix C we can see that the minimum may be explained with cross-sections of N, Cr, Mo and Ni. Their total cross

sections show a flat zone in energies equal to those of the minimum shown in figure 92. The maximum is then due to the influence of Ca present in the rock. The influence of Ca was also visible in all the other simulations where rock was present. Also in this cased hole simulation is present the discontinuities usually correlated with Hydrogen presence. The presence of Hydrogen is in mud invaded zone. We may say that corrections in case of while drilling logs should consider the effect of the casing. So, a correction in both, epithermal and thermal zone is advised to make a better comparison between cased hole and all the other situations. In figure 93 is shown the response of the tool in different position in the wellbore. The two configurations are again the centered one and the wall side one. In all previous simulations we saw that centered tool response is hugely affected by borehole effects and that wall side measurements are closer to results in 100% of simulated media. In this case instead we have a higher response for tool measuring in centered configuration. The difference between centered and wall side is not huge as in all the other cases. The higher response of the tool pushed against the wall of the borehole could due to the neutrons distribution in the borehole. To well understand it we need to perform a mesh simulation on the wellbore.

All the simulations which we complete to build and conclude the thesis are listed in table 10:

Simulation name	Running time [h]
All Water	3.64
All Mud	1.51
All Rock	11.6
Hole Water	4.97
Hole Mud	2.64
HolePhi15water	4.38
HolePhi30water	4.12
HolePhi50water	3.97
Phi15water	5.43
Phi30water	4.56
Phi50water	4.43
Allwaterprecise	5.51
Hydrogen	8.18
Meshdetector	14.36
Alloil	3.89
Allgas	3.11
Phi15oil	5.23

Phi15gas	4.54
Mudinvasion	55
Mudinvasionwaterphi15	55
Mudinvasionoilphi15	55
HolePhi15waterWall	4.38
HolePhi30waterWall	4.12
Holephi50waterWall	3.89
Phi15oilWall	5.54
Phi15gasWall	4.58
MudinvasionWall	55
Mudinvasionwaterphi15Wall	55
Mudinvasionoilphi15Wall	55
Casing	55
Cadmio	3.98

Tab.10, in column 1 are listed the names of our simulations, in 2 the running time.

Cadmium simulation was performed to avoid to presence of fast uncolided neutrons passing through the tool frame. The quantity of cadmium chose to this simulation was not enough to show reliable results. A moderator as paraffin was also advised to achieve better results. Libraries to define paraffin as moderator are not included in Serpent. Some example of compiled simulation is attached in Appendix E.

## 5 Conclusions

The purpose of the Thesis was to perform a numerical simulation, conducted by Serpent, a Monte Carlo Neutron Particle transport code software, of the neutron log response placed within a borehole which intercept a porous media. The porous media simulated should approximate a range of a hydrocarbon reservoir mineralized with oil. To better represent the phenomenology the system, hence, borehole-mineralized reservoir has been represented as follow: The stainless-steel tool with its detector and neutron source within a borehole (centred or pushed against the wall) of 10 cm of radios, filled of a water based mud with a known composition, invested zone characterized by mud saturation that varies with the radius and the presence of the hydrocarbon. The media was Calcite with porosity of 15%. This model approaches to a real system. To achieve this field representation, we had to describe every single component of the system by their chemical composition, in terms of atomic composition or mass fraction per unit volume of every nuclide. Hence, we had to describe: Water, it was assumed as pure water,

without any salts dissolved in, the mud was assumed a water-based mud, its composition was given by experts, the composition of hydrocarbons is an intermediate one and the reservoir rock was supposed to be pure Calcite, so defined by its chemical formula, furthermore we had to define metallic components of the system, the tool frame and the casing, the neutron source and the detector, thanks to information's furnished by experts and technicians we could define them. To characterise the response of the tool to each pure component we performed five preliminary simulations. Those fives were run assuming to immerge the tool in a 100% volume of water, mud, calcite, oil and gas respectively. The results of simulations were representing in terms of energy-volume integrated neutron flux in function of incident energy of the neutron at the detector, expressed in MeV. Results interpretation analysis shown that the response of the tool for neutron thermal energies is proportional to the amount of Hydrogen in the chemical composition of the single media. This means, with our given composition that, Gas shows the higher response and it is followed by oil, water and then rock that does not present Hydrogen in its composition. Mud shows the lowest response, it is possible to understand it looking at its chemical composition ad so to the cross-section of its components. Some of them as Barium, Chlorine, Potassium and Sulphur have capture cross sections that are almost superimposing their own total cross sections, especially for what concern thermal energy. This implies that mud adsorbs the main part of neutrons in this range of energy hence, shows the lowest response in terms of neutrons count in thermal energy.

Once the tool response to individual materials was characterized and we evaluated how the detector output behaves to any pure components we moved further to understand which ware the effects due to borehole and filling fluids. Firstly, two simplified cases were simulated, a homogeneous-isotropic with zero porosity formation with borehole filled first by mud only and then by water only. The obtained output showed how influence of drilling fluids may widely change the response of the neutron detectors in comparison to that of calcite only. Cross sections have been essential for the interpretation of the output. In Case of borehole filled with water the response is higher, that is due to the presence of Hydrogen. Presence of strong neutrons addressers in mud makes detector response lower for rock with borehole filled with it. We may also notice that borehole filled with mud showed ah higher response in thermal energies than mud only. This is due to the rock presence that contains Carbon and Oxygen, them scatters better than mud components the neutrons. After the simulations with borehole within a non-porous rock, we tried to understand how porosity could be effectively detected, to approximate better the media to a real case. To have an overview about the phenomena, we did three simulations with different porosities for our rock. In all cases the porous of the rock were all

saturated by water. In those simulations, the borehole was filled by water. The result of those three simulations shown the effect of porosity in rock volumes. The presence of water in rock formation gives a higher response respect to the simulation with 0% porosity. The results show also that effect of borehole filling fluids is more important than porosity effect in the case of 15% porosity, this case showed a higher response than 30% porosity simulation. 50% and 30% porosity showed a behaviour of their response that is proportional though the amount of water in the pores. To understand how borehole effects have affected water saturated rock measurements, specifically for 15% porosity case, we performed the same calculations of before but without borehole. Without borehole means that we have done another characterization in mono-media conditions, as we did for the first five cases discussed on the thesis, in which the tool was surrounded by a body of the same material. Thanks to those three simulations, we might say that thermalized neutron count made by the detector increases as well as the presence of Hydrogen in the pores increases and so when porosity increases too. Hence, the proportionality between the Hydrogen index and the porosity has already been confirmed. From the plots in possible to see that the signal of rock formation with 15% of porosity is the lowest one, so borehole effects are eliminated and the proportionality with HI is guaranteed. Once reached this step, we proceed to simulate a model that fits better a real case. To represent better the real case, we used mud as the borehole fluid and we considered the invasion of the rock formation by this mud. Furthermore, real problems consist substantially in four main configurations, that might happen separately or together: rock saturated by water, rock saturated by oil or rock saturated by gas. It is also possible to find a rock that is not saturate by any of the previous fluids. Therefore, in absence of rock porosity, HOIP is zero.

The approximation of invaded zone was thought such as a linear saturation versus distance model, where distance is calculated from the centre of the wellbore. Then, three simulations have been carried out. Each of them is performed with borehole filled by mud and a mud invasion into the rock. The purpose was to detect how mud filtrate disturbances may affect the measurements of HI. The obtained results, in any case, were a decreasing of the response on all the spectrum of the energies considered.

By comparing the result of “mud invaded” simulations, it is possible to appreciate that the response behaves in accordance with all the previous simulations. This accordance means that higher presence of hydrogen in the formation shows always a higher response in thermal neutron energy zone.

The extrapolation of the porosity is done generally with Thermalized part of the spectrum.

Also in the case of mud filtrations, simulations with tool in pushed against the borehole wall and in the centre of the borehole were performed. The results of wall pushed tool simulations were, again, less affected by borehole effect and, therefore, more reliable.

The last two simulations have been conducted to evaluate different responses of the tool in two different times of the well life, namely wireline and while drilling measurements. In the former borehole is uncased while in the latter we have casing.

To evaluate the influence of the casing on the neutron log detector responses we did these two simulations. The results were a disturbance in the thermic part of the spectrum that is due to the composition of the stainless-steel used for the casing. Those two simulations were carried on supposing the tool well centred in the borehole. In real cases tool is pushed against the borehole wall. The purpose of pushing the tool against the wall is to increase its resolution and so its reliability. To understand how the measurement was influenced by the position of the tool in the borehole we perform every simulation in both cases, centred tool and wall side tool. In most cases the result was the when the tool is pushed against the borehole wall the response is more like the response not affected by the borehole. Thus, when the tool is pushed against the wall, borehole effects are less affecting the measurement and the tool reproduces almost the response of the media. Only the simulation with casing shows the opposite trend. This is due to the disturbance of the steel.

Once analysis and the interpretations of the results were ended, it was possible to distinguish between different media and to understand how the presence of hydrogen may influence the measurements. By improving our model and performing an inversion algorithm it is possible to make an estimation of the total porosity of the rock. It is important to say that good comparison and estimation might be carried out if boundary condition are the same and just a parameter changes per time.

For instance, a good comparison was carried out among rocks saturated by water with different porosity and without wellbore effects. Also in the case of mud penetration simulations, into which we changed just the saturating fluid while porosity remained constant, we had a good possibility to compare results, and to check those results with the calibration models done at the beginning.

To conclude, the purpose of this thesis, that was to model a neutron log in different environmental conditions by using a Monte Carlo method, has been reached. A deeper effort about this topic must be done to develop an effective instrument to calculate porosity. An inversion algorithm and field measurements need to be done to overcome the limits of this thesis.

## List of symbols

$A_H$  =atomic mass of Hydrogen atoms in the material

$A_i$  =atomic mass of non-Hydrogen element i

$(C_H)_{\text{mass}}$  =partial concentration of Hydrogen per unit mass

$(C_H)_{\text{vol}}$  = partial concentration of Hydrogen per unit volume

$E$  =Neutrons' energy.

$E_i$  =neutron's nergy for a given state

$f(r, E)$  =Response function.

$HI_{\text{mf}}$  =Hydrogen index for mud

$HI$  =Hydrogen index

$HI_{\text{hc}}$  =Idrogen Index for hydrocarbons

$n_H$  =number of Hydrogen atoms in a molecule of the material

$n_i$  =number of non-Hydrogen atoms of element i in a molecule of the material

$n$  =neutron

$p$  =pressure

$p_1$  =atmospheric pressure

$p_2$  =reservoir pressure in accordance with lithostatic gradient

$R$  =Reaction rate integrated over volume and energy  $S$  =Source Term.

$R_w$  =Resistivity of the water

$R_{ox}$  =Resistivity of the fluxed zone

$R_t$  =True resistivity of the formation

$R_{mc}$  =Mud cake resistivity

$S_{x_0}$  =Saturation of Fluxed zone

$S_{\text{wirr}}$  =Irriducible water saturation

$S_{or}$  =Residual oil saturation

$T_1$  =Standard temperature

**T<sub>2</sub>=reservoir temperature in accordance with temperature gradient**

**V=Volume**

**V<sub>1</sub>=standard volume of a mole in standard condition.**

**V<sub>2</sub>=Unknown volume**

**y<sub>i</sub>=mole fraction in gas phase**

**γ=Photon**

**ϕ=Porosity**

**ϕ<sub>N</sub>=Neutron porosity**

**Φ=angular flux, vector which specify neutrons crossing a unit surface per unit time.**

**φ(r, E)=Flux function.**

**Ω=Given direction**

**ρ<sub>b</sub>=bulk density**

**$\tilde{\rho}$  =molar density of the gas.**

**$\tilde{\rho}_{ev}$ = average molar density of the gas.**

**Σ<sub>t</sub>=Total interaction Cross section.**

**Σ<sub>s</sub>=Scattering cross section.**

**$\ln \frac{E_0}{E_i}$  = Lethargy.**

### **List of acronyms**

**CNT=Compensated Neutron Tool**

**CNL=Compensated Neutron Logs**

**DNL=Dual energy Neutron Logs**

**GNT=Gamma ray Neutron Tool**

**HGNS=Highly Gamma Ray Neutrons probe**

**HOIP=Hydrocarbons Originally in Place**

**QCNT= SlimXtreme Compensated Neutron Tool**

**SCNT= Slim Compensated Neutron Porosity Too**

**SNP= Slim Neutron Probe**

**VTT= Valtion teknillinen tutkimuslaitos**

### **List of nuclides**

**H=Hydrogen**

**He=Helium**

**Be=Berilyum**

**C=Carbon**

**N=Nitrogen**

**O=Oxygen**

**Na=Sodium**

**Al=Alluminium**

**Si=Silicon**

**S=Sulphur**

**Cl=Chlorine**

**K=Potassium**

**Ca=Calcium**

**Cr=Cromium**

**Mn=Manganese**

**Fe=Iron**

**Ni=Nichel**

**Mo=Molibedenum**

**Cd=Cadmium**

**Ba=Barium**

**Ta=Tallium**

**Pu=Plutonium**

**Am=Americyum**

## 6 References

de l'Acad. Roy. des. Sciences (1733), 43–45; naturelle, générale et particulière Supplément 4 (1777), p. 46

Nuclear magnetic resonance and formation porosity, Matthias appeal, 2004

Becker, B., Dagan, R. and Lohnert, G. (2009) "Proof and implementation of the stochastic formula for ideal gas, energy dependent scattering kernel." *Ann. Nucl. Energy*, 36 (2009) 470-474. MCNPTM–A General Monte Carlo N–Particle Transport Code Version 4C Judith F. Briesmeister, Editor

Scienza e ingegneria dei materiali. Una introduzione ,Autore: William Callister,1985

Cetnar, J. (2006) "General solution of Bateman equations for nuclear transmutations." *Ann. Nucl. Energy*, 33 (2006) 640-645.

Basic Health Physics 25 Neutron Sources, Chartier, 2010

Revision of the ISO 8529 standards calculation of the (AmBe) neutron spectrum, J-L Chartier, 2014

E. R. (Ross) Crain, Crain's Petrophysical Handbook, January 2015

Neutron detectors, T.W. Crane and M.P. Baker

Well Logging for Earth Scientists, Authors: Ellis, Darwin V., Singer, Julian M, 2007

Dufek, J. and Valtavirta, V. (2014) "Time step length versus efficiency of Monte Carlo burnup calculations." *Ann. Nucl. Energy*, 72 (2014) 409-412.

Ellis, D.V. 1990. Some Insights on Neutron Measurements. *IEEE Trans. on Nuclear Science* 37 (2): 959

Cash well, E.D.; Everett, C.J. (1959). A Practical Manual on the Monte Carlo Method for Random Walk Problems (PDF). London: Pergamon Press]

Fridman, E., Shwageraus, W. and Galperin, A. (2008b) "Efficient generation of one-group cross sections for coupled Monte Carlo depletion calculations." *Nucl. Sci. Eng.*, 159 (2008) 37-47.

Fridman, E., Shwageraus, E. and Galperin, A. (2008a) "Implementation of multi-group cross-section methodology in BGCORE MC-depletion code." In proc. PHYSOR 2008, Interlaken, Switzerland, Sept. 14-19, 2008

Girard, J.F., Boucher, M., Legchenko, A., and Baltassat, J.M., "2D magnetic resonance tomography applied to karstic conduit imaging", *Journal of Applied Geophysics*, Vol. 63, No. 3-4, pp. 103-116, 2007/12/5.

Paul Grover, Petrophysics MSc Course Notes,

Haeck, W. and Verboomen, B. (2007) "An optimum approach to Monte Carlo burnup." *Nucl. Sci. Eng.*, 156 (2007) 180-196

Hilchie, Douglas W. (1990). *Wireline: A history of the well logging and perforating business in the oil fields*. Boulder, Colorado: Privately Published. p. 200.

NMR Properties of Reservoir Fluids George Hirasaki<sup>1</sup>, Matthias Appel<sup>2</sup>, Justin Freeman

Ikonen, T. (2013a) "FINIX - fuel behavior model and interface for multiphysics applications - code documentation for version 0.13.9." VTT-R-06563-13, VTT Technical Research Centre of Finland, 2013.

Isotalo, A. and Aarnio, P. (2011a) "Comparison of depletion algorithms for large systems of nuclides." *Ann. Nucl. Energy*, 38 (2011) 261-268.

Carlo Jacoboni e Paolo Lugli, *The Monte Carlo Method for Semiconductor Device Simulation* - Springer-Verlag

Central Limit Theorem by Robert D. Klauber July 7, 2015

Krouse, D. P.; Brereton, T.; Tamer, T.; Boteh, Z. I. (2014). "Why the Monte Carlo method is so important today". *WIREs Compute Stat.* 6: 386–392. doi:10.1002/wics.1314

Lands Highway Division, Lakewood, CO, Publication No. FHWA-IF-04-021, September 2003.

Serpent 1 User's Manual (March 6, 2013) Lappanen

Leppänen, J. (2013a) "Development of a dynamic simulation mode in the Serpent 2 Monte Carlo code." In proc. M&C 2013, Sun Valley, ID, May 5-9, 2013.

Leppänen, J. (2013b) "Modeling of nonuniform density distributions in the Serpent 2 Monte Carlo code." *Nucl. Sci. Eng.*, 174 (2013) 318-325.

V.McLane, editor ENDF-102 data formats and procedures for the evaluated nuclear data file ENDF-6, BNL-NCS-44945-01/04. Rev. Brookhaven National Laboratory, 2001

N. Metropolis; A.W. Rosenbluth; M.N. Rosenbluth; A.H. Teller & E. Teller (1953). "Equation of State Calculations by Fast Computing Machines". *Journal of Chemical Physics*. 21 (6):

D.L Price and K. Skold, "Introduction to Neutron Scattering" Methods of Experimental Physics 23A, 1 (1986)

K. O. Ott, W. A. Bezella, Introductory Nuclear Reactor Statics, American Nuclear Society, Revised edition (1989), 1989, ISBN: 0-894-48033-2

Pusa, M. and Leppänen, J. (2010) "Computing the matrix exponential in burnup calculations." Nucl. Sci. Eng., 164 (2010) 140-150.

Pusa, M. (2011) "Rational approximations to the matrix exponential in burnup calculations." Nucl. Sci. Eng., 169 (2011) 155-167.

Pusa, M. and Leppänen, J. (2012) "An efficient implementation of the Chebyshev rational approximation method (CRAM) for solving the burnup equations." In proc. PHYSOR 2012,

Pusa, M. (2013a) "Accuracy considerations for Chebyshev rational approximation method (CRAM) in burnup calculations." In proc. M&C 2013, Sun Valley, ID, May 5-9, 2013.

Pusa, M. (2013b) "Numerical methods for nuclear fuel burnup calculations." D.Sc. Thesis, Aalto University, 2013. (VTT Science 32)

Pusa, M. and Leppänen, J. (2013c) "Solving linear systems with sparse Gaussian elimination in the Chebyshev rational approximation method (CRAM)." Nucl. Sci. Eng., 175 (2013) 250-258. Knoxville, TN, Apr. 15-20, 2012

Fundamentals of Well-Log Interpretation, The Acquisition of Logging Data, Edited by O. Serra, Volume 15, Part A, Pages iii-vii, 1-423 (1984)

©Schlumberger August 2004 \*Mark of Schlumberger Produced by Marketing Communications, Houston. Neutron Porosity Tools

schlumberger log interpretation principal and application, 1989

Actinide Beryllium Neutron Source with Reduced Dispersion Characteristics. Background Information on AmBe Source Fabrication. Patent S-116,232., Louis D. Schulte, MET-1, 2011

How porosity is measured, Tony Smithson, 2012

Exploration geophysics material, Socco, 2017

Experimental techniques in nuclear and particles physics, Tavarner. S, 2010, IX, 306p., Hardcover, Springer

Radioactivity and uranium content of some cretaceous shales, central great plains Harry A. Tourtelot, 1978

Wightman, W. E., Jalinoos, F., Sirles, P., and Hanna, K. (2003). "Application of Geophysical Methods to Highway Related Problems." Federal Highway Administration, Central Federal

Valtavirta, V., Ikonen, T., Viitanen, T. and Leppänen, J. (2014b) "Simulating Fast Transients with Fuel Behavior Feedback Using the Serpent 2 Monte Carlo Code." In proc. PHYSOR 2014, Kyoto, Japan, Sep. 28 - Oct. 3, 2014.

The Use of Bentonite in Drilling Mud, Andy Varoshotis, 2016

Fluid Mechanics in porous media materials, Viberti, 2017

## **6.1 Web references**

[1] [https://education.jlab.org/glossary/neutron\\_emission.html](https://education.jlab.org/glossary/neutron_emission.html)

[2] [https://www.vacutec-gmbh.de/fileadmin/user/Prospekt\\_He-3\\_Neutron\\_Detectors.pdf](https://www.vacutec-gmbh.de/fileadmin/user/Prospekt_He-3_Neutron_Detectors.pdf)

[3] <https://www.oecd-nea.org/janis/>

[4] [http://www.globaldrillchem.com/Sito della techint](http://www.globaldrillchem.com/Sito_della_techint)

[5] <http://www.irochemical.com/>

[6] <http://petrowiki.org/PetroWiki>

[7] <http://www.glossary.oilfield.slb.com/>

[8] <http://www.halliburton.com/en-US/default.page>

APPENDIX A) Stainless Steel specificatios.

GRADES		Chemical composition (cast analysis) (1)(7) of stainless steel flat products										
Name Designation EN	EN Number	Designation AISI/ASTM	C	Si	Mn	P max	S	N	Cr	Mo	Ni	Others
<b>AUSTENITIC</b>												
X12CrNiN17-7-5	1.4372	201	50.15	51.00	5.50 to 7.50	0.045	50.015	0.05 to 0.25	16.00 to 18.00		3.50 to 5.50	
X12CrNiN18-9-5	1.4373	202	50.15	51.00	7.50 to 10.50	0.045	50.015	0.05 to 0.25	17.00 to 19.00		4.00 to 6.00	
X2CrNiMn17-7-5	1.4371		50.030	51.00	6.00 to 8.00	0.045	50.015	0.15 to 0.20	16.00 to 17.00		3.50 to 5.50	
X2CrNiCuNb17-8-3	1.4597		50.10	52.00	6.50 to 8.50	0.045	50.030	0.15 to 0.30	16.00 to 18.00	51.00	52.00	Cr:2.00 to 3.50; B: 0.0005 to 0.0050
X1TiCrNiMn19-6-6	1.4369		0.07 to 0.15	0.50 to 1.00	5.00 to 7.50	0.030	50.015	0.20 to 0.30	17.50 to 19.50		6.50 to 8.50	
X10CrNi18-8	1.4310	301	0.05 to 0.15	52.00	52.00	0.045	50.015	50.11	16.00 to 19.00	50.80	6.00 to 9.50	
X3CrNi17-7	1.4319	301 L	50.07	51.00	52.00	0.045	50.030	50.11	16.00 to 18.00		6.00 to 8.00	
X3CrNi18-7	1.4318	301 LN	50.030	51.00	52.00	0.045	50.015	0.10 to 0.20	16.50 to 18.50		6.00 to 8.00	
X3CrNi18-9	1.4305	303	50.10	51.00	52.00	0.045	50.030	50.10	17.00 to 19.00		8.00 to 10.00	Cr:1.00
X3CrNi18-9	1.4301	304	50.07	51.00	52.00	0.045	50.015	50.11	17.50 to 19.50		8.00 to 10.50	
X3CrNi18-10	1.4311	304 LN	50.030	51.00	52.00	0.045	50.015	0.12 to 0.22	17.50 to 19.50		8.50 to 11.50	
X3CrNi18-10	1.4948	304 H	0.04 to 0.08	51.00	52.00	0.035	50.015	50.11	17.00 to 19.00		8.00 to 11.00	
X3CrNi18-9	1.4307	304 L	50.030	51.00	52.00	0.045	50.015	50.11	17.50 to 19.50		8.00 to 10.50	
X3CrNi19-11	1.4306	304 LN	50.030	51.00	52.00	0.045	50.015	50.11	18.00 to 20.00		10.00 to 12.00	
X3CrNi19-9	1.4315	304 N	50.06	51.00	52.00	0.045	50.015	0.12 to 0.22	18.00 to 20.00		8.00 to 11.00	
X3CrNi18-12	1.4303	305	50.06	51.00	52.00	0.045	50.015	50.11	17.00 to 19.00		11.00 to 13.00	
X15CrNiSi20-12	1.4828		50.20	1.50 to 2.50	52.00	0.045	50.015	50.11	19.00 to 21.00		12.00 to 14.00	
X12CrNi25-13	1.4833	309 S	50.15	51.00	52.00	0.045	50.015	50.11	22.00 to 24.00		19.00 to 22.00	
X3CrNi25-21	1.4845	310 S	50.10	51.00	52.00	0.045	50.015	50.11	24.00 to 26.00		19.00 to 22.00	
X3CrNiMo17-12-2	1.4401	316	50.07	51.00	52.00	0.045	50.015	50.11	16.50 to 18.50	2.00 to 2.50	10.50 to 13.00	
X3CrNiMo17-3-3	1.4436	316	50.05	51.00	52.00	0.045	50.015	50.11	16.50 to 18.50	2.50 to 3.00	10.50 to 13.00	
X3CrNiMo17-12-2	1.4404	316 H	0.04 to 0.10	50.75	52.00	0.045	50.030	0.10 to 0.16	16.00 to 18.00	2.00 to 3.00	10.00 to 14.00	
X3CrNiMo18-14-3	1.4435	316 L	50.030	51.00	52.00	0.045	50.015	50.11	16.50 to 18.50	2.00 to 2.50	10.00 to 13.00	
X3CrNiMo17-12-3	1.4432	316 L	50.030	51.00	52.00	0.045	50.015	50.11	17.00 to 19.00	2.50 to 3.00	12.50 to 15.00	
X3CrNiMo17-1-2	1.4406	316 LN	50.030	51.00	52.00	0.045	50.015	50.11	16.50 to 18.50	2.00 to 3.00	10.50 to 13.00	
X3CrNiMo17-13-3	1.4429	316 LN	50.030	51.00	52.00	0.045	50.015	0.12 to 0.22	16.50 to 18.50	2.50 to 3.00	11.00 to 14.00	
X3CrNiMo117-12-2	1.4571	316 Ti	50.08	51.00	52.00	0.045	50.015	0.12 to 0.22	16.50 to 18.50	2.00 to 2.50	10.50 to 13.50	Ti:5 x C to 0.70
X3CrNiMoN17-12-2	1.4580	316 CB	50.08	51.00	52.00	0.045	50.015	50.11	16.50 to 18.50	2.00 to 2.50	10.50 to 13.50	Nb:10 x C to 1.00
<b>AUSTENITIC</b>												
X3CrNiMo18-15-4	1.4438	317 L	50.030	51.00	52.00	0.045	50.015	50.10	18.00 to 20.00	3.00 to 4.00	13.00 to 16.00	
X3CrNiMo18-12-4	1.4434	317 LN	50.030	51.00	52.00	0.045	50.015	0.10 to 0.20	16.50 to 19.50	3.00 to 4.00	10.50 to 14.00	
X3CrNiMo17-13-5	1.4439	317 L/N	50.030	51.00	52.00	0.045	50.015	0.12 to 0.22	16.50 to 18.50	4.00 to 5.00	12.50 to 14.50	
X3CrNi17-8-10	1.4541	321	50.08	51.00	52.00	0.045	50.015	50.11	17.00 to 19.00		9.00 to 12.00	Ti:5 x C to 0.70
X3CrNi17-8-10	1.4878	321 H	50.10	51.00	52.00	0.045	50.015	50.11	17.00 to 19.00		9.00 to 12.00	Ti:5 x C to 0.80
X3CrNi18-10	1.4550	347	50.08	51.00	52.00	0.045	50.015	50.11	17.00 to 19.00		9.00 to 12.00	Nb:10 x C to 1.00
X3CrNi18-10	1.4550	347 H	0.04 to 0.10	50.75	52.00	0.045	50.015	50.11	17.00 to 19.00		9.00 to 12.00	Nb:8 x C to 1.00
X1CrNi25-21	1.4335	50.20	50.20	50.25	52.00	0.025	50.010	50.11	24.00 to 26.00	50.20	20.00 to 22.00	
X1CrNiMo25-22-2	1.4466	310 H/LN	50.020	50.70	52.00	0.025	50.010	0.10 to 0.16	24.00 to 26.00	2.00 to 2.50	21.00 to 23.00	
X1CrNi18-13-4	1.4381		50.015	50.70	52.00	0.025	50.010	50.11	16.50 to 18.50	50.20	14.00 to 16.00	
X1CrNiMoCu17-2-4	1.4583		50.020	50.70	52.00	0.030	50.010	50.11	26.00 to 28.00	3.00 to 4.00	30.00 to 32.00	
X1CrNiMoCu25-25-5	1.4537		50.020	50.70	52.00	0.030	50.010	0.17 to 0.25	24.00 to 26.00	4.70 to 5.70	24.00 to 27.00	
X1CrNiMoCu25-20-5	1.4539	904 L	50.020	50.70	52.00	0.030	50.010	50.15	19.00 to 21.00	5.00 to 5.00	24.00 to 26.00	
X1CrNiMoCu20-18-7	1.4547		50.020	50.70	52.00	0.030	50.010	0.18 to 0.25	19.50 to 20.50	6.00 to 7.00	17.50 to 18.50	
X1CrNiMoCu24-22-8	1.4552		50.020	50.50	52.00	0.030	50.005	0.45 to 0.55	23.00 to 25.00	7.00 to 8.00	21.00 to 23.00	
X1CrNiMoCuNi21-22-6	1.4659		50.020	50.70	2.00 to 4.00	0.030	50.010	0.35 to 0.50	23.00 to 25.00	5.50 to 6.50	21.00 to 23.00	
X1CrNiMoCuNi25-20-7	1.4529		50.020	50.50	51.00	0.030	50.010	0.15 to 0.25	19.00 to 21.00	6.00 to 7.00	24.00 to 26.00	
X3CrNiMo25-18-6-5	1.4565		50.030	51.00	5.00 to 7.00	0.030	50.015	0.30 to 0.60	24.00 to 26.00	4.00 to 5.00	16.00 to 19.00	
X12NiCu35-16	1.4864	330	50.015	1.00 to 2.00	52.00	0.045	50.015	50.11	15.00 to 17.00		33.00 to 37.00	
X12NiCu35-16	1.4835		0.05 to 0.12	1.40 to 2.50	51.00	0.045	50.015	0.12 to 0.20	20.00 to 22.00		10.00 to 12.00	Ce:0.03 to 0.08
X10NiCuAl13-2-1	1.4876		50.12	50.30	52.00	0.030	50.015	50.11	19.00 to 23.00		30.00 to 34.00	Al:0.15 to 0.60; Ti:0.15 to 0.60
X8NiCuCr32-27	1.4877		0.04 to 0.08	50.20	51.00	0.020	50.015	50.11	26.00 to 28.00		31.00 to 33.00	Al:0.025; Ce:0.05 to 0.10; Nb:0.60 to 1.00
X8NiCuNi9-10	1.4818		0.04 to 0.08	1.00 to 2.00	51.00	0.045	50.015	0.12 to 0.20	18.00 to 20.00		9.00 to 11.00	Ce:0.03 to 0.08
X8NiCuNi35-25	1.4854		0.04 to 0.08	1.20 to 2.00	52.00	0.040	50.015	0.12 to 0.20	24.00 to 26.00		34.00 to 36.00	Ce:0.03 to 0.08

Figura A1: Chemical compositions of Austenitic Stainless Steel. In the columns are listed: Name of the steel, En Number designation, Austenitic designation. Then the chemical composition in mass fraction for C, Si, Mn, P, S, N, Cr, Mo, Ni and others.

Chemical composition (cast analysis) <sup>(1)(7)</sup> of stainless steel flat products														
EN	Name Designation EN	EN Number Designation	Designation AISI/ASTM	C	Si	Mn	P max	S	N	Cr	Mo	Ni	Others	
GRAD E3	X2CrNiMoN22-5-3 <sup>(8)</sup>	1.4462 <sup>(9)</sup>	2205	≤0.030	≤1.00	≤2.00	0.035	≤0.015	0.10 to 0.22	21.00 to 23.00	2.50 to 5.50	4.50 to 6.50		
	X2CrNi24-4 <sup>(8)</sup>	1.4362 <sup>(9)</sup>	2304	≤0.030	≤1.00	≤2.00	0.035	≤0.015	0.05 to 0.20	22.00 to 24.00	0.10 to 0.60	3.50 to 5.50	Co:0.10 to 0.80	
	X2CrNiCN23-4	1.4555		≤0.030	≤1.00	≤2.00	0.035	≤0.015	0.05 to 0.20	22.00 to 24.00	0.10 to 0.60	3.50 to 5.50	Co:1.00 to 3.00	
	X2CrNiMoN25-7-4 <sup>(8)</sup>	1.4410 <sup>(9)</sup>	2507	≤0.030	≤1.00	≤2.00	0.035	≤0.015	0.24 to 0.35	24.00 to 26.00	3.00 to 4.50	6.00 to 8.00		
	X2CrNiMoCN25-6-3	1.4507	295	≤0.030	≤0.70	≤2.00	0.035	≤0.015	0.20 to 0.30	24.00 to 26.00	3.00 to 4.00	6.00 to 8.00	Co:1.00 to 2.50	
	X2CrNiMoCN25-7-4	1.4501		≤0.030	≤1.00	≤1.00	0.035	≤0.015	0.20 to 0.30	24.00 to 26.00	3.00 to 4.00	6.00 to 8.00	Co:0.50 to 1.00; W: 0.50 to 1.00	
	X2CrNiMoSi18-5-3	1.4424		≤0.030	1.40 to 2.00	1.20 to 2.00	0.035	≤0.015	0.05 to 0.10	18.00 to 19.00	2.50 to 3.00	4.50 to 5.20		
	X2CrNiMoN29-7-2 <sup>(8)</sup>	1.4477 <sup>(9)</sup>		≤0.030	≤0.50	0.80 to 1.50	0.030	≤0.015	0.30 to 0.40	28.00 to 30.00	1.50 to 2.60	5.80 to 7.50	Co:0.80	
	X2CrNi12	1.4003		≤0.030	≤1.00	≤1.50	0.040	≤0.015 <sup>2)</sup>	≤0.030	16.50 to 12.50		0.30 to 1.00		
	X2CrNi12	1.4512	409	≤0.030	≤1.00	≤1.00	0.040	≤0.015		10.50 to 12.50			Ti:6xC to 0.65	
	X2CrNi12	1.4516		≤0.08	≤0.70	≤1.50	0.040	≤0.015		10.50 to 12.50		0.50 to 1.50	Ti:0.05 to 0.35	
	X6Cr13	1.4000	410S	≤0.08	≤1.00	≤1.00	0.040	≤0.015 <sup>2)</sup>		12.00 to 14.00				
X6Cr13	1.4002	405	≤0.08	≤1.00	≤1.00	0.040	≤0.015 <sup>2)</sup>		12.00 to 14.00			Al: 0.10 to 0.30		
X2CrNiMoTi15-2	1.4589		429 <sup>(8)</sup>	≤0.08	≤1.00	≤1.00	0.040	≤0.015	13.50 to 15.50	0.20 to 1.20	1.00 to 2.50		Ti: 0.30 to 0.50	
X1CrNi615	1.4595			≤0.020	≤1.00	≤1.00	0.025	≤0.015	≤0.020	14.00 to 16.00			Nb: 0.20 to 0.60	
X6Cr17	1.4016	430		≤0.025	≤1.00	≤1.00	0.040	≤0.015 <sup>2)</sup>	≤0.015	16.00 to 18.00			Ti: 0.30 to 0.60	
X2CrNi17	1.4520			≤0.025	≤0.50	≤0.50	0.040	≤0.015	≤0.015	16.00 to 18.00			Nb:12xC to 1.00	
X2CrNi17	1.4511			≤0.05	≤1.00	≤1.00	0.040	≤0.015 <sup>2)</sup>		16.00 to 18.00		1.20 to 1.60		
X6CrNi17-1	1.4017		434	≤0.08	≤1.00	≤1.00	0.040	≤0.015 <sup>2)</sup>		16.00 to 18.00				
X6CrMo17-1	1.4113		434	≤0.08	≤1.00	≤1.00	0.040	≤0.015 <sup>2)</sup>		16.00 to 18.00				
X2CrNi17	1.4510		439	≤0.05	≤1.00	≤1.00	0.040	≤0.015 <sup>2)</sup>		16.00 to 18.00			Ti:4xC to Ni:0.15 to 0.80 <sup>2)</sup>	
X2CrMoTi17-1	1.4513			≤0.025	≤1.00	≤1.00	0.040	≤0.015	≤0.020	16.00 to 18.00	0.80 to 1.40		Ti: 0.30 to 0.60	
X2CrMo18-2	1.4521		444	≤0.025	≤1.00	≤1.00	0.040	≤0.015	≤0.030	17.00 to 20.00	1.80 to 2.50		Ti:4xC to Ni:0.15 to 0.80 <sup>2)</sup>	
X6CrMoNi17-1	1.4526		436	≤0.08	≤1.00	≤1.00	0.040	≤0.015	≤0.040	16.00 to 18.00	0.80 to 1.40		Nb:7xC to Ni:0.10 to 1.00	
X2CrTiNb18	1.4509			≤0.030	≤1.00	≤1.00	0.040	≤0.015	17.50 to 18.50				Nb:3xC to 0.30 to 1.00; Ti:0.10 to 0.60	
X2CrNi27	1.4590			≤0.030	≤1.00	≤1.00	0.040	≤0.015	16.00 to 17.50				Nb: 0.35 to 0.55; Zr: 7xC to Ni:0.15	
X18CrNi28	1.4749		446	0.15 to 0.20	≤1.00	≤1.00	0.040	≤0.015	0.15 to 0.25	26.00 to 29.00				
X10CrNiSi7	1.4713			≤0.12	0.50 to 1.00	≤1.00	0.040	≤0.015	6.00 to 8.00				Al: 0.50 to 1.00	
X10CrNiSi13	1.4724			≤0.12	0.70 to 1.40	≤1.00	0.040	≤0.015	12.00 to 14.00				Al: 0.70 to 1.20	
X10CrNiSi25	1.4762			≤0.12	0.70 to 1.40	≤1.00	0.040	≤0.015	23.00 to 26.00				Al: 1.20 to 1.70	
X2CrMoTi29-4	1.4592			≤0.025	≤1.00	≤1.00	0.030	≤0.010	≤0.045	26.00 to 30.00	3.50 to 4.50		Ti:4xC to Ni:0.15 to 0.80 <sup>2)</sup>	
MARTENSITIC <sup>(10)</sup>	X12Cr13	1.4006	410	0.08 to 0.15	≤1.00	≤1.50	0.040	≤0.015 <sup>2)</sup>		11.50 to 13.50			≤0.75	
	X19Cr13	1.4024		0.12 to 0.17	≤1.00	≤1.00	0.040	≤0.015 <sup>2)</sup>		12.00 to 14.00				
	X20Cr13	1.4021	420	0.16 to 0.25	≤1.00	≤1.00	0.040	≤0.015 <sup>2)</sup>		12.00 to 14.00				
	X30Cr13	1.4028	420	0.26 to 0.35	≤1.00	≤1.50	0.040	≤0.015 <sup>2)</sup>		12.00 to 14.00				
	X39Cr13	1.4031	420	0.36 to 0.42	≤1.00	≤1.00	0.040	≤0.015 <sup>2)</sup>		12.50 to 14.50				
	X46Cr13	1.4034	420	0.43 to 0.50	≤1.00	≤1.00	0.040	≤0.015 <sup>2)</sup>		12.50 to 14.50				
	X50CrNi15	1.4116			0.45 to 0.55	≤1.00	≤1.00	0.040	≤0.015 <sup>2)</sup>	14.00 to 15.00	0.50 to 0.80		V: 0.10 to 0.20	
	X55CrMo14	1.4110			0.48 to 0.60	≤1.00	≤1.00	0.040	≤0.015 <sup>2)</sup>	13.00 to 15.00	0.50 to 0.80		1560.15	
	X39CrMo14	1.4419			0.36 to 0.42	≤1.00	≤1.00	0.040	≤0.015	13.00 to 14.50	0.80 to 1.00			
	X39CrMo17-1	1.4122			0.33 to 0.45	≤1.00	≤1.50	0.040	≤0.015 <sup>2)</sup>	15.50 to 17.50	0.80 to 1.30			
	X39CrNi13-4	1.4313			≤0.05	≤0.70	≤1.50	0.040	≤0.015	12.00 to 14.00	0.30 to 0.70	3.50 to 4.50		
	X40CrNiMo16-5-1	1.4418			≤0.06	≤0.70	≤1.50	0.040	≤0.015 <sup>2)</sup>	15.00 to 17.00	0.80 to 1.50	4.00 to 6.00		
X10CrNiMo12-5-2	1.4422			≤0.020	≤0.50	≤2.00	0.040	≤0.003	11.00 to 13.00	1.30 to 1.80	4.00 to 5.00	Co:0.20 to 0.80		
X10CrNiMo12-7-3	1.4423			≤0.020	≤0.50	≤2.00	0.040	≤0.003	≤0.020	11.00 to 13.00	2.30 to 2.80	6.00 to 7.00	Co:0.20 to 0.80	
PH <sup>(10)</sup>	X5CrNiCuNb16-4	1.4542	630	≤0.07	≤0.70	≤1.50	0.040	≤0.015 <sup>2)</sup>		15.00 to 17.00	≤0.60	3.00 to 5.00	Co:3.00 to 5.00; Nb: 5xC to 0.45	
	X7CrAlNi17-7	1.4568	631	≤0.09	≤0.70	≤1.00	0.040	≤0.015		16.00 to 18.00		6.50 to 7.80 <sup>2)</sup>	Al: 0.70 to 1.50	

Figure A2 Chemical compositions of Duplex, Ferritic and Martensitic Stainless Steel. In the columns are listed: Name of the steel, En Number designation, Austenitic designation. Then the chemical composition in mass fraction for C, Si, Mn, P, S, N, Cr, Mo, Ni and others.

APPENDIX B) Serpent Users manual tables

Type	Description	Parameters
inf	all space	-
px	plane perpendicular to x-axis	$x_0$
py	plane perpendicular to y-axis	$y_0$
pz	plane perpendicular to z-axis	$z_0$
sph	sphere	$x_0, y_0, z_0, r$
cylx	circular cylinder parallel to x-axis	$y_0, z_0, r, x_1, x_2$
cyly	circular cylinder parallel to y-axis	$x_0, z_0, r, y_1, y_2$
cylz or cyl	circular cylinder parallel to z-axis	$x_0, y_0, r, z_1, z_2$
sqc	square cylinder parallel to z-axis	$x_0, y_0, r, r_0$
cube	cube	$x_0, y_0, z_0, r$
cuboid	cuboid	$x_1, x_2, y_1, y_2, z_1, z_2$
hexxc	x-type hexagonal cylinder parallel to z-axis	$x_0, y_0, r, r_0$
hexyc	y-type hexagonal cylinder parallel to z-axis	$x_0, y_0, r, r_0$
hexxprism	x-type hexagonal prism parallel to z-axis	$x_0, y_0, r, z_1, z_2$
hexyprism	y-type hexagonal prism parallel to z-axis	$x_0, y_0, r, z_1, z_2$
cross	cruciform cylinder parallel to z-axis	$x_0, y_0, r, d, r_0$
pad	(see description below)	$x_0, y_0, r_1, r_2, \theta_1, \theta_2$
conx	cone oriented in the x-axis	$x_0, y_0, z_0, r, h$
cony	cone oriented in the y-axis	$x_0, y_0, z_0, r, h$
conz or cone	cone oriented in the z-axis	$x_0, y_0, z_0, r, h$
dode	dodecagonal cylinder parallel to z-axis	$x_0, y_0, r_1, r_2$
octa	octagonal cylinder parallel to z-axis	$x_0, y_0, r_1, r_2$
plane	general plane	$A, B, C, D$
quadratic	general quadratic surface	$A, B, C, D, E, F, G, H, J, K$

Figure B1 Surface type card in Serpent code. (Lappanen, 2015)

Param.	Description	Comments
dr	Reaction multiplier	Determines the response function
dv	Detector volume	Used for normalization
dc	Detector cell	Defines the cell where the reactions are scored
du	Detector universe	Defines the universe where the reactions are scored
dm	Detector material	Defines the material where the reactions are scored
dl	Detector lattice	Defines the lattice where the reactions are scored
de	Detector energy grid	Defines the energy bins for the response function
dx	Detector mesh	Defines the x-mesh where the reactions are scored
dy	Detector mesh	Defines the y-mesh where the reactions are scored
dz	Detector mesh	Defines the z-mesh where the reactions are scored
dt	Detector type	Special detector types
ds	Surface current detector	Defines surface for current detector

Figure B2 Detector cards parameters. (Lappanen, 2015)

	MT	Reaction mode
Material total reactions	0	None
	-1	Total
	-2	Total capture
	-3	Total elastic
	-5	Total (n,2n)
	-6	Total fission
	-7	Total fission neutron production
	-8	Total fission energy deposition
	-9	Majorant
ENDF Reaction modes	1	Total
	2	Elastic scattering
	16	(n,2n)
	17	(n,3n)
	18	Total fission
	19	First-chance fission
	20	Second-chance fission
	51	Inelastic scattering to 1st excited state
	52	Inelastic scattering to 2nd excited state
	...	
	90	Inelastic scattering to 40th excited state
	91	Continuum inelastic scattering
	102	(n, $\gamma$ )
	103	(n,p)
	104	(n,d)
	105	(n,t)
	106	(n, $^3\text{He}$ )
107	(n, $\alpha$ )	

Figure B3 Detector response function cards. (Lappanen, 2015) (McLane, 2001)

Param.	Description	Comments
sw	Source weight	Determines the relative importance of the source
sc	Source cell	Defines the cell where the neutrons are started
sm	Source material	Defines the material where the neutrons are started
sp	Source point	Defines the coordinates of a point source
sx, sy, sz	Source boundaries	Defines the boundaries of the source distribution
sd	Source direction	Defines the source direction vector
se	Source energy	Multiple uses
sb	Source energy bins	Defines a bin-wise energy spectrum
sr	Source reaction	Defines the source reaction
ss	Source surface	Defines a surface source

Figure B4 Sources parameter cards. (Lappanen, 2015)

### APPENDIX C) Components Cross-Sections.

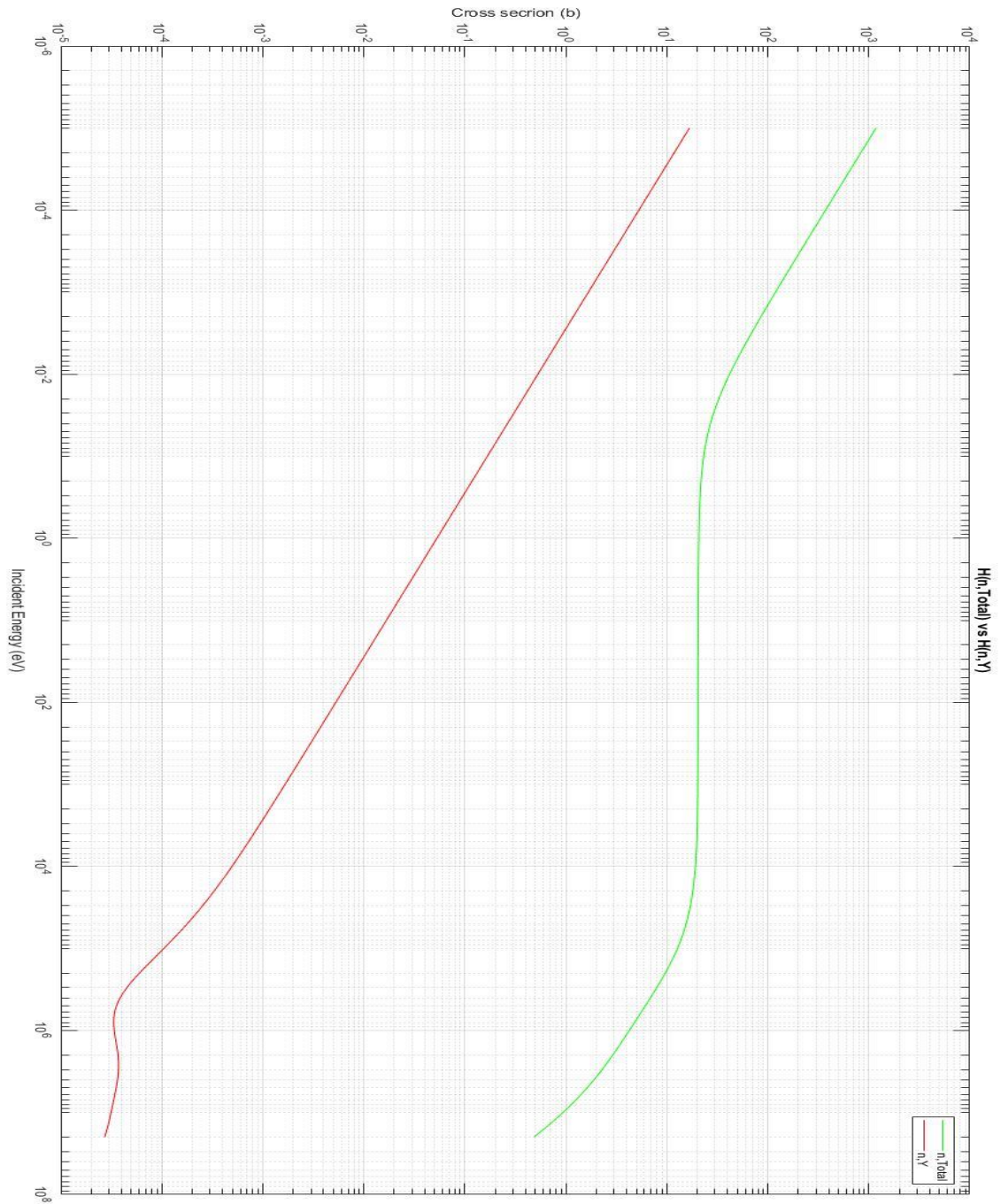


Fig.C1 Comparison between total cross section (Green) of Hydrogen and its capture cross section (Red). In the abscissae are Incident Energies in eV while in ordinates are represented cross section in barns. Hydrogen Carputer cross section contributes to the total in little part. Its major contribution is in low energy zone. Hydrogen is contained in all fluid used in the thesis [3]

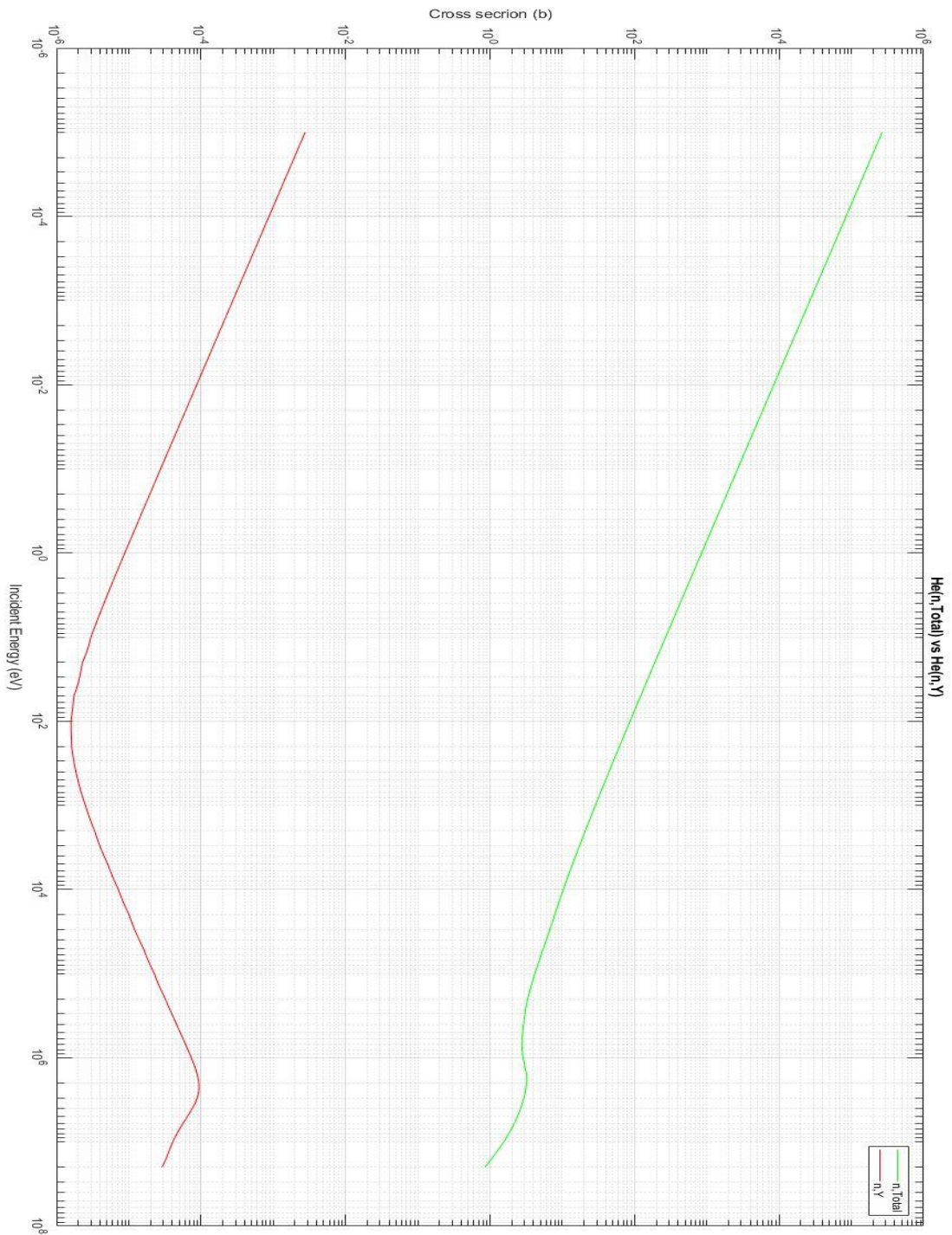


Fig. C2 Comparison between total cross section (Green) of Helium and its capture cross section (Red). In the abscissae are represented Incident Energies in eV while in ordinates are represented cross section in barns. Helium, Carputer cross section contributes to the total in little part. Its major contribution is in very low and very high energy zone. Helium is the gas which fills the detector. [3]

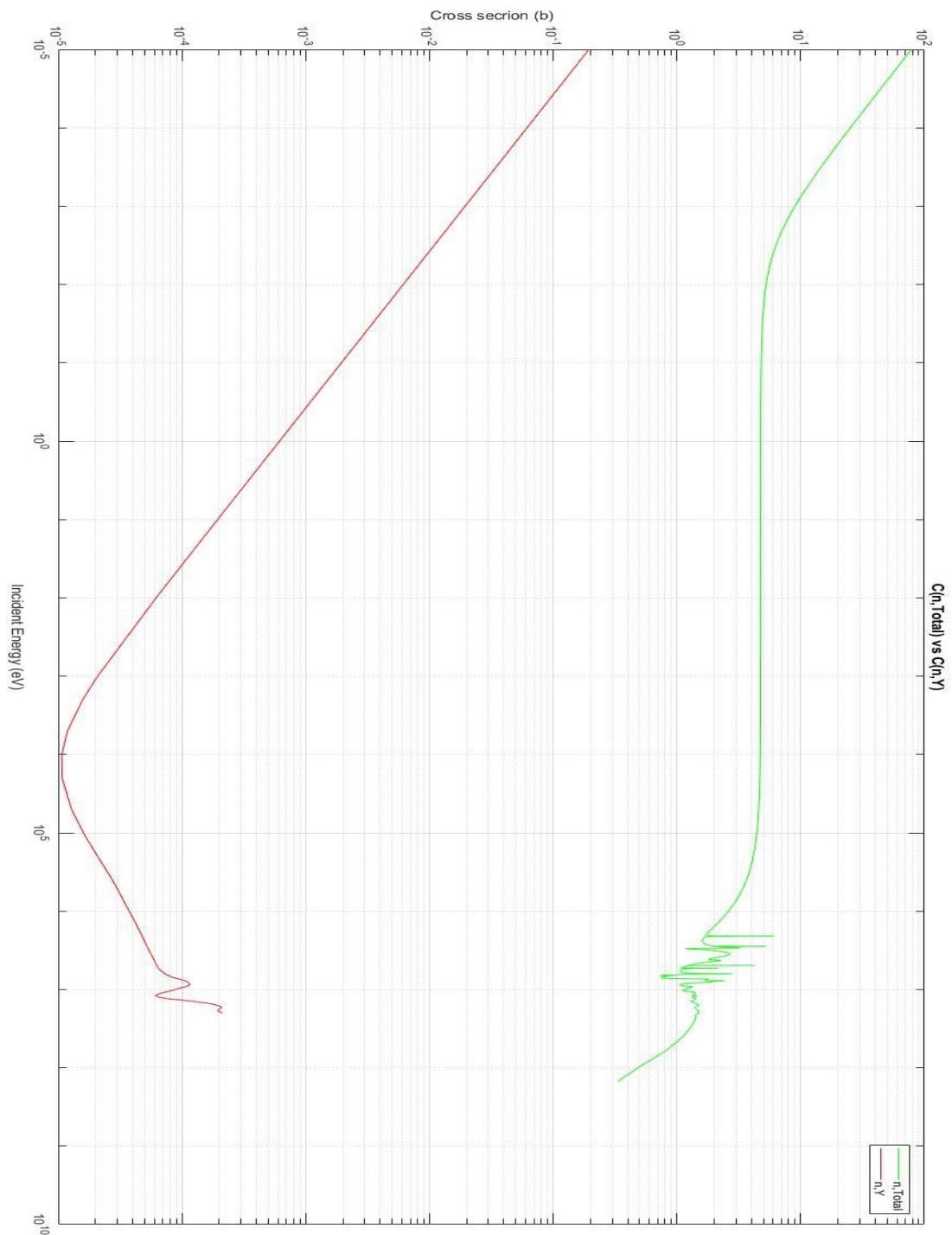


Fig. C3 Comparison between total cross section (Green) of Carbon and its capture cross section (Red). In the abscissae are represented Incident Energies in eV while in ordinates are represented cross section in barns. Carbon Capture cross section contributes to the total in little part. Its major contribution is in low energy zone. Resonance is presence for total cross section in high energy zone. Carbon is contained in Hydrocarbons, Steel and in Calcite [3]

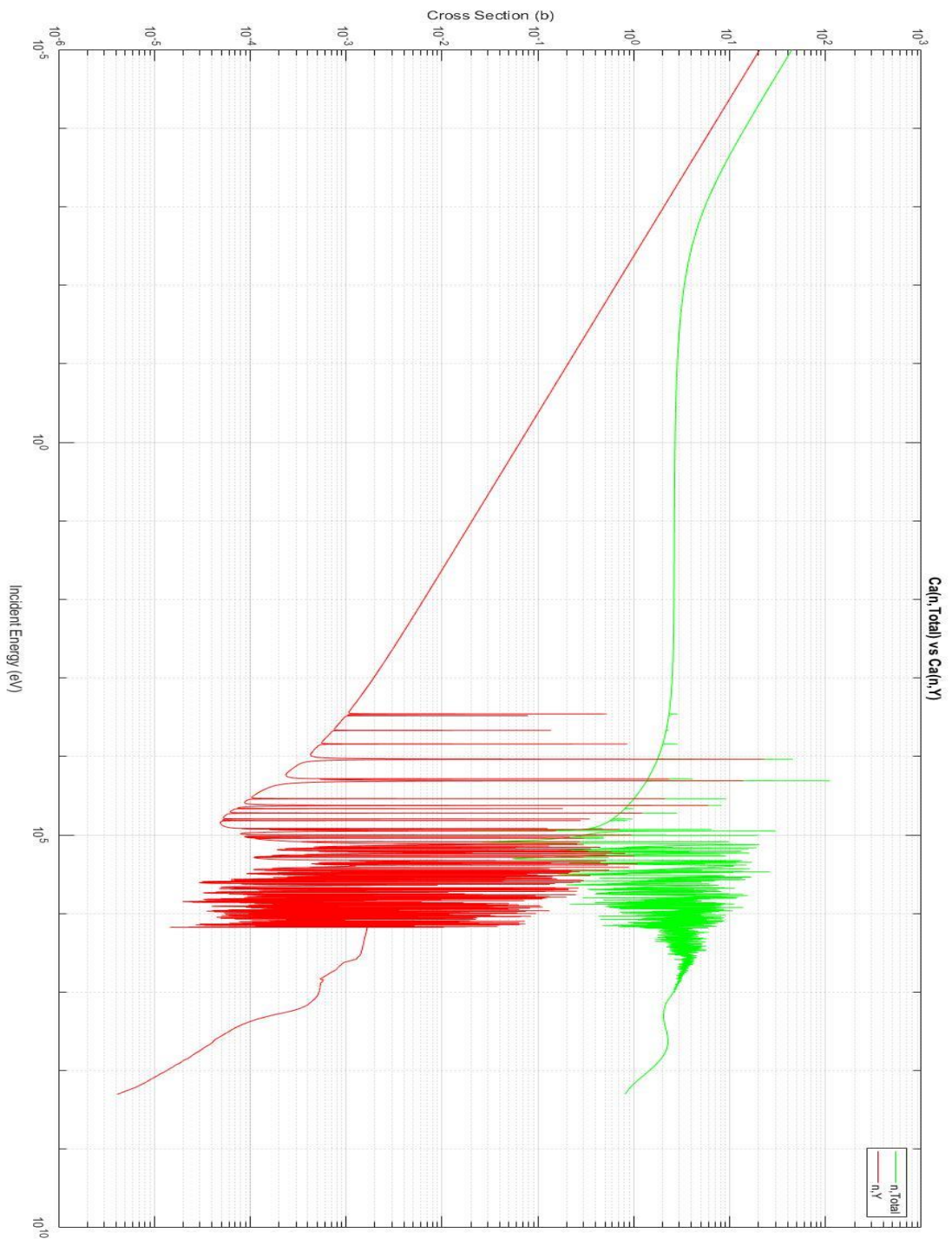


Fig. C4 Comparison between total cross section (Green) of Calcium and its capture cross section (Red). In the abscissae are represented Incident Energies in eV while in ordinates are represented cross section in barns. Calcium Carputer cross section contribution is relevant to the total cross section in low energy zone. At High energy huge resonance is present. Calcium is contained in the rock formation. [3]

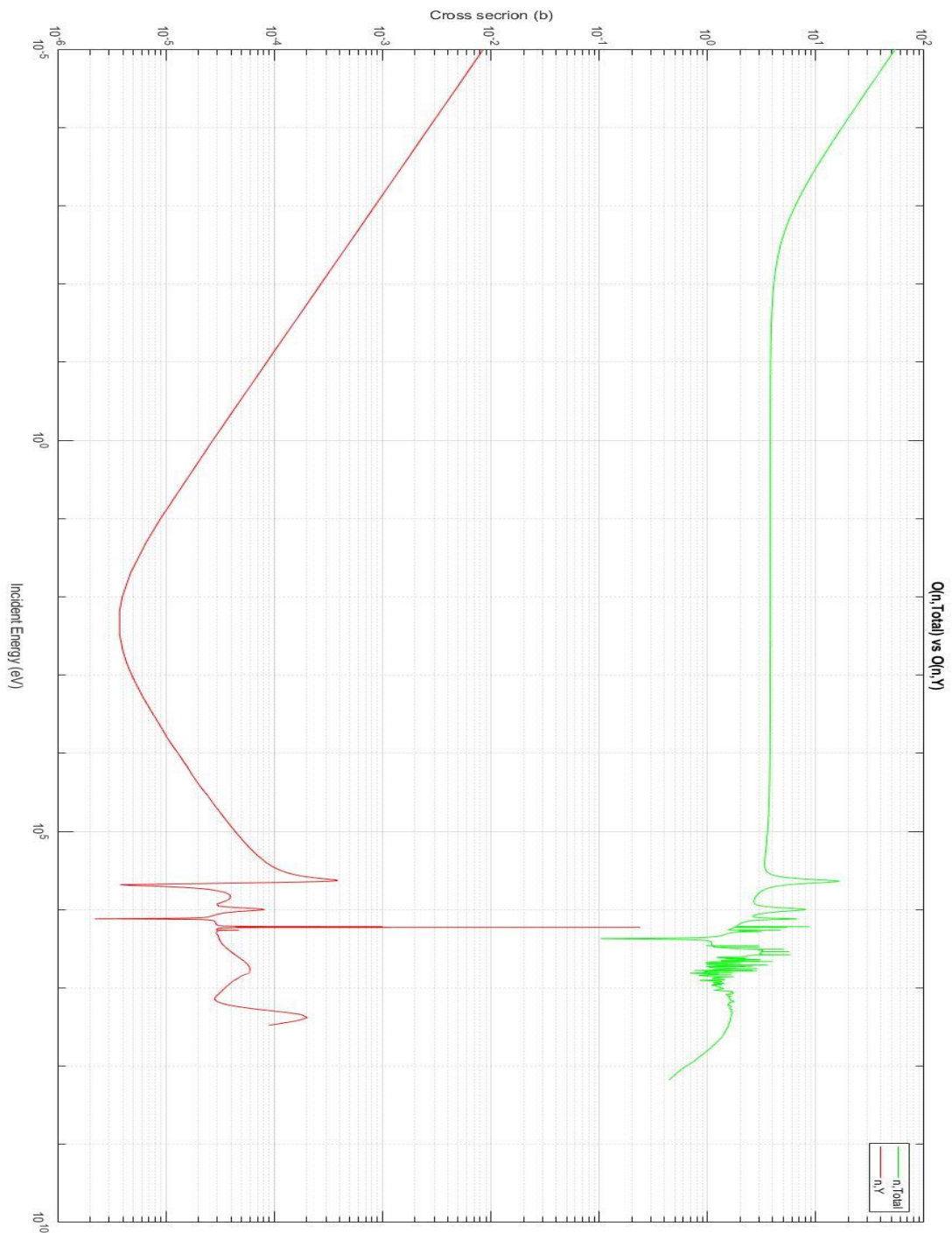


Fig. C5 Comparison between total cross section (Green) of Oxygen and its capture cross section (Red). In the abscissae are represented Incident Energies in eV while in ordinates are represented cross section in barns. Oxygen Carputer cross section contributes little to the total cross section in low energy zone. At High energy resonance is present. Oxygen is present in mud, water and in Calcite [3]

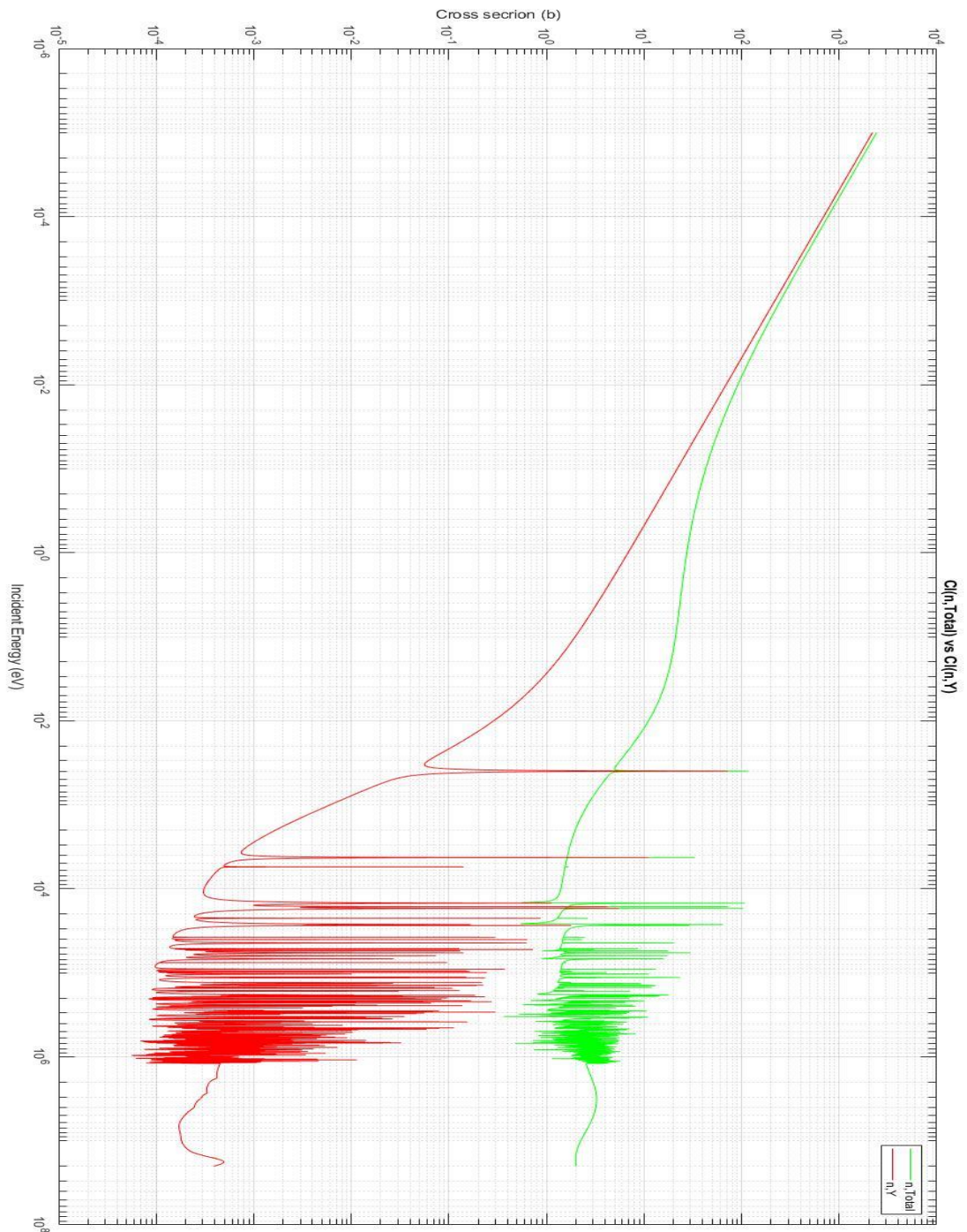


Fig. C6 Comparison between total cross section (Green) of Chlorine and its capture cross section (Red). In the abscissae are represented Incident Energies in eV while in ordinates are represented cross section in barns. Chlorine Capture cross section practically superimpose is Trent with the total cross section in low energy zone. At High energy high resonance is present. Chlorine is present in mud [3]

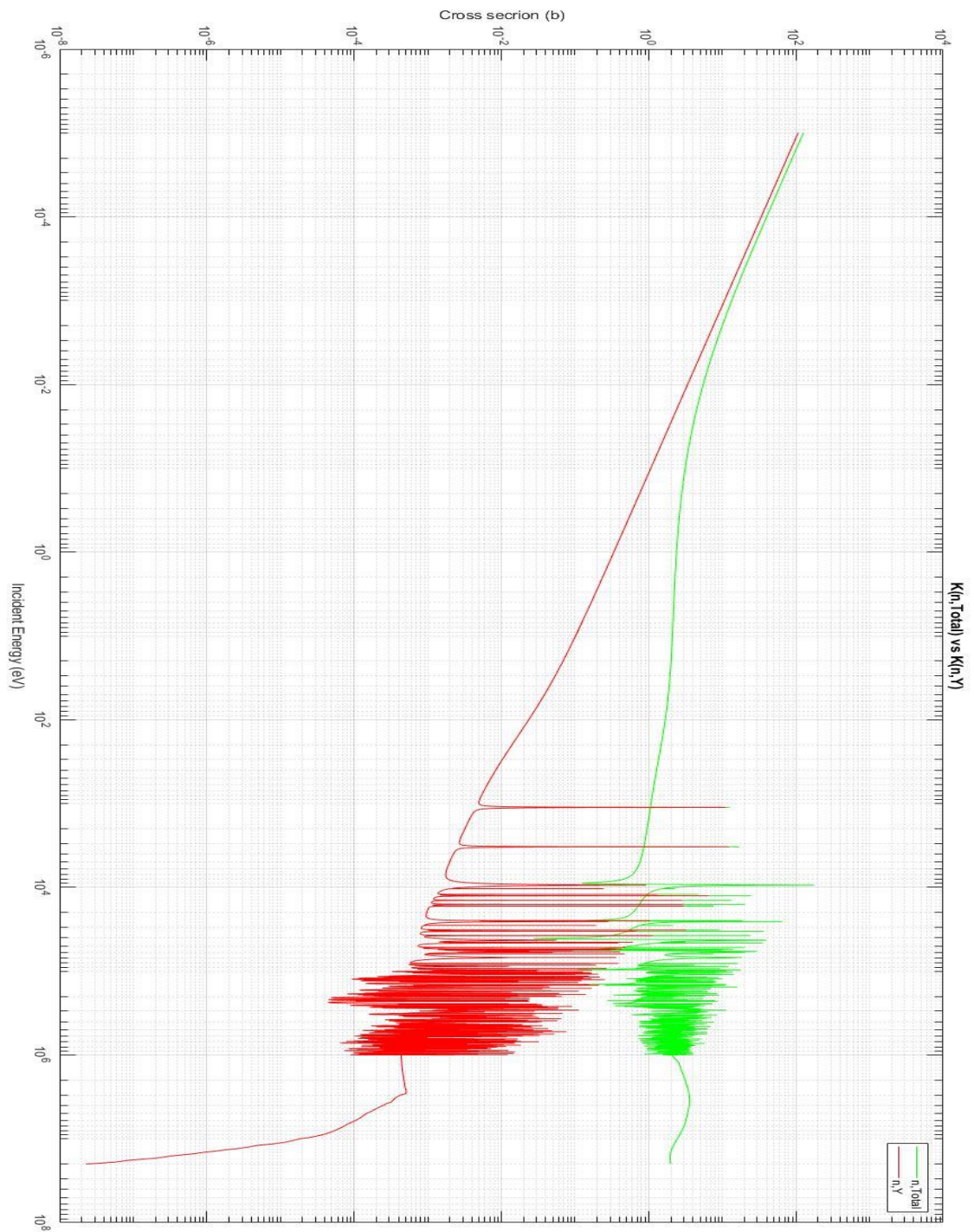


Fig. C7 Comparison between total cross section (Green) of Potassium and its capture cross section (Red). In the abscissae are represented Incident Energies in eV while in ordinates are represented cross section in barns. Potassium Carputer cross section practically superimpose is Trent with the total cross section in low energy zone. At High energy high resonance is present. Potassium is present in mud [3]

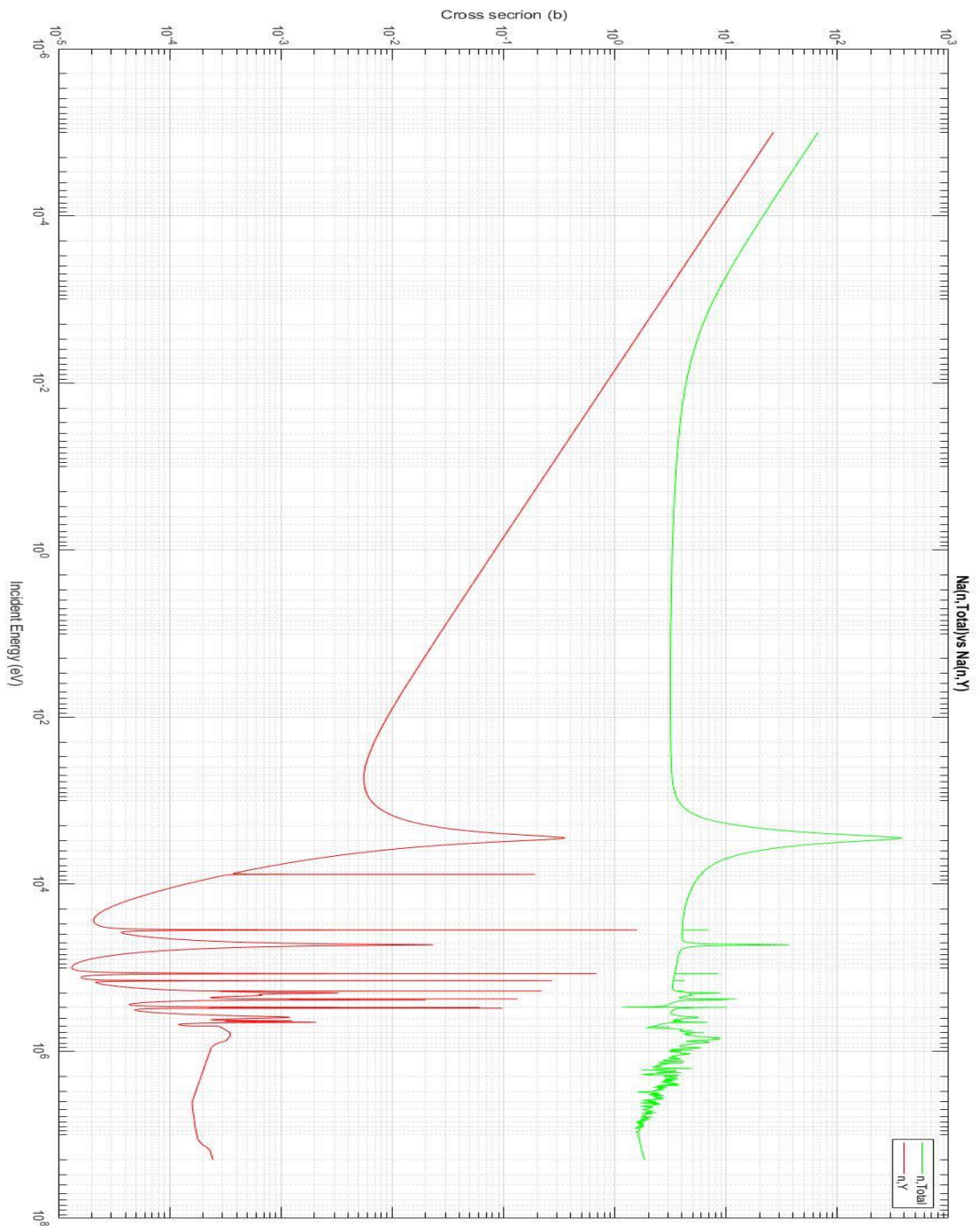


Fig. C8 Comparison between total cross section (Green) of Sodium and its capture cross section (Red). In the abscissae are represented Incident Energies in eV while in ordinates are represented cross section in barns. Sodium Capture cross section has a big contribution on the total cross section in low energy zone. At High energy resonance is present. Sodium is present in mud [3]

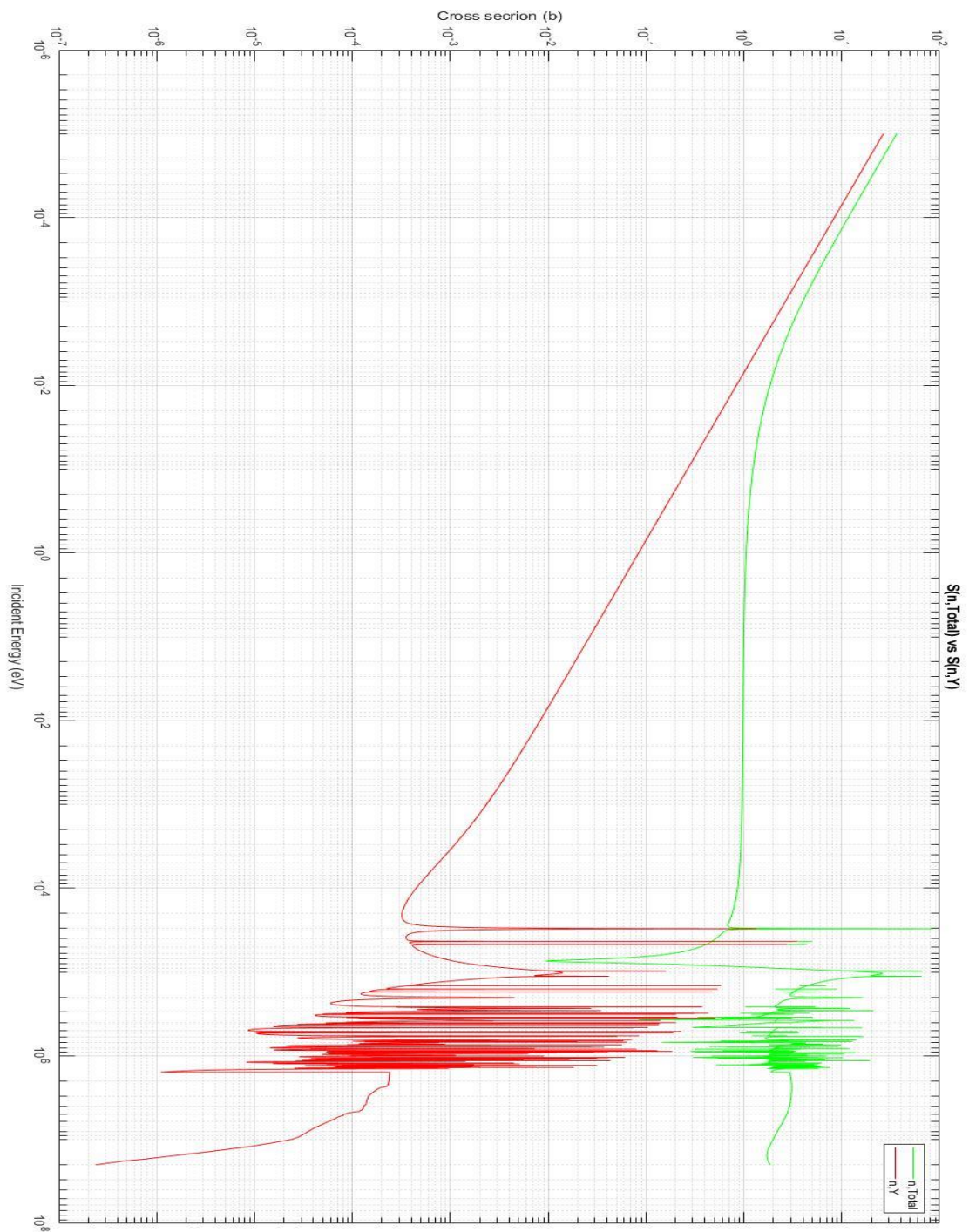


Fig. C9 Comparison between total cross section (Green) of Sulphur and its capture cross section (Red). In the abscissae represents Incident Energies in eV while in ordinates are represented cross section in barns. Sulphur Capture cross section practically superimpose is Trent with the total cross section in low energy zone. At High energy high resonance is present. Sulphur is present in mud [3]

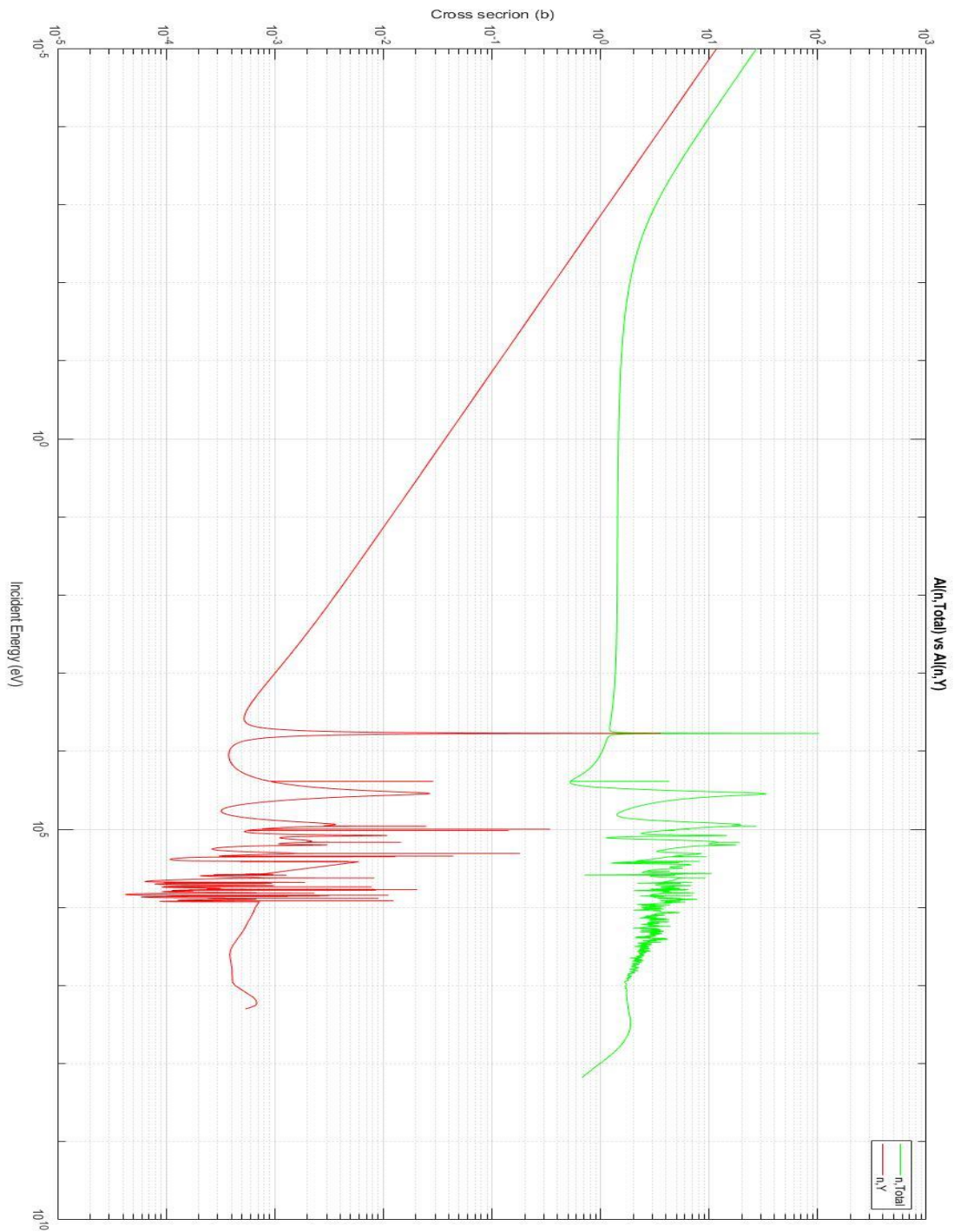


Fig. C10 Fig. C11 Comparison between total cross section (Green) of Aluminum and its capture cross section (Red). In the abscissae are represents Incident Energies in eV while in ordinates are represented cross section in barns. Aluminum Carputer cross section has a big contribution on the total cross section in low energy zone. At High energy resonance is present. Aluminum is present in mud [3]

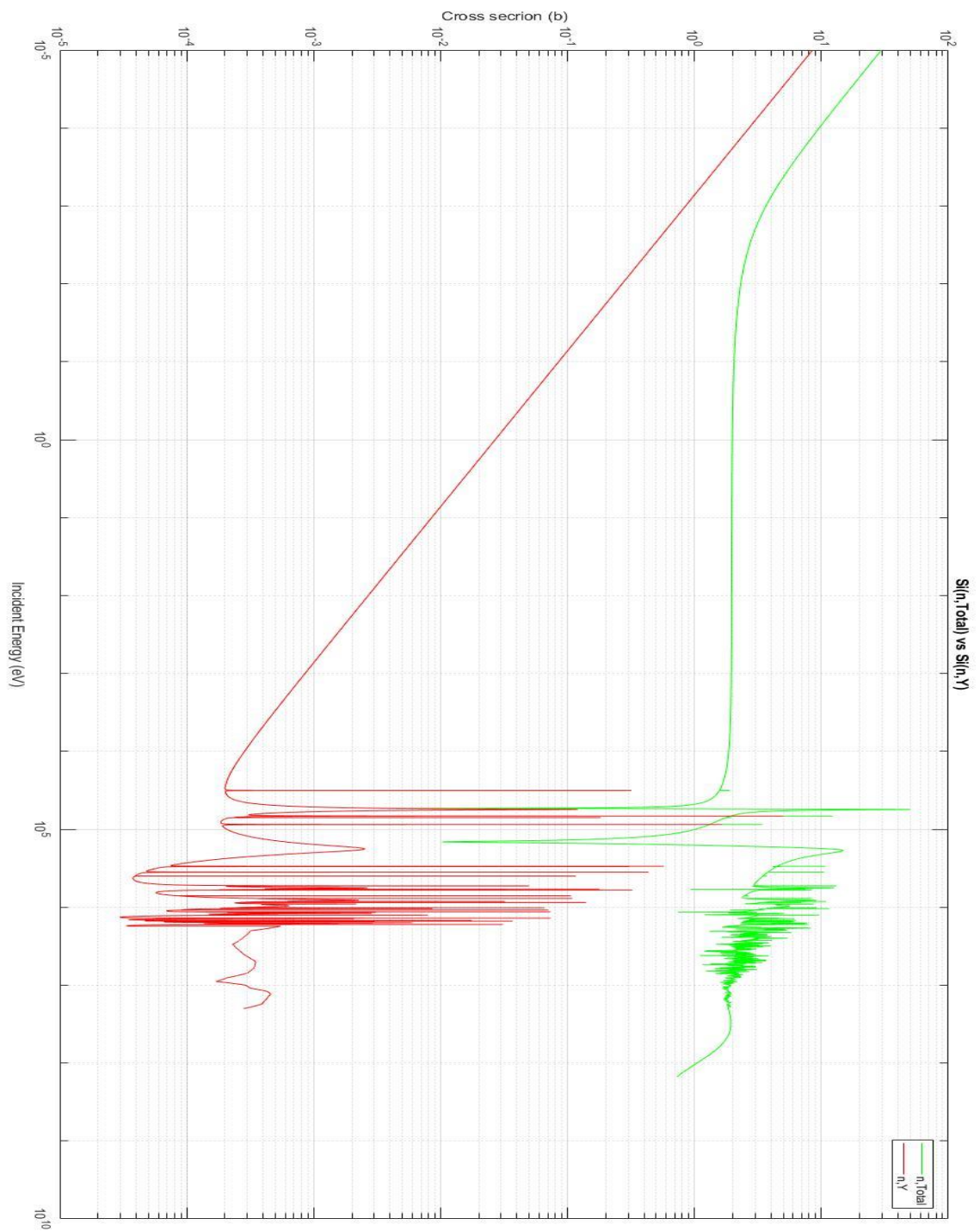


Fig. C12 Comparison between total cross section (Green) of Silicon and its capture cross section (Red). In the abscissae are represented Incident Energies in eV while in ordinates are represented cross section in barns. Silicon Capture cross section has a big contribution on the total cross section in low energy zone. At High energy resonance is present. Silicon is present in mud [3]

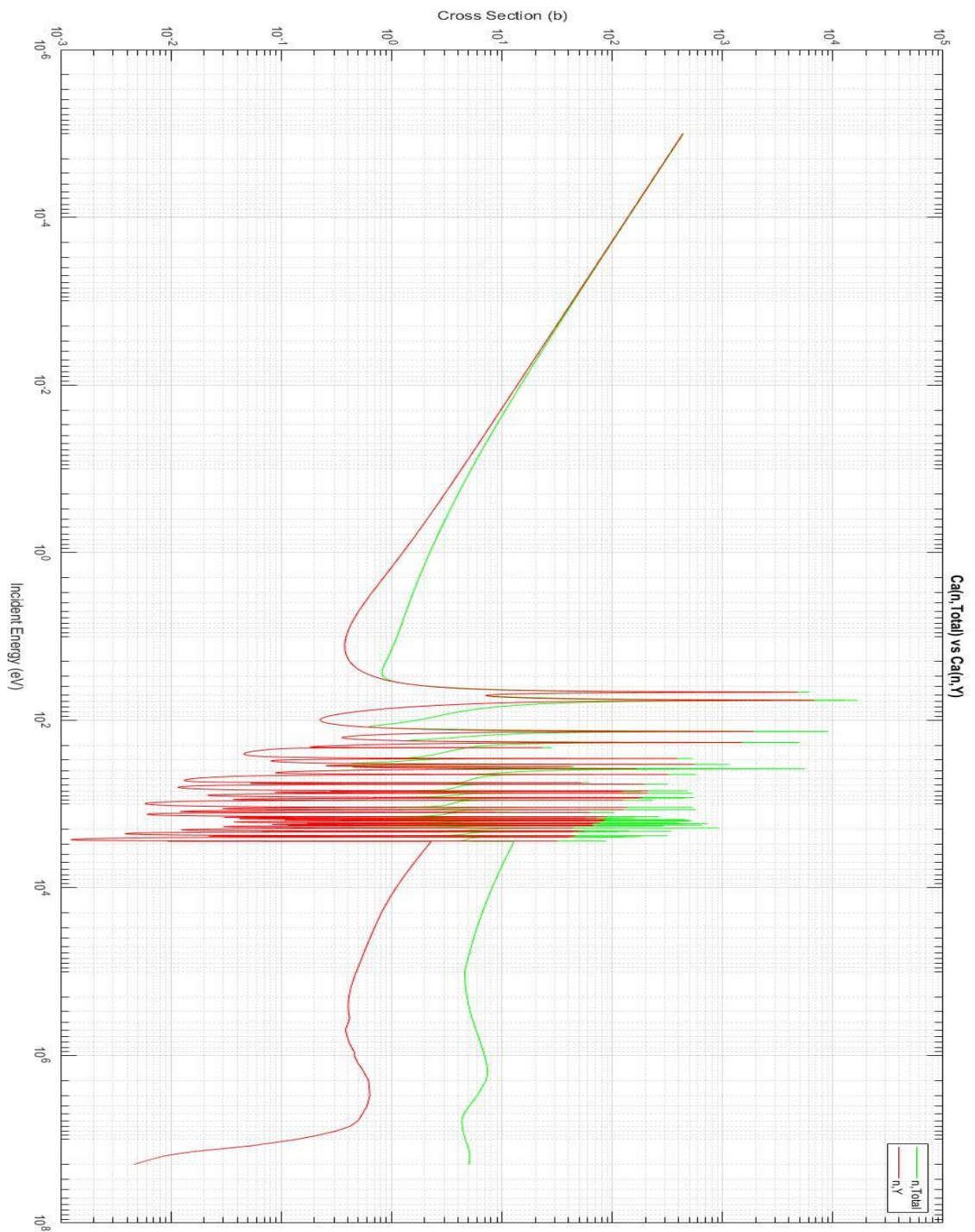


Fig. C13 Comparison between total cross section (Green) of Barium and its capture cross section (Red). In the abscissae are represented Incident Energies in eV while in ordinates are represented cross section in barns. Barium Capture cross section practically superimpose is trend with the total cross section in Thermal and epithermal energy zone. At High energy high resonance is present and the width between the two-cross section increases. Barium is present in mud [3]

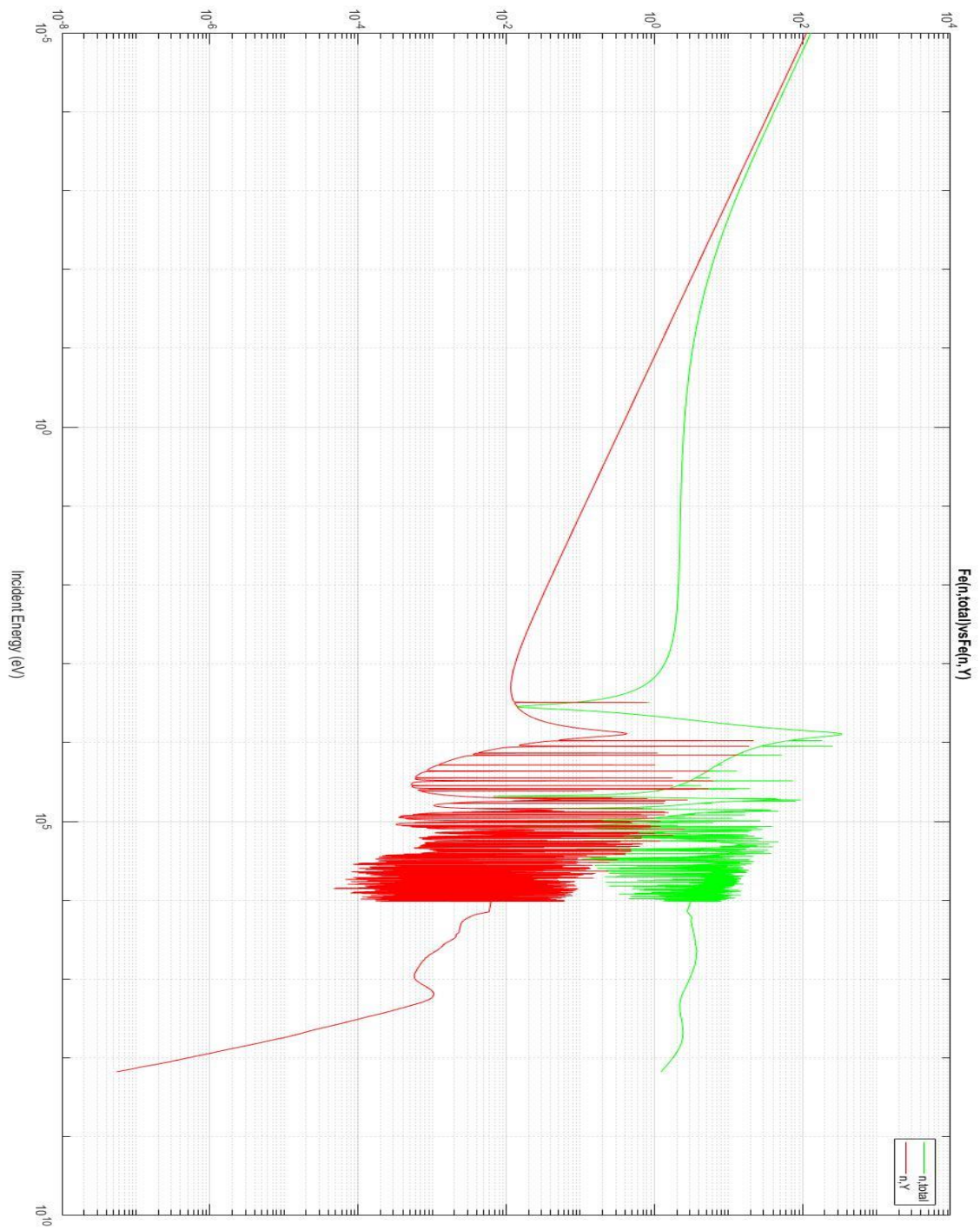


Fig. C14 Comparison between total cross section (Green) of Iron and its capture cross section (Red). In the abscissae are represented Incident Energies in eV while in ordinates are represented cross section in barns. Iron Capture cross section practically superimpose is trend with the total cross section in low energy zone. At High energy high resonance is present. Iron is present in Steel [3]

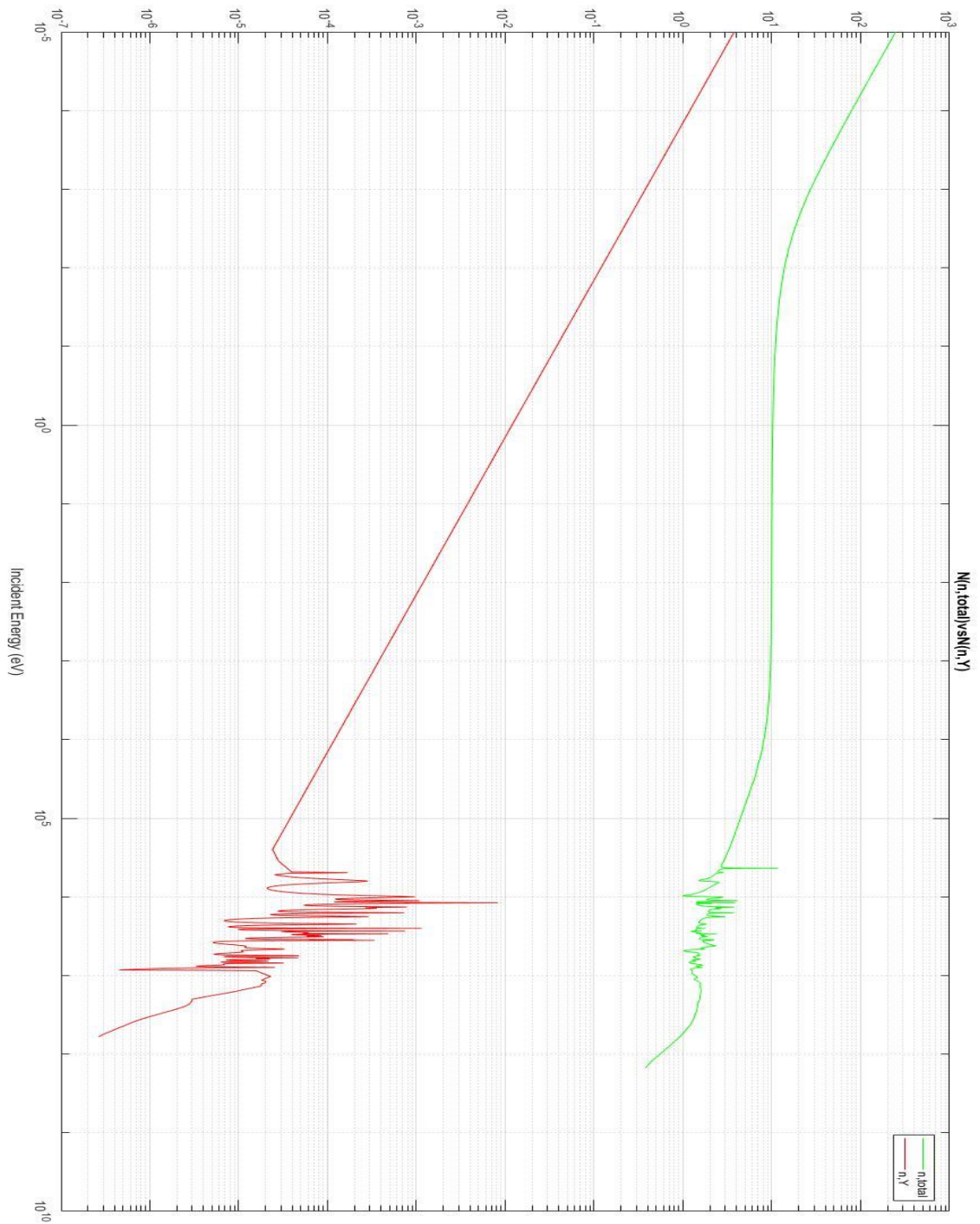


Fig. C15 Comparison between total cross section (Green) of Nitrogen and its capture cross section (Red). In the abscissae are represents Incident Energies in eV while in ordinates are represented cross section in barns. Nitrogen Carputer cross section contributes to the total in little part. Its major contribution is in low energy zone. Resonance is presence for total cross section in high energy zone. Nitrogen is contained in Steel. [3]

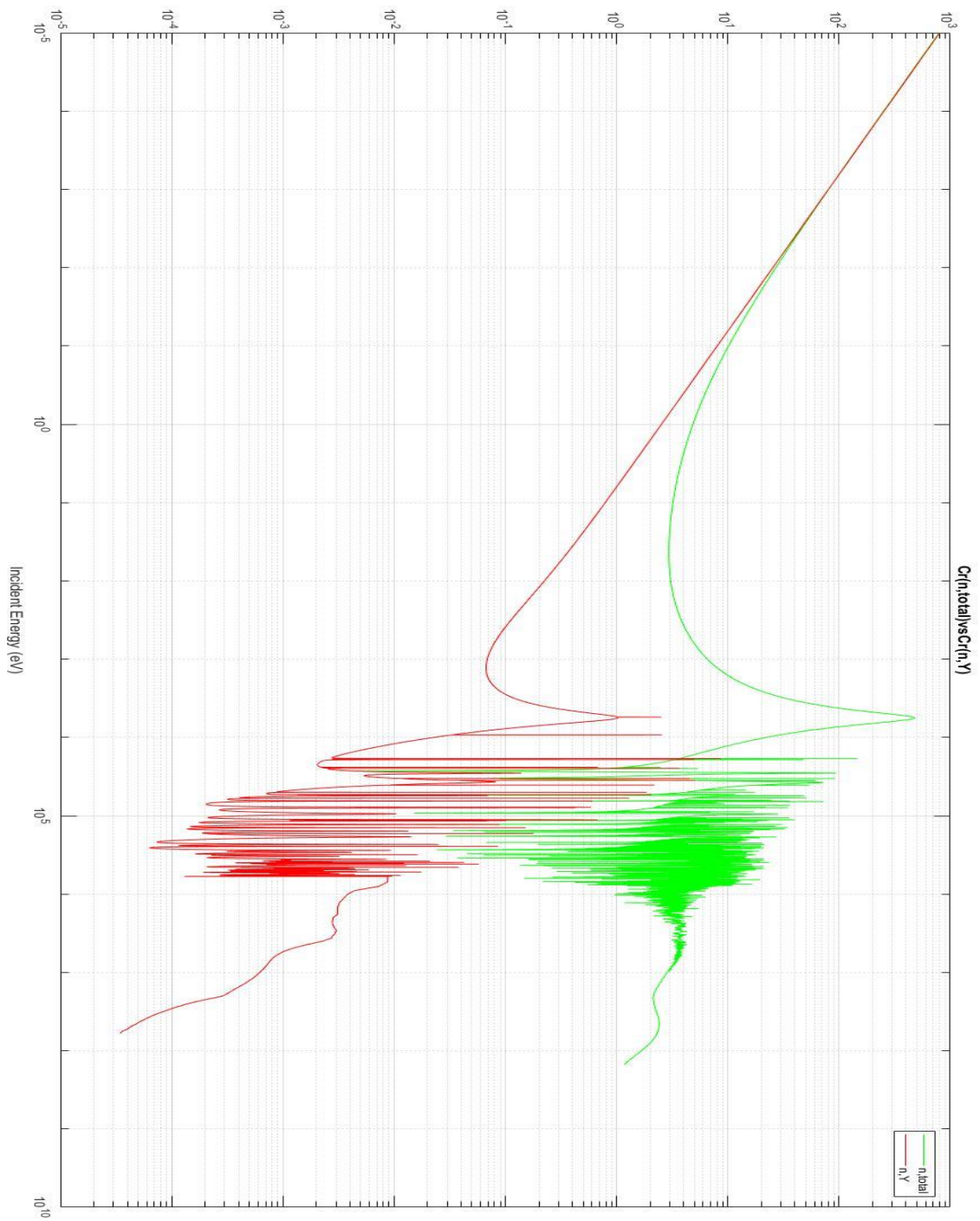


Fig. C16 Comparison between total cross section (Green) of Chromium and its capture cross section (Red). In the abscissae are represents Incident Energies in eV while in ordinates are represented cross section in barns. Chromium Carputer cross section practically superimpose is trend with the total cross section in low energy zone. At High energy high resonance is present. Chromium is present in Steel [3]

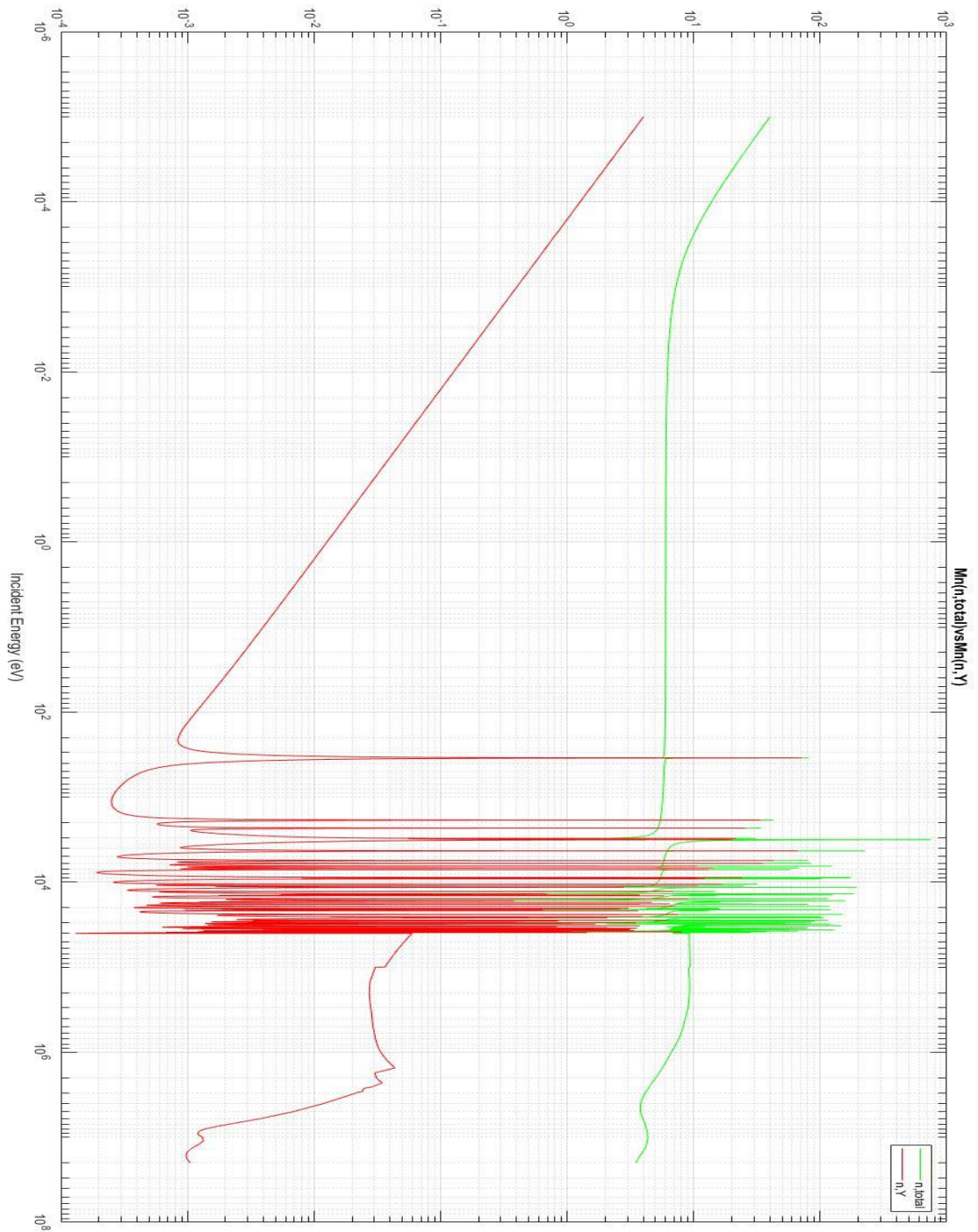


Fig. C17 Comparison between total cross section (Green) of Molybdenum and its capture cross section (Red). In the abscissae are represents Incident Energies in eV while in ordinates are represented cross section in barns. Molybdenum Carputer cross section has a big contribution on the total cross section in low energy zone. At High energy high resonance is present. Molybdenum is present in Steel [3]

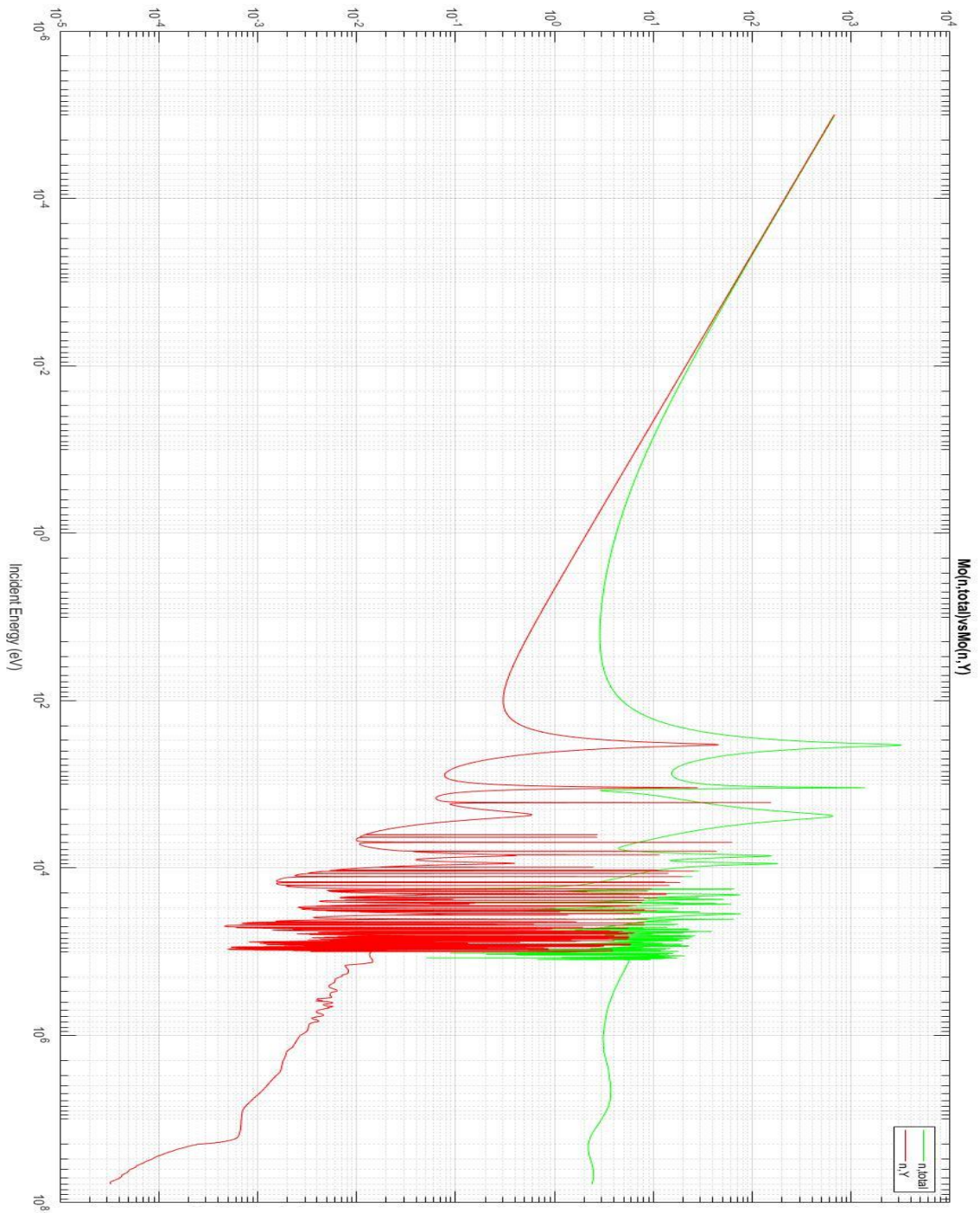


Fig. C18 Comparison between total cross section (Green) of Manganese and its capture cross section (Red). In the abscissae are represented Incident Energies in eV while in ordinates are represented cross section in barns. Manganese Carputer cross section practically superimpose is trend with the total cross section in low energy zone. At High energy high resonance is present. manganese is present in Steel [3]

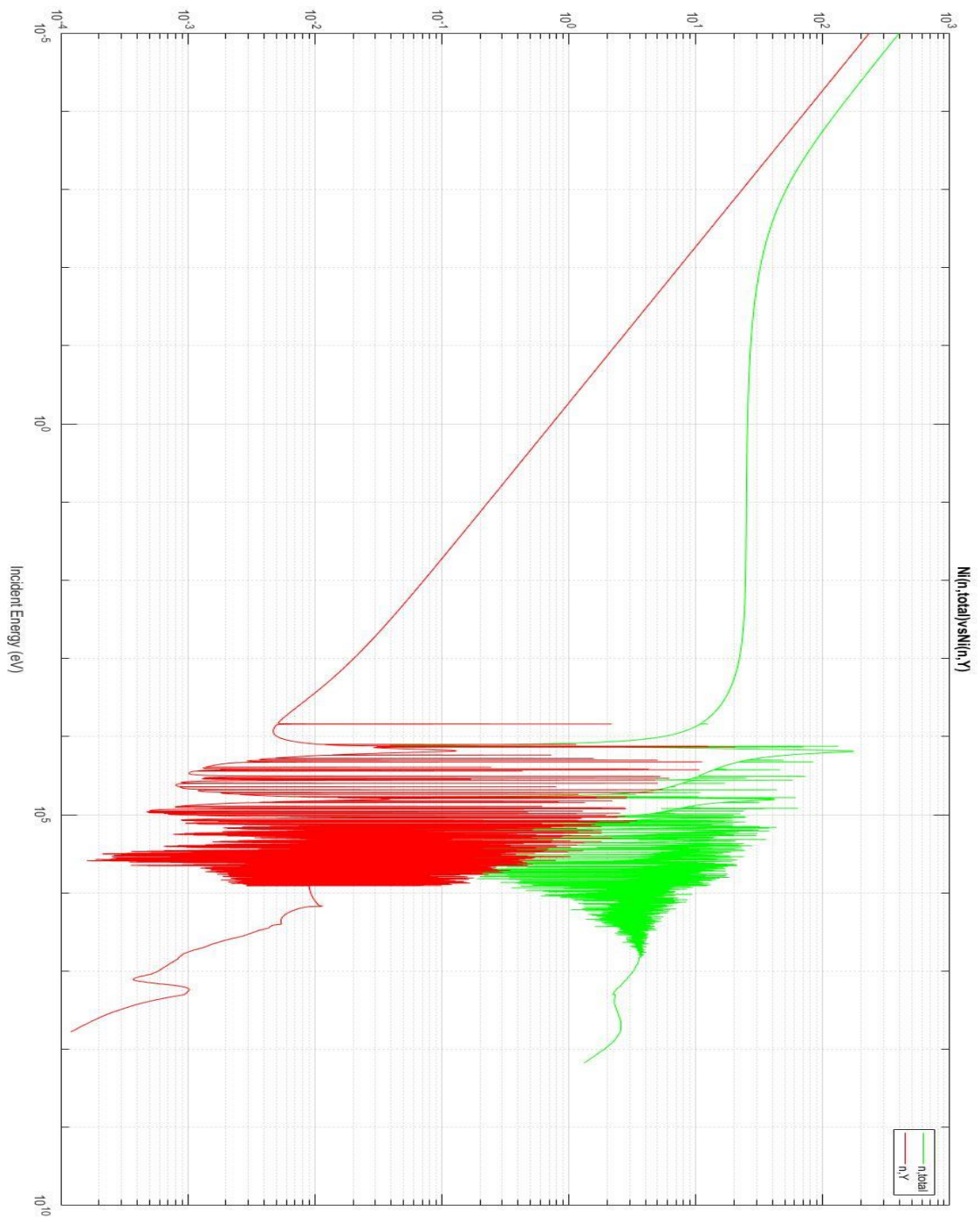


Fig. C19 Comparison between total cross section (Green) of Nichol and its capture cross section (Red). In the abscissae are represented Incident Energies in eV while in ordinates are represented cross section in barns. Nichol Carputer cross section has a big contribution on the total cross section in low energy zone. At High energy high resonance is present. Nichol is present in Steel [3]

## APPENDIX D) Simulations Output

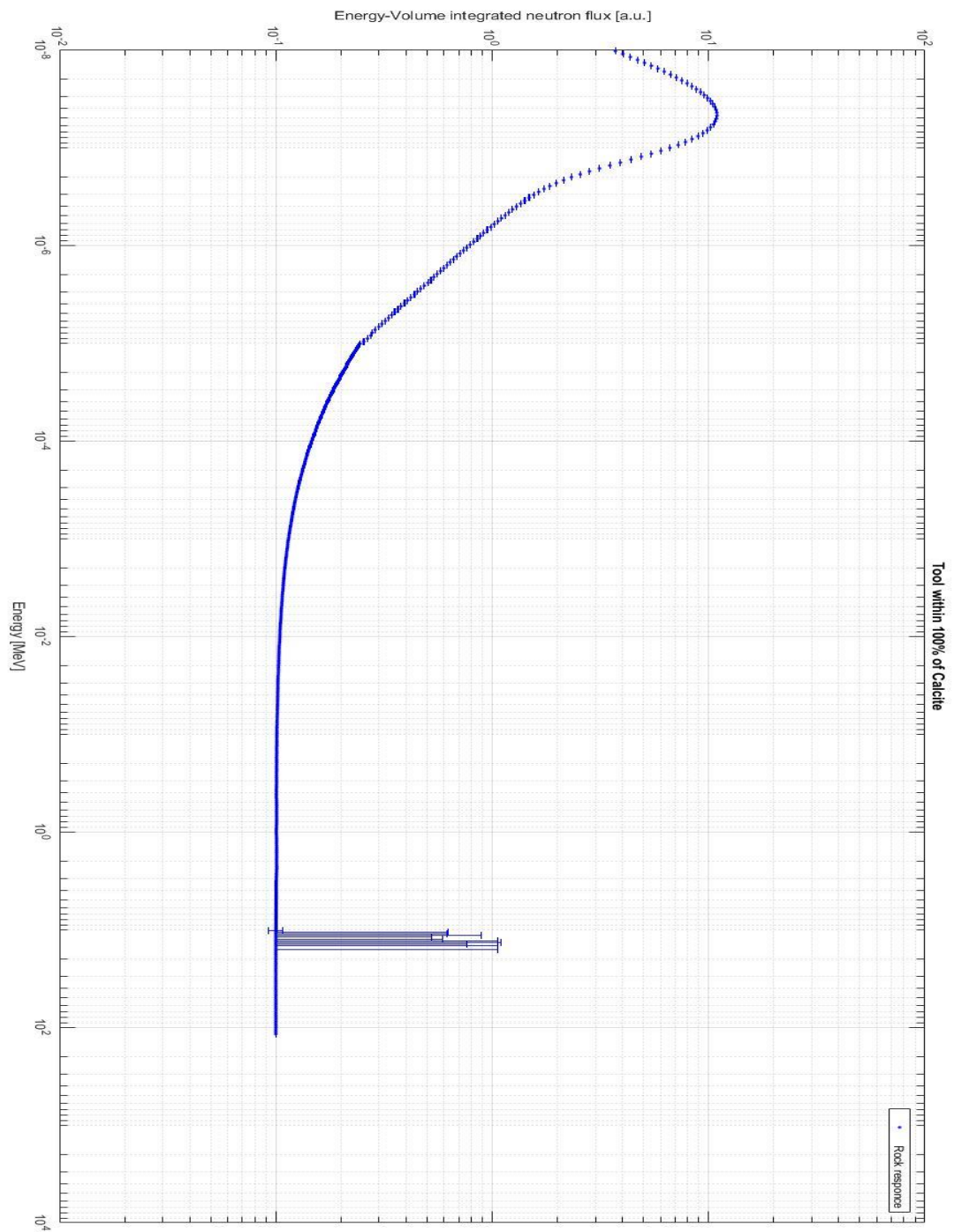


Figure D 1 Tool immersed in 100% of Calcite, in ordinates are plotted Energy-Volume integrated neutron flux [a.u.], in abscises are plotted detector incident energies expressed in MeV.

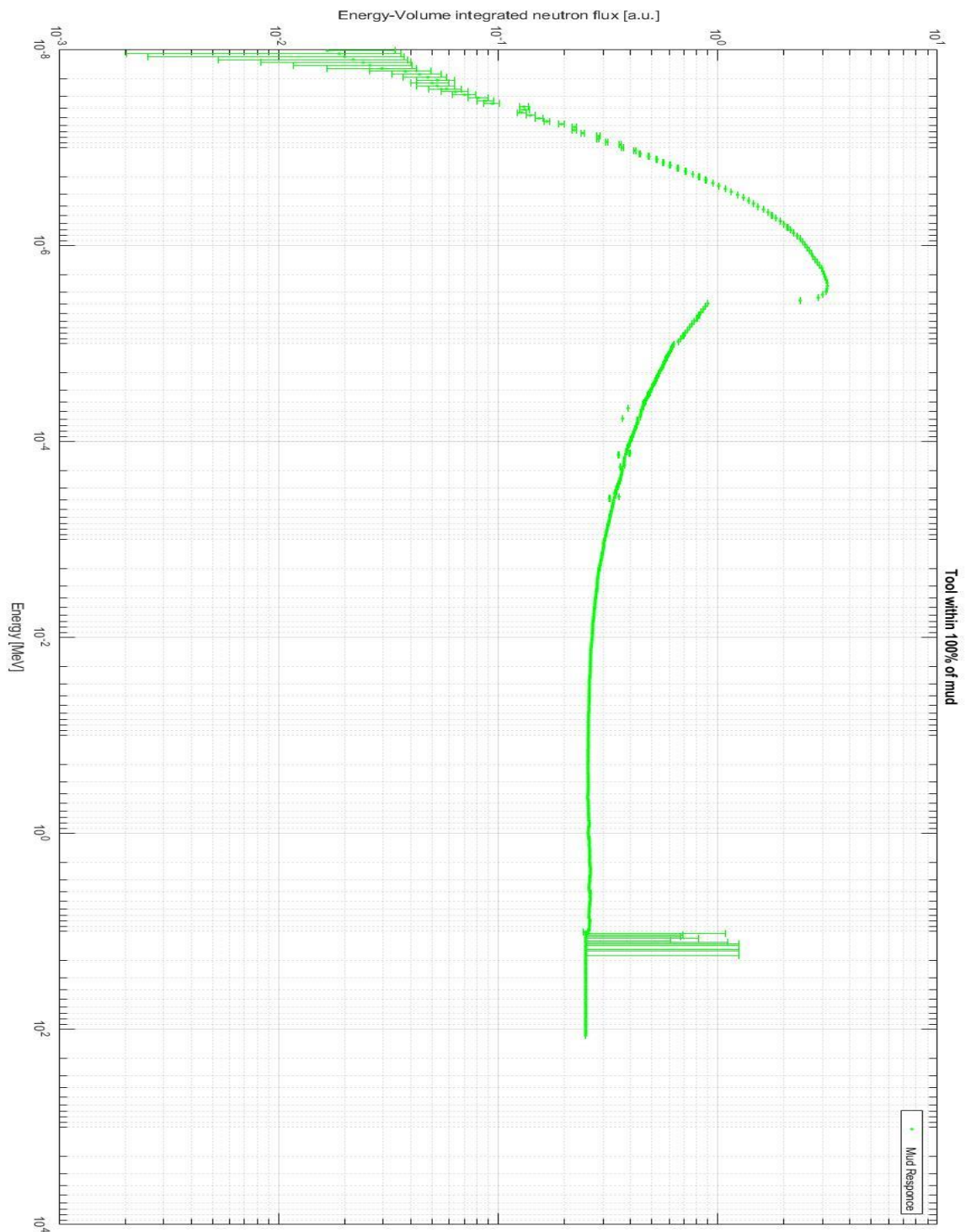


Figure D 2 Tool immersed in 100% of water-based mud, in ordinates are plotted Energy-Volume integrated neutron flux [a-u], in abscises are plotted detector incident energies expressed in MeV.

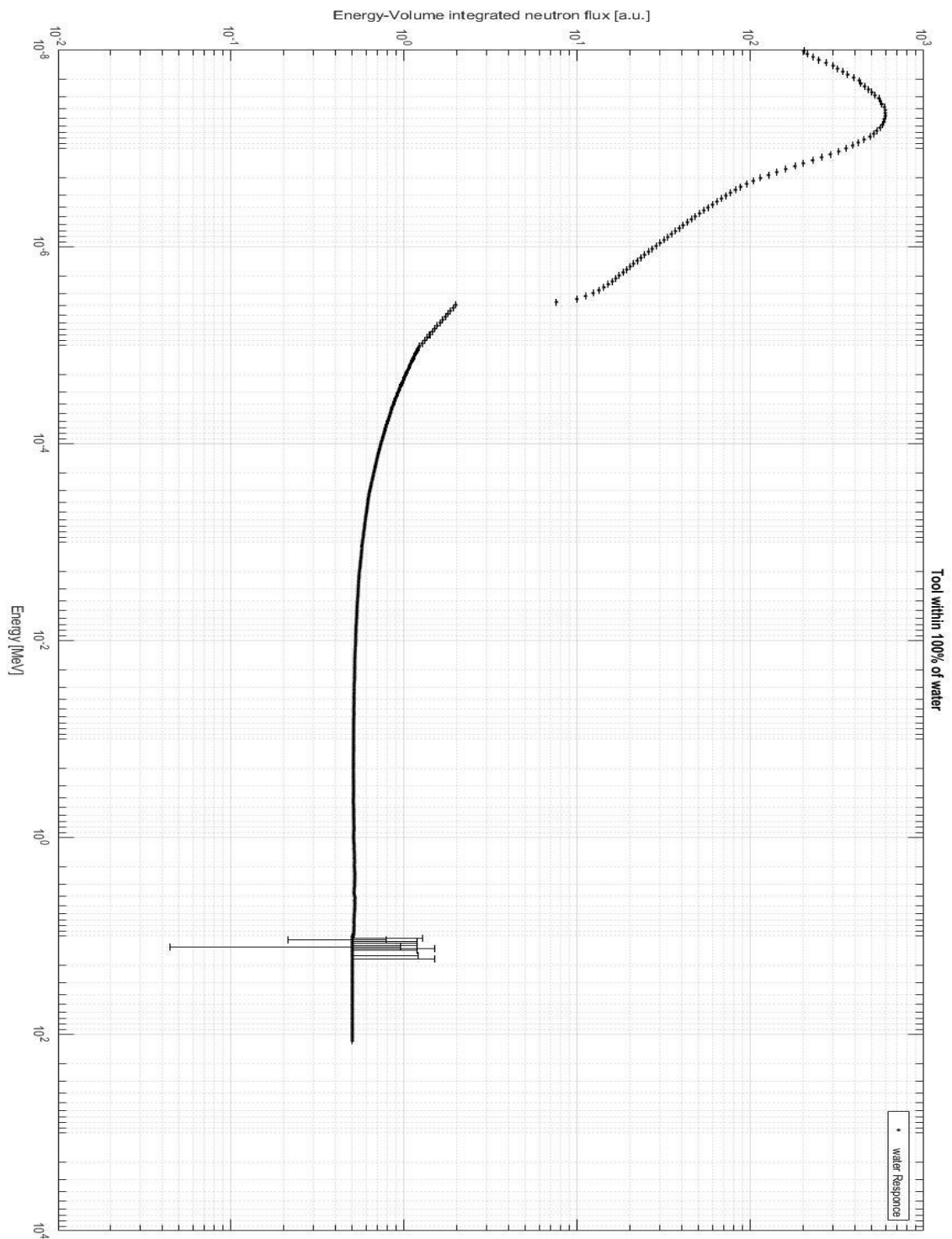


Figure D 3 Tool immersed in 100% of pure water, in ordinates are plotted Energy-Volume integrated neutron flux [a-u], in abscises are plotted detector incident energies expressed in MeV.

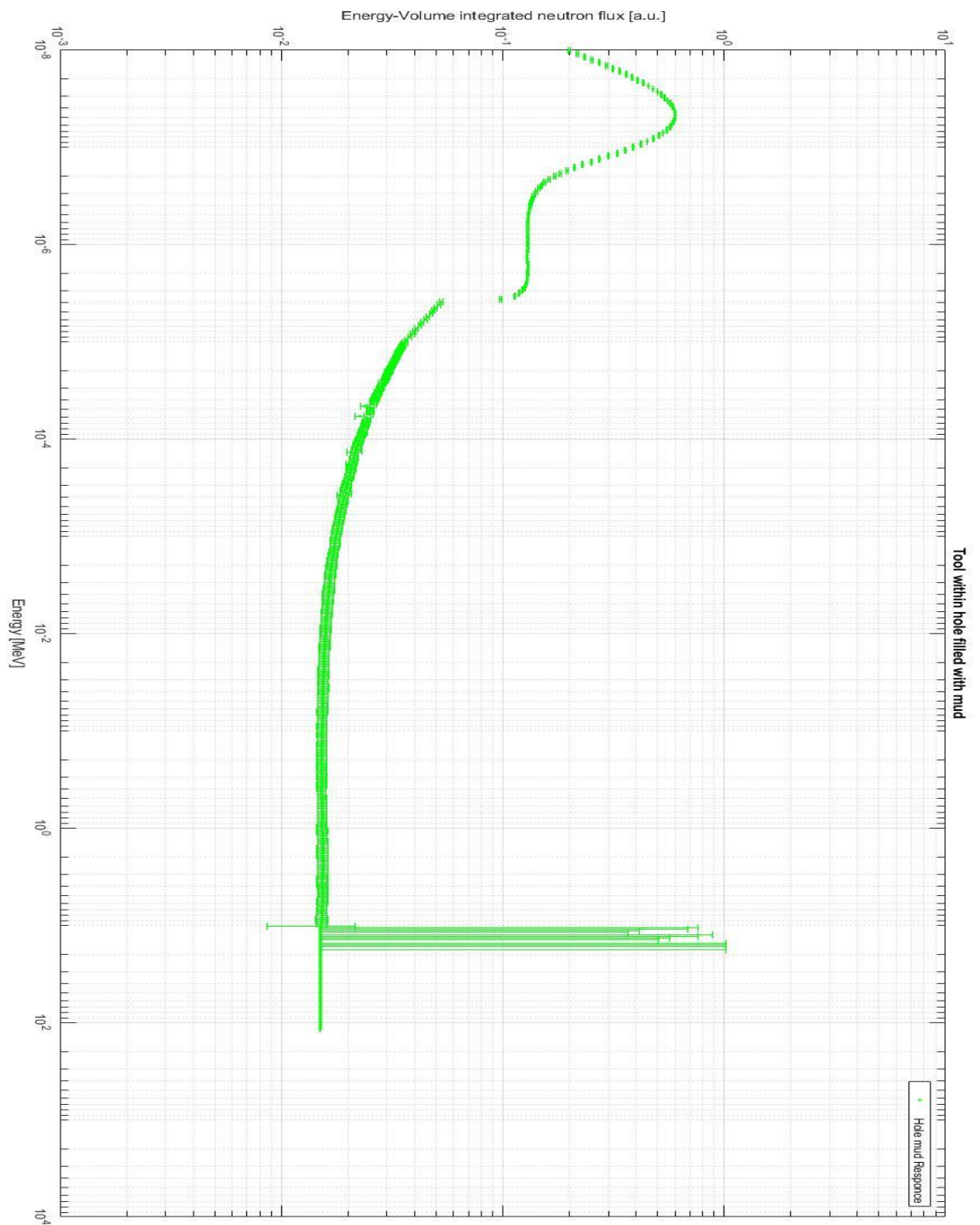


Figure D 4 Tool immersed within a borehole filled by water-based mud. The radius of the borehole is 10 cm. The borehole is drilled in 100% of Calcite, in ordinates are plotted Energy-Volume integrated neutron flux [a-u], in abscises are plotted detector incident energies expressed in MeV.

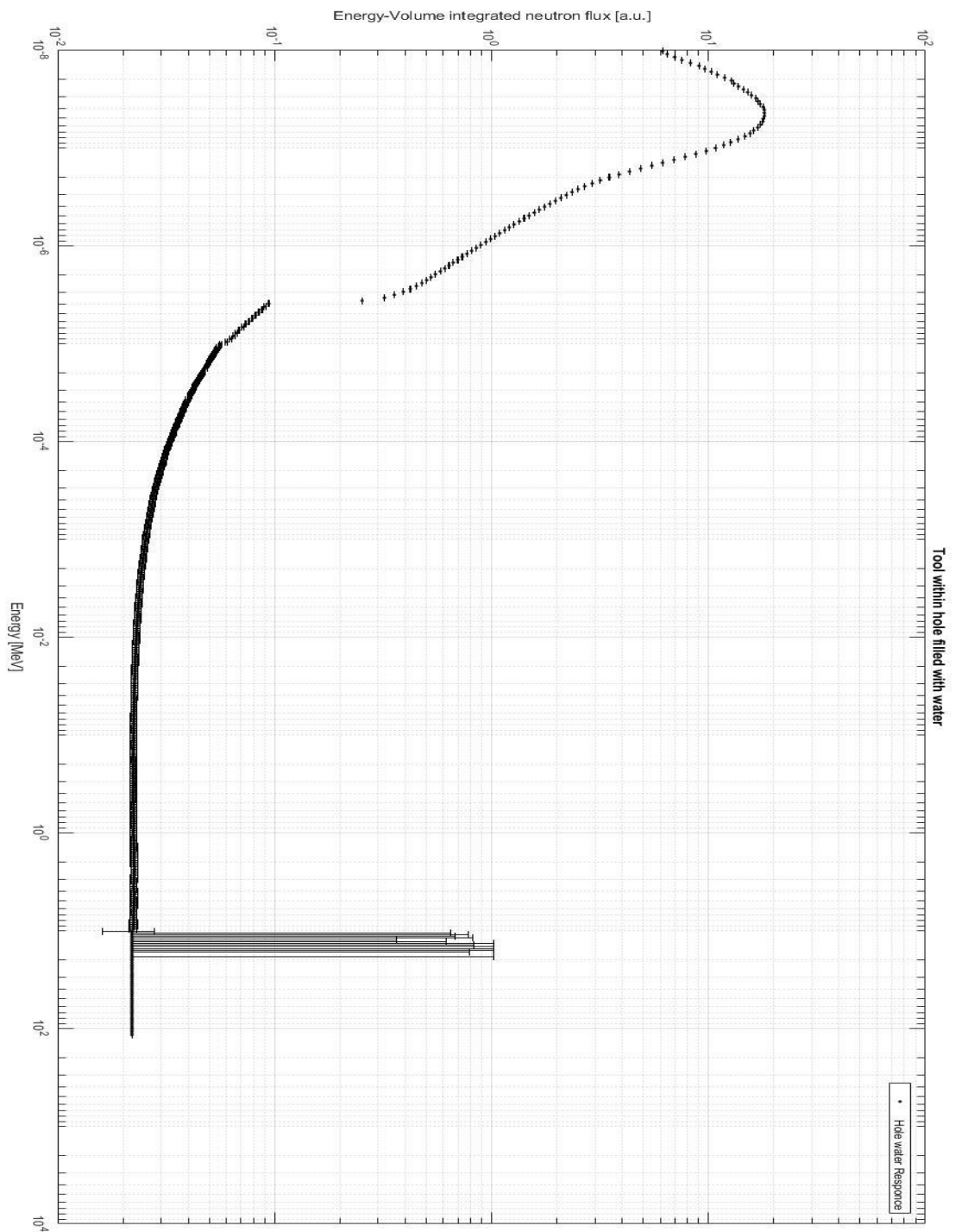


Figure D 5Tool immersed within a borehole filled by pure water. The radius of the borehole is 10 cm. The borehole is drilled in 100% of Calcite, in ordinates are plotted Energy-Volume integrated neutron flux [a-u], in abscises are plotted detector incident energies expressed in MeV

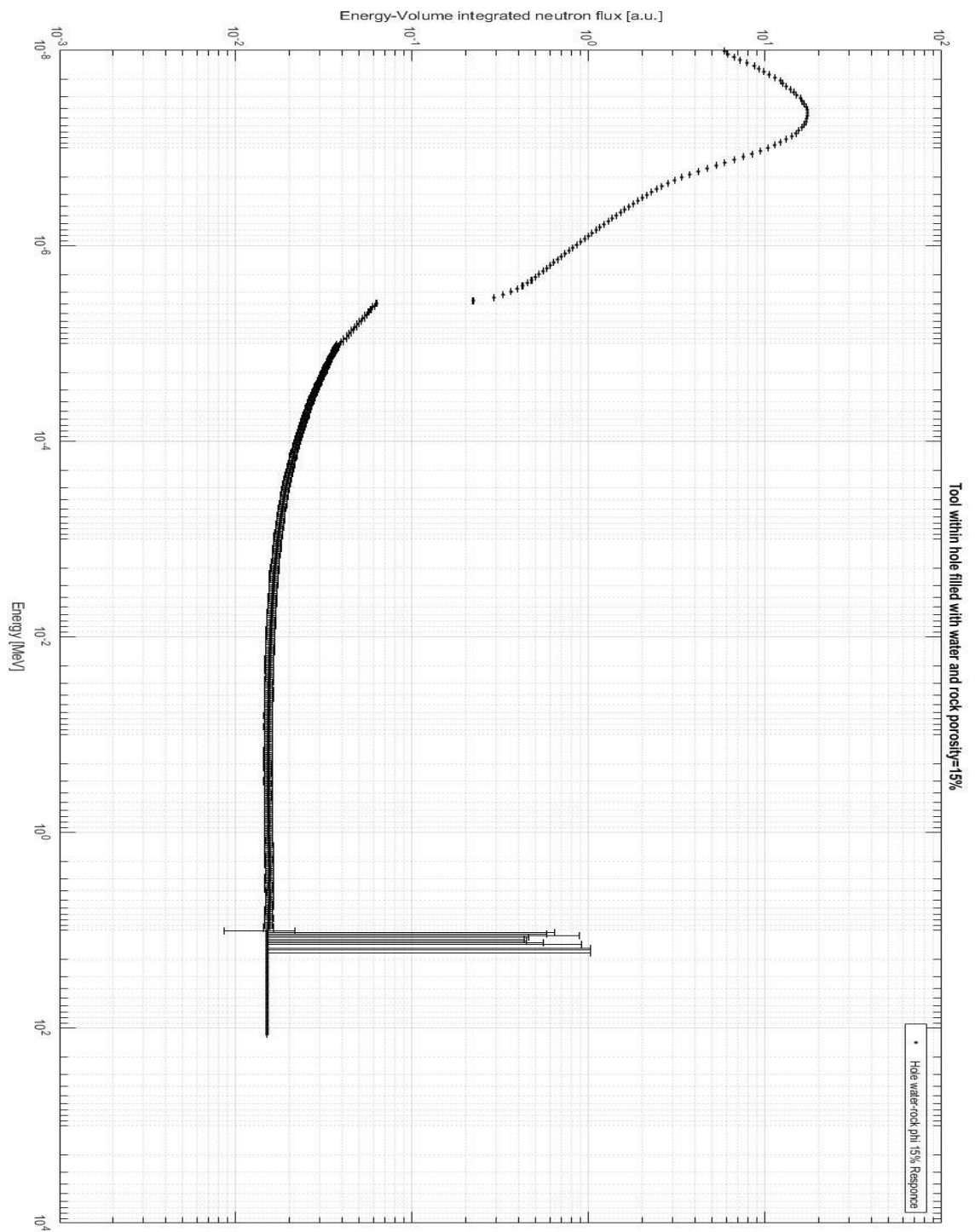


Figure D 6Tool immersed within a borehole filled by pure water. The radius of the borehole is 10 cm. The borehole is drilled in 100% of Calcite with a porosity of 15%, saturated by pure water only. In ordinates are plotted Energy-Volume integrated neutron flux [a-u], in abscises are plotted detector incident energies expressed in MeV.

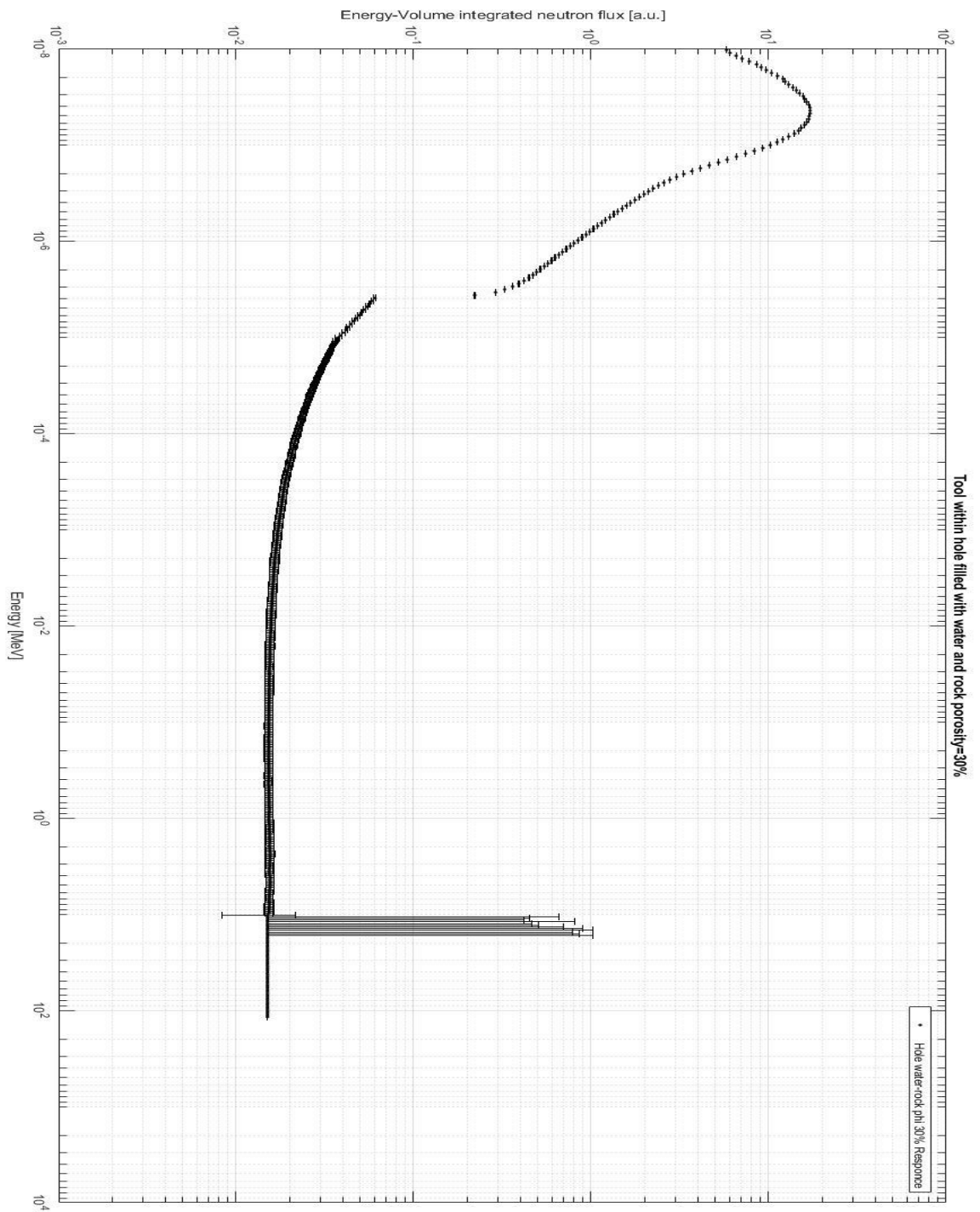


Figure D 78 Tool immersed within a borehole filled by pure water. The radius of the borehole is 10 cm. The borehole is drilled in 100% of Calcite with a porosity of 30%, saturated by pure water only. In ordinates are plotted Energy-Volume integrated neutron flux [a-u], in abscises are plotted detector incident energies expressed in MeV

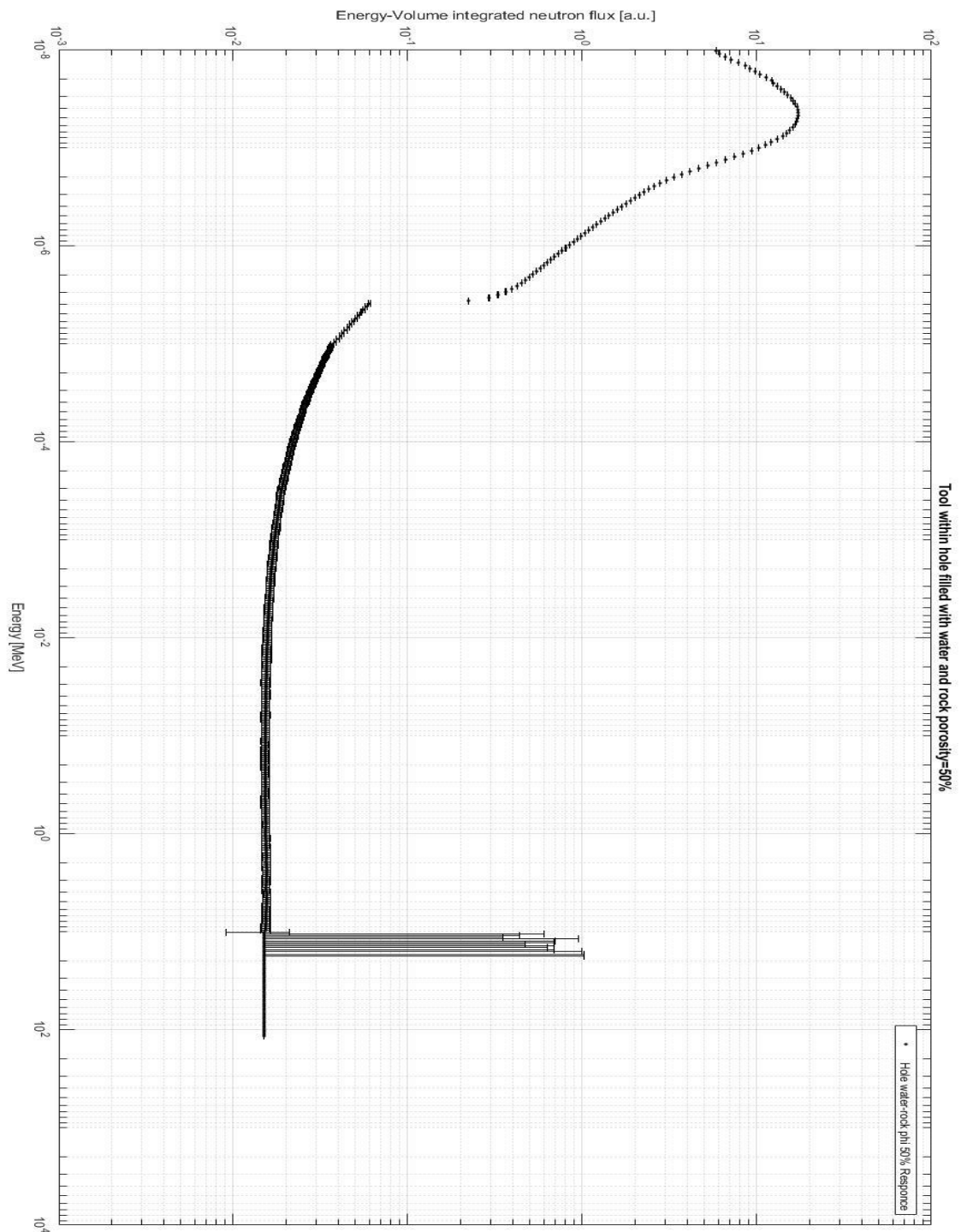


Figure D 910Tool immersed within a borehole filled by pure water. The radius of the borehole is 10 cm. The borehole is drilled in 100% of Calcite with a porosity of 50%, saturated by pure water only. In ordinates are plotted Energy-Volume integrated neutron flux [a-u], in abscises are plotted detector incident energies expressed in MeV

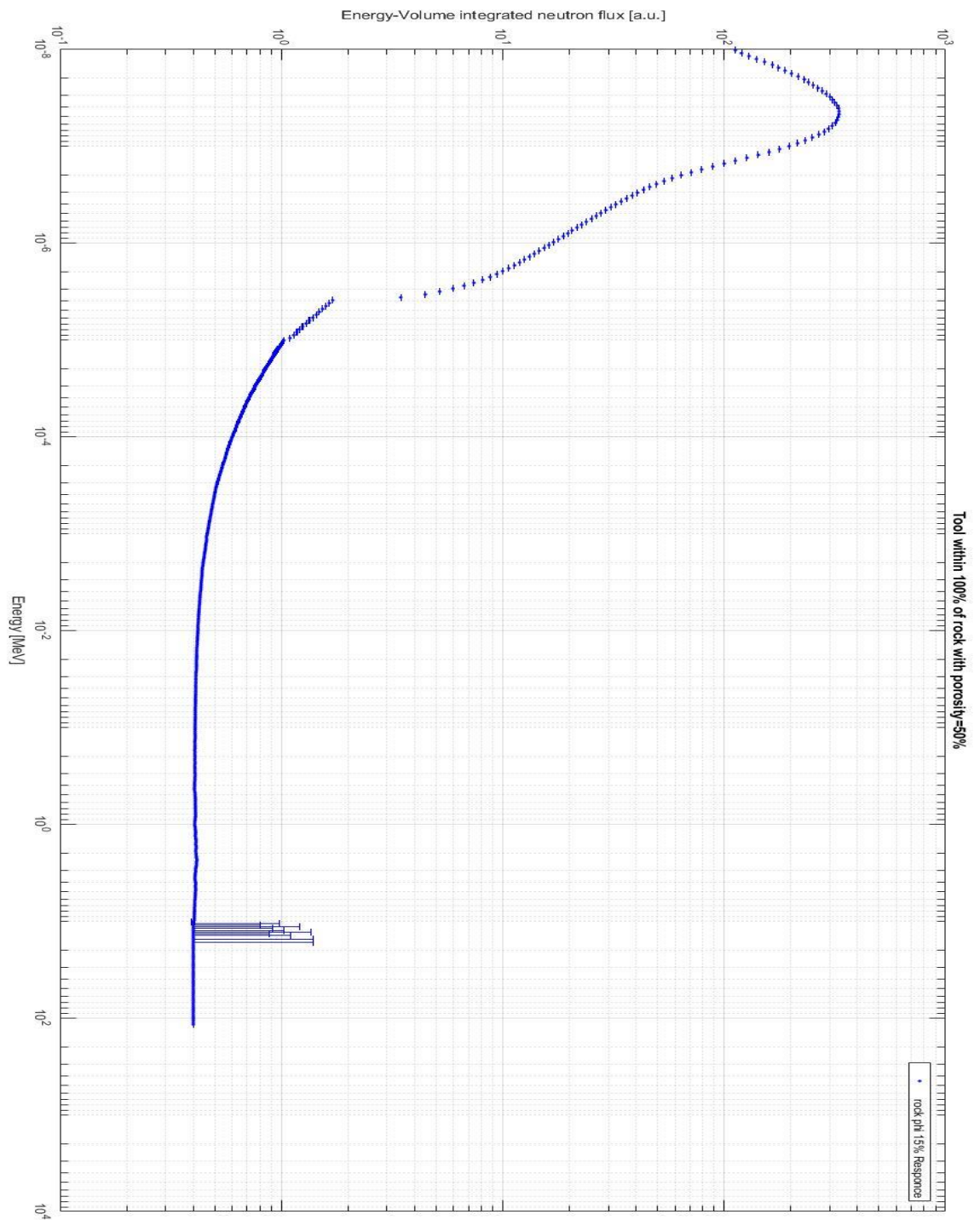


Figure D 11 Tool immersed within 100% of Calcite with porosity of 50% saturated by pure water. The radius of the borehole is 10 cm. In ordinates are plotted Energy-Volume integrated neutron flux [a-u], in abscises are plotted detector incident energies expressed in MeV

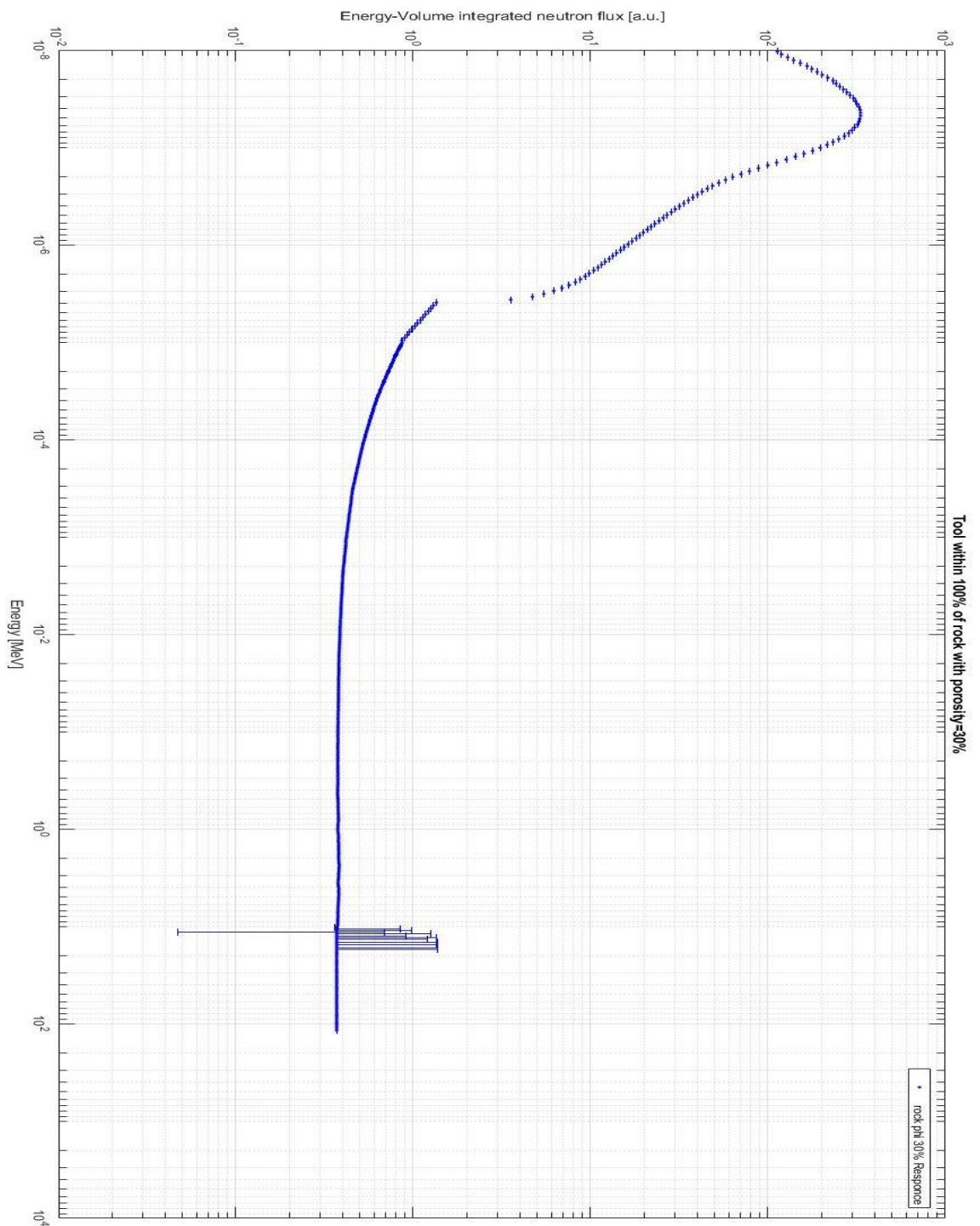


Figure D 12 Tool immersed within 100% of Calcite with porosity of 30% saturated by pure water. The radius of the borehole is 10 cm. In ordinates are plotted Energy-Volume integrated neutron flux [a-u], in abscises are plotted detector incident energies expressed in MeV

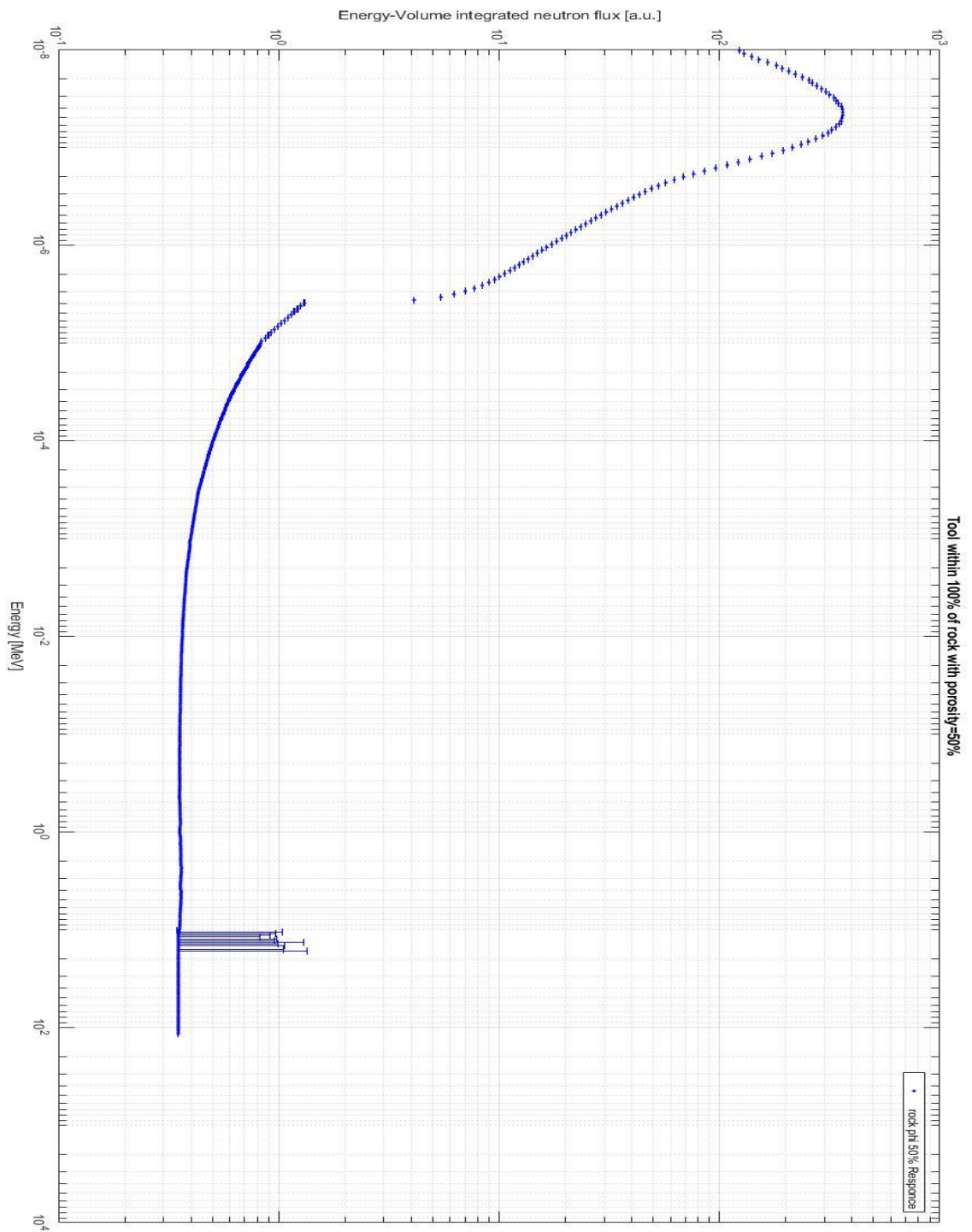


Figure D 13 Tool immersed within 100% of Calcite with porosity of 15% saturated by pure water. The radius of the borehole is 10 cm. In ordinates are plotted Energy-Volume integrated neutron flux [a-u], in abscises are plotted detector incident energies expressed in MeV

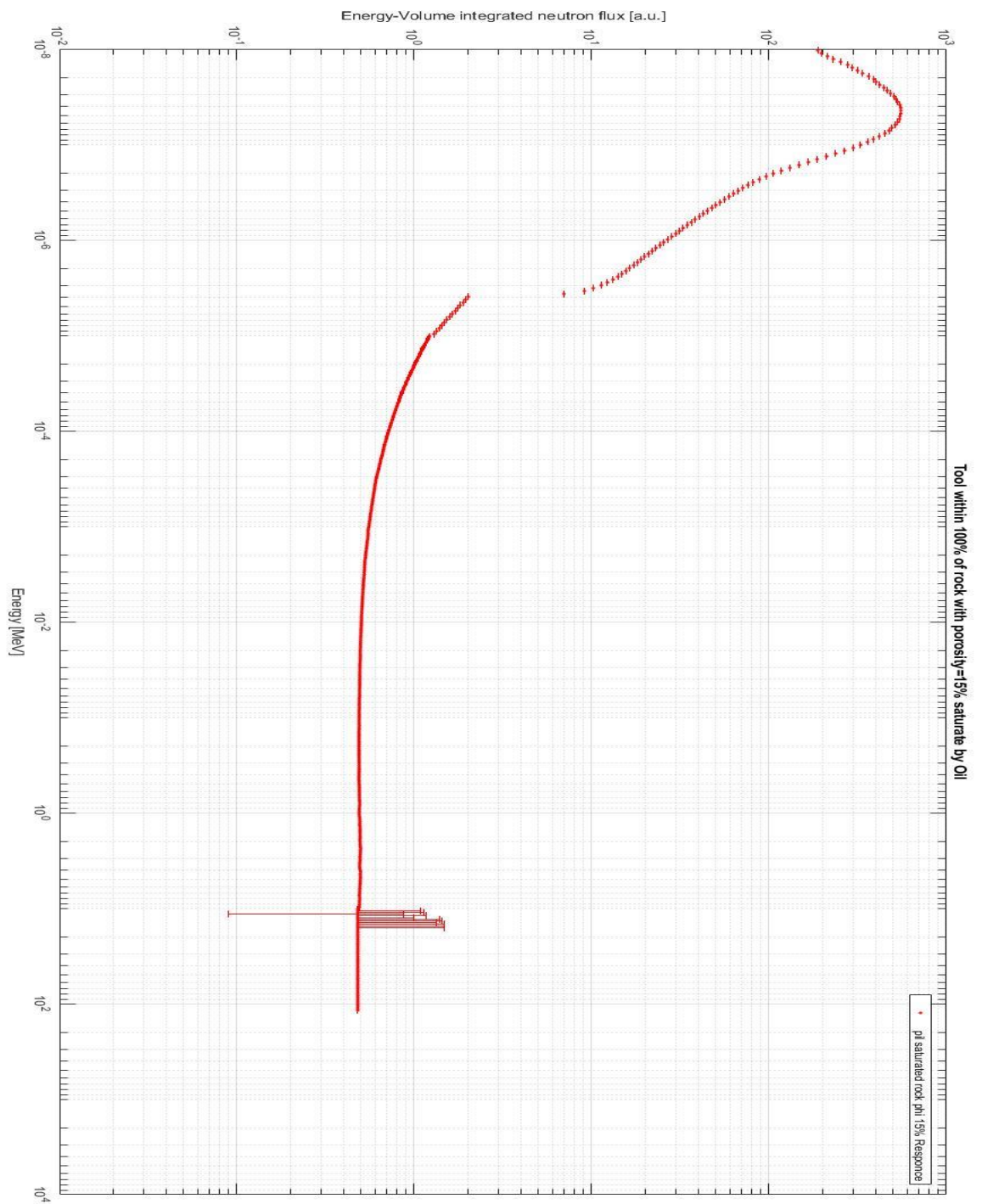


Figure D 14 Tool immersed within 100% of oil. In ordinates are plotted Energy-Volume integrated neutron flux [a.u.], in abscises are plotted detector incident energies expressed in MeV

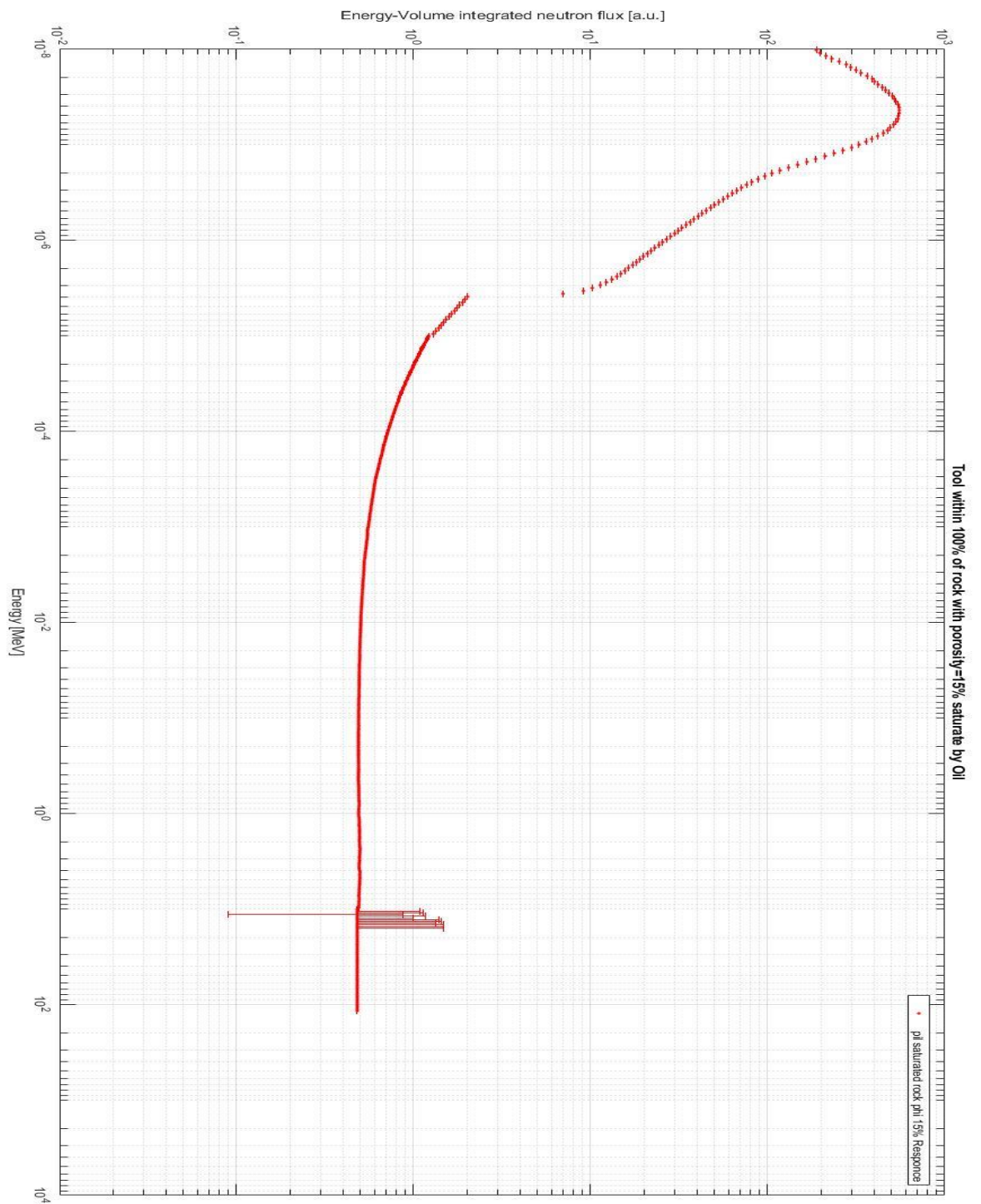


Figure D 15 Tool immersed within a borehole filled by pure water. The radius of the borehole is 10 cm. The borehole is drilled in 100% of Calcite with a porosity of 15%, saturated by oil only. In ordinates are plotted Energy-Volume integrated neutron flux [a-u], in abscises are plotted detector incident energies expressed in MeV.

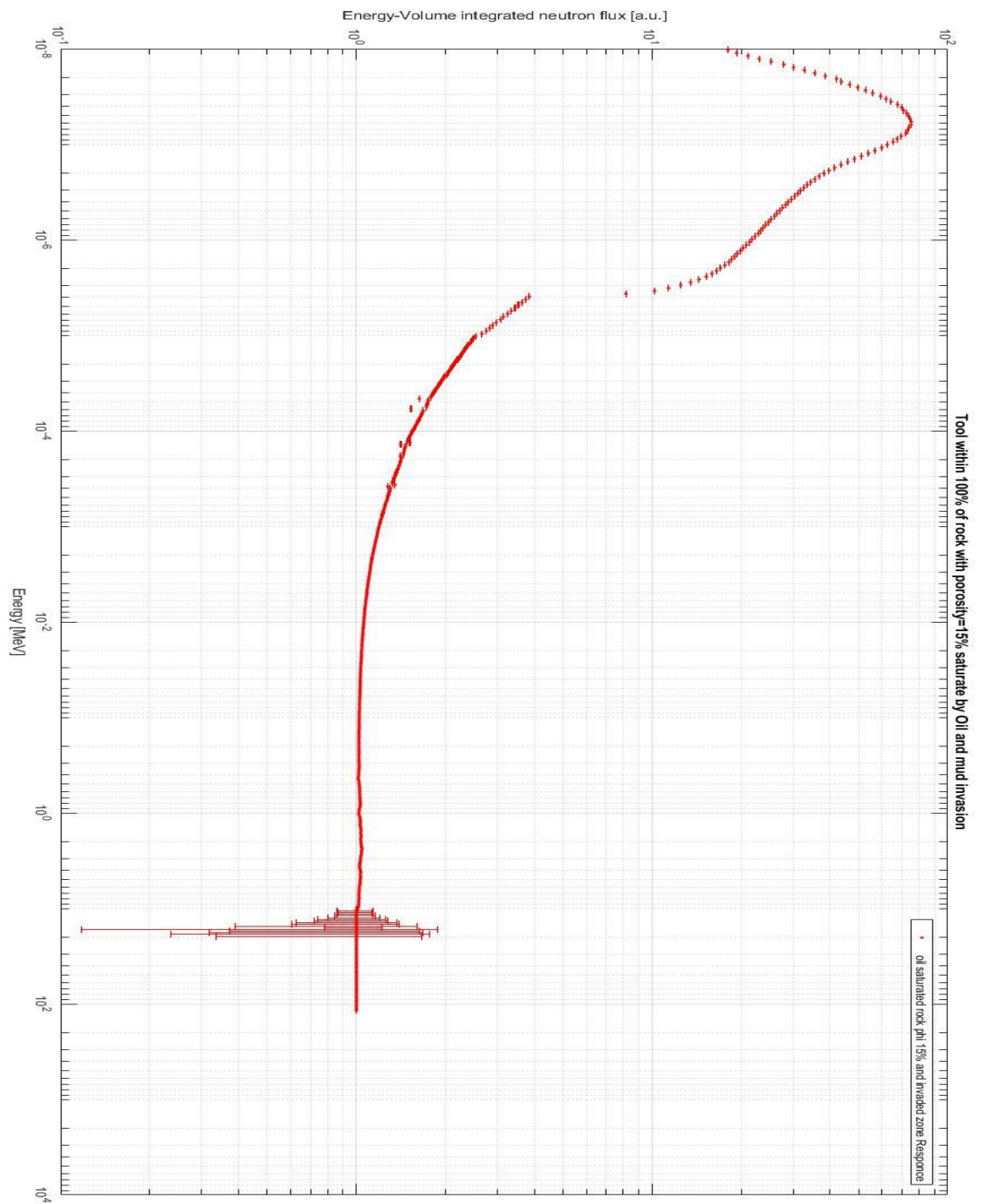


Figure D 16 Tool immersed within a borehole filled by pure water. The radius of the borehole is 10 cm. The borehole is drilled in 100% of Calcite with a porosity of 15%, saturated by oil only. Is also simulated the mud invasion, the invaded zone is wide 20cm from the wall of the borehole. In ordinates are plotted Energy-Volume integrated neutron flux [a-u], in abscises are plotted detector incident energies expressed in MeV.

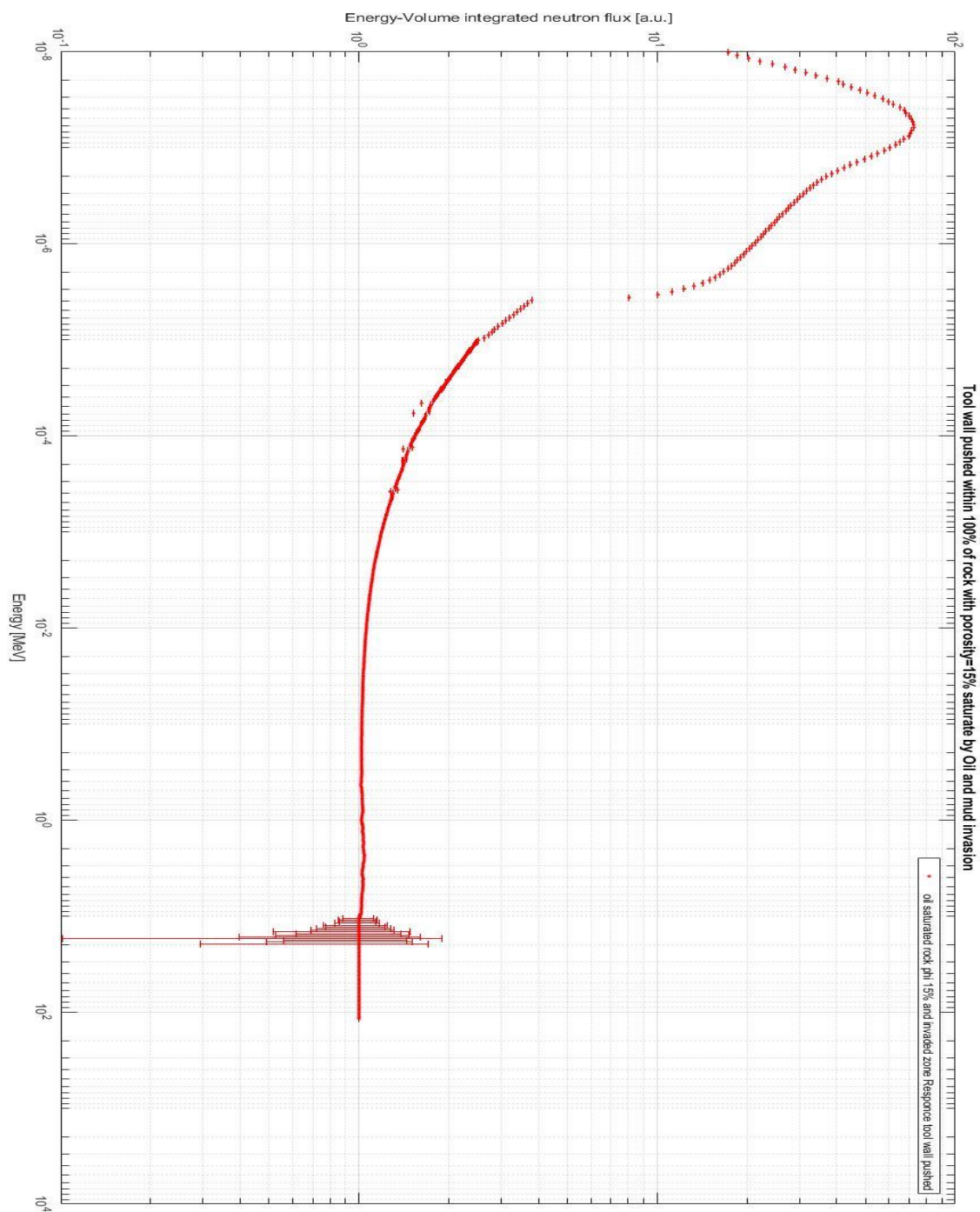


Figure D 17 Tool immersed within a borehole filled by pure water. The radius of the borehole is 10 cm. The borehole is drilled in 100% of Calcite with a porosity of 15%, saturated by oil only. Is also simulated the mud invasion, the invaded zone is wide 20cm from the wall of the borehole. In this simulation the tool is pushed against the borehole's wall. In ordinates are plotted Energy-Volume integrated neutron flux [a-u], in abscises are plotted detector incident energies expressed in MeV.

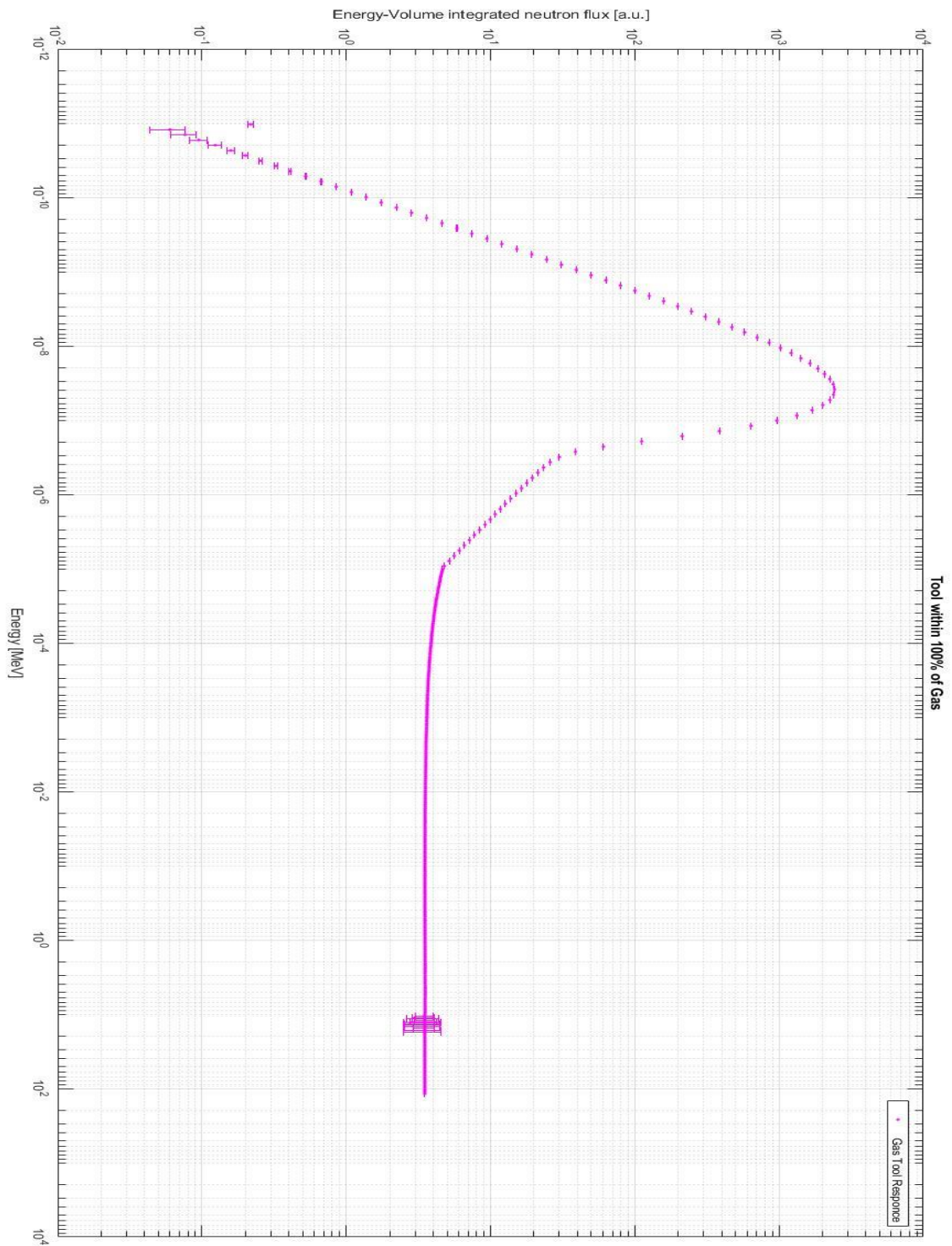


Figure D 18 Tool immersed within 100% of gas. In ordinates are plotted Energy-Volume integrated neutron flux [a-u], in abscises are plotted detector incident energies expressed in MeV.

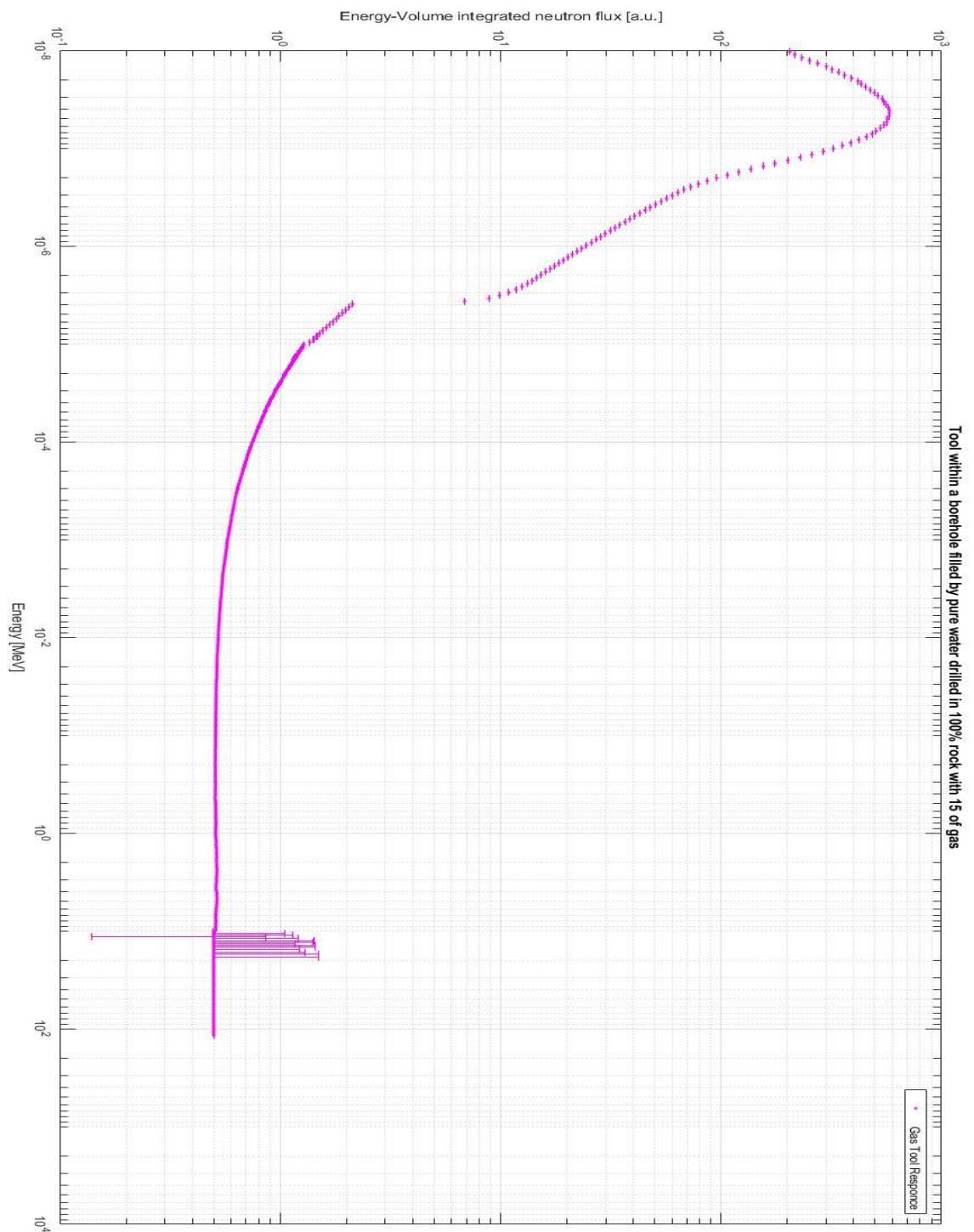


Figure D 19 Tool immersed within a borehole filled by pure water. The radius of the borehole is 10 cm. The borehole is drilled in 100% of Calcite with a porosity of 15%, saturated by gas only. In ordinates are plotted Energy-Volume integrated neutron flux [a-u], in abscises are plotted detector incident energies expressed in MeV.

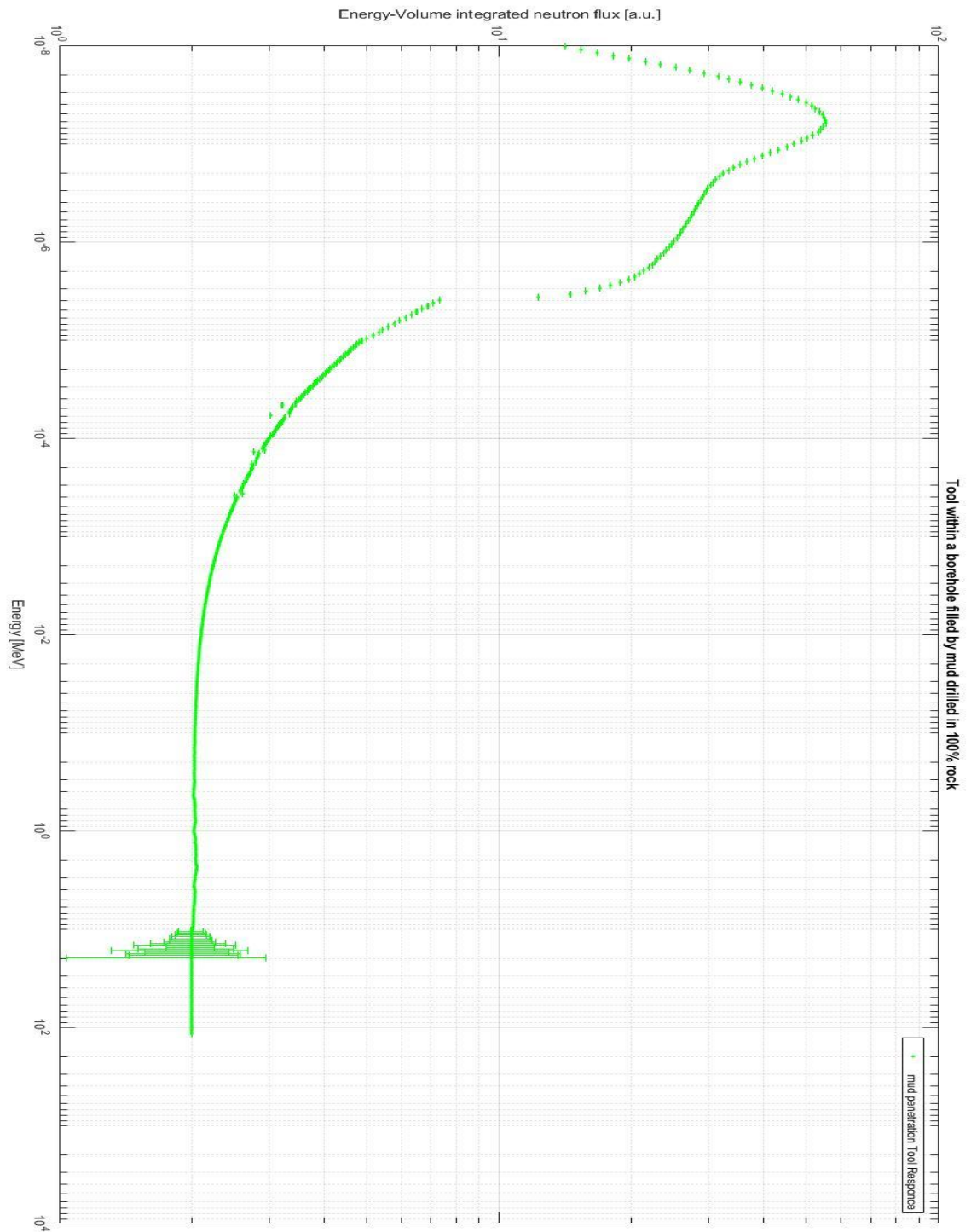


Figure D 20 Tool immersed within a borehole filled by water-based mud. The radius of the borehole is 10 cm. The borehole is drilled in 100% of Calcite, in ordinates are plotted Energy-Volume integrated neutron flux [a-u], in abscises are plotted detector incident energies expressed in MeV

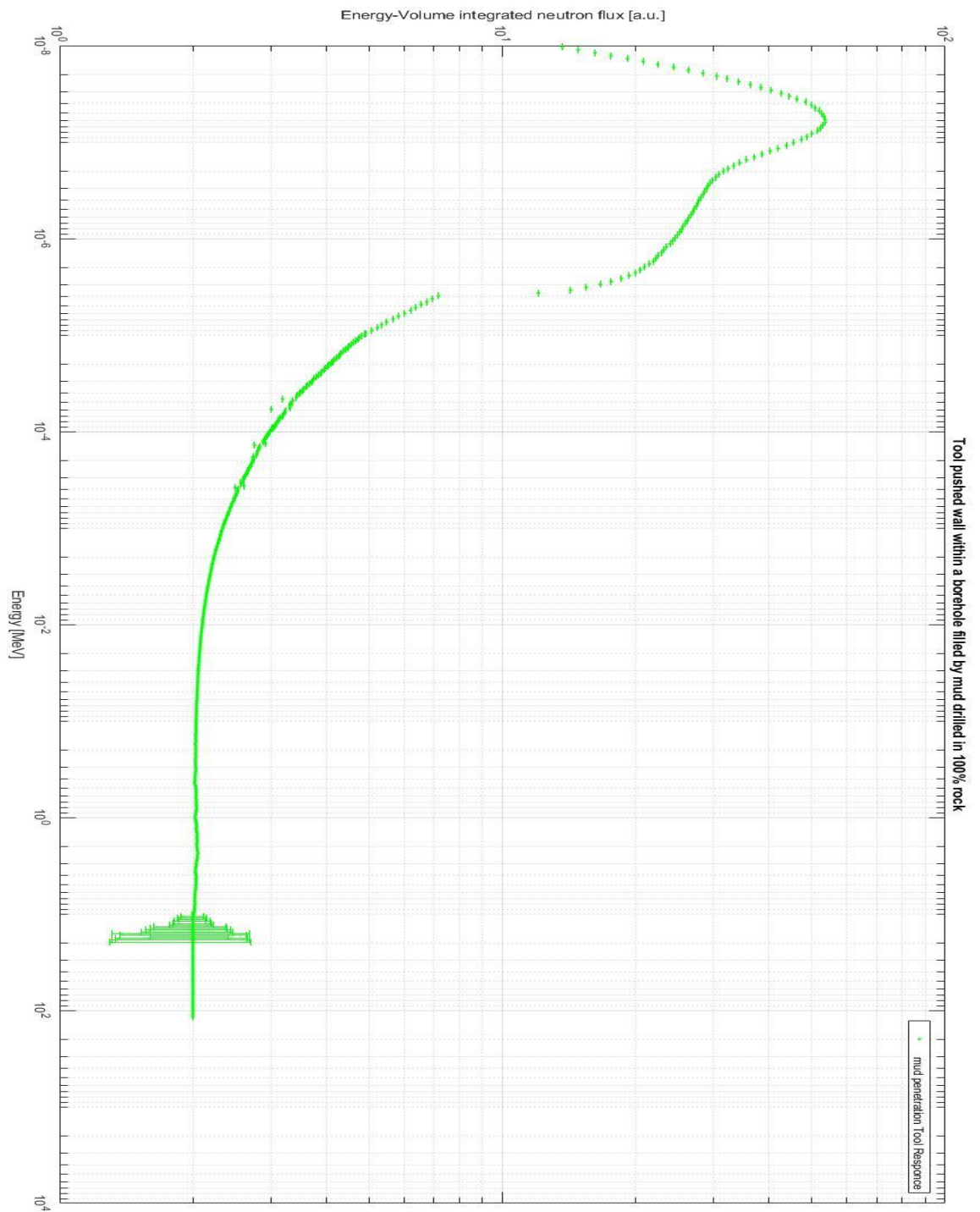


Figure D 21 Tool immersed within a borehole filled by water-based mud. The radius of the borehole is 10 cm. The borehole is drilled in 100% of Calcite. The tool is pushed against borehole's wall. In ordinates are plotted Energy-Volume integrated neutron flux [a-u], in abscises are plotted detector incident energies expressed in MeV

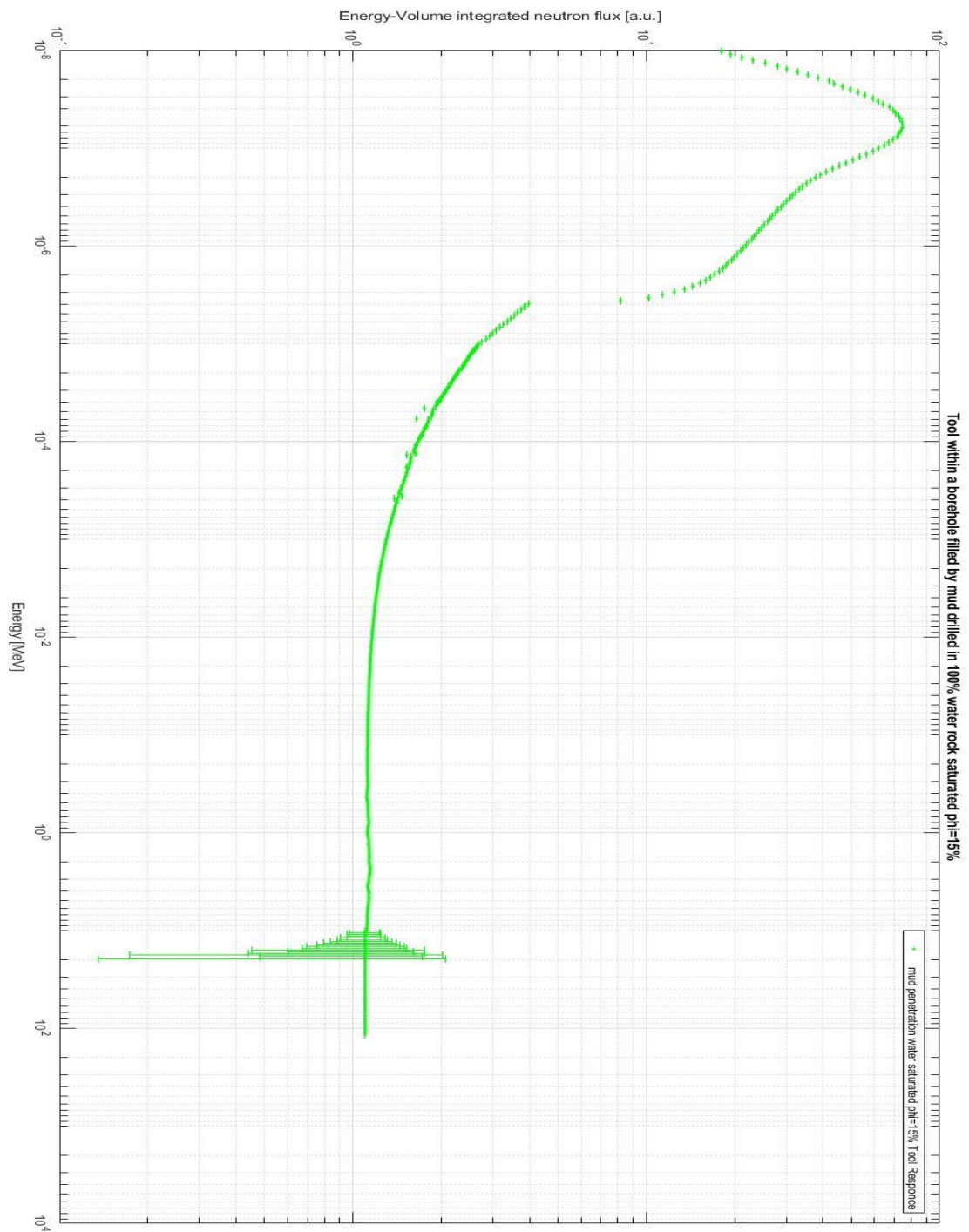


Figure D 22 Tool immersed within a borehole filled by water-based mud. The radius of the borehole is 10 cm. The borehole is drilled in 100% of Calcite with 15% of porosity, in this case porosity is void. The mud invasion is simulated, its extension is 20cm through the rock from the wall of the borehole. in ordinates are plotted Energy-Volume integrated neutron flux [a-u], in abscises are plotted detector incident energies expressed in MeV

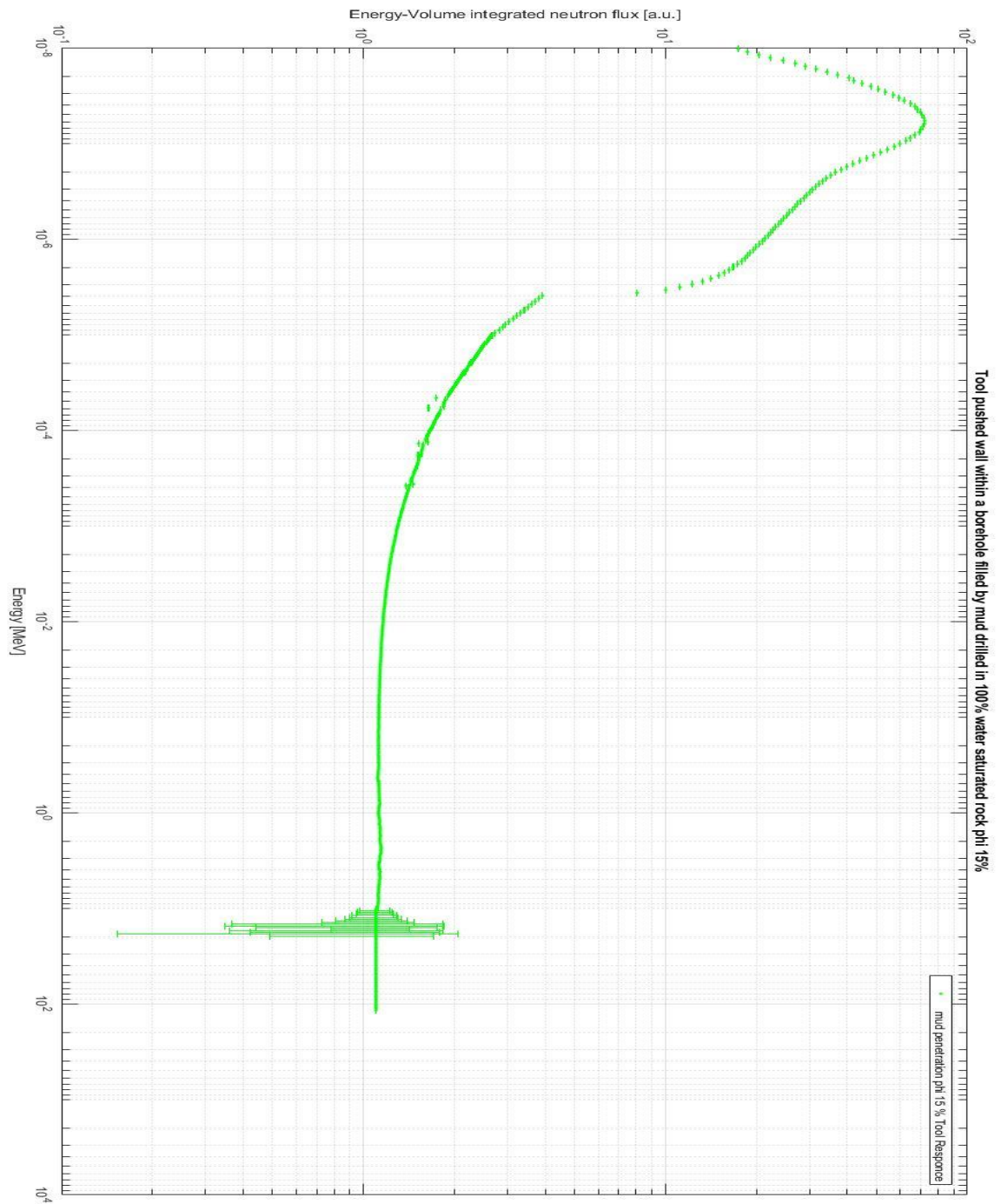


Figure D 23 Tool immersed within a borehole filled by water-based mud. The radius of the borehole is 10 cm. The borehole is drilled in 100% of Calcite with 15% of porosity, in this case porosity is void. The mud invasion is simulated, its extension is 20cm through the rock from the wall of the borehole. Here the tool is pushed against the wall of the borehole. In ordinates are plotted Energy-Volume integrated neutron flux [a-u], in abscises are plotted detector incident energies expressed in MeV

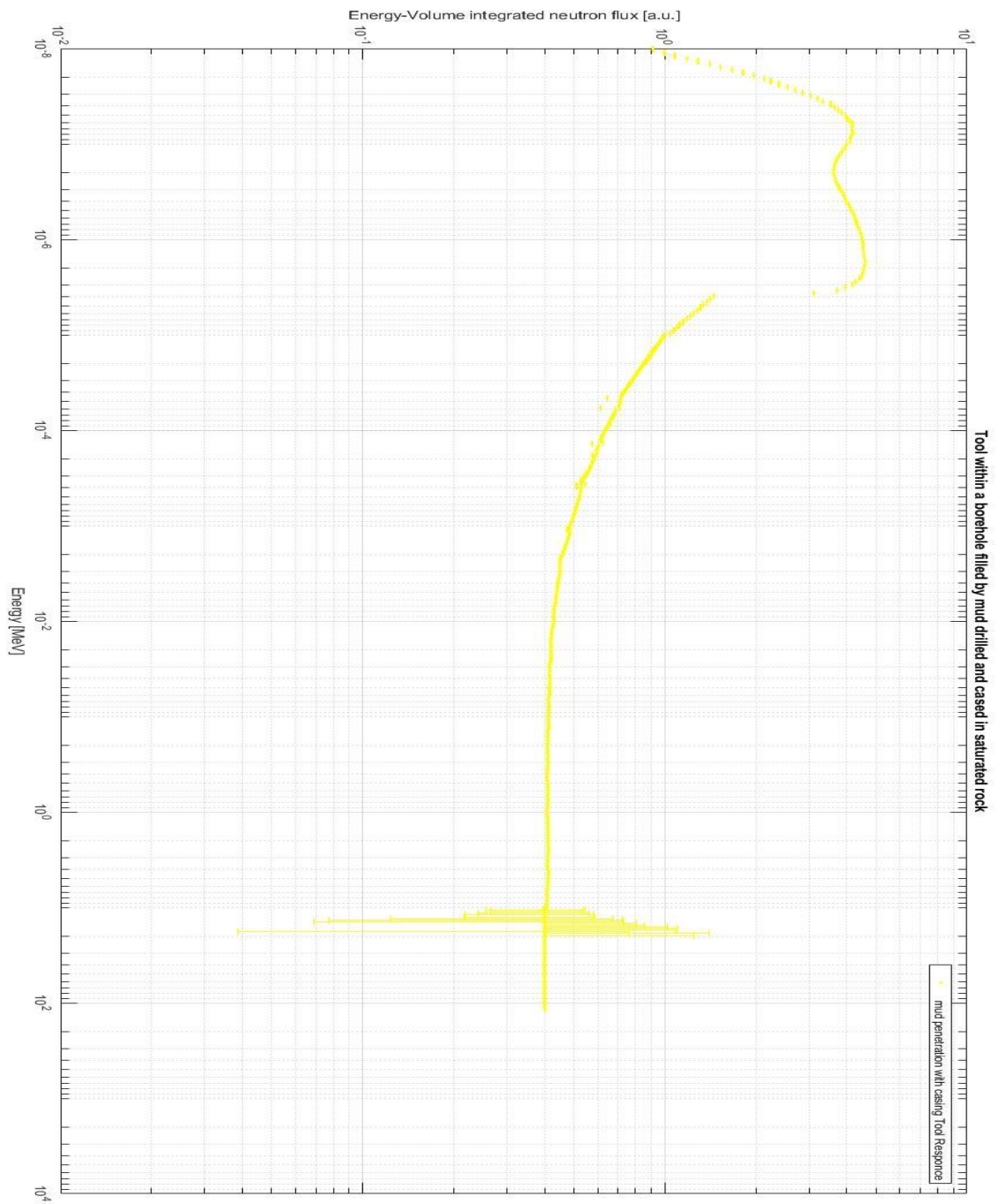


Figure D 24 Tool immersed within a borehole filled by water-based mud. The radius of the borehole is 10 cm. The borehole is drilled in 100% of Calcite with 15% of porosity, in this case porosity is void. The mud invasion is simulated, its extension is 20cm through the rock from the wall of the borehole. The test is done in wireline condition so Casing string is simulated. in ordinates are plotted Energy-Volume integrated neutron flux [a-u], in abscises are plotted detector incident energies expressed in MeV

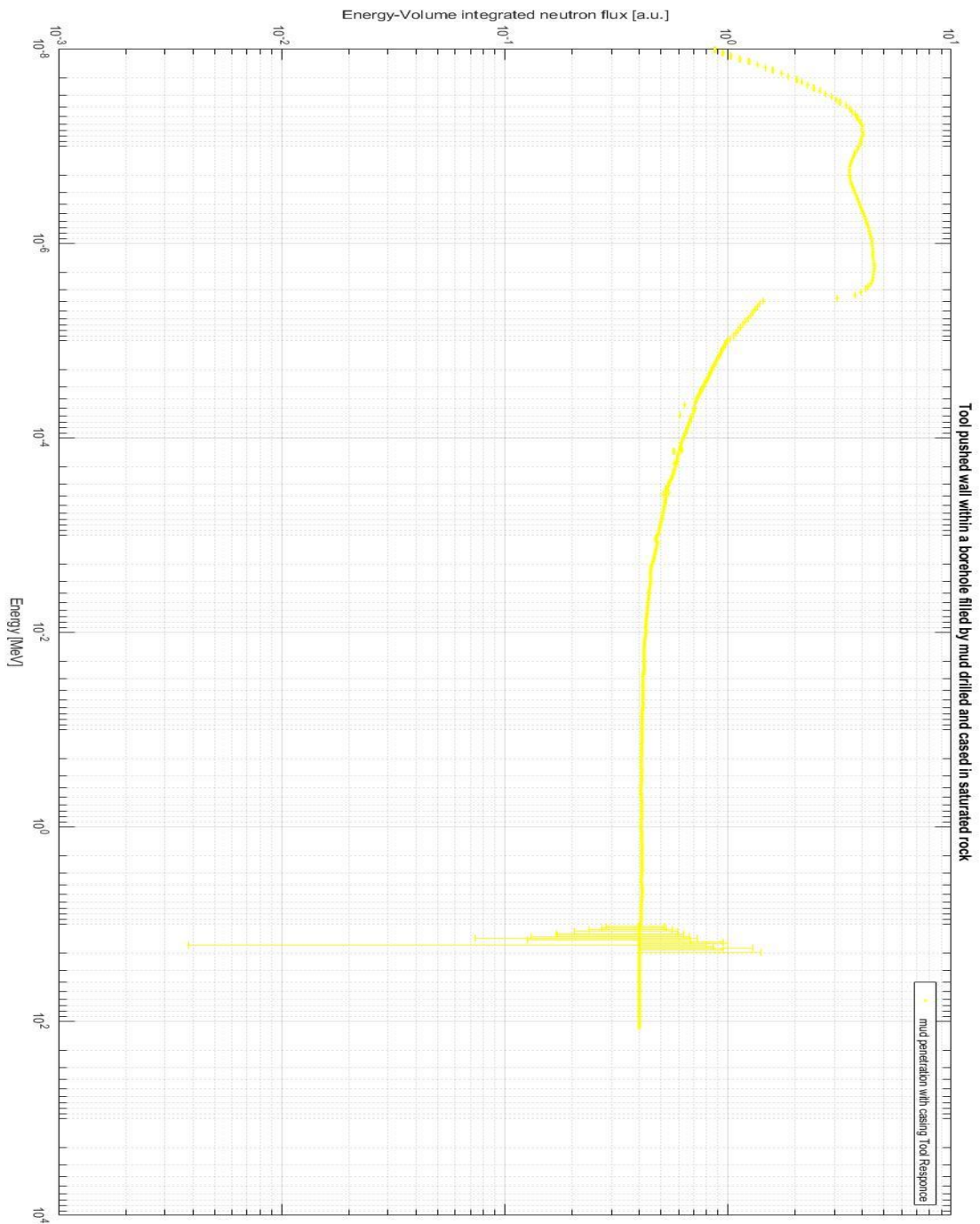


Figure D 25 Tool immersed within a borehole filled by water-based mud. The radius of the borehole is 10 cm. The borehole is drilled in 100% of Calcite with 15% of porosity, in this case porosity is void. The mud invasion is simulated, its extension is 20cm through the rock from the wall of the borehole. The test is done in wireline condition so Casing string is simulated. Here the tool is pushed against the borehole's wall. In ordinates are plotted Energy-Volume integrated neutron flux [a-u], in abscises are plotted detector incident energies expressed in MeV

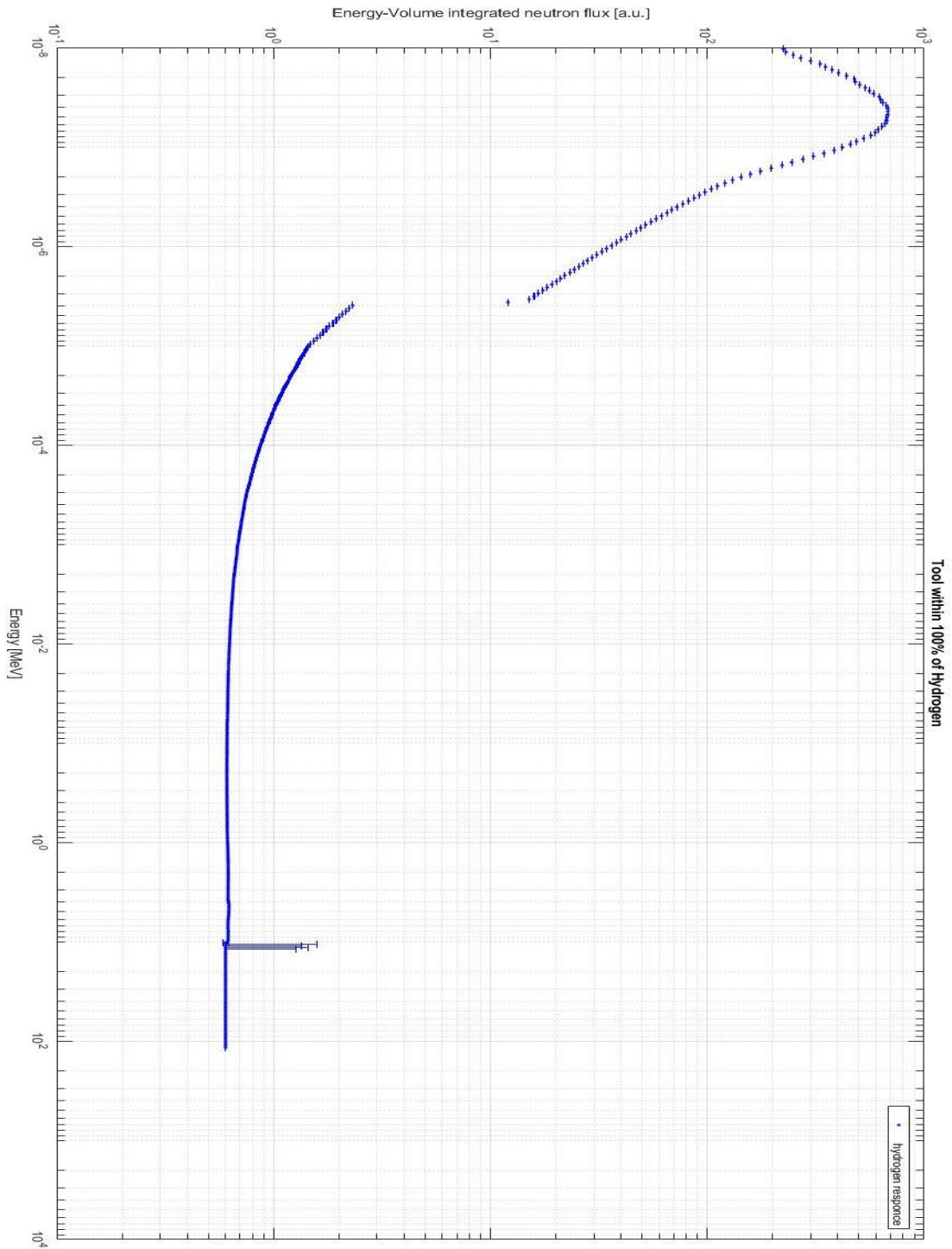


Figure D 26 Tool immersed in 100% of Hydrogen. In ordinates are plotted Energy-Volume integrated neutron flux [a-u], in abscises are plotted detector incident energies expressed in MeV

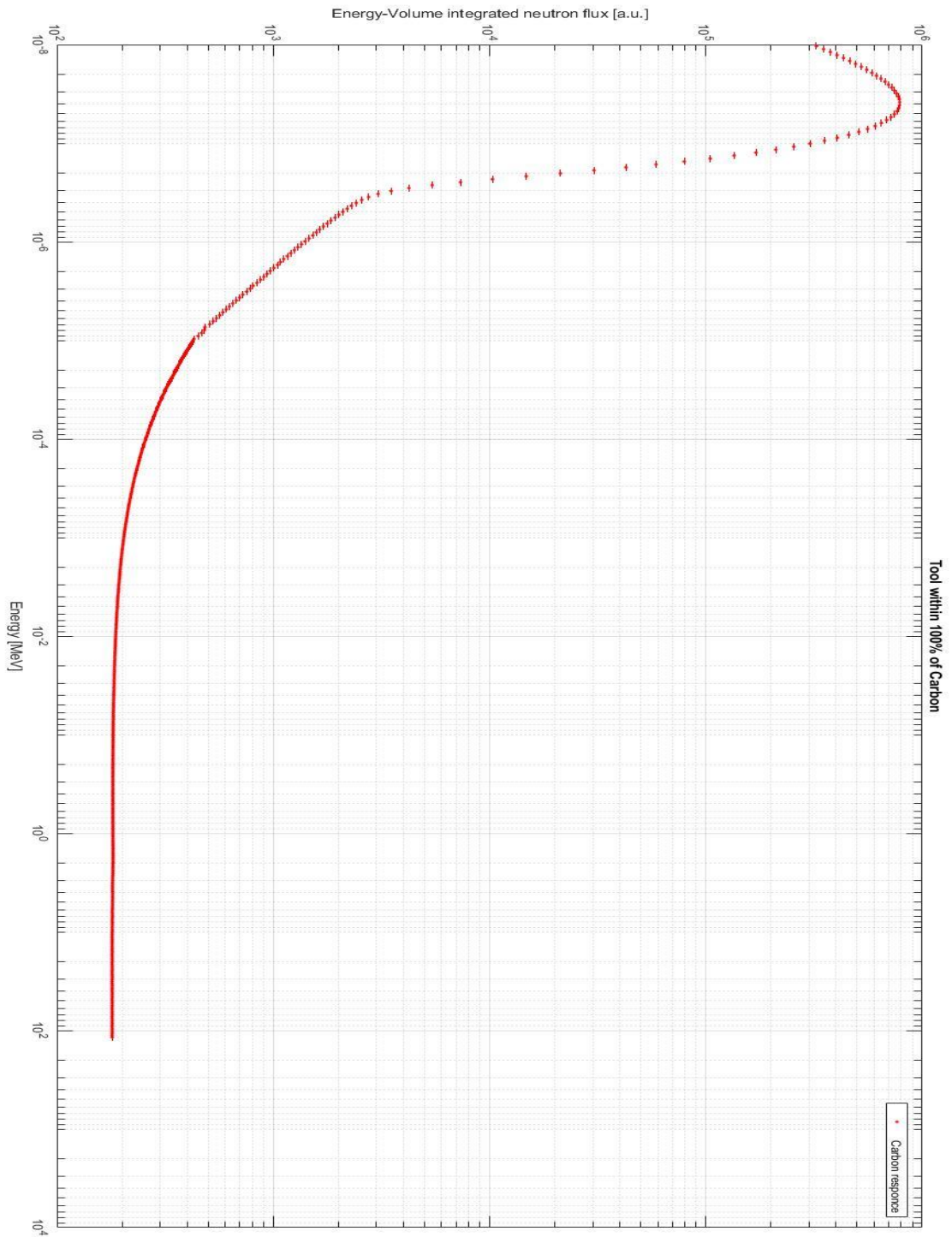


Figure D 27 Tool immersed in 100% of Carbon. In ordinates are plotted Energy-Volume integrated neutron flux [a-u], in abscises are plotted detector incident energies expressed in MeV

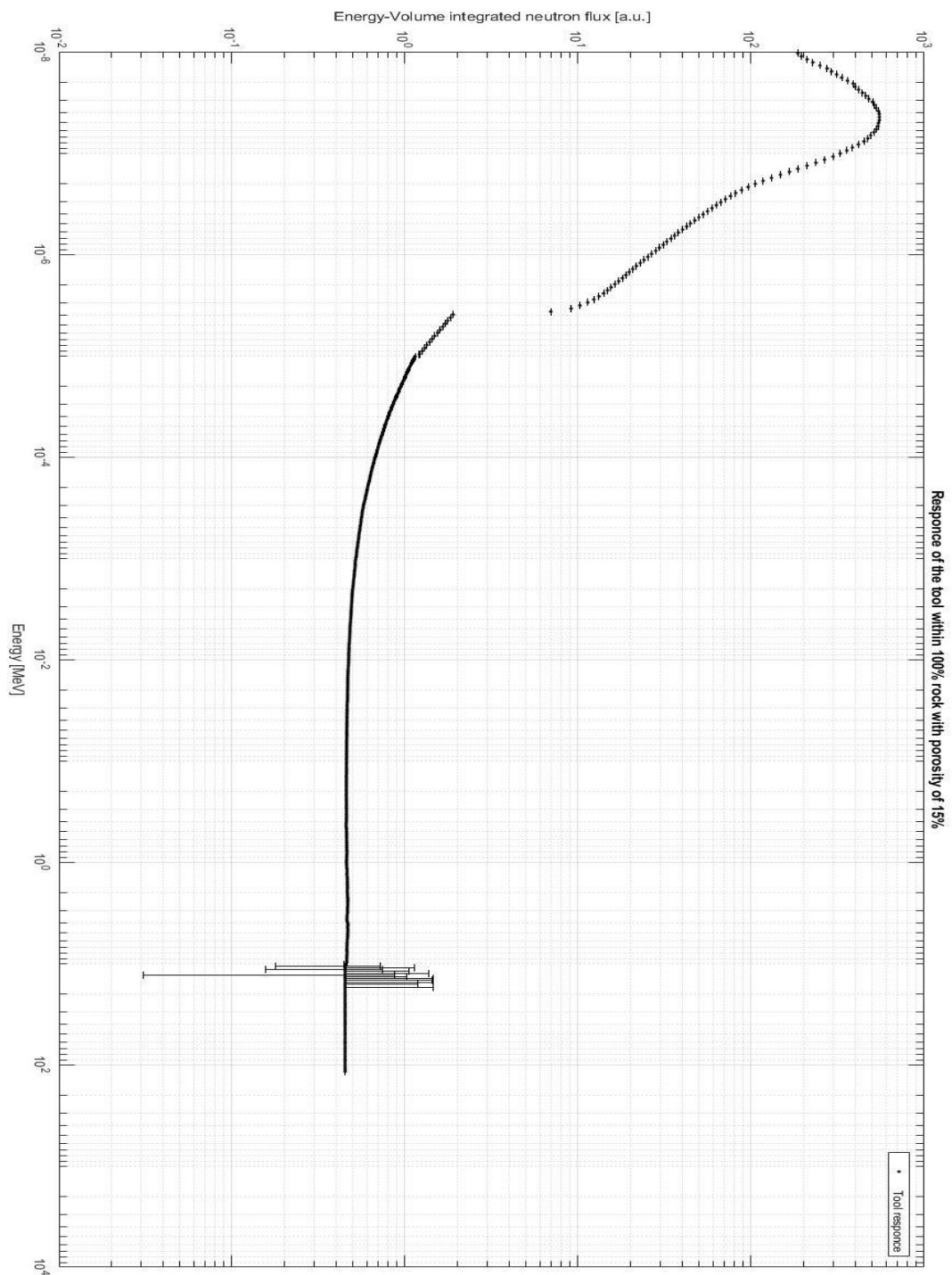


Figure D 28 Tool immersed in 100% of Calcite with porosity of 15% saturated by pure water. Tool immersed in 100% of Hydrogen. In ordinates are plotted Energy-Volume integrated neutron flux [a-u], in abscises are plotted detector incident energies expressed in MeV

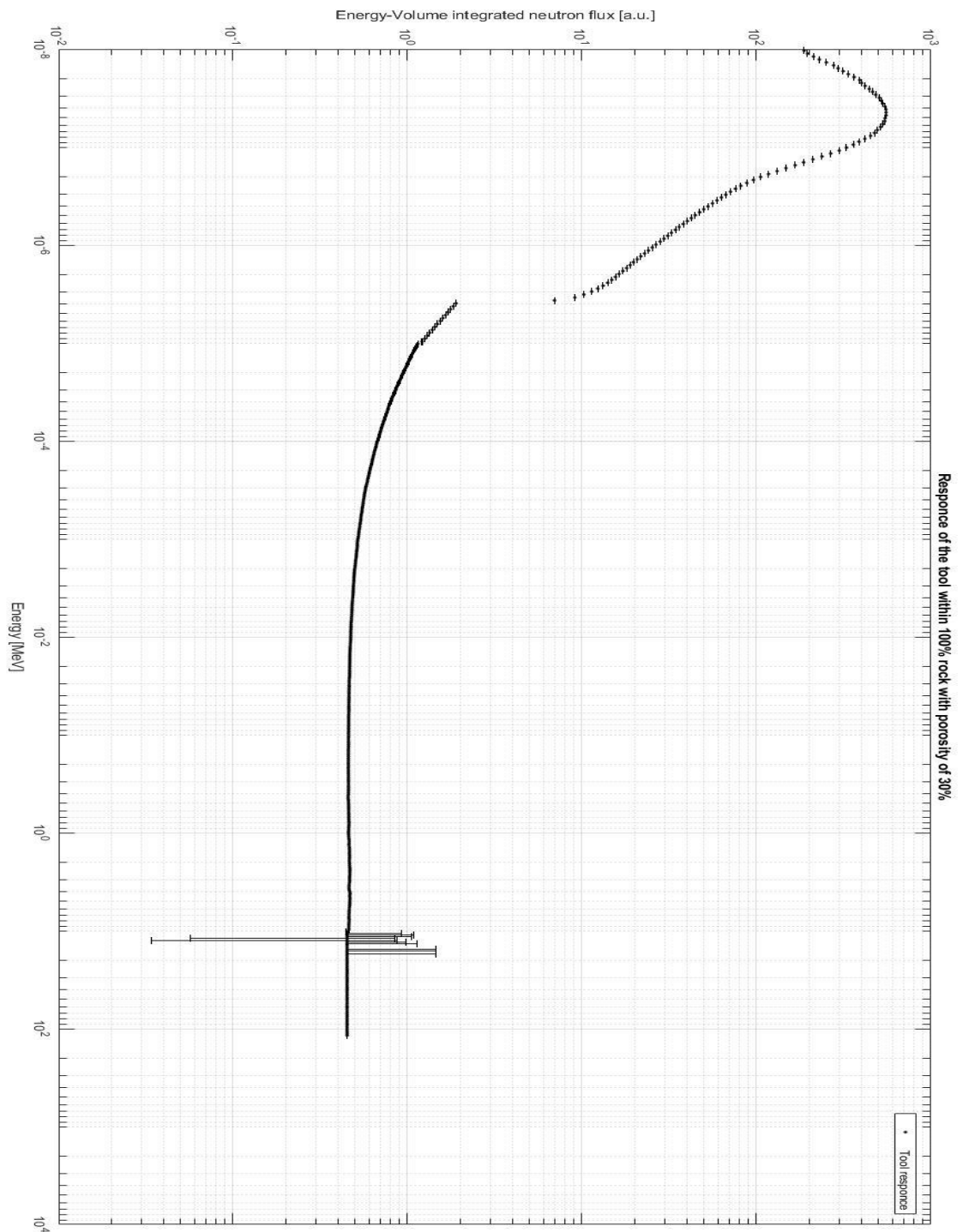


Figure D 29 Tool immersed in 100% of Calcite with porosity of 30% saturated by pure water. Tool immersed in 100% of Hydrogen. In ordinates are plotted Energy-Volume integrated neutron flux [a-u], in abscises are plotted detector incident energies expressed in MeV

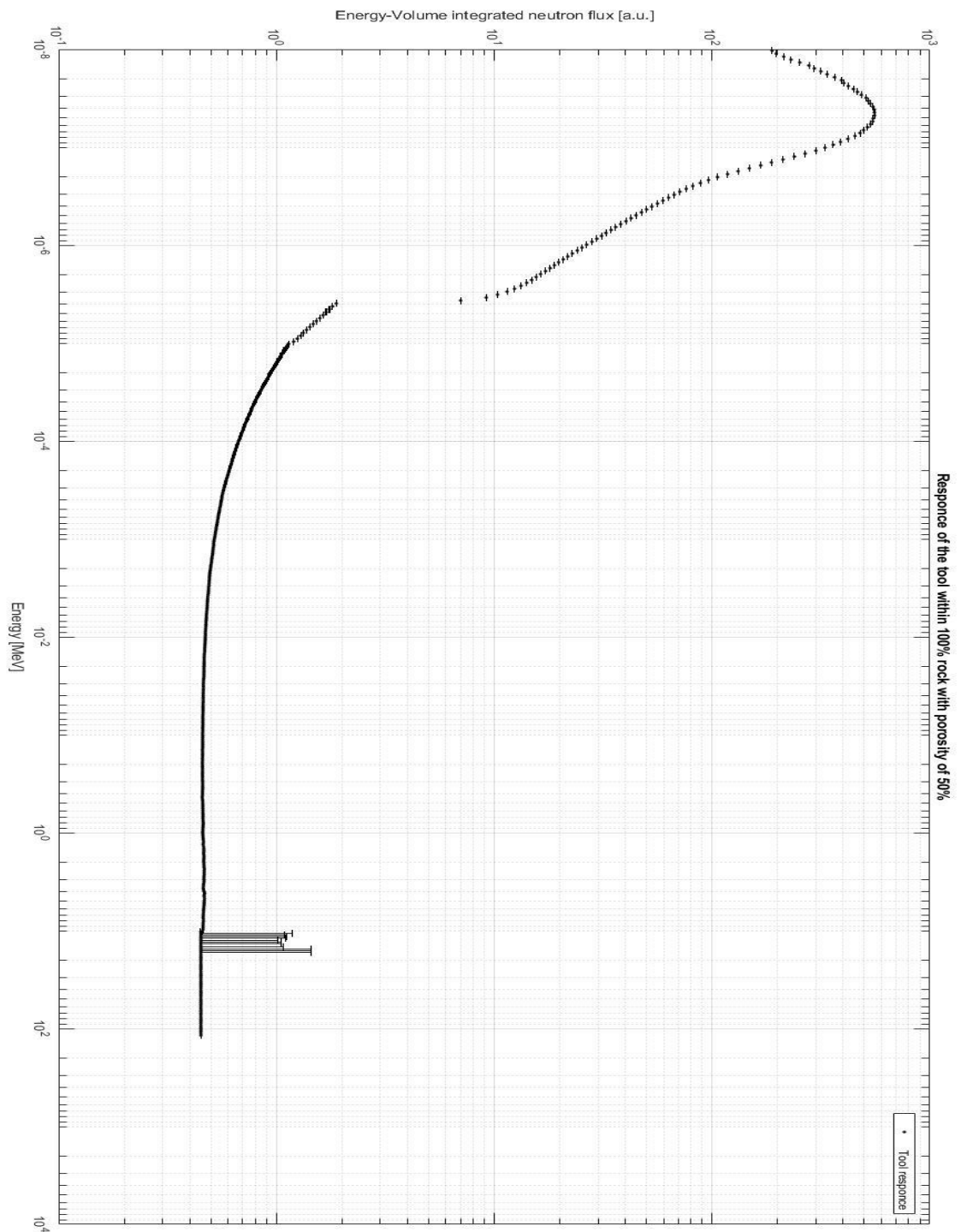


Figure D 30 Tool immersed in 100% of Calcite with porosity of 50% saturated by pure water. Tool immersed in 100% of Hydrogen. In ordinates are plotted Energy-Volume integrated neutron flux [a-u], in abscises are plotted detector incident energies expressed in MeV

## APPENDIX E) Compiled Programs

Example E1) Simulation 1, AllROCK.

```
%ALLROCK PROGRAM, THE TOOL IS IMMERGED IN 100% OF CALCITE

%geometry of the rock
surf earth inf

%geometry of the hole
surf hole cyl 0.000 0.000 5.0

%definition univers 0 body of infinity rock with an hole filled
with universe 3

cell 1 0 rock -earth hole
cell 2 0 outside earth
cell 3 0 fill 3 -hole

%Materials definition:
%To define material we need to define its nuclides, the adopted
convention is this <Z><A>.<id>.
%Where <Z> is the element, <A> is the isotope mass number (three
digits) and <id> is the libray id. For example Carbon is defined
"6000.03c". The library id is referred to temperature in K, .03c
means 300K.

%Rock definition, composition of rock in wt%, density 2,71g/cm3.

mat rock 2.71          rgb 200 200 200
20000.03c -0.4 % wt% of Calcium
8016.03c  -0.4 % wt% of Oxigen
6000.03c  -0.2 % wt% of Carbon

%Steel definition, composition in wt%, density 7,5g/cm3

mat steel 7.5          rgb 100 100 100
6000.03c  -0.0006%C
26000.03c -0.73555 %Fe
14000.03c -0.007 %Si
25055.03c -0.15 %Mn
16000.03c -0.00015 %S
7014.03c  -0.0002 %N
24000.03c -0.17 %Cr
42000.03c -0.115 %Mo
28000.03c -0.6 %Ni

%Source materia definition, called AmBe, Chemical composition is
AmO2Be, composition expressed in wt%, density, 3,7g/cm3.

mat AmBe 3.7          rgb 255 0 0
95241.03c -0.18 %Am
8016.03c  -0.02 %O
4007.03c  -0.8 %Be
```

**%Detector material definition**

```
mat He3 sum          rgb 0 255 0
2003.03c -1.0
```

**%Water definition**

```
mat water 1.0        rgb 200 200 255
8016.03c -0.89
1001.03c -0.11
```

**%Water based mud definition**

```
mat mud 1.380        rgb 204 102 0
1001.03c -0.072 %H
6000.03c -0.0023 %C
8016.03c -0.66 %O
11022.03c -0.0019 %Na
13027.03c -0.0053 %Al
14000.03c -0.0069 %Si
16000.03c -0.0376 %S
17000.03c -0.0102 %Cl
19000.03c -0.0428 %K
56130.03c -0.1609 %Ba
```

**%External source mode definition**

```
set nps 50000000
```

```
src 1 sc 6 sb 7
4E-1 0.0
1.0 0.4
3.0 1.4
4.0 1.0
6.0 5.8
7.5 3.4
10.0 7.00
```

**%Moderator library definition**

```
therm MyThermLib hwj3.00t
set acelib "/xs/sss_jeff311u.xsdata"
```

**%geometry of the tool**

```
surf bottom1 pz -234
surf top1 pz 188
surf bottom2 pz -3.0
surf top2 pz 3.0
```

**%tool definition**

```
pin 1
AmBe 0.5
steel 1.0
rock
```

```
pin 2
steel 1.0
rock
```

```
pin 4
He3 0.5
steel 1.0
rock
```

```
surf botdet1 pz 62
surf topdet1 pz 72
```

```
cell 4 3 rock -bottom1
cell 5 3 fill 2 bottom1 -bottom2
cell 6 3 fill 1 bottom2 -top2
cell 7 3 fill 2 top2 -botdet1
cell 8 3 fill 4 botdet1 -topdet1
cell 9 3 fill 2 topdet1 -top1
cell 12 3 rock top1
```

**%Definition of the detector and its energy grid**

```
ene energy 3 400 10e-6 12e1
ene energy2 3 100 1e-8 10e-6
det 1 de energy du 0 dv 31.14 dr 103 He3
det 2 de energy2 du 0 dv 31.14 dr 103 He3
```

**%Geometry Plot**

```
plot 1 1000 1000 0 40 -40 400 -400
plot 2 1000 1000 0 100 100 100 100
plot 3 1000 1000 0 30 -30 100 -100
```

---

Example E2), Simulation 6, PHI15WATER.

```
%SIMULATION "PHI15WATER". IN THIS SIMULATION THE TOOL IS CENTRED  
IN THE BOREHOLE, DRILLING FLUID IS WATER AND ROCK IS CALCITE.  
CALCITE IS SIMULATED WITH A POROSITY OF 15% SATURATED BY WATER. |
```

```
%geometry of the rock
```

```
surf earth inf
```

```
%geometry of the hole
```

```
surf hole cyl 0.000 0.000 5.0
```

```
%definition univers 0 body of infinity rock with an hole filled  
with universe 3
```

```
cell 1 0 rock15water -earth hole
```

```
cell 2 0 outside earth
```

```
cell 3 0 fill 3 -hole
```

```
%materials
```

```
mat rock15water 2.45 moder MyThermLib 1001 rgb 200 200 220  
20000.03c -0.34 %Ca  
8016.03c -0.4735 %O  
6000.03c -0.17 %C  
1001.03c -0.0165 %H
```

```
mat steel 7.5 rgb 100 100 100  
6000.03c -0.0006 %C  
26000.03c -0.73555 %Fe  
14000.03c -0.007 %Si  
25055.03c -0.15 %Mn  
16000.03c -0.00015 %S  
7014.03c -0.0002 %N  
24000.03c -0.17 %Cr  
42000.03c -0.115 %Mo  
28000.03c -0.6 %Ni
```

```
mat AmBe 3.7 rgb 255 0 0  
95241.03c -0.18 %Am  
8016.03c -0.02 %O  
4007.03c -0.8 %Be
```

```
mat He3 sum rgb 0 255 0  
2003.03c -1.0 %He
```

```
mat water 1.0 moder MyThermLib 1001 rgb 0 0 255  
8016.03c -0.89 %O  
1001.03c -0.11 %H
```

```
mat mud 1.380
1001.03c -0.072 %H
6000.03c -0.0023 %C
8016.03c -0.66 %O
11022.03c -0.0019 %Na
13027.03c -0.0053 %Al
14000.03c -0.0069 %Si
16000.03c -0.0376 %S
17000.03c -0.0102 %Cl
19000.03c -0.0428 %K
56130.03c -0.1609 %Ba
```

#### %External source definition

```
set nps 50000000
```

```
src 1 sc 6 sb 7
```

```
4E-1 0.0
1.0 0.4
3.0 1.4
4.0 1.0
6.0 5.8
7.5 3.4
10.0 7.00
```

#### %Moderator library definition

```
therm MyThermLib hwj3.00t
set acelib "/xs/sss_jeff311u.xsdata"
```

#### %geometry of the tool and tool definition

```
surf bottom1 pz -234
surf top1 pz 188
surf bottom2 pz -3.0
surf top2 pz 3.0
```

```
pin 1
AmBe 0.5
steel 1.0
water
```

```
pin 2
steel 1.0
water
```

```
pin 4
He3 0.5
steel 1.0
```

---

```
surf botdet1 pz 62
surf topdet1 pz 72
```

```
cell 4 3 water -bottom1
cell 5 3 fill 2 bottom1 -bottom2
cell 6 3 fill 1 bottom2 -top2
cell 7 3 fill 2 top2 -botdet1
cell 8 3 fill 4 botdet1 -topdet1
cell 9 3 fill 2 topdet1 -top1
cell 12 3 water top1
```

%then I have to score total capture into He3 due to neutrons collision into universe 0 (volume of integration=>everything) with an energy interval of 0->15MeV, so my idea was:

```
ene energy 3 400 10e-6 12e1
ene energy2 3 100 1e-8 10e-6
det 1 de energy du 0 dv 31.14 dr 103 He3
det 2 de energy2 du 0 dv 31.14 dr 103 He3
```

%Geometry plot

```
plot 1 1000 1000 0 40 -40 400 -400
plot 2 1000 1000 0 100 100 100 100
plot 3 1000 1000 0 30 -30 100 -100
```

Example E3), simulation 23, WallPenetrationOil.

```
%PROGRAM "WALLPENETRATIONOIL", THE TOOL IS IMMERSGED IN A BOREHOLE
OF 10cm RADIUS, THE FILLING FLUID IS WATER-BASED MUD. PENETRATION
ZONE IS 20cm WIDE FROM THE WALL OF THE BOREHOLE. ROCK BODY HAS 15%
OF POROSITY, OIL SATURATED. IRRIDUCIBLE WATER SATURATION IS 0,15.
RESIDUAL OIL SATURATION IS 0,05 IN INVADED ZONE.
```

%geometry of the rock

```
surf earth inf
```

%geometry of the hole and the invased zone.

```
surf hole cyl 0.000 -3.50 4.5 %Borehole
surf mudc cyl 0.000 -3.50 5.0 %Mudcake
surf m1 cyl 0.000 -3.50 6.0 %Invaded zone
surf m2 cyl 0.000 -3.50 7.0
surf m3 cyl 0.000 -3.50 8.0
surf m4 cyl 0.000 -3.50 9.00
surf m5 cyl 0.000 -3.50 10.0
surf m6 cyl 0.000 -3.50 11.0
surf m7 cyl 0.000 -3.50 12.0
surf m8 cyl 0.000 -3.50 13.0
surf m9 cyl 0.000 -3.50 14.0
surf m10 cyl 0.000 -3.50 15.0
```

%definition univers 0 body of infinity rock with an hole filled with universe 3

```
cell 2 0 outside earth
cell 1 0 rock15wateroil -earth m10
```

```
%definition univers 0 body of infinity rock with an hole filled
with universe 3
```

```
cell 2 0 outside earth
cell 1 0 rock15wateroil -earth m10
```

```
%Defining of penetration definition
```

```
cell 14 0 mud1 -m1 mudc
cell 15 0 mud2 -m2 m1
cell 16 0 mud3 -m3 m2
cell 17 0 mud4 -m4 m3
cell 18 0 mud5 -m5 m4
cell 19 0 mud6 -m6 m5
cell 20 0 mud7 -m7 m6
cell 21 0 mud8 -m8 m7
cell 22 0 mud9 -m9 m8
cell 23 0 mud10 -m10 m9
cell 24 0 mudcake -mudc hole
cell 3 0 fill 3 -hole
```

```
%Materials definitions
```

```
%Mud cake, mud cake is thought without liquid part. For us liquid
part was water. Thus, mudcake composition is without O and H
```

```
mat mudcake sum rgb 50 20 20
11022.03c -0.00717 %Na
13027.03c -0.0199 %Al
14000.03c -0.026 %Si
16000.03c -0.1416 %S
17000.03c -0.0384 %Cl
19000.03c -0.1612 %K
56130.03c -0.6057 %Ba
```

```
%Invaded zone
```

```
mat mud1 sum moder MyThermLib 1001 rgb 103 80 65
20000.03c -0.34 %Ca
1001.03c -0.01266 %H
6000.03c -0.1762 %C
8016.03c -0.439 %O
11022.03c -0.000228 %Na
13027.03c -0.000636 %Al
14000.03c -0.000828 %Si
16000.03c -0.004512 %S
17000.03c -0.001224 %Cl
19000.03c -0.005136 %K
56130.03c -0.019296 %Ba
```

```

mat mud2 sum      moder MyThermLib 1001      rgb 120 133 119
20000.03c -0.34   %Ca
1001.03c   -0.0133 %H
6000.03c   -0.1781   %C
8016.03c   -0.439    %O
11022.03c  -0.000209 %Na
13027.03c  -0.000583 %Al
14000.03c  -0.000759 %Si
16000.03c  -0.004136 %S
17000.03c  -0.001122 %Cl
19000.03c  -0.004708 %K
56130.03c  -0.017687 %Ba

```

```

mat mud3 sum      moder MyThermLib 1001      rgb 150 150 130
20000.03c -0.34   %Ca
1001.03c   -0.0139 %H
6000.03c   -0.1801   %C
8016.03c   -0.4394   %O
11022.03c  -0.00019   %Na
13027.03c  -0.000529 %Al
14000.03c  -0.00069   %Si
16000.03c  -0.00376   %S
17000.03c  -0.00102   %Cl
19000.03c  -0.00428   %K
56130.03c  -0.01608   %Ba

```

```

mat mud4 sum      moder MyThermLib 1001      rgb 165 155 133
20000.03c -0.34   %Ca
1001.03c   -0.0145   %H
6000.03c   -0.1821   %C
8016.03c   -0.43945  %O
11022.03c  -0.000171 %Na
13027.03c  -0.000477 %Al
14000.03c  -0.000621 %Si
16000.03c  -0.003383 %S
17000.03c  -0.000918 %Cl
19000.03c  -0.003851 %K
56130.03c  -0.014472 %Ba

```

```

mat mud5 sum      moder MyThermLib 1001      rgb 170 165 140
20000.03c -0.34   %Ca
1001.03c   -0.0151   %H
6000.03c   -0.184   %C
8016.03c   -0.4395   %O
11022.03c  -0.000152 %Na
13027.03c  -0.000424 %Al
14000.03c  -0.000552 %Si
16000.03c  -0.003008 %S
17000.03c  -0.000816 %Cl
19000.03c  -0.003424 %K
56130.03c  -0.012864 %Ba

```

```

mat mud6 sum      moder MyThermLib 1001   rgb 180 170 150
20000.03c -0.34    %Ca
1001.03c   -0.0157  %H
6000.03c   -0.186    %C
8016.03c   -0.4396  %O
11022.03c  -0.000133 %Na
13027.03c  -0.000371 %Al
14000.03c  -0.000483 %Si
16000.03c  -0.002632 %S
17000.03c  -0.00714 %Cl
19000.03c  -0.002995 %K
56130.03c  -0.011256 %Ba

```

```

mat mud7 sum      moder MyThermLib 1001   rgb 188 179 155
20000.03c -0.34    %Ca
1001.03c   -0.0164  %H
6000.03c   -0.188    %C
8016.03c   -0.4397  %O
11022.03c  -0.0001139 %Na
13027.03c  -0.000318 %Al
14000.03c  -0.000414 %Si
16000.03c  -0.002256 %S
17000.03c  -0.000611 %Cl
19000.03c  -0.002568 %K
56130.03c  -0.009647 %Ba

```

```

mat mud8 sum      moder MyThermLib 1001   rgb 190 185 160
20000.03c -0.34    %Ca
1001.03c   -0.01699 %H
6000.03c   -0.1899 %C
8016.03c   -0.4398 %O
11022.03c  -0.000095 %Na
13027.03c  -0.000265 %Al
14000.03c  -0.000345 %Si
16000.03c  -0.00187 %S
17000.03c  -0.00051 %Cl
19000.03c  -0.002139 %K
56130.03c  -0.008040 %Ba

```

```

mat mud9 sum      moder MyThermLib 1001   rgb 210 193 180
20000.03c -0.34    %Ca
1001.03c   -0.01762 %H
6000.03c   -0.1919 %C
8016.03c   -0.4398 %O
11022.03c  -0.000076 %Na
13027.03c  -0.000211 %Al
14000.03c  -0.000276 %Si
16000.03c  -0.001504 %S
17000.03c  -0.000408 %Cl
19000.03c  -0.001712 %K
56130.03c  -0.006432 %Ba

```

```

mat mud10 sum      moder MyThermLib 1001  rgb 235 250 233
20000.03c -0.34   %Ca
1001.03c  -0.01824 %H
6000.03c  -0.1939   %C
8016.03c  -0.4399   %O
11022.03c -0.000057 %Na
13027.03c -0.000159 %Al
14000.03c -0.000207 %Si
16000.03c -0.001128 %S
17000.03c -0.000306 %Cl
19000.03c -0.001283 %K
56130.03c -0.004824 %Ba

```

#### %Mud definition

```

mat mud 1.380      moder MyThermLib 1001  rgb 204 102 0
1001.03c  -0.072   %H
6000.03c  -0.0023   %C
8016.03c  -0.66    %O
11022.03c -0.0019   %Na
13027.03c -0.0053   %Al
14000.03c -0.0069   %Si
16000.03c -0.0376   %S
17000.03c -0.0102   %Cl
19000.03c -0.0428   %K
56130.03c -0.1609   %Ba

```

#### %Porous rock definition

```

mat rock15wateroil 2.4475 moder MyThermLib 1001  rgb 54 150 69
20000.03c -0.34   %Ca
8016.03c  -0.440125 %O
6000.03c  -0.19977875 %C
1001.03c  -0.02009625 %H

```

#### %Rock Definition

```

mat rock 2.71      rgb 200 200 200
20000.03c -0.4   %Ca
8016.03c  -0.4   %O
6000.03c  -0.2   %C

```

#### %Stainless-steel definition

```

mat steel 7.5      rgb 100 100 100
6000.03c  -0.0006   %C
26000.03c -0.73555   %Fe
14000.03c -0.007    %Si
25055.03c -0.15    %Mn
16000.03c -0.00015   %S
7014.03c  -0.0002   %N
24000.03c -0.17    %Cr
42000.03c -0.115   %Mo
28000.03c -0.6     %Ni

```

### %Source definition

```
mat AmBe 3.7          rgb 255 0 0
95241.03c -0.18 %Am
8016.03c  -0.02 %O
4007.03c  -0.8  %Be
```

### %Detector definition

```
mat He3 sum          rgb 0 255 0
2003.03c -1.0  %He
```

### %water definition

```
mat water 1.0  moder MyThermLib 1001  rgb 200 200 255
8016.03c -0.89 %O
1001.03c -0.11 %H
```

%external source definition, a higher number of neutrons is needed to perform a better statistic.

```
set nps 1000000000
```

```
src 1 sc 6 sb 7
```

```
4E-1  0.0
1.0   0.4
3.0   1.4
4.0   1.0
6.0   5.8
7.5   3.4
10.0  7.00
```

### %moderator library definition

```
therm MyThermLib hwj3.00t
set acelib "/xs/sss_jeff311u.xsdata"
```

### %geometry of the tool

```
surf bottom1 pz -234
surf top1     pz  188
surf bottom2 pz -3.0
surf top2     pz   3.0
```

### %tool definition

```
pin 1
AmBe 0.5
steel 1.0
mud
```

```
pin 2
steel 1.0
mud
```

```
pin 4
He3 0.5
steel 1.0
mud
```

```

surf botdet1 pz 62
surf topdet1 pz 72

cell 4 3 fill 6 -bottom1
cell 5 3 fill 2 bottom1 -bottom2
cell 6 3 fill 1 bottom2 -top2
cell 7 3 fill 2 top2 -botdet1
cell 8 3 fill 4 botdet1 -topdet1
cell 9 3 fill 2 topdet1 -top1
cell 12 3 fill 6 top1

%Definition of mud pin

pin 6
mud 10.0
rock

%then I have to score total capture into He3 due to neutrons
collision into universe 0 (volume of integration=>everything) with
an energy interval of 0->15MeV, so my idea was:

ene energy 3 400 10e-6 12e1
ene energy2 3 100 1e-8 10e-6
det 1 de energy du 0 dr 103 He3
det 2 de energy2 du 0 dr 103 He3

%Geometry plot

plot 1 1000 1000 0 40 -40 400 -400
plot 2 1000 1000 0 100 100 100 100
plot 3 1000 1000 0 20 -20 20 -20

```

## APPENDIX F) Example of Serpent Output

%11°Coloms rappresent the mean value, 12°rappresent standar deviation from mean value:

```

ExOutput = [
  1  1  1  1  1  1  1  1  1  1  2.48114E-01 0.01697
  2  2  1  1  1  1  1  1  1  1  2.63563E-01 0.01600
  3  3  1  1  1  1  1  1  1  1  2.83442E-01 0.01504
  4  4  1  1  1  1  1  1  1  1  3.13483E-01 0.01502
  5  5  1  1  1  1  1  1  1  1  3.57415E-01 0.01337
  6  6  1  1  1  1  1  1  1  1  3.90106E-01 0.01382
  7  7  1  1  1  1  1  1  1  1  4.29610E-01 0.01236
  8  8  1  1  1  1  1  1  1  1  5.62988E-01 0.01014
  9  9  1  1  1  1  1  1  1  1  6.45071E-01 0.00943
 10 10  1  1  1  1  1  1  1  1  7.17314E-01 0.01111
 11 11  1  1  1  1  1  1  1  1  7.70304E-01 0.00926
 12 12  1  1  1  1  1  1  1  1  7.36940E-01 0.00985
 13 13  1  1  1  1  1  1  1  1  7.87665E-01 0.00888
 14 14  1  1  1  1  1  1  1  1  8.57637E-01 0.00860
 15 15  1  1  1  1  1  1  1  1  9.39048E-01 0.00849
 16 16  1  1  1  1  1  1  1  1  1.03107E+00 0.00806
 17 17  1  1  1  1  1  1  1  1  1.19571E+00 0.00741
 18 18  1  1  1  1  1  1  1  1  1.30675E+00 0.00711
 19 19  1  1  1  1  1  1  1  1  1.39013E+00 0.00714
 20 20  1  1  1  1  1  1  1  1  1.92085E+00 0.00607
 21 21  1  1  1  1  1  1  1  1  1.96290E+00 0.00631
 22 22  1  1  1  1  1  1  1  1  1.91064E+00 0.00623
 23 23  1  1  1  1  1  1  1  1  2.07411E+00 0.00554
 24 24  1  1  1  1  1  1  1  1  2.24897E+00 0.00578
 25 25  1  1  1  1  1  1  1  1  2.43570E+00 0.00530
 26 26  1  1  1  1  1  1  1  1  2.83112E+00 0.00436
 27 27  1  1  1  1  1  1  1  1  3.29952E+00 0.00473
 28 28  1  1  1  1  1  1  1  1  3.27474E+00 0.00428
 29 29  1  1  1  1  1  1  1  1  3.55360E+00 0.00432
 30 30  1  1  1  1  1  1  1  1  4.26428E+00 0.00393
 31 31  1  1  1  1  1  1  1  1  4.24827E+00 0.00374
    .
    .
    .
 93 93  1  1  1  1  1  1  1  1  1.14701E+01 0.00083
 94 94  1  1  1  1  1  1  1  1  1.11644E+01 0.00090
 95 95  1  1  1  1  1  1  1  1  1.09210E+01 0.00086
 96 96  1  1  1  1  1  1  1  1  1.06507E+01 0.00079
 97 97  1  1  1  1  1  1  1  1  1.03919E+01 0.00076
 98 98  1  1  1  1  1  1  1  1  1.01936E+01 0.00075
 99 99  1  1  1  1  1  1  1  1  9.93566E+00 0.00082
100 100 1  1  1  1  1  1  1  1  9.64219E+00 0.00077
];

```

Figure E 1 Detector Output for Energy-integrated neutron flux: The results for each detector are written in a 13-column table, one bin value per row. The variable is named "DET.name", where "name" is the detector name. The values in each column are: 1. Value index (total number in "DET\_VALS") 2. Energy bin index (total number in "DET\_EBINS") 3. Universe bin index (total number in "DET\_UBINS") 4. Cell bin index (total number in "DET\_CBINS") 5. Material bin index (total number in "DET\_MBINS") 7.2 Detector output 106 6. Lattice bin index (total number in "DET\_LBINS") 7. Reaction bin index (total number in "DET\_RBINS") 8. Z-mesh bin index (total number in "DET\_ZBINS") 9. Y-mesh bin index (total number in "DET\_YBINS") 10. X-mesh bin index (total number in "DET\_XBINS") 11. Mean value 12. Relative statistical error 13. Total number of scores (Lappanen,2015)

%Third column represent the mean energy of the bin, first and second are the minimum and maximum energy boundaries of the bin.

```
ExOutput2E = [
1.00000E-08 1.07152E-08 1.03576E-08
1.07152E-08 1.14815E-08 1.10984E-08
1.14815E-08 1.23027E-08 1.18921E-08
1.23027E-08 1.31826E-08 1.27426E-08
1.31826E-08 1.41254E-08 1.36540E-08
1.41254E-08 1.51356E-08 1.46305E-08
1.51356E-08 1.62181E-08 1.56769E-08
1.62181E-08 1.73780E-08 1.67981E-08
1.73780E-08 1.86209E-08 1.79994E-08
1.86209E-08 1.99526E-08 1.92867E-08
2.13796E-08 2.29087E-08 2.06661E-08
2.29087E-08 2.45471E-08 2.21441E-08
2.45471E-08 2.63027E-08 2.37279E-08
2.63027E-08 2.81838E-08 2.54249E-08
2.81838E-08 3.01995E-08 2.72433E-08
3.01995E-08 3.23594E-08 2.91917E-08
3.23594E-08 3.46737E-08 3.12794E-08
3.46737E-08 3.71535E-08 3.35165E-08
3.71535E-08 3.98107E-08 3.59136E-08
3.98107E-08 4.26580E-08 3.84821E-08
4.26580E-08 4.57088E-08 4.12343E-08
4.57088E-08 4.89779E-08 4.41834E-08
4.89779E-08 5.24807E-08 4.73434E-08
5.24807E-08 5.62341E-08 5.07293E-08
5.62341E-08 6.02560E-08 5.43574E-08
6.02560E-08 6.45654E-08 5.82450E-08
6.45654E-08 6.91831E-08 6.24107E-08
6.91831E-08 7.41100E-08 6.68743E-08
.
.
.
4.67735E-06 5.01187E-06 4.84461E-06
5.01187E-06 5.37032E-06 5.19110E-06
5.37032E-06 5.75440E-06 5.56236E-06
5.75440E-06 6.16595E-06 5.96017E-06
6.16595E-06 6.60693E-06 6.38644E-06
6.60693E-06 7.07946E-06 6.84320E-06
7.07946E-06 7.58578E-06 7.33262E-06
7.58578E-06 8.12831E-06 7.85704E-06
8.12831E-06 8.70964E-06 8.41897E-06
8.70964E-06 9.33254E-06 9.02109E-06
9.33254E-06 1.00000E-05 9.66627E-06
];
```

Figure E 2Output of energy grid detector: If an energy bin structure is defined, the corresponding bin boundaries are written in variable "DETE". The variable has three columns: 1. Lower energy boundary of bin 2. Upper energy boundary of bin 3. Mean energy of bin